Aérojoules project: Vertical Axis Wind Turbine

Michael O'Connor

Master Thesis

presented in partial fulfillment
of the requirements for the double degree:
"Advanced Master in Naval Architecture" conferred by University of Liege
"Master of Sciences in Applied Mechanics, specialization in Hydrodynamics, Energetics and Propulsion" conferred by Ecole Centrale de Nantes
developed at l'Institut Catholique d'Arts et Métiers (ICAM), Nantes
in the framework of the

"EMSHIP"
Erasmus Mundus Master Course
in "Integrated Advanced Ship Design"

Ref. 159652-1-2009-1-BE-ERA MUNDUS-EMMC

Supervisor: Mr Jean-François Largeau, l'Institut Catholique d'Arts et Métiers (ICAM), Nantes.

Reviewer: Prof. Pierre Ferrant, Ecole Centrale Nantes.

Nantes, January 2014

CONTENTS

TABLE OF FIGURES:

LIST OF TABLES

1. SUMMARY

The objective of the Aérojoules project is to optimise the design of a Darrieus type Vertical Axis Wind Turbine and assess its validity of use as small scale electrical power generation in the 'Pay de la Loire' region.

It is well known that flow phenomena over a VAWT is complex and difficult to predict. A good understanding of flow characteristics is needed to predict torque and net power at various wind speeds, minimise stall effects, allow reliable starting, minimise loads and in particular fluctuating loads leading to excessive fatigue, understand tangential and radial forces and identify flow characteristics in the wake of the turbine to better understand interference effects.

Detailed 3D unsteady CFD analyses has been undertaken using the CFD program Star CCM+ to better analyse and predict flow over a VAWT. Such analysis has been compared with published articles and model tests with the aim to provide a reliable model for future applications.

Also detailed model testing has been conducted in a wind tunnel at various angles of attack, to measure lift forces and understand flow characteristics. Further wind tunnel testing has been conducted at full scale and compared with predicted results. A good comparison between static and dynamic foil wind tunnel behavior as well as between model and full scale is obtained.

The designed turbine uses a fixed pitch, yet helicoidal 3-bladed VAWT made of composite material. Its use in the marine industry and in particular on cargo ships is further investigated. It is also compared with a concept design which alters the angle of attack of the turbine over a rotation, allowing better control of turbine characteristics for a more reliable prediction of performance.

2. INTRODUCTION

A Darrieus type[12] VAWT has been designed for use as small scale electrical power generation in the 'Pay de la Loire' region. This project will continue the work conducted by Mr. Christian José Bottero as part of his EMSHIP master thesis conducted at l'Institut Catholique d'Arts et Métiers (ICAM) in 2010/2011[3]. The project is called the 'Aérojoules project'[4] which includes the collaboration of numerous companies in the French region 'Pays de la Loire'. It is in line with the regions strategy of developing a local renewable energy sector[5] and also the greater French[6] and European[7] strategy of increasing the amount of electrical generation from renewable sources in the years to come.

This report is more specifically focused on understanding the aerodynamics of a VAWT. Such aerodynamic flow was found to be non-linear and complicated to predict and control. A thorough guide of the theory of Darrieus type VAWT's will be presented and various means of aerodynamic prediction methods from numerical empirical, numerical Computational Fluid Dynamics (CFD) and experimental have been performed. A good understanding of the limitations and capabilities of such prediction software has been developed and recommendations on their suitability in the Aérojoules project have been provided.

The designed helicoidal 3-bladed turbine has had a particular focus with some design guidance on optimising blade aerodynamics. Helicoidal blades in a VAWT do provide complications in flow dynamics, with differing angles of attack along the span of a blade and stall phenomena occurring at any instant in time. Understanding such aerodynamics is important when designing

[1] Sutherland H, Berg D, Ashwill T; A *Retrospective of VAWT Technology*, Sandia National Laboratories, New Mexico, 2012.
[2] Paraschivoiu I, *Wind Turbine Design – With Emphasis on Darrieus Concept*, Presses internationals Polytechnique, Québec, Canada,2009.
[3] Bottero C , *Aérojoules project: Vertical Axis Wind Turbine;* Master's Thesis; 'EMSHIP' program in 'Integrated Advanced Ship Design', West Pomeranian University of Technology, Szczecin, 2011.
[4] Breluzeau J, *Projet collaboratif Aérojoules : une éolienne 300 W sur le marché en 2012...*, Océan Vital Fondation, 11/04/2012, http://www.fondationoceanvital.com/Actualites/Projet-collaboratif-Aerojoules-une-eolienne-300-W-sur-le-marche-en-2012. (Accessed 26 June 2013).
[5] J Auxiette, *The tide is turning for marine renewable energy in the French region pays de la Loire*; http://www.mre-paysdelaloire.com/presentation/ , Pay de la Loire regional council, June 2013. (Accessed June 26 2013).
[6] ADEMA, '*French know how in the field of RENEWABLE ENERGIES'*, French Environment and Energy Management Agency, Angers, April 2012, pg. 2. (Accessed 26 June 2013).
[7] Georgescu A, *'Introductory course to offshore wind turbines'*, University of Liege, 10th December 2012, Liège, slide 3

such a turbine to minimise unnecessary blade loading and vibration and obtain optimum power efficiencies.

When optimising flow however the design intended purpose must be known and fully understood. The use of turbines as electrical generators was also assessed with some optimal wind conditions for a suitable system.

In studying the blade aerodynamics some novel concepts have been proposed for further analysis. It was found that by controlling the pitch angle of the blades the negative effects of stall phenomena can be avoided, better turbine control can be obtained and potentially higher power coefficients achieved. However further analysis was needed.

Also a small study was conducted on the merits of using such a turbine on board various cargo ships whilst underway. The turbine was assessed as an electrical generator and as a means to reduce the ships wind resistance.

Previous work conducted by Mr. Christian José Bottero at ICAM regarding blade aerodynamics involved 2 dimensional CFD simulations of various NACA air foils; for both rapid assessment of the most appropriate foil, and of VAWT forces, torque and expected power.

2D CFD methods however have been shown to not agree with the physical reality. Blade aerodynamics are complex and to fully capture the real flow it must be analysed in the 3rd dimension. A successful 3D CFD model has not been implemented to date within the project, with time and computer hardware limitations present.

A CFD 3D model contradicts a concept designer's aim for rapid assessment, especially in early stages of a project; but is important to fully capture the real flow present in a VAWT.

The ultimate questions are; what is the real flow in a Darrieus VAWT? How can it be understood and assessed with accuracy but in a realistic time period? How does a good understanding of VAWT flow phenomena aid in making design decisions.

As the performance of a wind turbine is dependent on the wind flow phenomena created over a rotating air foil blade. This is a good place to commence such questions.

'The wind'.

3. WIND ENERGY

The technology of extracting energy from the wind has evolved dramatically over the last few Decades. The re-emergence of the wind as a significant source of the world's energy must rank as one of the significant developments of the late 20th century[8]. The advent of the steam engine, followed by the appearance of other technologies for converting fossil fuels to useful energy, would seem to have forever relegated to insignificance the role of the wind in energy generation. However, the re-emergence of wind energy as a major source of global energy production has been attributed to 5 main factors[8]:

1. There was a **need**. A global awareness developed of the finiteness of the earth's fossil fuel reserves and possible adverse effects of burning these fuels prompted people to look for alternatives.
2. There was the **potential**. Wind exists all over the world and in some areas with considerable energy density. Wind has been widely used in the past for transportation and mechanical power. There is no reason why it couldn't be used again.
3. There was the **technological capacity**. Developments in other fields of engineering when applied to wind turbines could revolutionise the way they are used.
4. There was a **vision**. The vision began well before the 1960's with such individuals as Poul Cour, Albert Betz, Palmer Putnam, Percy Thomas to name a few.
5. There was **political will**. Government support was needed to carry out research, development & testing; to provide regulatory reform to allow wind turbines to interconnect with electrical networks; and to offer incentives to help the deployment of the new technology. This has been done in various countries with governments offering incentives and the Aérojoules project is an example of a government led initiative.

3.1 OVERVIEW WIND TURBINES

3.1.1 Generators

A wind turbine is 'a device which converts the power in the wind into electricity'.[8] This is worth noting, as methods used pre-industrial revolution to convert the wind power into mechanical power was done by a device called a wind mill. This predominately was used to transport water via a large pump, which has a slightly different power vs. speed curve.

Thus it must be noted all wind energy devices must be studied in terms of their design purpose. Each energy use (such as mechanical or electrical) from the wind must be studied independently as the power-speed characteristics will differ.

It is important to consider the load and the energy when first assessing wind turbines.

The wind turbine will convert wind energy into aerodynamic wind force to produce a net positive torque on a rotating shaft, resulting first in the production of mechanical power and then its transformation of electricity to a generator. Energy is only produced when there is sufficient wind energy available, and the amount of energy produced is dependent on the electrical energy extracted from the prevailing winds.

3.1.2 Wind turbine classification

Wind turbines are classified into 2 main categories, depending on the axis of rotation of the shaft. This is Horizontal Axis Wind Turbines (HAWT) & Vertical Axis Wind Turbines (VAWT).[9]

HAWTs capture kinetic energy with a propeller type rotor and their rotational axis is parallel to the direction of the wind. A yawing mechanism to move the turbine into the direction of the wind is needed with these turbines and the electrical generator is located high in the propeller hub.

Some examples of various concept designs of HAWTs over the years is shown below in figure 1 and a modern large HAWT design is shown in figure 2. HAWTs are the most common in use today.[10]

---

[8] Manwell J, McGowen J, Roger A; *Wind energy explained: Theory, design & application*, 2nd edition, John Wiley & sons ltd, 2009,pg 1,2

[9] Paraschivoiu I; *Wind Turbine Design – With Emphasis on Darrieus Concept*, Presses internationales Polytechnique, 2009, Canada, pg. 1,2

[10] Ashwill T, Berg D, Sutherland H ; *A retrospective of VAWT technology*, SANDIA report, SAND2012-0304, Sandia National laboratories, California, USA, Jan 2012, pg. 13

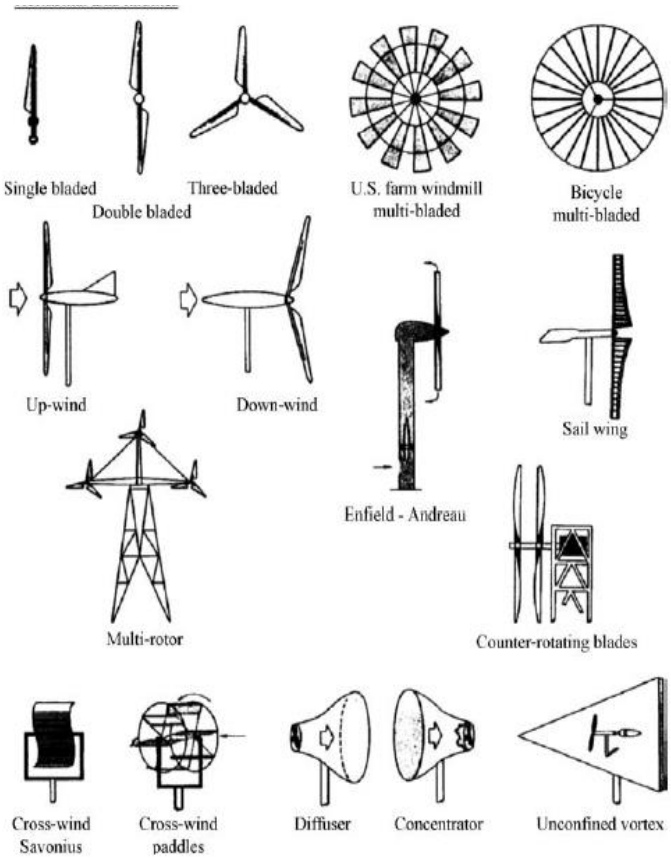

Figure 1: Various concepts for HAWTs

Figure 2: Modern HAWT's

VAWTs use straight or curved bladed rotors with the rotating axis perpendicular to the wind. The rotor is located below the turbine and they can operate in all wind directions.

VAWTs tend to come in two main configurations; the Savonius & the Darrieus turbines. The savonius turbine uses momentum transfer (or drag) to generate power and the Darrieus turbine uses aerodynamic forces (the lift force of an air foil)[11].

The Savonius turbine is characterised by its high torque and low speed, while the Darrieus turbine is characterised by its high speed and high efficiency.

Some examples of a wide array of VAWTs concepts developed are contained in figure 3.[12]

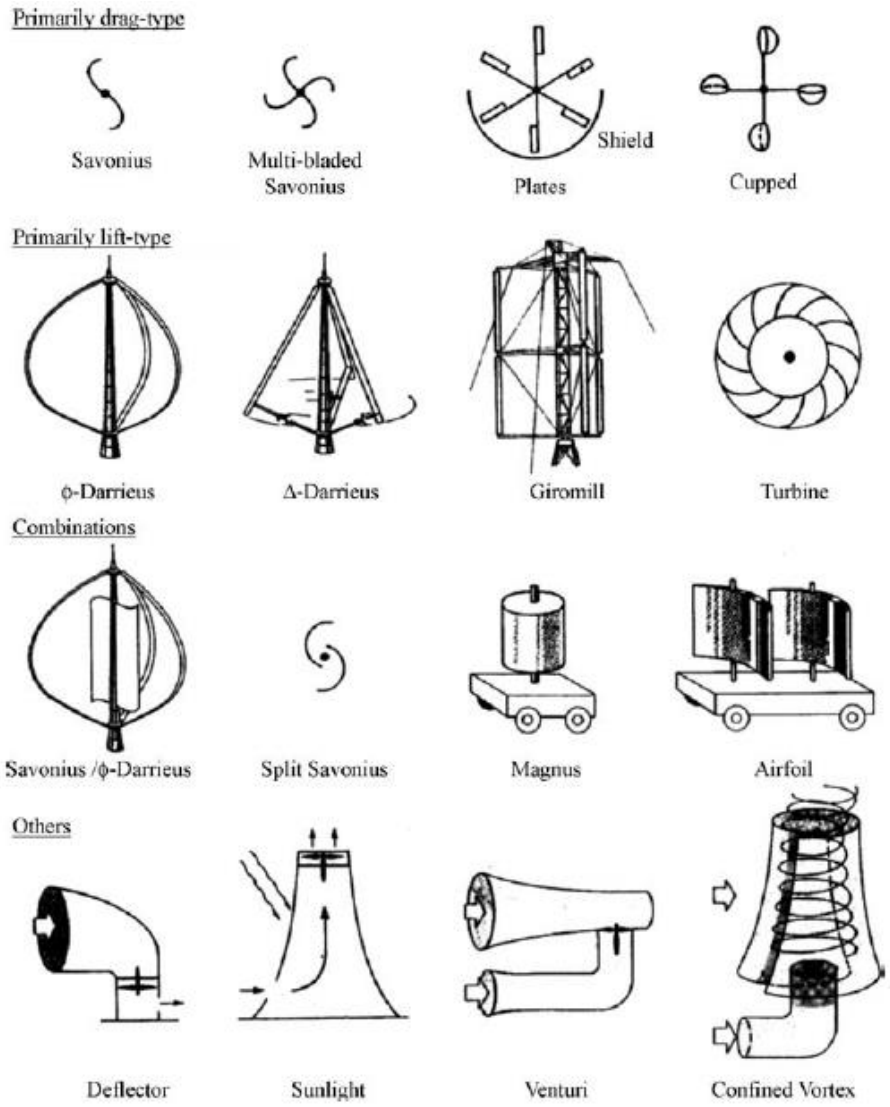

Figure 3: Vertical axis Wind Turbine concepts

[11] Ashwill T, Berg D, Sutherland H ; *A retrospective of VAWT technology*, SANDIA report, SAND2012-0304, Sandia National laboratories, California, USA, Jan 2012, pg. 13

[12] Manwell J, McGowen J, Roger A; *Wind energy explained: Theory, design & application*, 2nd edition, John Wiley & sons ltd, 2009,pg 10

3.2 DARRIEUS TYPE VAWT

The focus of this study will be on the optimisation of the VAWT Darrieus type.

The Darrieus configuration was patented by the French inventor Georges Jean Marie Darrieus in France in 1925 and in the US in 1931[13].This configuration was reinvented in the late 1960s in Canada by Rangi, South and Templin[14] and has had many concept design proposals of various forms since. Some examples are shown below.

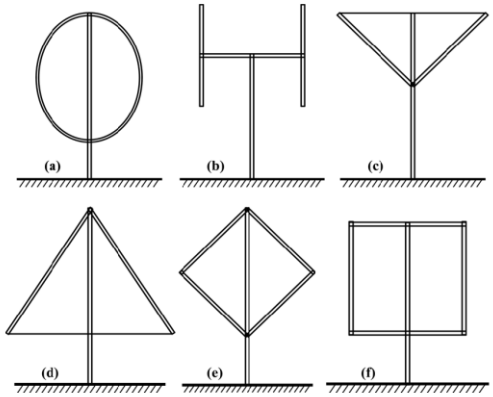

Figure 4: Various Darrieus type VAWTs

The full-Darrieus-rotor VAWT based on the original Darrieus model is contained in figure 5 below.

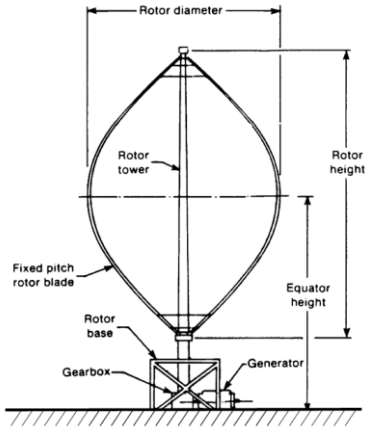

Figure 5: Full Darrieus type VAWTs

[13] G.J.M. Darrieus, *Turbine Having Its Rotating Shaft Transverse to the Flow of Current*, U.S. Patent #1834018, December, 1931.

[14] Sutherland H, Berg D, Ashwill T; *A Retrospective of VAWT Technology*, Sandia National Laboratories, New Mexico, 2012,pg 14

Figure 6 is an overview of the power coefficient (Cp) vs. the blade tip speed ratio (ratio of blade tip speed to wind velocity) of various wind turbines[15]. It is based on both theoretical calculations using momentum theory and experimental results gathered by various scientific research bodies over the years, and was published in the 1980's. The most significant research conducted on a VAWT at the time of publication was that conducted at Sandia Laboratories, a DOE Laboratory located at Albuquerque, New Mexico.[16] Figure 7 shows experimental results of a 17m height, 60KW VAWT and shows the importance of blade tip speed ratio in obtaining the optimum energy extraction coefficient.

What is important for large scale electrical power generation is the speed of the rotor, as it determines the size of the electrical generator. As can be seen from the curve the two suitable types of turbines with higher speeds for electrical power generation for a given size, based on blade tip speed ratio are the 2 bladed and often these days 3 blades horizontal wind turbine and the Darrieus type VAWT.

As the HAWT has a variable pitch mechanism their power coefficient is flatter making it efficient to extract power over a range of wind speeds and shaft rpms. The Darrieus type turbine has only been assessed with fixed pitch blades so its efficiency curve is limited to a particular wind speed to rotor rpm ratio.

Also to note, is the low Cp value for the Darrieus turbine operating at low tip speed ratios. The correspondingly low shaft power is insufficient to overcome friction so the Darrieus turbine needs a mechanical assist to get its tip speed up to at least twice the wind speed. At tip speed ratios above two, the Darrieus is able to extract enough power from the wind to accelerate itself up to the desired operating angular velocity of maximum efficiency.[17] Such a phenomenon is caused by what is termed 'stall effect' and is a major consideration when designing a VAWT and will be discussed further in chapter 4.

[15] Johnson G; Wind Energy Systems, electronic edition, Manhatton KS, May 2005, pg. 26
[16] Worstell, M. H.: *Aerodynamic Performance of the 17- Metre-Diameter Darrieus Wind Turbine*, Sandia Laboratories Report SAND78-1737, January 1979.
[17] Johnson G; Wind Energy Systems, electronic edition, Manhatton KS, May 2005, pg. 26

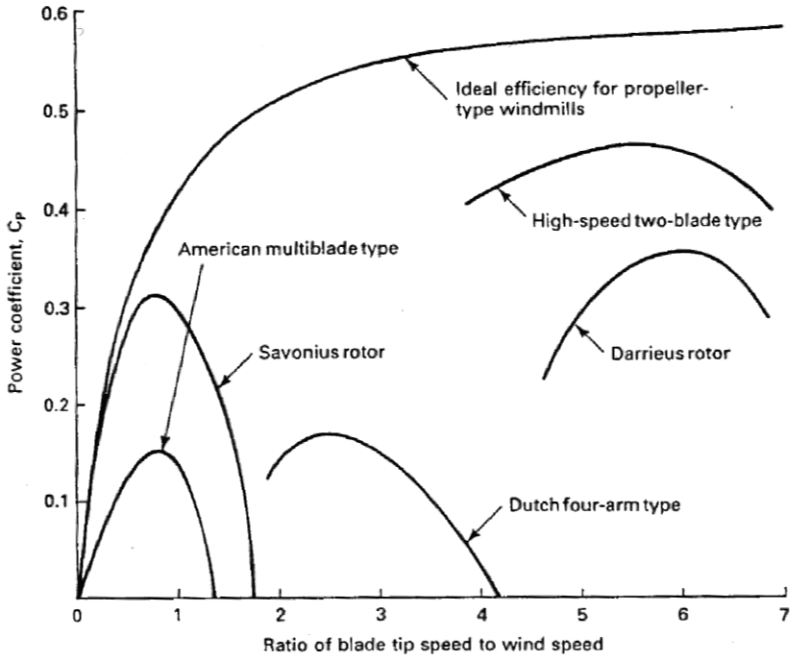

Figure 6: Power coefficient vs. blade tip speed ratio of various wind turbines.

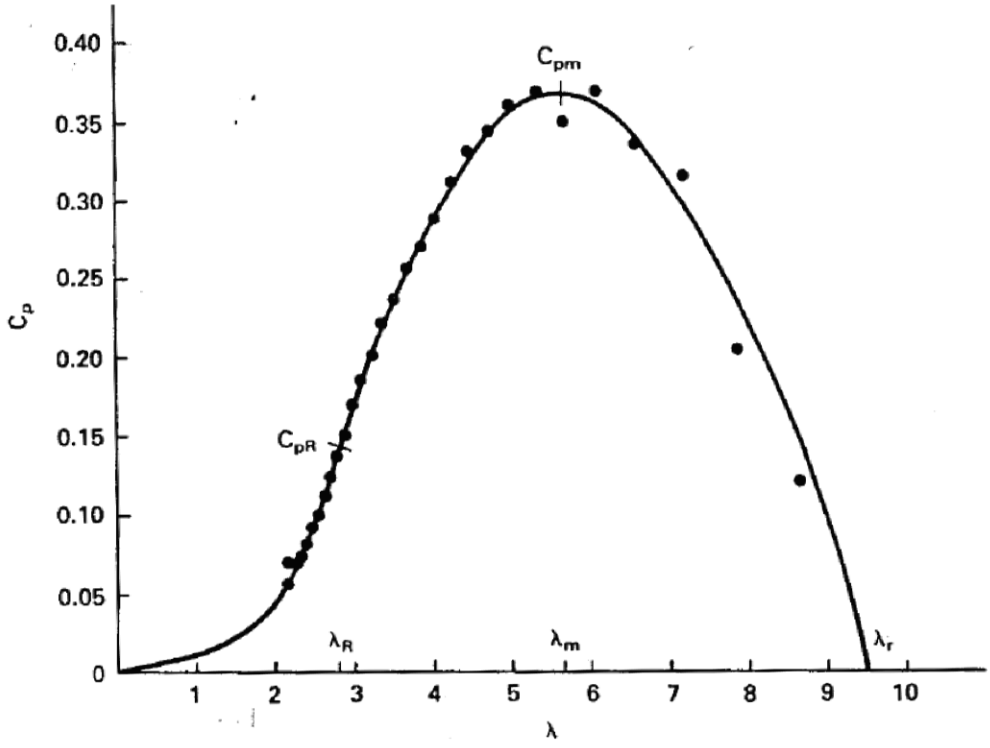

Figure 7: Coefficient of performance Cp versus tip-speed ratio for Sandia 17-m Darrieus turbine. Two blades; 42 rpm.

It is generally accepted that VAWT's have not had the same level of research and development funding as the HAWT and many concepts are still in development.[18]

Some early design issues experienced with Darrieus type VAWT such as fatigue issues due to the cyclic nature of the loading has contributed to this[19], however it is important to note some important technological advancements that have helped in the product development of wind turbines[20] and have also aided in a renewed interest in VAWT's.

- **Material science**: has brought new composites for the blades and alloys for the metal components. Improving structural strength, fatigue, weight and manufacturability. Early VAWT were made of Aluminium, where these days composite materials are more widely used which can better handle fatigue and enhance manufacturability[21]
- **Computer science**: facilitates more rapid design, analysis, monitoring and control. In particular the use of Computational Fluid Dynamics (CFD) to study the fluid flow, which will be a large part of this study.
- **Aerodynamics**: design methods of air foil blades for the aeronautical industry have been now used in the wind energy industry.
- **Analytical design & analysis methods:** design analysis is more accurate and rapid.
- **Testing and monitoring**: performance is more easily understood and verified using a vast array of commercially available sensors and data collection devices.
- **Power electronics:** can help to connect the turbine smoothly to the electrical network, allow variable speed rotation which can reduce cyclic loads and fatigue and optimise efficiency by allowing an optimum blade tip speed ratio to be achieved.

In many respects VAWTs are considered relatively simple devices. Fixed geometry blades, usually only 2 or 3 in number, easy access to the generator for maintenance, no yaw control or power regulation system is required. However such simplicity does not extend to the turbine aerodynamics. The blade elements travel along circular paths through air, whose relative speed

[18] Paraschivoiu I; *Wind Turbine Design – With Emphasis on Darrieus Concept*, Presses internationales Polytechnique, 2009, Canada, pg. 29
[19] Sutherland H, Berg D, Ashwill T; *A Retrospective of VAWT Technology,* Sandia National Laboratories, New Mexico, 2012,pg 14
[20] Manwell J, McGowen J, Roger A; *Wind energy explained: Theory, design & application*, 2nd edition, John Wiley & sons ltd, 2009,pg 20
[21] Bottero C **,** *Aérojoules project: Vertical Axis Wind Turbine;* Master's Thesis; 'EMSHIP' program in 'Integrated Advanced Ship Design', West Pomeranian University of Technology, Szczecin, 2011. Pg. 76

and direction are constantly changing[22]. A diagram that better emphasises this concept is contained in figure 8 below. It shows the circular path in which the air foil is operating and the direction of the incoming wind. The relative angle between the foil velocity vector and the wind velocity vector will change at each point in a 360 degree rotation.

Due to this changing blade velocity relative to the wind, Darrieus turbine blades operate with unsteady, non-linear, interfering aerodynamics[23]. This provides variation in structural loading and creates difficulty in accurately predicting and optimising the power output due to the varying and turbulent flow. Understanding blade aerodynamics is the key to accurately assessing performance of a VAWT.

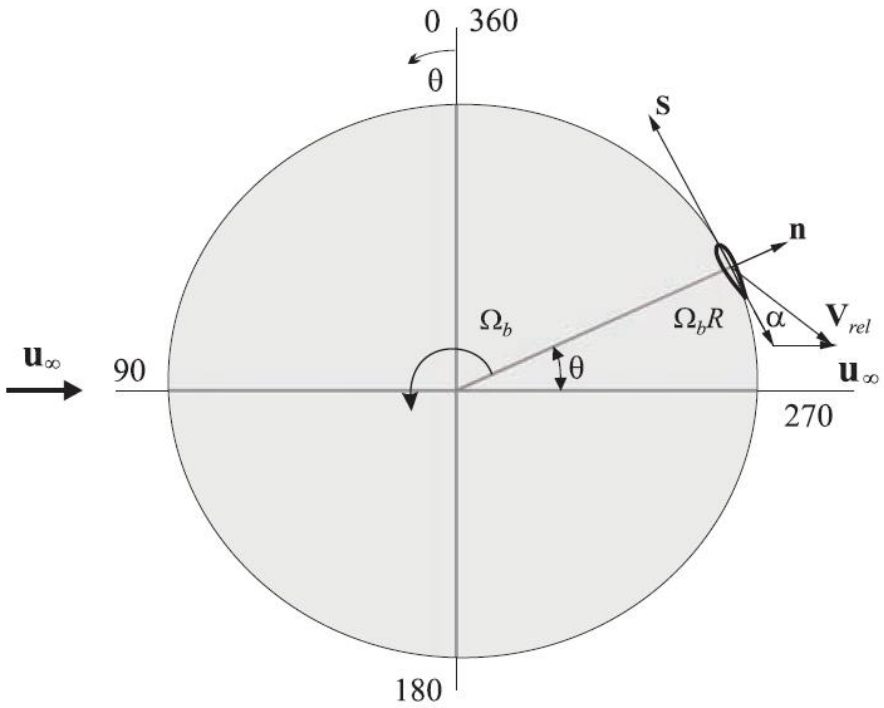

Figure 8: Circular path of a VAWT blade

[22] Klimas P, *Darrieus Rotor Aerodynamics*, Sandia National Laboratories, Advanced Energy Projects Division, Albuquerque, USA

4. THEORY OF VAWT AERODYNAMICS:

A VAWT experiences complex fluid flow over a rotating foil. The reason such a flow is complex is the constantly changing angle of attack and inlet velocity over the foil during each revolution. This section aims at simplifying the problem and explain using Blade Element Momentum (BEM) theory via the actuator disc model the flow characteristics of a VAWT. By using such a model and combining it with interference effects and known flow phenomena such as stall effect obtained through experiments; 2 key advantages are possible.

- Flow is easily understood and explained.
- Rapid assessment is achievable.

4.1 VAWT FLOW CHARACTERISTICS:

It is possible to simplify the analysis of a VAWT flow by studying the variation in angle of attack and inlet velocity over a full 360 degrees turn. The angle of attack and inlet velocity is very much dependent on wind speed and rotational velocity of the turbine.

A study of the various factors that determine major flow characteristics over an airfoil is contained below.

This analysis is based on an airfoil of chord **c** rotating at a speed **n** and exposed to a free stream wind velocity of speed $\mathbf{V_1}$. At the rotor, the velocity has reduced its magnitude to $\mathbf{V_a}$ due to the induction factor. This is explained well in Beri & Yao[23] by use of the actuator disc model of a wind turbine shown in Figure 9. This simple model, generally attributed to Betz[24] can be used to determine the power, the thrust of the wind on the ideal rotor and the effect of the rotor operation on the local wind field.

[23] Beri H, Yao Y**:** *Double Multiple Stream Tube Model and Numerical Analysis of Vertical Axis Wind Turbine* ; Department of Manufacturing and Automation, Harbin Institute of Technology, Harbin, China, published May 2011, (http://www.SciRP.org/journal/epe)

[24] Ragheb M, Ragheb A:*Wind Turbines Theory - The Betz Equation and Optimal Rotor Tip Speed Ratio, Fundamental and Advanced Topics in Wind Power*, Dr. Rupp Carriveau (Ed.), ISBN: 978-953-307-508-2,2011; InTech, Available from: http://www.intechopen.com/books/fundamental-and-advanced-topicsin-wind-power/wind-turbines-theory-the-betz-equation-and-optimal-rotor-tip-speed-ratio

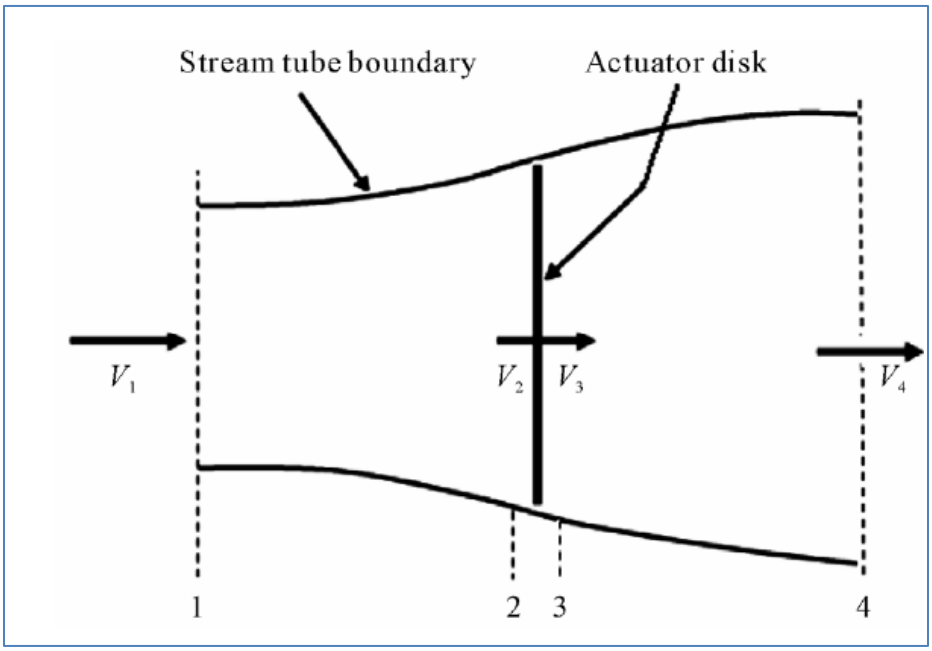

Figure 9: Actuator disc model of a wind turbine.

This is the simplest of models of a VAWT wind turbine but a good place to start, for understanding the flow and comparing various variables and there effect on turbine performance. Some initial assumptions of such a model include:

- Homogenous, incompressible, steady state fluid flow with no frictional drag.
- The pressure increment or thrust per unit area is constant over the disk.
- The rotational component of the velocity in the slipstream is zero.
- There is continuity of velocity through the disc.
- An infinite number of blades.

What is most notable about the model is it exemplifies absolute ideal conditions for a VAWT. Interference effects between blades and over a complete revolution are ignored and eddy effects in the slipstream are also ignored. However by a applying a simplistic model combined with some knowledge of blade behavior, interference effects and wake flow a good understanding of the limitations and possibilities of a VAWT can be obtained.

The axial induction factor "***a***" is defined as the fractional decrease in wind velocity between the free stream and the rotor plane. Thus the wind at the rotor plane is defined as the average of the up-stream and down-stream wind speeds.

Then:

$$a = \frac{V_1 - V_2}{V_1} \quad (3.1a)$$

$$V_2 = V_1(1-a) \quad (3.1b)$$

$$V_4 = V_1(1-2a) \quad (3.2)$$

$$V_2 = \frac{V_1 + V_4}{2} \quad (3.3)$$

Maximum power from such a model was derived by Betz to be when a = 1/3. Thus this can be used to estimate the induction velocity for power estimates in ideal conditions.

$$C_P = 4a(1-a)^2 \quad (3.4a)$$

$$(C_P)_{\max} = \frac{16}{27} = 0.5926 \quad (3.4b)$$

When a = 1/3

Also worth noting is the variation in the speed of the air before ($\mathbf{V_1}$) and after ($\mathbf{V_4}$) passing through the turbine. Logically, the difference in the kinetic energy of the flow was transformed or dissipated in the process. This is very important when looking at interference effects from the turbine wake of each foil on a single turbine, especially if 3 foils are employed on a single rotor. These effects will all be considered and discussed further in 4.3 and chapter 8. Initially the Betz model assumes no interference between the wind flow as the blade performs a complete revolution. As a VAWT will encounter the free stream wind flow twice, this is difficult to perfect, however can be analysed and interference minimised. If interference can be minimised, there is no reason to assume a VAWT cannot perform as good or better than a HAWT, as it has 2 attempts to extract as much energy as possible from the wind.

4.2 WIND VELOCITY AND BLADE ANGLE OF ATTACK

As it can be seen from figure 10, the total incident velocity on the turbine blade is obtained by combining the free stream component and the rotational component, which can be expressed in the equations below.

The ratio between the blade tip speed and the speed of the incident flow is known as the tip Speed ratio (λ) and its expression can be found in equation 3.6 below.

$$V_t = R\,\omega \tag{3.5}$$

$$\lambda = \frac{V_t}{V_a} = \frac{R\,\omega}{V_a} \tag{3.6}$$

V_t is the blade tip speed, while V_a is the induction speed, which is actually V_2 in 3.3.

As the blade tip speed is often much higher than the speed of the incident flow for a VAWT this will have the largest influence on the angle of attack of the wind over the foil.

To obtain the magnitude of the total incident velocity, the airfoil can be divided into a component parallel to its chord (V_c) and one normal to it (V_n). The expressions can be found in the equations below, and the total incident velocity can be expressed as in equation 3.10.

$$V_c = V_t + V_a\,\cos\theta \tag{3.7}$$

$$V_n = V_a\,\sin\theta \tag{3.8}$$

$$V_r = \sqrt{V_c^2 + V_n^2} \tag{3.9}$$

$$V_r = \sqrt{V_a\left(\frac{R\,\omega}{V_a} + \cos\theta\right)^2 + V_a\,\sin^2\theta} \tag{3.10a}$$

$$= V_a\sqrt{\left(\lambda + \cos\theta\right)^2 + \sin^2\theta} \tag{3.10b}$$

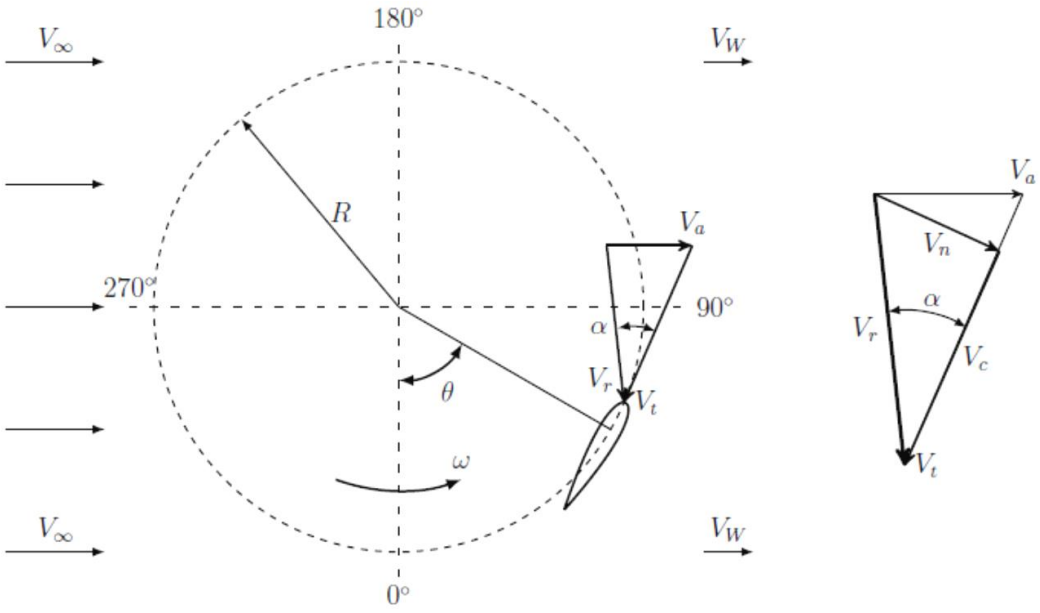

Figure 10: VAWT schematic view and velocity diagram.

Thus as the angle of attack over the airfoil is constantly changing during a revolution, the incident velocity magnitude is also changing. This variation of the flow velocity leads to a variation in the local Reynolds number. Depending on the foil type and range of Reynolds number this may have an associated effect on the flow conditions present over the foil.

$$Re = \frac{c V_r}{\nu} \tag{3.11}$$

The magnitude on the angle of attack also is very important when considering flow conditions present over the turbine and force coefficients at an instant in time. This is defined as the angle between the direction of the incident flow and the chord of the airfoil. Looking at Figure 10 this is the sum of the turbine tangential velocity and the wind induction velocity.

$$\alpha = \tan^{-1}\left(\frac{V_n}{V_c}\right) \tag{3.12}$$

Replacing $\mathbf{V_n}$ and $\mathbf{V_c}$ from the equations 3.7 and 3.8, the incident angle can be written as in the equation below.

$$\alpha = \tan^{-1}\left(\frac{\sin\theta}{(\lambda + \cos\theta)}\right) \tag{3.13}$$

From these equations we can obtain an inlet velocity and an angle of attack for each angle over a 360 degree cycle for a given angular velocity and free wind velocity. An example of this variation in angle of attack of a 360 degree revolution at various blade tip speed ratios is contained in figure 11 below.

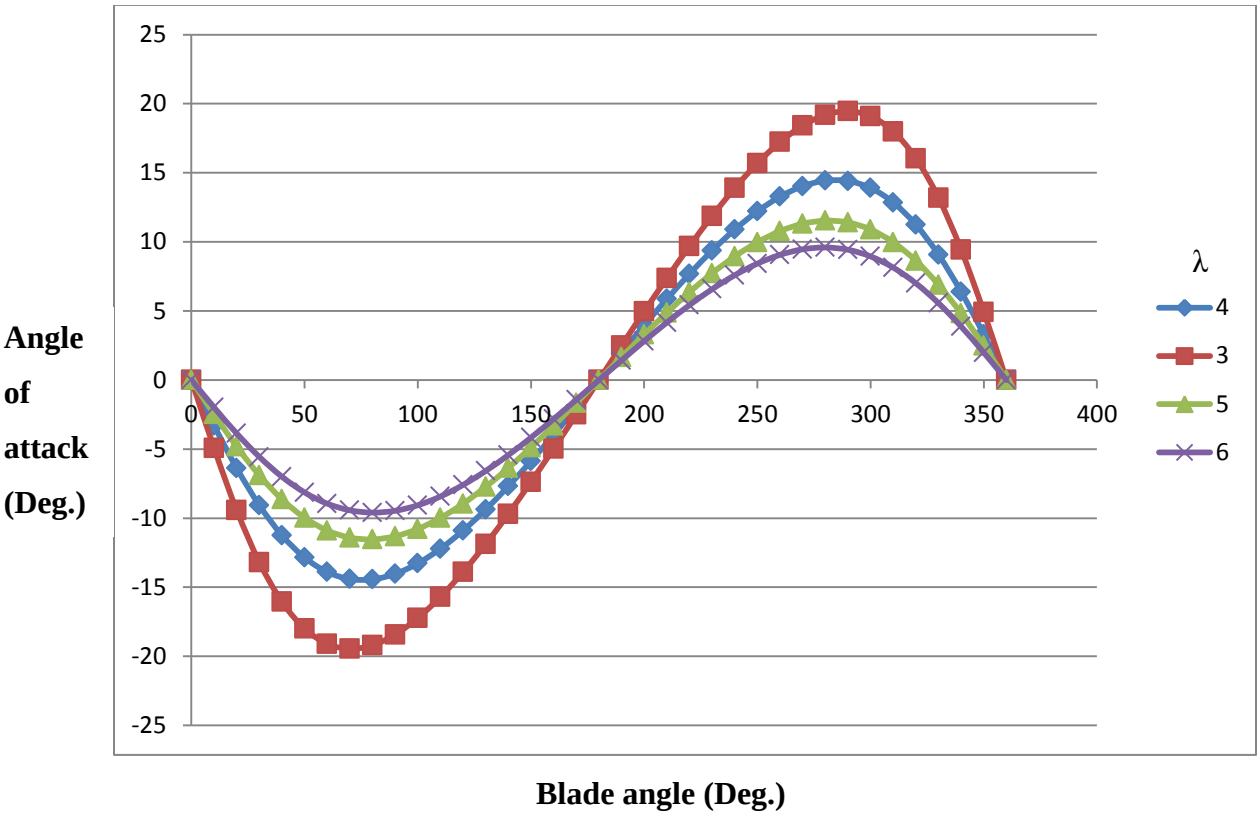

Figure 11: Airfoil angle of attack vs blade angle at various tip speed ratios.

Note: angle of attack is positive relative to the leading edge blade.

Depending on the type of airfoil used and its characteristics the blade angle of attack is very important in determining the blade lift forces and foil aerodynamics. Using the NACA 0012 foil as an example the maximum lift force available from turbine blade is obtained at a blade angle of attack of 13 degrees shown in Figure 12.[25] After this angle blade aerodynamics becomes unstable and a sudden drop in lift force occurs. This is a phenomena called stall, and in the static condition

[25] Gerontakos P, Lee T: *Investigation of flow over an oscillating airfoil;* Department of Mechanical Engineering, McGill University, Montreal, Canada. J. Fluid Mech. (2004), vol. 512, pp. 313–341. 2004 Cambridge University Press

is associated with a complete separation of the boundary layer at the leading edge which culminates in the bursting of a the boundary separation bubble. However it should be noted such analysis has been undertaken at a Reynolds number of 1.35 x 10^5, and not only is the blade angle of attack changing but also the blade inlet velocity, which will be linked to a particular Reynolds number. The location of the sudden drop in blade lift forces may vary depending on the airfoil type and the blade Reynolds number. This is an area that will be investigated further with model tests and CFD analysis.

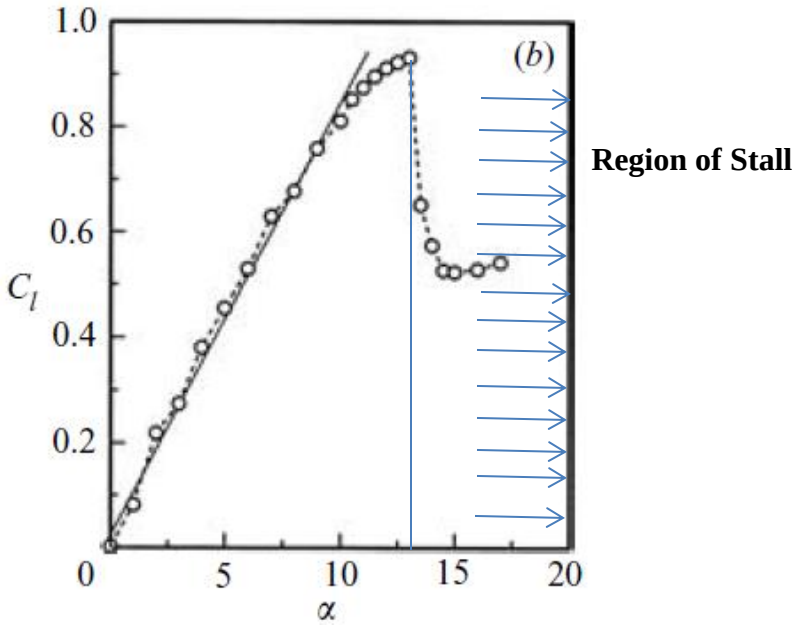

Figure 12: Lift coefficient vs Angle of attack for a NACA 0012 airfoil.

Figure 13 & 14 illustrates an example of the changing Reynolds number vs Blade angle for various blade tip speed ratios (λ) for a NACA 0012 airfoil of a chord of 0.1 at wind inlet speed of 10 m/s and also 5m/s using an optimum induction factor of **a**=1/3.

It highlights over the lifetime of a turbine it will operate over variable Reynolds numbers; both for 1 revolution and also over a range of wind speeds. Thus it is important to have accurate and relevant air foil data in regards to lift and drag coefficients over a range of Reynolds numbers.

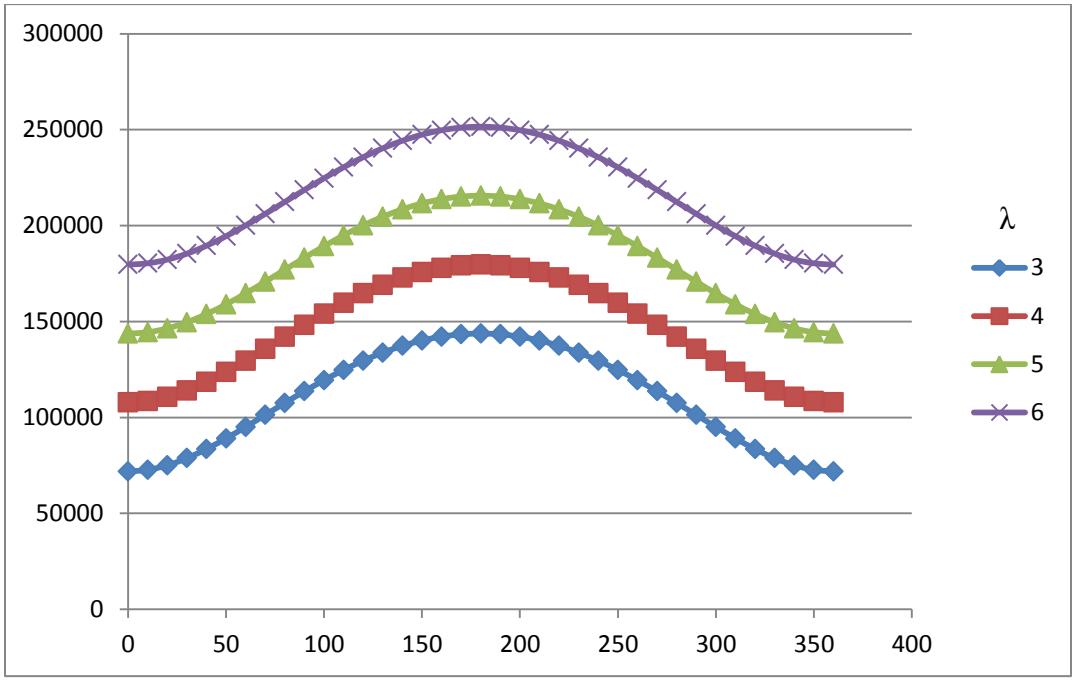

Figure 13: Reynolds number vs Blade angle at various tip speed ratios at a wind speed of 10 m/s.

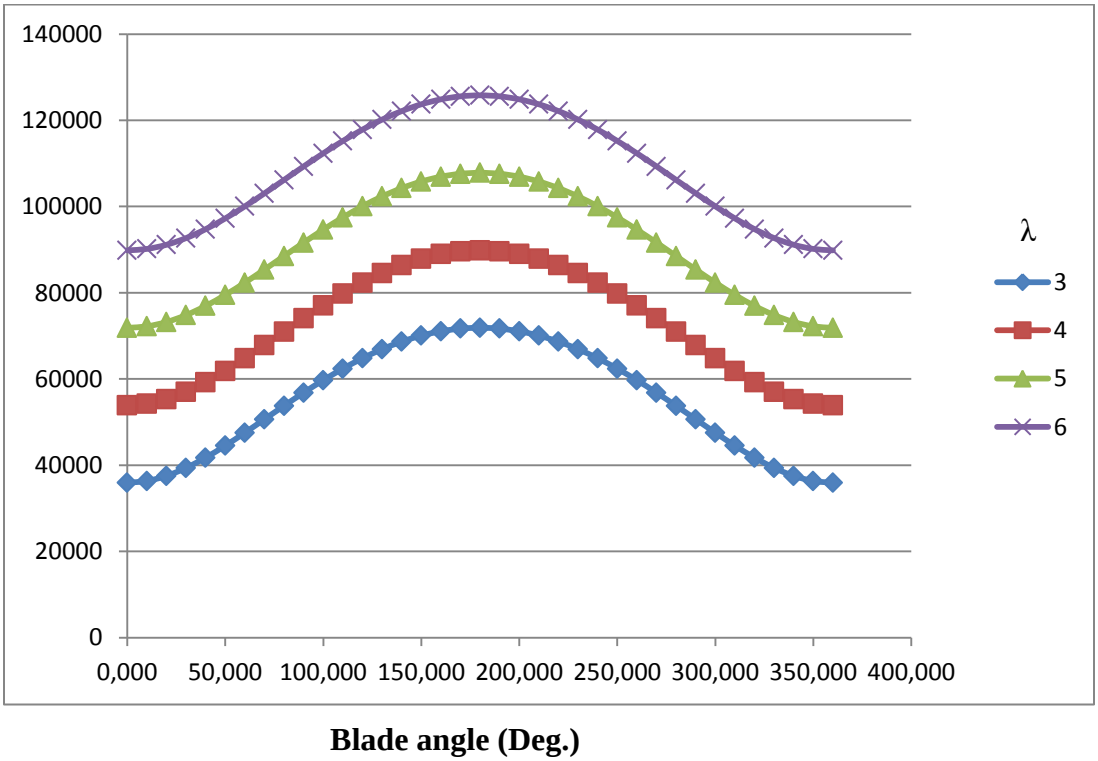

Figure 14: Reynolds number vs Blade angle at various tip speed ratios for a wind speed of 5m/s.

4.3 INTERFERENCE

It is well known that each foil will create a disturbance in the wind flow. This disturbance will not only be associated with the air the foil displaces but also the wake created by the foil. For ideal conditions it is important that the next blade passing through the displaced area of the proceeding blade does so without any interference from the previous blades wake. Thus the time period that each blade disturbs an air zone must be calculated.

The time taken for the disturbed wind to reestablish itself (t_w) and the time required for the next blade to move into the zone of the previous blade (t_s) should be calculated.

These times are as follows:

$$t_s = \frac{2\pi}{n\omega}[\text{sec}] \qquad 3.14$$

$$t_w = \frac{s}{V}[\text{sec}] \qquad 3.15$$

V is the wind speed, s is the length of the disturbed wind speed (size of the wake), ω is the angular velocity and n is the number of blades.

The length of the disturbed wind speed is dependent on many factors, but the most important is chord length. So it is planned to adjust the above equation and related disturbed length of wind speed with chord length, however at this stage more analysis of blade aerodynamics is needed to develop such a relation.

For optimal conditions, factors which will affect the design include of the number of blades, the turbine frequency, the chord length and the turbine radius.

Also it should be noted that each blade will cross the free stream wind twice. So for ideal conditions it may be wise to allow for some time for free stream velocity to pass through the turbine before the next blade enters the zone, allowing a full free stream wind velocity at each blade encounter.

All these factors can be combined to obtain an ideal turbine frequency, radius, chord length and number of blades.

If $t_s > t_w$, some wind is unaffected or allowed to flow through the turbine unaffected at the first encounter. If $t_w > t_s$, some wind is not allowed to flow through the rotor and will disturb the blade aerodynamics of the proceeding blade. The maximum power extraction occurs when the two

times are approximately equal, or when $t_s > t_w$ and the unaffected wind is encountered for in the 2nd blade passing. The optimum will hence depend on the number of blades, frequency of rotation and radius. At this stage setting $t_s > t_w$ is more complicated and a thorough analysis of blade aerodynamics is needed to understand the size of the wake and the degree of unaffected flow. Setting t_w equal to t_s yields the equations below;

$$t_s \approx t_w$$
$$\frac{2\pi}{n\omega} \approx \frac{s}{V} \Rightarrow \frac{n\omega}{V} \approx \frac{2\pi}{s} \qquad 3.16$$

Thus optimal rotational frequency can be defined as:

$$\omega_{optimal} \approx \frac{2\pi V}{ns} \qquad 3.17$$

Consequently, for optimal power extraction, the rotor blade must rotate at a rotational frequency that is related to the speed of the oncoming wind. This rotor rotational frequency decreases as the radius of the rotor increases and can be characterised by calculating the optimal TSR; $\lambda_{optimal}$ as shown in the equation below.

$$\lambda_{optimal} \approx \frac{\omega_{optimal} r}{V} \approx \frac{2\pi}{n}\left(\frac{r}{s}\right) \qquad 3.18$$

Further analysis will be conducted of this optimal speed when a better understanding of the blades wake is known.

4.4 FORCES OVER THE AIRFOIL

Once flow velocity and angle of attack of a turbine are known the forces over the blade can be calculated. Such forces are responsible for both radial and tangential loads on the turbine and also output torque and power generated. It is important to analyse forces both in the radial and tangential direction. Radial direction will influence the rotor and turbine structure while tangential forces will influence the torque generated. It should also be noted the net force direction is dependent on wind direction, unlike the torque generated over a cycle which is considered independent of wind direction.

Analysing figure 15 below, the forces on the airfoil can be divided into a drag force (Fd) parallel to the incident flow and a lift force (Fl), perpendicular to the flow direction. Forces are further divided into tangential (Ft), and radial forces (Fr), which are more appropriate for the design of the VAWT for power generation.

These forces can be expressed as a function of both the non-dimensional force coefficients and the blade dimensions, as seen in the equations below for the lift and drag force.

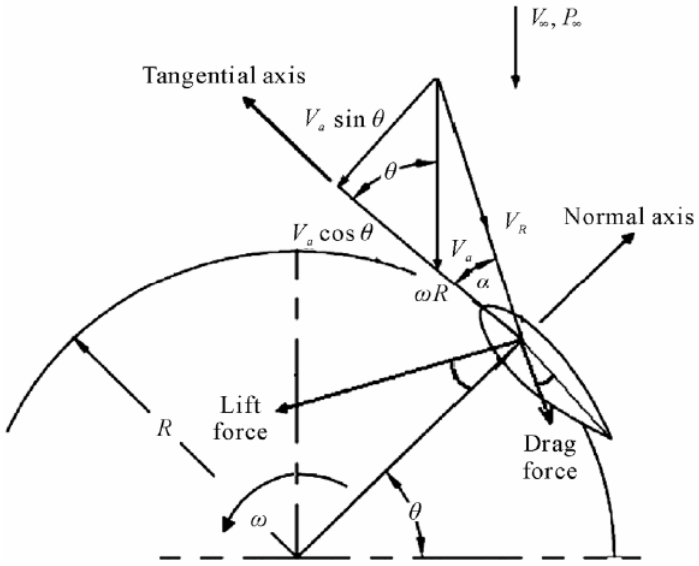

Figure 15: Forces over the rotating foil.

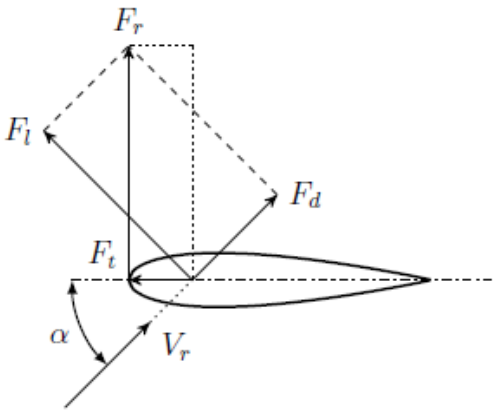

Figure 16: Forces over the rotating foil.

$$F_l = \frac{1}{2}\rho\, c\, l\, C_l\, V_r^2 \tag{3.19}$$

$$F_d = \frac{1}{2}\rho\, c\, l\, C_d\, V_r^2 \tag{3.20}$$

To obtain the tangential and radial forces, the lift and the drag must be calculated in the tangential and radial direction and then added to find the expression of the tangential force and the radial force, as seen in the equations below.

$$F_t = F_l \sin\alpha - F_d \cos\alpha \tag{3.21}$$

$$F_t = \frac{1}{2}\rho\, c\, l\, V_r^2 \left(C_l \sin\alpha - C_d \cos\alpha\right) \tag{3.22}$$

$$F_r = F_l \cos\alpha + F_d \sin\alpha \tag{3.23}$$

$$F_r = \frac{1}{2}\rho\, c\, l\, V_r^2 \left(C_l \cos\alpha + C_d \sin\alpha\right) \tag{3.24}$$

Cd is comprised of both lift induced drag and frictional induced drag. Frictional induced drag is a function of the Reynolds number while pressure drag is a function of the blade geometry, angle of attack and also Reynolds number.

The lift and drag coefficients of various NACA type airfoils can be obtained by experimental results or CFD analysis. Also there are many published results of Lift coefficients of various NACA airfoils which can be utilised to verify experimental and numerical analysis. Initial analysis was conducted using a NACA 0012 airfoil as lift coefficients are readily available and

can be easily compared with experiment results and CFD numerical analysis. What is very important however is to find an article with identical Reynolds numbers to compare flow characteristics.

4.5 TORQUE AND POWER OUTPUT

The torque generated by the airfoil is dependent on the incident flow and the angle of attack. Thus it will vary over one complete cycle as can be seen from the equations below.

$$M_t = F_t\, R \tag{3.25}$$

It is important, however, to have an averaged or mean value of the generated torque and therefore, of the gross power output. As the motion of the airfoil is periodic, the mean torque over a turn (Mta) can be derived as follows:

$$M_{ta} = \frac{1}{2\pi} \int_0^{2\pi} F_t(\theta)\, R \, \mathrm{d}\theta. \tag{3.26}$$

This can be assessed over a 360 degree cycle and at each instant in time over a cycle the torque of each blade can be calculated. The sum of each blade torque at a moment in time is then calculated, and then the average over a cycle can be computed. An example is given below of a 3 blade VAWT utilising a blade tip speed ratio of 3 and a wind speed of 10m/s.

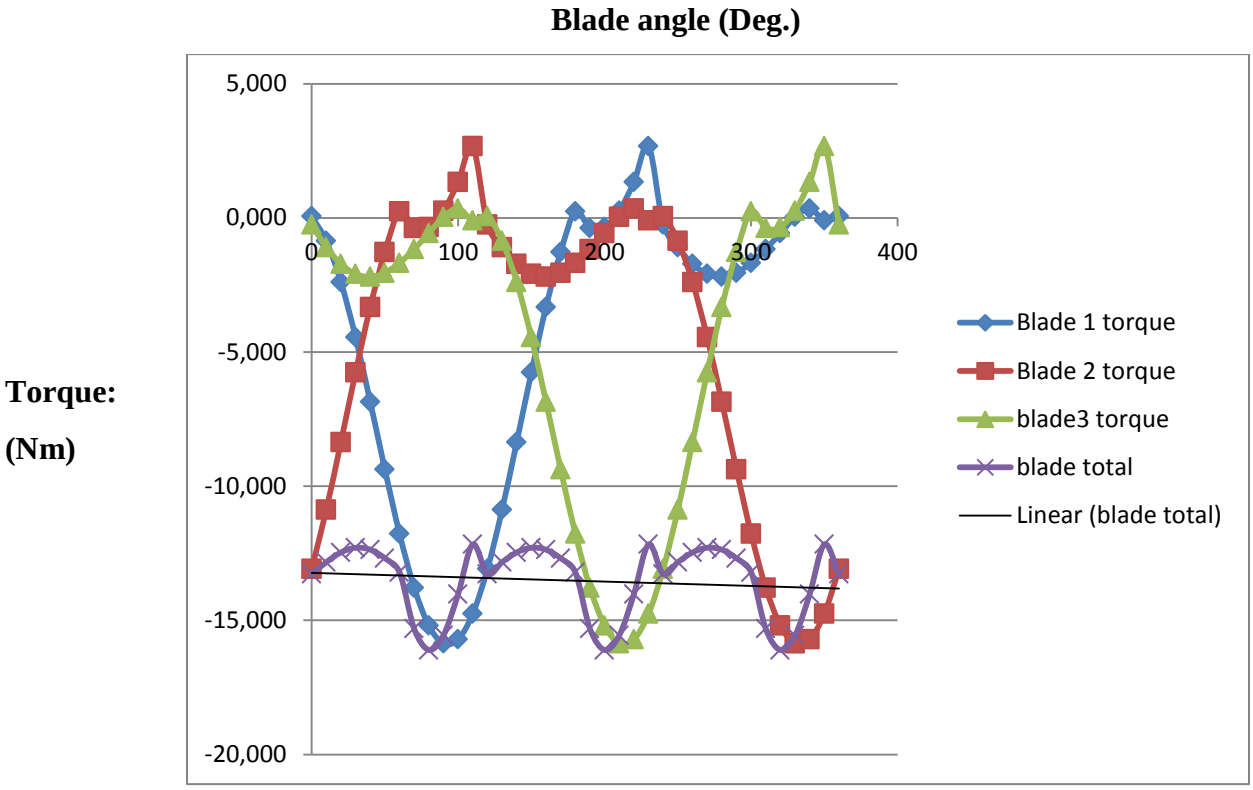

Figure 17: Blade torque vs foil angle

The average torque for the turbine (M_{Ta}) will be the summation of the N_B blades at a moment in time, as shown in the figure 17 above.

Finally, the mean power output of the turbine can be computed considering its rotational speed, as shown in the equation.

$$P_a = M_{Ta}\,\omega \tag{3.27}$$

This last expression can be used to assess the efficiency of different designs, comparing it to the maximum theoretical available power in the free stream. The ratio between the extracted power from the wind and the total power available in the free stream is known as the power coefficient or efficiency of the turbine and can be expressed as in the equation below.

$$C_P = \frac{P_a}{P_w} \tag{3.28}$$

$$= \frac{P_a}{\frac{1}{2}\rho S V_\infty^3} \tag{3.29}$$

4.6 CYCLING LOADING

This has always been an area of difficulty in designing a VAWT, as due to cyclic loads fatigue can be a large problem. Using the same example the cyclic loads of radial and tangential forces for each blade individually and combined is shown below:

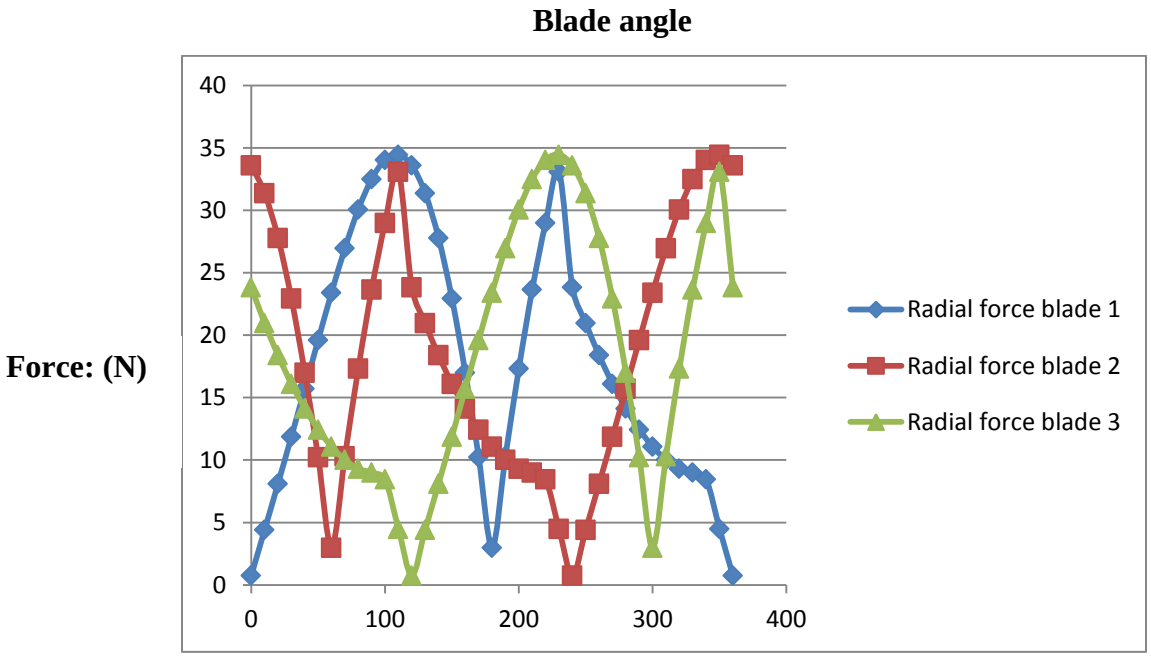

Figure 18: Radial forces over a foil revolution

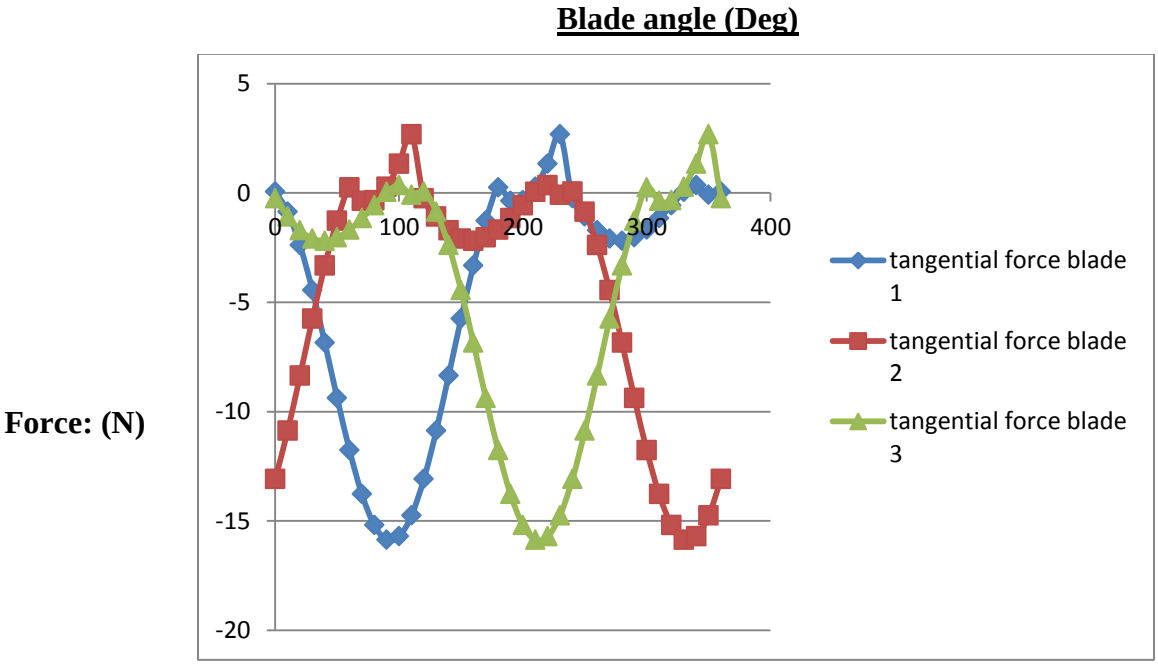

Figure 19: Tangential forces over a foil revolution

As is shown in the previous graphs there is cyclic loading over a rotation of a VAWT. Such cyclic loading will contribute to fatigue loading of the turbine. As discussed previously fatigue has been one issue that has hindered the development of VAWT's, however due to advancements in material science with the use of composite materials & advancements in electronics with variable speed rotation control; this issue can be better controlled.

4.7 DYNAMIC STALL

Static stall has already been discussed, which includes a series of complex aerodynamic phenomena, beginning with transition to turbulence, shear layer instability, vortex formation and flow separation. Its effects are seen in a sudden loss in lift force associated with a particular angle of attack.

Dynamic stall has similar effects such as a sudden loss in lift force however occurs due to a dynamic change in blade angle of attack. As discussed VAWT turbine blades operate with a constantly changing angle of attack. The only equivalent could be made with pitch control used on a helicopter blade to control lift. This phenomenon has led to several experiments studying flapping foils. Such experiments can be equally utilised in studying the flow phenomena of a VAWT.

When an airfoil experiences a time dependent change of its angle of incidence, an unsteady flow separation might occur, causing what is known as dynamic stall.

Various experiments over the years have been conducted aiming at better understanding the phenomena of dynamic stall. Most experiments have been conducted to solve the practical problem of stall over a helicopter blade rotor. The work of Lee & Gerontakos[26] was particularly noted in comparing both static and dynamic stall via experimental analysis on a NACA 0012 foil. Such experiments have shown that the predominant feature of dynamic stall is the formation over the upper surface of an airfoil an energetic vortex like disturbance and its shedding over the leading edge. This induces a non-linear fluctuating pressure field and produces transient variations in forces and moments that are fundamentally different from their steady state

[26] Gerontakos P, Lee T: *Investigation of flow over an oscillating airfoil;* Department of Mechanical Engineering, McGill University, Montreal, Canada. J. Fluid Mech. (2004), vol. 512, pp. 313–341. 2004 Cambridge University Press

counterparts. After the leading edge-vortex passes the airfoil trailing edge and goes into the wake, the flow progresses to a state of full separation over the upper surface.[27]

Wang[27] further investigated dynamic stall but more specifically focused on VAWT's and summarised well dynamic stall phenomena present into 4 key stages.

- An attached flow at low angles of attack.
- The development of the leading edge vortex
- The shedding of the leading edge vortex from the suction surface causing the full stall of the blade
- The reattachment of the flow to the suction surface.

The phenomenon of dynamic pitching was shown to actually improve the blade lift coefficients and delay the effects of stall (or increase the angle of attack at which the loss of lift forces occurs). Figure 20 shows results of experiments conducted by Lee & Gerontakos of the dynamic pitching of a NACA 0012 airfoil.

[27] Wang S, Ingham D, Ma L, Pourkashanian M, Tao Z: *Turbulence modelling of deep dynamic stall at relatively low Reynolds number:* Journal of fluids and structures, science direct, 2012 Elsevier Ltd.

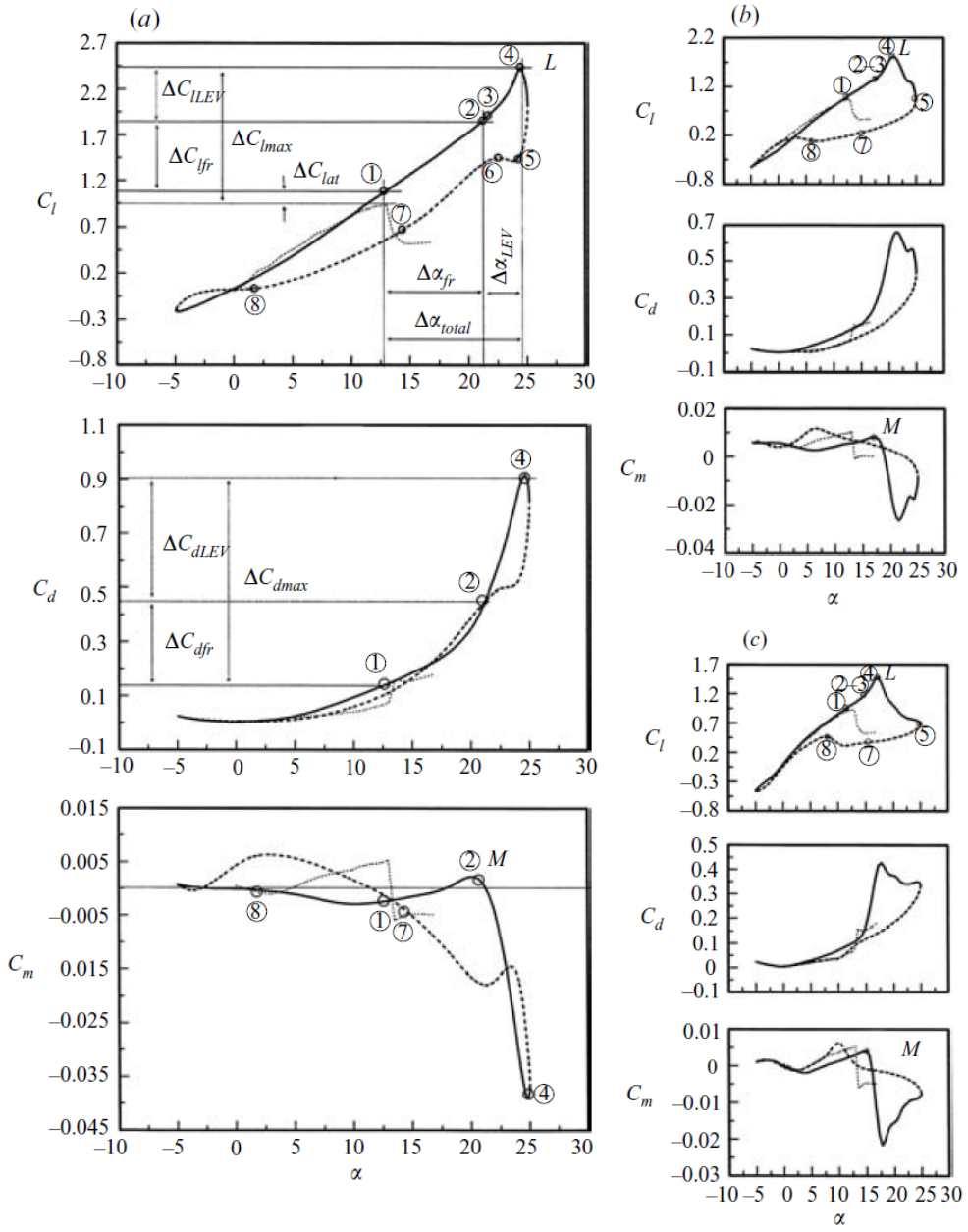

FIGURE 8. Variation of dynamic load-loops with reduced frequency for $\alpha(t) = 10° + 15°\sin\omega t$. (*a*) $\kappa = 0.1$, (*b*) $\kappa = 0.05$, (*c*) $\kappa = 0.025$. ①, onset of flow reversal; ②, end of upward spread of flow reversal; ③, turbulent breakdown; ④, lift stall; ④–⑤, full stall; ⑥, onset of secondary vortex; ⑦, onset of flow reattachment; ⑧, end of flow reattachment. ——, increasing α; ····, decreasing α; · · · ·, static values; *M*, moment stall; *L*, lift stall.

Figure 20: NACA 0012 airfoil dynamic load –loops with changing frequency.

Some interesting conclusions from the above figure that could be utilised in the design of a VAWT's include:

- As the frequency of pitching decreases, the stall angle of attack is lower and the lift coefficient is less.
- As the frequency of pitching increases, the stall angle of attack is higher and the maximum lift coefficient is higher.

Such conclusions agree with theoretical and experimental results previously shown on VAWT's, that higher efficiencies can be achieved at high blade tip speed ratios. As stall angles at higher blade tip speed ratios and lift coefficients will be increased due to a higher pitching frequency. The operation at higher blade tip speed ratios will also reduce the chances of stall occurrence, as shown previously in figure 20 the maximum blade angle of attack will be decreased.

Experiments more specifically related to VAWT's conducted by Fujisawa and Shibuya[28] using Particle Image Velocimetry (PIV), showed that as a consequence of the dynamic stall, two sets of counter rotating vortices are detached from the airfoil at different intervals and then travel downstream growing in size. It was observed that the size of the rotating vortices increases as the tip speed ratio decreases.

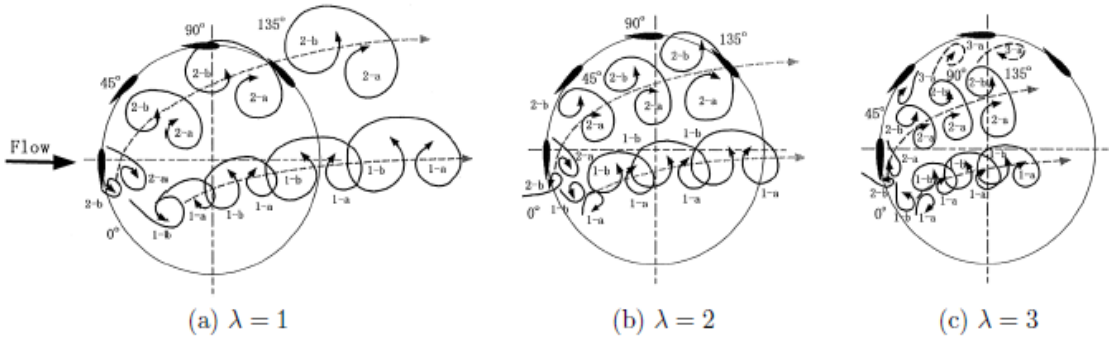

Figure 21: Illustration of dynamic stall.

Dynamic stall induces non-linear unsteady flow that is very difficult to predict. Not only is it a major contributor to variable loading and fatigue due to the sudden changes in lift forces, but it is also a major contribution to vibration and noise generation. For a small VAWT operating in a residential area this is a very important design characteristic.

Understanding dynamic stall is thus a key parameter in understanding the flow over a VAWT and designing a turbine for optimum aerodynamic efficiency. It has been shown that the dynamic

[28] Fujisawa N, Shibuya S; *Observations of dynamic stall on darrieus wind turbine blades*. Journal of Wind Engineering and industrial Aerodynamics, 2001, pg. 201-214.

pitching can have a positive influence on blade lift forces and efficiency; however avoiding dynamic stall is paramount in providing a turbine with lower blade force fluctuations and better understood and predictable air flow.

4.8 NOTES ON DESIGN:

Empirical methods based on Blade Element Momentum (BEM) theory and some known experimental phenomena such as static and dynamic stall are a good starting point in understanding the flow and assessing the main design drivers. A similar empirical method that incorporate interference factors, upstream and downstream wind velocity and accounts for blade tip speed losses will be discussed further in chapter 8.

BEM methods do have a distinct advantage; they simplify the problem and allow rapid assessment. Once a good understanding of flow phenomena is achieved forces can be generated and an estimate of average power over a cycle predicted. To obtain the maximum possible power interference effects must be minimised. To estimate interference the wake must be known and easily analysed over various blade angle of attacks and Reynolds numbers. With a good knowledge of stall effects turbines can be designed at a blade tip speed ratio to maximise lift and avoid stall phenomena.

This is the next focus of the study, to better understand flow phenomena of the blade using both computer generated numerical simulations with the program StarCCM+ and by performing experimental tests.

5. EXPERIMENTAL ANALYSIS

Experimental analysis was conducted at the ICAM wind tunnel and the CSTB Jules Verne wind tunnel. The ICAM wind tunnel is limited in size, capable of testing small foils individually, while the CSTB tunnel is capable of full scale testing.

Experimental testing is the best way to study the real flow phenomena experienced in a VAWT. However regarding full scale testing it is also the most expensive with a turbine being constructed and tested.

This section aims at describing the advantages and disadvantages of experimental analysis, its use in understanding blade aerodynamics and how its results can be used to make design decisions and combined with other forms of analysis to provide a useful prediction model.

A good understanding of flow over a turbine blade can be obtained by both small scale and large scale model testing. Various test methods and tools were used and aerodynamic flow although complex became more easily understood.

5.1 ICAM WIND TUNNEL:

Initial experiments were conducted in the ICAM wind tunnel in Nantes, France. Such a tunnel can test foils of 0.2m in span length at wind speeds of 20 m/s and 40m/s by using a 2 speed motor connected to a fan. Plans were underway to use a frequency convertor to better control the speed of the wind to have a wider range of Reynolds numbers tested. However this was not undertaken during the scope of this study.

The Wind tunnel is currently set up for teaching, and not for specific research purposes. Testing methods used were sufficient to understand some flow phenomena, but more accurate means of testing and analysis has been proposed for the future.

Figure 22:ICAM wind tunnel configuration.

5.2 MEASUREMENT TECHNIQUES AND SENSORS AVAILABLE:

The ICAM wind tunnel is a small wind tunnel designed for single blade testing. The measurement techniques, sensors available and hence resources at hand to understand and measure the real flow are contained herein.

5.2.1 Wall flow visualisation techniques.

The test area contains an approx. 0.5m long square Perspex section to visualise the flow over a blade. There are 5 potential measurement points above the tunnel to insert a measurement device inside the flow while the wind tunnel is in operation. These are shown in Figure 23

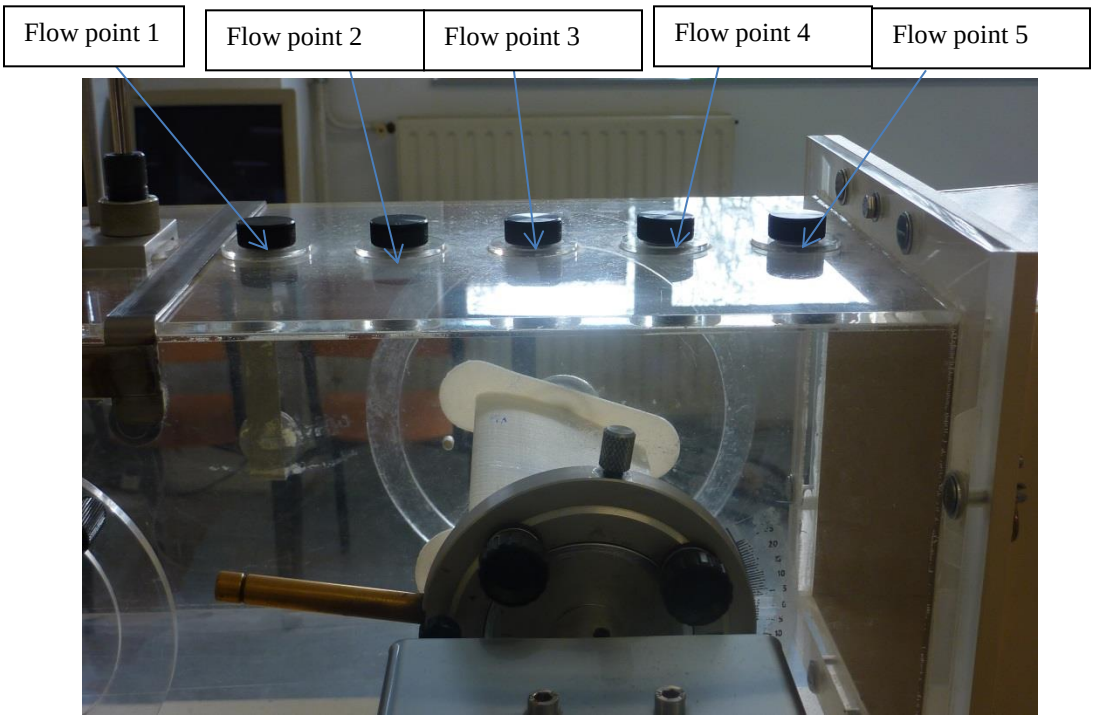

Figure 23: Flow test points.

The distance from the blade leading edge as a function of chord length at each flow point in Figure 23 is shown in the table below.

1	2	3	4	5
0.8c	0.2c (fwd.)	0.4c (aft)	TE	0.6c + c

Table 1: Distances of flow point measurements as a function of chord length.

Flow visualisation methods were used to study the nature of the flow (being lamina, turbulent or highly turbulent) and the direction of the flow at various blade pitch angles.

This is the simplest and less expensive method to understand the flow. By visualising it and placing something inside the flow and observing the results.

The following two methods were utilised to understand better the turbine flow characteristics, especially the turbine wake and turbulence regions.

- **String method**

It was proposed to use string on the low pressure side of a fixed turbine blade at various chord lengths along the blade to better understand the flow conditions. In particular flow direction and degree of turbulence.

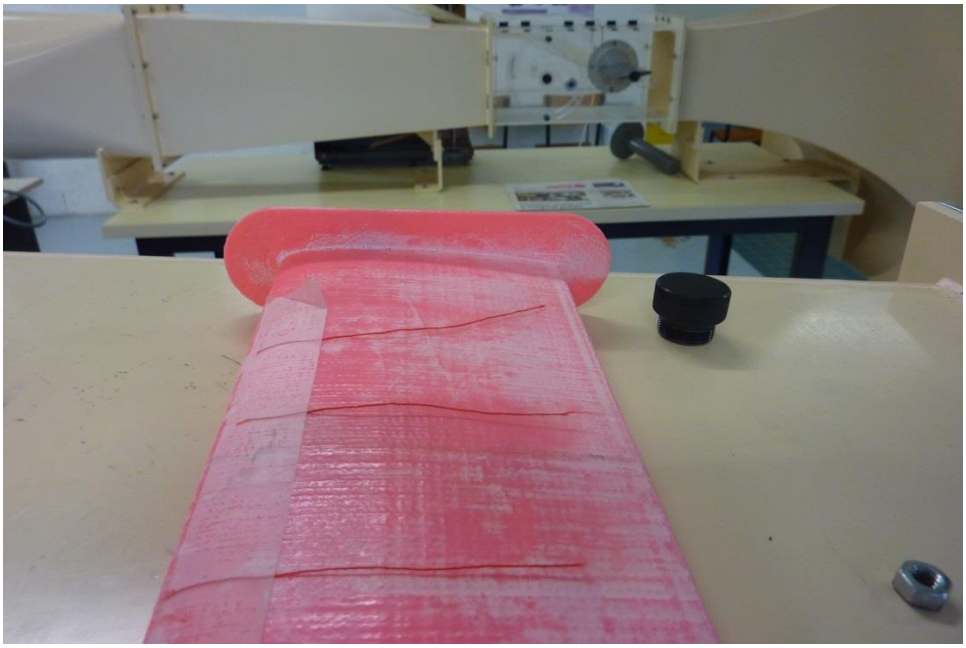

Figure 24: Example of string method at foil surface.

Also string was used on a steel rod at various horizontal and vertical distances from the foil for the same purpose; however a wider range of air space measurement could be achieved.

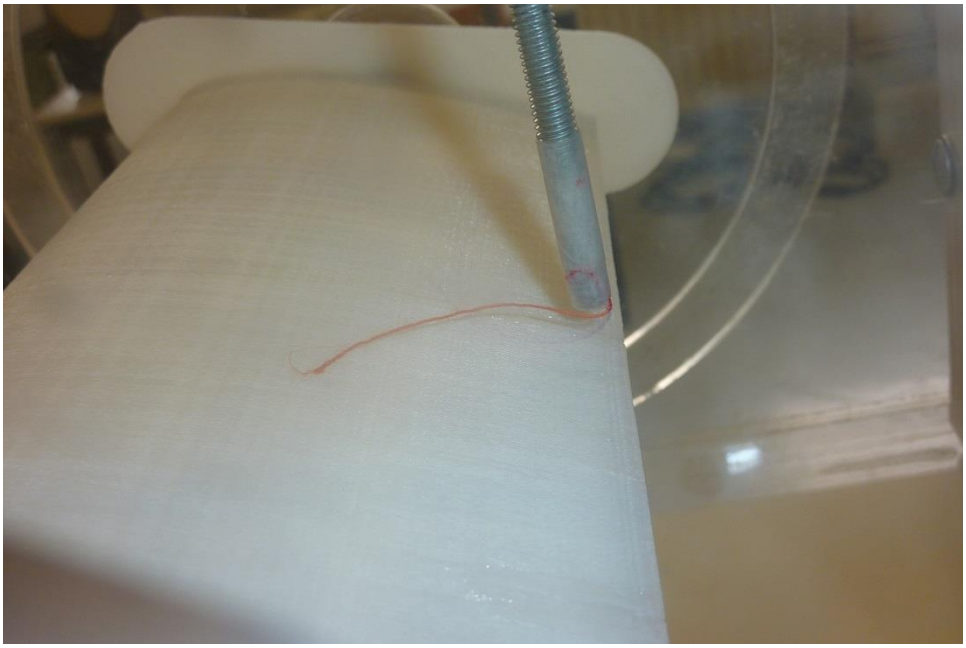

Figure 25: String method on a steel rod.

- **Ink droplets:**

Ink droplets were utilised over the blade low pressure surface to better understand the nature of the flow created at various angle of attacks along the blade.

Figure 26: Static ink droplet before the fan is started.

This was a very cheap and effective method in studying the flow over the surface of the blade.

5.2.2 Velocity measurements:

Hot-bulb anemometry

To better understand the speed of the flow a testo 490 manual hot-bulb anemometer was used at various horizontal and vertical distances from the foil. The anemometer is designed to measure wind speeds from 0.1m/s to 60 m/s. Such a device gave an indication of the velocity magnitude present in the wind at various points around the blade and at various angles of attack. Although it only measures speed and due to the unsteady flow present some measurements were an average of a range of fluctuating values, it did show some trends in flow behavior.

5.2.3 Aerodynamic forces

By varying the velocity and the angle of attack we can potentially model 1 entire revolution of a VAWT. However this only includes static effects and does not include dynamic effects.

The first experiment aim was to obtain lift and drag coefficients at various blade angles of attack using a load cell (strain gauge). The NACA 0012 & 2415 foils were utilised.

By the use of the load cell in a wind tunnel by varying the blade angle of attack and maintaining the same Reynolds number we can measure the lift and drag forces on the blade. From the lift and drag forces we can obtain the lift and drag coefficients.
This can be compared with CFD results and previous articles for validation.

Figure 27: Load cell and foil blade arrangement.

5.3 MODELS:

By using a 3D virtual printer and the extrusion process air foils were printed for use in the wind tunnel of a chord length of 0.1m with the material Acrylonitrile Butadiene Styrene (ABS). The NACA 0012 foil profile and the NACA 2415 profile were printed with good accuracy. Two foils of each were printed and a comparison was made between a rough blade and a smooth blade. The rough blade was very mildly sanded to remove major surface imperfections, and the smooth blade was sanded to a very fine tolerance.

Figure 28: ABS Rough blade.

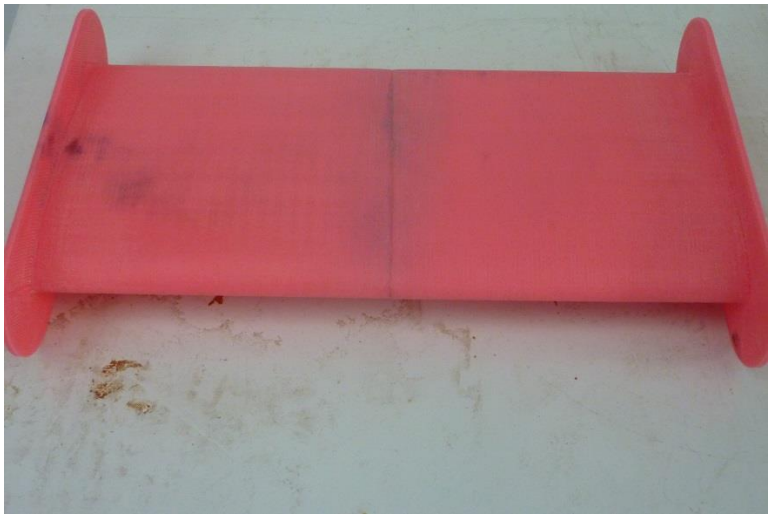

Figure 29: ABS smooth blade.

5.4 EXPERIMENTAL RESULTS AND ANALYSIS:

5.4.1 Flow visualisation:

The initial method for using string on the surface was considered not appropriate as it became difficult to accurately stick the string and keep the string on the blade due to the erratic flow behavior of the wind. The ink method used provided a good understanding of surface flow phenomena. The surface bubble was measured at each angle of attack present. Results are contained in table 2 and 3 and Figure 30 shows the length of the trailing edge bubble after flow is stopped.

Real time visual analysis of the flow over an airfoil can be easily seen using the ink droplets method. Depending on the angle of attack the ink will move quickly (often jump) from the leading edge aft when the wind is turned on. The distance that the droplet travels aft depends on the amount of reverse flow, which is dependent on the foil angle of attack. At an angle of 5 degrees angle of attack the bubble is stagnant at 1.5 cm from the trailing edge for the NACA 0012 foil and 2 cm for the NACA 2415 foil. This increases to 2 and 3 cm respectively for an increase in angle of attack to 10 degrees.

When the angle of attack is moved higher, and outside the static stall angle of attack for both blades, a completely different flow phenomena is present. Flow is erratic, it moves span wise and moves both towards the leading edge and aft to the trailing edge. It is non-linear, and appears very unpredictable.

For future use it would be interesting to compare the size of the ink bubble stagnation point at various angles of attack with a CFD Large Eddy Simulation (LES). More information on LES is contained in 7.5.

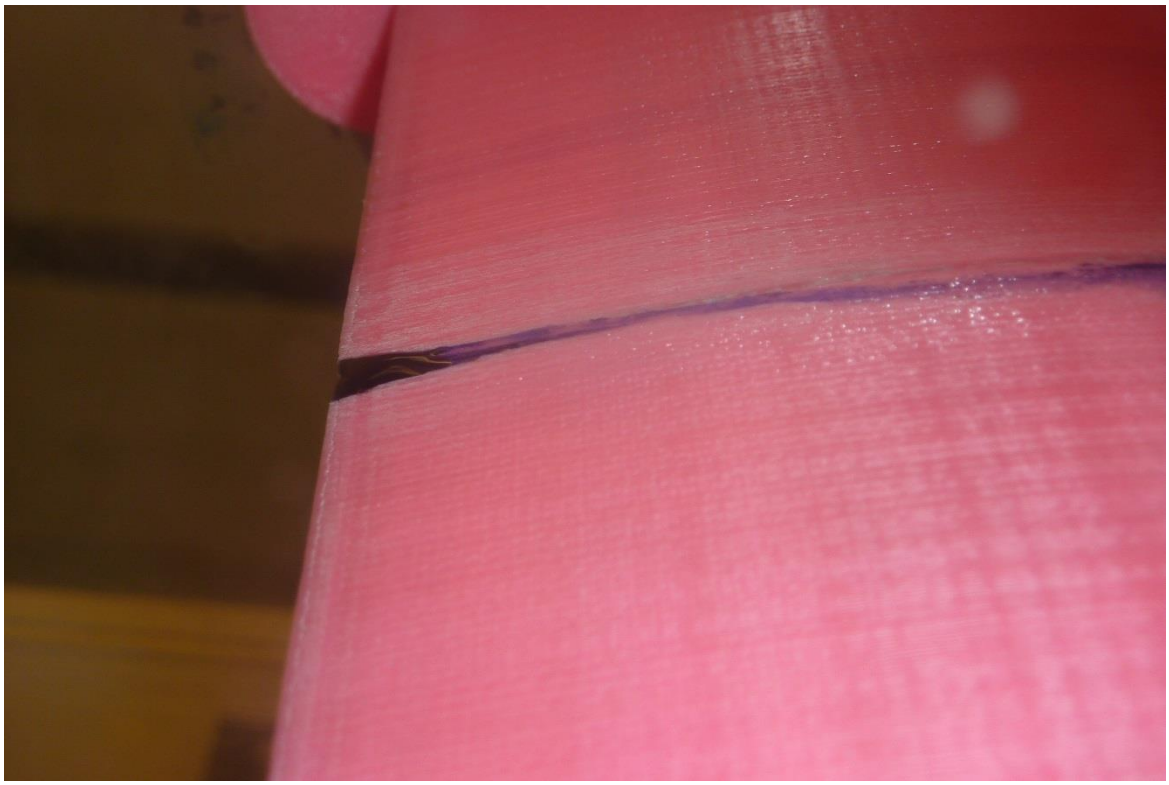

Figure 30: Ink bubble developed at the blade trailing edge of NACA 0012 air foil – 5 deg.

Angle of attack	Ink droplet observations:
5	Started at leading edge and jumped to trailing edge. Droplet is stagnant 1.5cm from trailing edge.
10	Started at leading edge and jumped to trailing edge. Droplet is longer at 2 cm length from trailing edge. Some ink fell over trailing edge.
15	Much slower to move aft, very erratic, jumped everywhere. Moved transversely to 5cm from centre.
20	Some of the droplet jumped aft, but also some has stayed at the leading edge. Movement is fwd. and aft, and right and left. Most of the droplet eventually moved to the trailing edge.

Table 2: Ink droplet results on the NACA 0012 smooth foil.

Angle of attack:	Ink droplet observations:
5	Even flow over blade. Ink gathered at trailing edge, 2cm left at trailing edge.
10	Jumped to leading edge. 3 cm on the leading edge.
15	Reverse flow: however not full reverse flow. Bubble moves to the trailing edge but slowly. Bubble moves transversely.
20	Reverse flow. Very erratic flow and messy. Bubble started at the trailing edge but moved towards the leading edge.

Table 3: Ink droplet results on the NACA 2415 smooth foil.

Using string on a metal rod was also tested over a range of blade angles and test points. Although interference effects may be present as you are placing a 0.5mm rod in front of the slipstream, it did identify regions of high turbulence and reverse flow.

The regions over the blade of high turbulence and reverse flow definitely increase as the blade angle of attack increases. A noticeable point is above the angle of stall of 13 degrees for the NACA 0012 blade and 17 degrees for the NACA 2415 blade. Above this point the entire section tested encountered some form of excessive string vibration or reverse flow. Indicating turbulence, unsteady flow and vortices present.

Detailed results are contained in Annex A. Such results could be further analysed to identify the size and length of the turbulent flow present at each angle of attack and compare this with a CFD LES simulation. However time further prevented this analysis.

One advantage of string is you can get an idea of the rotational flow in the blade slipstream in turbulent regions, and in linear regions the direction of flow.

5.4.2 Hot-bulb anemometry

Detailed results have been obtained of this method over a large spatial region around the blade. Unfortunately the results only give a velocity magnitude and not a direction. Time constraints prevented a detailed analysis of these results, but they are available in Annex A for assessment.
A common trend however was found in this method also. Above the static stall angle of attack flow velocity was much harder to measure, with erratic fluctuations.

5.4.3 Aerodynamic forces:

It must be said there are limitations by using a wind tunnel of such size that should be considered. Due to the size of the foil compared with the size of the tunnel area, as the foil is moved to higher angles of attack the foil causes a blockage of the flow through the tunnel. The Pitot tube differential pressure reading decreases and consequently the inlet flow velocity over the blade will decrease. By the use of a frequency converter in the future this problem could be rectified. It is assumed at this stage that such differences in velocity are negligible; however it should be noted when analysing results.
Also at higher angles of attack in particular there are interference effects between the walls of the wind tunnel that should be considered. When attempting the higher velocity of 40m/s this is particularly evident.
Below are the results of the lift coefficient vs blade angles of attack for the NACA0012 foil and the NACA 2415 foil. The NACA 0012 foil was tested at both smooth and rough foil surface types and compared with the article by Gerontakos[26] presented in Chapter 4 at the same Reynolds number of 1.35×10^5. The NACA 2415 was tested with just a smooth foil surface using an article by Ghods[29] of the University of British Columbia in 2001 with a Reynolds number of 3.3×10^5.

[29] Ghods M: *THEORY OF WINGS AND WIND TUNNEL TESTING OF A NACA 2415 AIRFOIL:* Technical Communication for Engineers, University of British Columbia, July 2001. http://www.ewp.rpi.edu/hartford/~ferraj7/ET/Other/References/Ghods2001.PDF; accessed Dec 14, 2013.

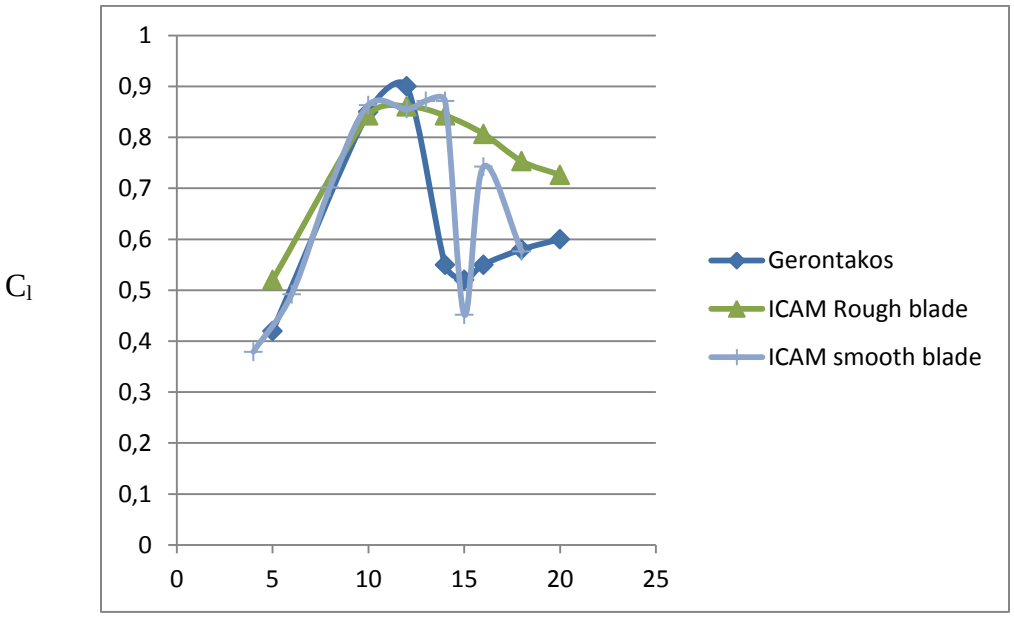

C_l

Angle of attack (Deg.)

Figure 31: Blade NACA 0012 Cl vs Blade angle of attack.

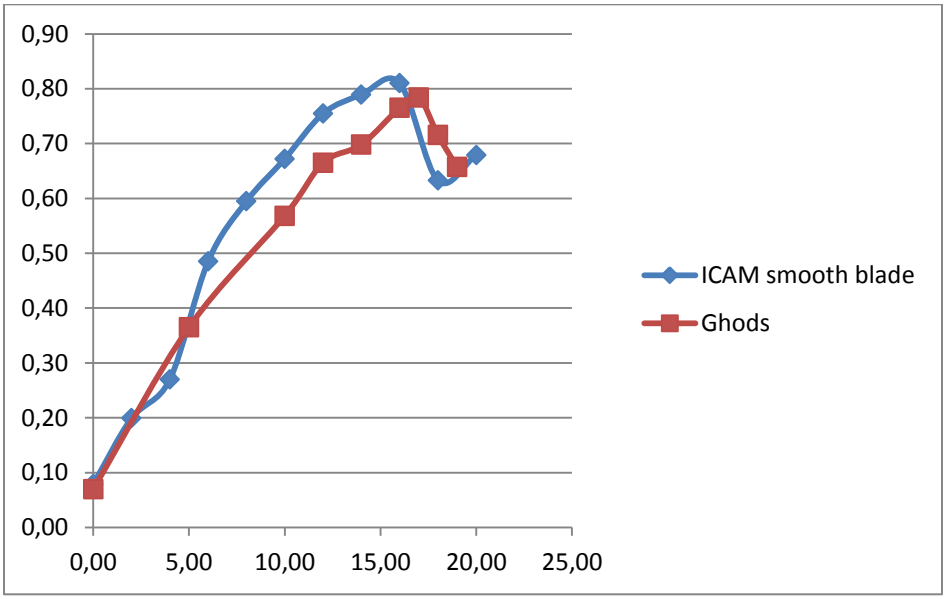

C_l

Angle of attack (Deg.)

Figure 32: Blade 2415 Cl vs Blade angle of attack.

Some observations of results include:

- The NACA 0012 smooth foil delayed the stall angle by 2 degrees.
- The NACA 0012 rough blade foil did not accurately estimate the lift coefficient in the stalled condition.

- In the stall condition it is most difficult to predict lift forces. The strain gauge readings were just read visually, and large fluctuations are noticeable.
- The NACA 2415 foil over predicted the lift coefficient by a factor of 10% however the stall angle was considered the same. It should be noted the difference in Reynolds numbers between the article ($3.3x10^5$) and the wind tunnel ($1.35x10^5$).

Measuring lift and drag coefficients in this way is a very effective way of obtaining blade foil force data, and comparing this with CFD simulations.

However there were some minor problems with the experimental set up that may have affected the results. At higher blade angle of attacks there is excessive vibration on the blades which affects the readings of the strain gauge. This vibration is caused by either flow blockage and interference, due to the size of the tunnel compared to the blade, the phenomena of stall, or a combination of both.

The strain gauge can also be coupled to a computer for a mean average reading; however for these simulations just a visual readout was obtained, which provides an extra margin of error.

5.5 FUTURE WORK:

In reality the VAWT has a constantly changing speed and angle of attack. It is proposed to alter the turbine blade angle of attack to resemble that of a VAWT in real time. This will better capture dynamic effects of the flow of the turbine blade.

Measuring instruments needed:

- Stepper motor for change of angle.
- Frequency convertor. (Change of motor speed to maintain the same wind velocity for various angles of attack).
- Hot wire anemometer and/or Particle Image velocimetry.

By using a stepper motor to change the angle of attack we can look at another design option, which is the possibility to change the blade pitch during a revolution, to optimise the torque for a complete revolution. This option adds another complexity in the need for a control system to alter the blade pitch, however allows far greater control of the lift forces and blade aerodynamics. By maintaining a constant blade angle of attack we can eliminate the effects of stall; which is created at angle of attacks were turbulent aerodynamics creates flow irregularities which are difficult to predict and understand.

By the use of a stepper motor we can monitor the energy lost by the stepper motor in changing the angle of attack and factor this value in the calculation of the total power coefficient.

Such a design option will be studied further in later chapters.

Examples of the use of a stepper motor in such experiments can be found in literature where flapping foil experiments are conducted to study the flow over helicopter rotor blades. A good example is in Lee & Gerontakos.[30]

It is also recommended to limit the testing speed between 0 and 30m/s as this will minimise interference effects experienced at high wind speeds. Otherwise a larger wind tunnel and larger motor and fan are necessary.

A more advanced method of measuring the flow is also proposed. As the blade will be dynamic to accurately capture flow field at various instants in time with accuracy and precision either hot wire anemometers or Particle Image Velocimetry is proposed.

[30] Gerontakos P, Lee T: *Investigation of flow over an oscillating airfoil;* Department of Mechanical Engineering, McGill University, Montreal, Canada. J. Fluid Mech. (2004), vol. 512, pp. 313–341. 2004 Cambridge University Press

6. CSTB WIND TUNNEL NANTES – FULL SCALE MODEL TESTING.

6.1 TEST 1: SEPT. 2012.

On the 13th and 14th of September 2012 the real scale model has been placed in the wind tunnel CTSB in Nantes. Below are some observations and results of the test as documented by Visonneau & Funck[31]. The wind turbine configuration with dimensions in the wind tunnel is contained in Figure 33 below.

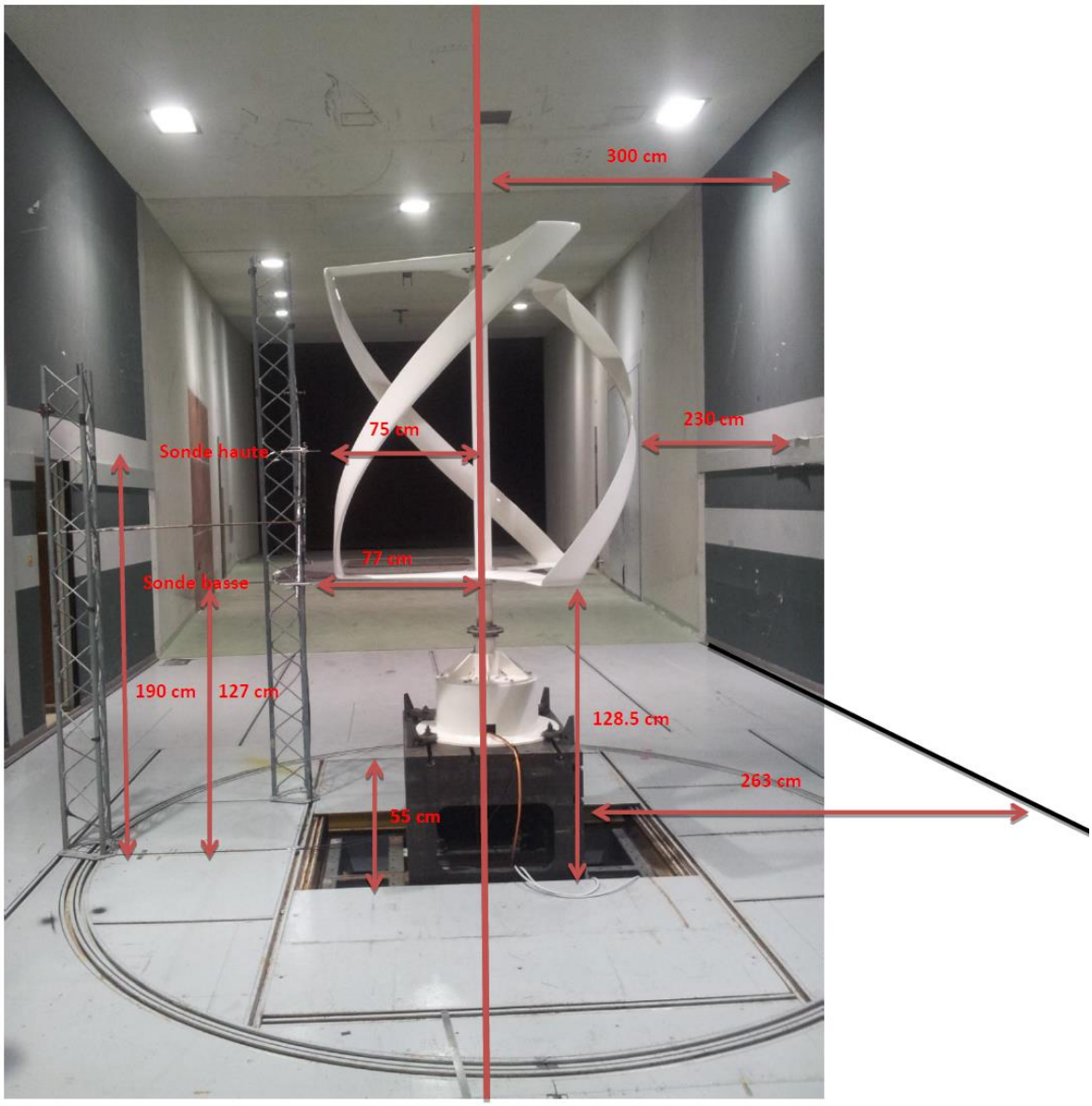

Figure 33: Wind tunnel configuration.

[31] Visonneau V, Funck J : Project Aérojoules – Rapport phase A1; ICAM, Rapport de mémoire Scientifique, 2013.

Testing was conducted at wind speeds of 5, 6, 7 & 10m/s. some observations of initial testing are contained below.

- Structural vibration is high; a fastening system was needed on top of the turbine above the shaft.
- Bending of the blades occurred, particularly at higher rpm.

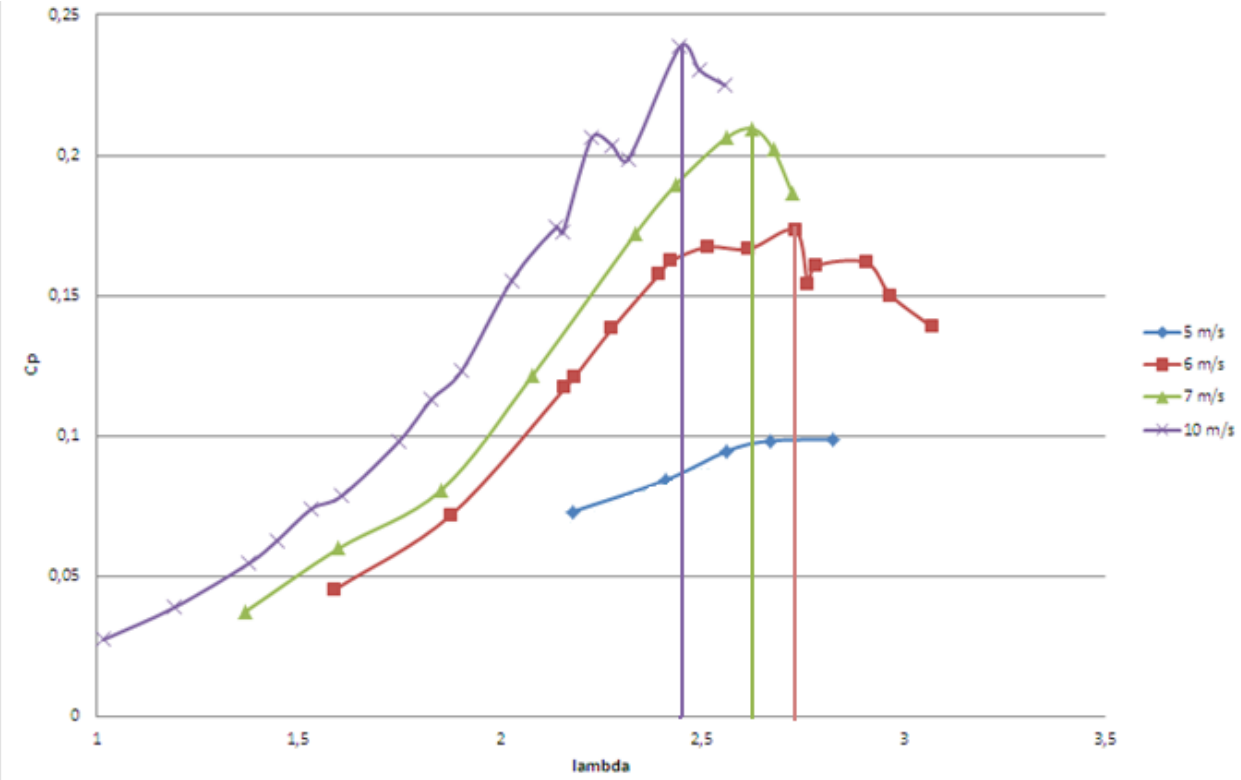

Figure 34: Wind tunnel test results- power coefficient vs blade tip speed ratio at various wind speeds.

- Higher power coefficients are obtained with higher wind speeds for the same blade tip speed ratio as shown in Figure 34 above.
- Optimum efficiencies depend on the wind speed – as the wind speed increases, the optimum blade tip speed ratio will decrease.
- Tests were undertaken only over a small range of blade tip speed ratios from 1 to 3.
- Power efficiencies were not as expected and the electrical power available was calculated in the order of 100W at 7m/s and 300W at 10m/s. This was considered below the goals of the project, and the next model was planned to have an increases swept area to aim for an electrical power output of 300W at 7m/s.

6.2 TEST 2: JAN 2014

Further full scale model tests were conducted on the 21st and 22nd of January 2014 in the wind tunnel CTSB in Nantes. This was on a modified design however, with a radius of 0.7m and an increase height of 2.4m. A photo of the model in the wind tunnel is contained in Figure 35.
What is noticeable is the use of a cable to attach the top shaft to a fixed point. This was due to excessive vibration of the free end of the shaft.

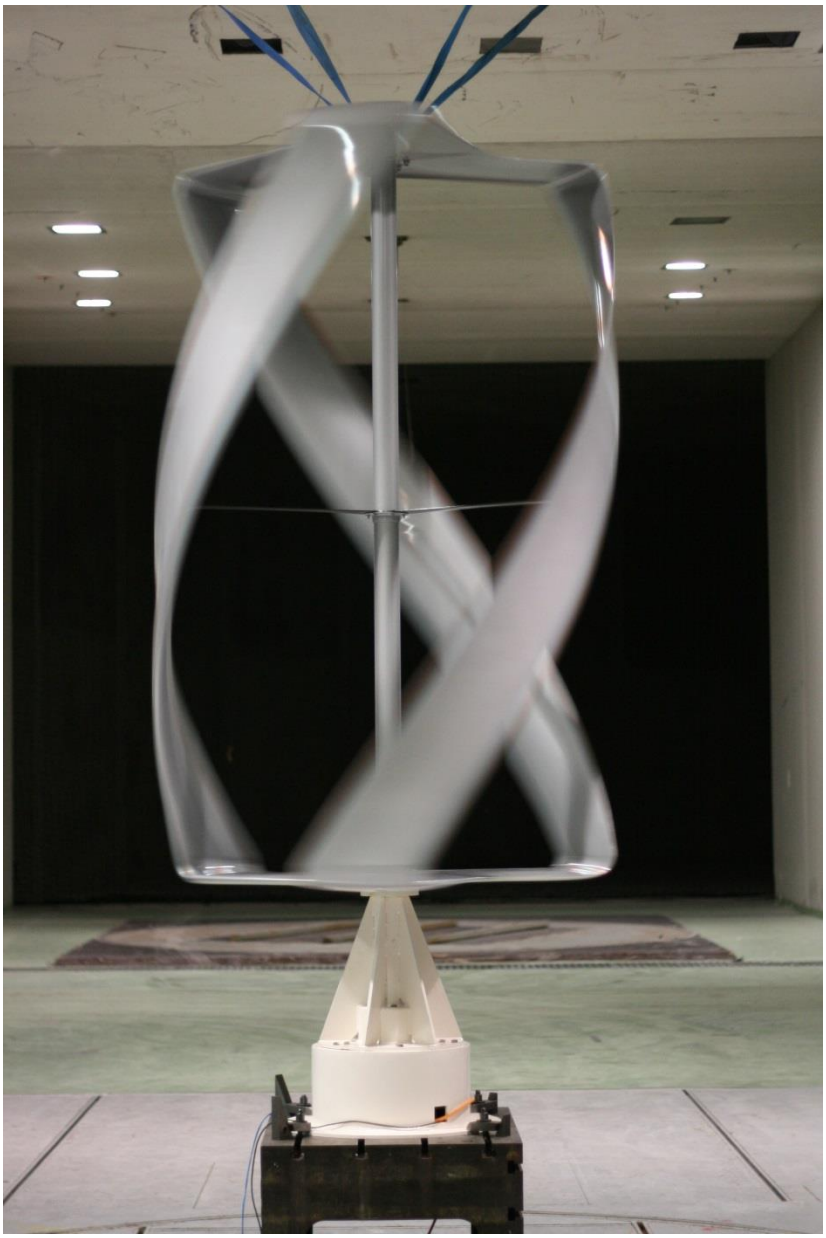

Figure 35: Model test 2, CSTB Wind Tunnel, Nantes.

Unfortunately model test results are not available for inclusion in this report, but when available it would be interesting to compare with the predicted QBlade results below. More description of the wind turbine performance software is contained in 8.2.

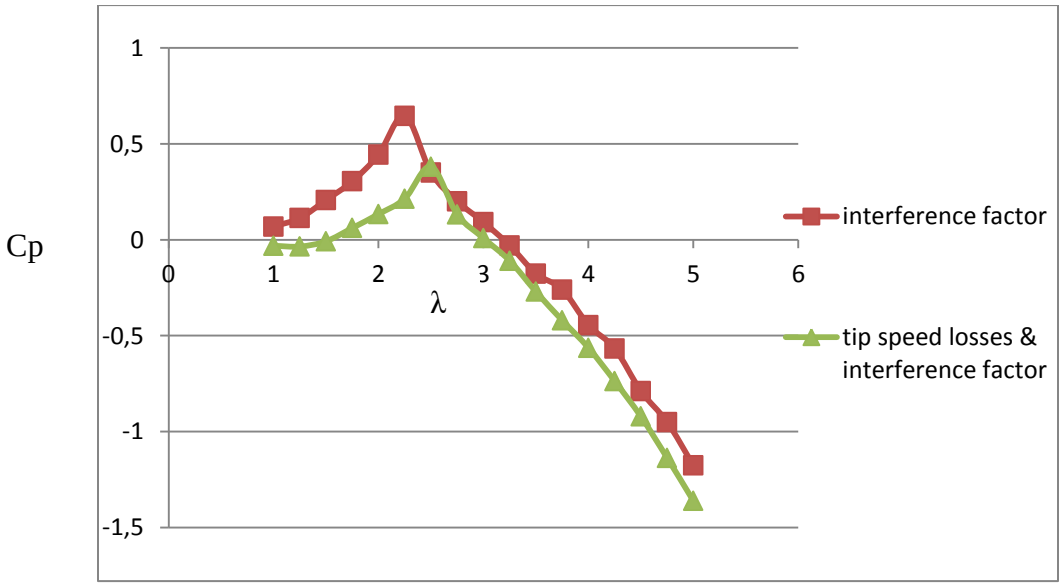

Figure 36: Q-blade predicted model test results.

7. COMPUTATIONAL FLUID DYNAMICS (CFD)

'The dawn of the twentieth century marked the beginning of the numerical solution of differential equations in mathematical physics and engineering'[32].CFD is the numerical simulation of a physical problem by the use of digital computers.[33]

7.1 BACKGROUND:

The ability of CFD to compute complex physical phenomena mathematically is an area of interest in the study of the flow over a vertical axis wind turbine. The mechanics of incompressible fluids is regulated by the Navier-Stokes equations. These equations dictate not position but velocity. It is the description of the velocity of the fluid at a given point in space and time. The equations are shown below:

7.2 NAVIER STOKES EQUATIONS

The Navier-Stokes equations can be formulated in three equations: continuity equations, the momentum balance equations and the energy balance equations

7.2.1 Continuity equations*:*

$$\frac{\partial \rho}{\partial t} + \underline{\nabla} \cdot (\rho \underline{v}) = S_m \qquad 5.1$$

The definition of the above terms from left to right includes:

- Time derivative of density
- Convection.
- Source – responsible for the production or destruction of mass.

7.2.2 Momentum Balance equations:

[32] Chung T, *Computational Fluid Dynamics*, Cambridge University Press 2002
[33] Le Touzé D; *An intro to Computational Fluid Dynamics*, 2013 EMSHIPS course notes, Ecole Centrale Nantes, France.

$$\frac{\partial(\rho \underline{v})}{\partial t}+\underline{\nabla}\cdot(\rho \underline{v}\underline{v})=-\underline{\nabla}p+\underline{\nabla}\cdot\left[\mu\left(\underline{\nabla}\underline{v}+\underline{\nabla}\underline{v}^{T}\right)-\frac{2}{3}\underline{\nabla}\cdot\underline{v}\underline{\underline{I}}\right]+\rho\underline{g}+\underline{F} \quad (5.2)$$

The definition of the above terms from left to right includes:

- Unsteady term – related to the time variation of momentum.
- Convection.
- Pressure gradient.
- Divergence of stress tensor – in relation to viscous effects.
- Gravity
- External forces.

7.2.3 Energy Balance Equations:

$$\frac{\partial \rho E}{\partial t}+\underline{\nabla}\cdot(\underline{v}(\rho E+p))=-\underline{\nabla}\cdot\left[\sum_{j}h_{j}J_{j}\right]+S_{h} \quad (5.3)$$

The definition of the above terms from left to right includes:

- Unsteady term
- Convection
- Generic diffusion term
- Source

For an incompressible flow these equations can be simplified into the equations below.

$$\frac{\partial u_i}{\partial x_i}=0 \quad (5.4)$$

Unsteadiness; Convection; Pressure effects; viscous effects; Volume forces (gravity)

$$\frac{\partial u_i}{\partial t}+u_k\frac{\partial u_i}{\partial x_k}=-\frac{1}{\rho}\frac{\partial p}{\partial x_i}+\nu\frac{\partial^2 u_i}{\partial x_k \partial x_k}+f_i \quad (5.5)$$

7.2.4 Navier stokes equations in CFD:

There are only few occasions when Navier stokes equations can be solved analytically, and due to the nature of the complex flow in a VAWT, the equations must be solved numerically.

As will be discussed further fluid flow over a body involves a combination of laminar and turbulent effects, and it is the turbulent effects which are often difficult to capture in a numerical CFD code. In particular within a reasonable computational time and amount of installed computer hardware.

The RANS (Reynolds Averaged Navier-Stokes) methodology is the most common CFD approach for engineering applications. It involves Navier-Stokes equations resolution and turbulence modeling giving reasonable CPU-requirements with complex flows. It consists of averaging the conservation equations over a sufficiently long time period in order to lose every turbulent fluctuation but keeping the time dependence of the averaged quantities. Initially the RANS method was used to simulate flow over a 3D foil.

In implementing a CFD analysis on an air foil various steps are necessary.

- Firstly a computer generated model must be designed and exported into a CFD program for analysis. The CFD program utilised is STARCCM+ and the 3D model has been generated in the CAD program SOLIDWORKS.
- Apply initial and boundary conditions to the physical problem.
- The domain must be discretised. Thus changed from the continuous domain to a discretised domain. The domain is divided into a grid and equations are solved at each grid point. Grid points are connected together by what is called a mesh. There are various methods of discretisation and the method of discretisation and type of mesh are strongly dependent.
- The finite volume method of discretisation is the most common for use over a turbine blade and will be used in this study using the CFD simulation program StarCCM+
- The resolution of the CFD simulation is obtained by an implicit linear system
- The number of grid points and size of the mesh is very important in finding a balance between solution accuracy and acceptable computer time and storage capacity. As the smaller the grid the greater the accuracy, but more computer time and space is needed. Thus the solution must converge to an acceptable level of tolerance within an acceptable time period.

What is of importance is the type of turbulence model used and the type or size of mesh used. These two parameters are interdependent and various combinations were trialed and validated with model tests to obtain the optimum balance of solution accuracy, time and computing power.

7.3 TURBULENCE MODELING:

Another complexity in the numerical simulation of fluid flow over a foil surface is turbulence. This area has been a subject of research for some time. Some early studies of turbulence modeling include work done by Launder & Spalding[34], Ferziger & Peric[35]& Wilcox[36].

The choice of a turbulence model is always a difficult problem. A list of the most commonly used turbulence models was provided by DeGennero[37]used in RANS simulations. They are contained in 19.2 and are ordered by categories according to computational effort.

Each model is a different method of solving the turbulence problem and some are coupled with near wall treatment. The wall function in StarCCM+ consists of the possibility to couple RANS simulations and turbulence models with a predetermined resolution of the boundary layer. Its use is very dependent on the size of mesh used and available computer power, as it is known that strong variations in temperature and velocity exist close to the boundary. To resolve such variations it often requires a very fine mesh and high computational power. To overcome this problem a standard shape for temperature and velocity can be given as a function of distance to the wall (linear in the laminar sub-layer and logarithmic in the turbulent boundary layer). By using a wall function it is possible to resolve the boundary layer with a low number of cells and reconstruct 'artificially' the wall stresses.

The previous simulation work at ICAM done by Bottero utilised the realizable k-epsilon model developed by the USA National Aeronautics & Space administration in 1994[38]. It incorporates mathematical constraints on the Reynolds stresses consistent with the physics of turbulent flows. This implies a better performance for flows with rotation, detachment & recirculation which is

[34] Launder B, Spalding D; *The numerical computation of turbulent flows: Computer methods in applied mechanics and Engineering*, Imperial College of Science & Technology, London, 1974.
[35] Ferziger J, Peric M*; Computational Methods of Fluid Dynamics*, 3rd edition, Springer, 2002.
[36] Wilcox D; *Turbulence modeling for CFD*, DCW Industries Inc, California, 2006.
[37] DeGennero M*; Computational Fluid Dynamics and Computational Aeroacoustics for Turbomachinery Applications with emphasis on High-Speed Propellers and Vertical Axis Wind Turbines*, Universita Degli Studi Di Napoli Federico II, 2010.
[38] Shih T, Liou W, Shabbir A, Yang Z, Zhu J*; A new k-epsilon eddy viscosity model for high Reynolds number turbulent flows: model development and validation. Computers & Fluids*, USA National Aeronautics & Space Administration, 1994. Pg. 227-238.

similar to the flow pattern of a VAWT. Also a 2 layer approach was implemented using all y+ wall treatment. Both these two models were unable to converge on a solution in 3D and did not accurately simulate the flow in 2D.

The Spalart-Allmaras model[39] which was utilised successfully in a 2D simulation by Ribeiro, Awruch & Gomes in 2011[40] is also available in StarCCM+. Its use previously however has been utilised for HAWT which has less complex flow than the VAWT.

The models used at ICAM using StarCCM+ and the RANS equations include the k-epsilon model and the Spalart-Allmaras model.

At the beginning of 2013 a research agreement has been reached with Dublin City University. So results could be compared with other CFD packages and turbulence models. Dublin City University uses the Fluent CFD software package. Two other turbulence models could be used in fluent and compared with the results obtained using StarCCM+. Some preliminary 2D modeling was conducted by Mr. David Baillergeau[41] of ICAM and compared with Dublin City University results. An overview of the various turbulence models used and some observations is contained in 19.3.

However using CFD over a VAWT rotating blade is an area of particular interest and further analysis in the research community is needed due to its complex nature. 'Some of the most complex and least understood phenomena in the field of Computational Fluid Dynamics (CFD) are associated with the description of the flow past rotating blades'.[42]

CFD is very powerful in optimising a design, as rapid simulations can be undertaken without the need for model testing or full scale testing for verification each time a small design change is implemented. However due to the complex nature of the flow accuracy is very important and a CFD simulation must be reliable and accurate. One must note that complex flow simulations are challenging and error prone and it takes a lot of engineering expertise to obtain validated solutions.[43]

The initial aim of the CFD simulations and model testing of an air foil was to obtain an accurate CFD RANS model of estimating the aerodynamic flow over the turbine blade. Once confidence

[39] Spalart P, Allmaras S; *A one-equation turbulence model for aerodynamic flows*, AIAA Paper 92-0439.
[40] Ribeiro A, Awruch A, Gomes H: *An airfoil optimization technique for wind turbines*, Graduate Program in Mechanical Engineering, Federal University of Rio Grande do Sul, Brazil. SciVerse, science direct, 30 Dec 2011.
[41] Baillergeau D; *Vertical Axis Wind Turbines: Aérojoules project*. ICAM, Nantes, France, 04/07/2013.
[42] Paraschivoiu I, *Wind Turbine Design – With Emphasis on Darrieus Concept*, Presses internationals Polytechnique, Québec, Canada,2009. Pg. 35
[43] Chung T, *Computational Fluid Dynamics*, Cambridge University Press 2002

is obtained in the CFD methodology then the 3 bladed VAWT can be simulated and multiple simulations can be achieved with an eye to optimising the VAWT design. This will allow accurate prediction of turbine design loads and aerodynamic efficiency. It will also allow a better understanding of the turbine wake and interference effects can be understood. This is important when assessing viable options for use of the turbine.

However as will be discussed further the RANS method of simulating the complex flow was found to be not appropriate for VAWT's and more complex numerical simulation methods were needed.

7.4 INITIAL SIMULATIONS:

Due to the complex nature of the flow over a VAWT, a 2D model cannot accurately reflect the flow over a turbine blade. This was particularly shown by Kitsios[44] as in the regions outside the uncontrolled stall angle of attack, 2D CFD models illustrate poor agreement with experimental measurements and a 3D simulation is needed. As the designed VAWT blade will pass through the uncontrolled stall angle of attack during a cycle, it was decided to directly attempt to simulate the flow using a 3 Dimensional model.

As known articles are available for the NACA 0012 foil, this was the initial foil used to model a simple 3D static flow over the foil.

It is recognised that the real flow is not static, but dynamic. However as this was the first attempt in the project to successfully model a 3d simulation, it was desired to start with a simple static foil, with known data for validation. This will allow various CFD models to be tested and validated with articles and also model tests in the ICAM wind tunnel.

7.4.1 Geometry:

In running a CFD simulation and especially in 3 dimensions it is very important to accurately define the geometry. The geometry will define the simulation space assessed. Too large a geometry may waste simulation time and create an unnecessarily large file; while too small geometry may not accurately assess the total flow over a foil and exclude important information, particularly defining the blade wake.

[44] V. Kitsios, R. k. Numerical simulation of lift enhancement on a NACA airfoil using ZNMF jets. *Center forTurbulence Research proceedings of the summer program*, 2006.

Kitsios[47] provided some useful information defining the minimum necessary geometry needed to accurately assess the entire flow over a foil blade. Importantly he included some minimum span requirements to contain an accurate representation of the flow, using an extruded blade.

His initial recommendations included LC –LN- LZ = 28c -6c - 1c. In the span wise direction due to the complexity of the flow he concluded that 1c was too small, and recommended a minimum value of 2c be used in this direction to accurately predict the lift coefficient.

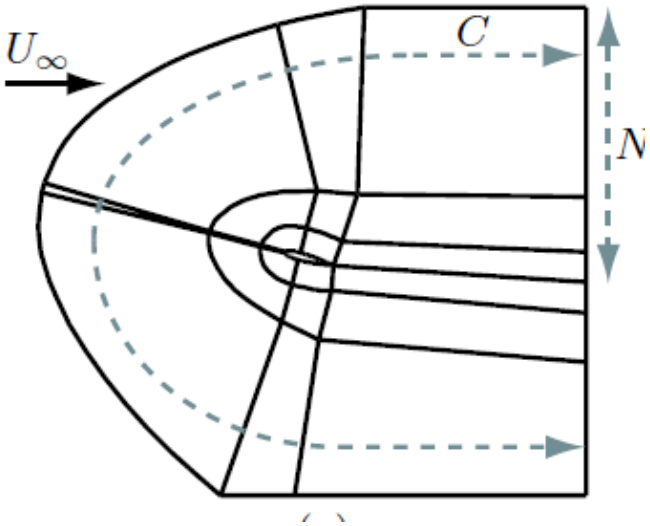

Figure 37: Kitsios recommended geometry for assessing flow over an airfoil.

For simplicity an extruded blade was initially used to assess the flow.

Initially to be able to accurately compare with known articles and the test blade in the ICAM wind tunnel a NACA 0012 blade was used, with a chord length of 0.1m.

Using a wind speed of 20m/s this also accurately reflected a common Reynolds number for assessment of 1.35×10^5.

The geometry modelled is shown in figure 38.

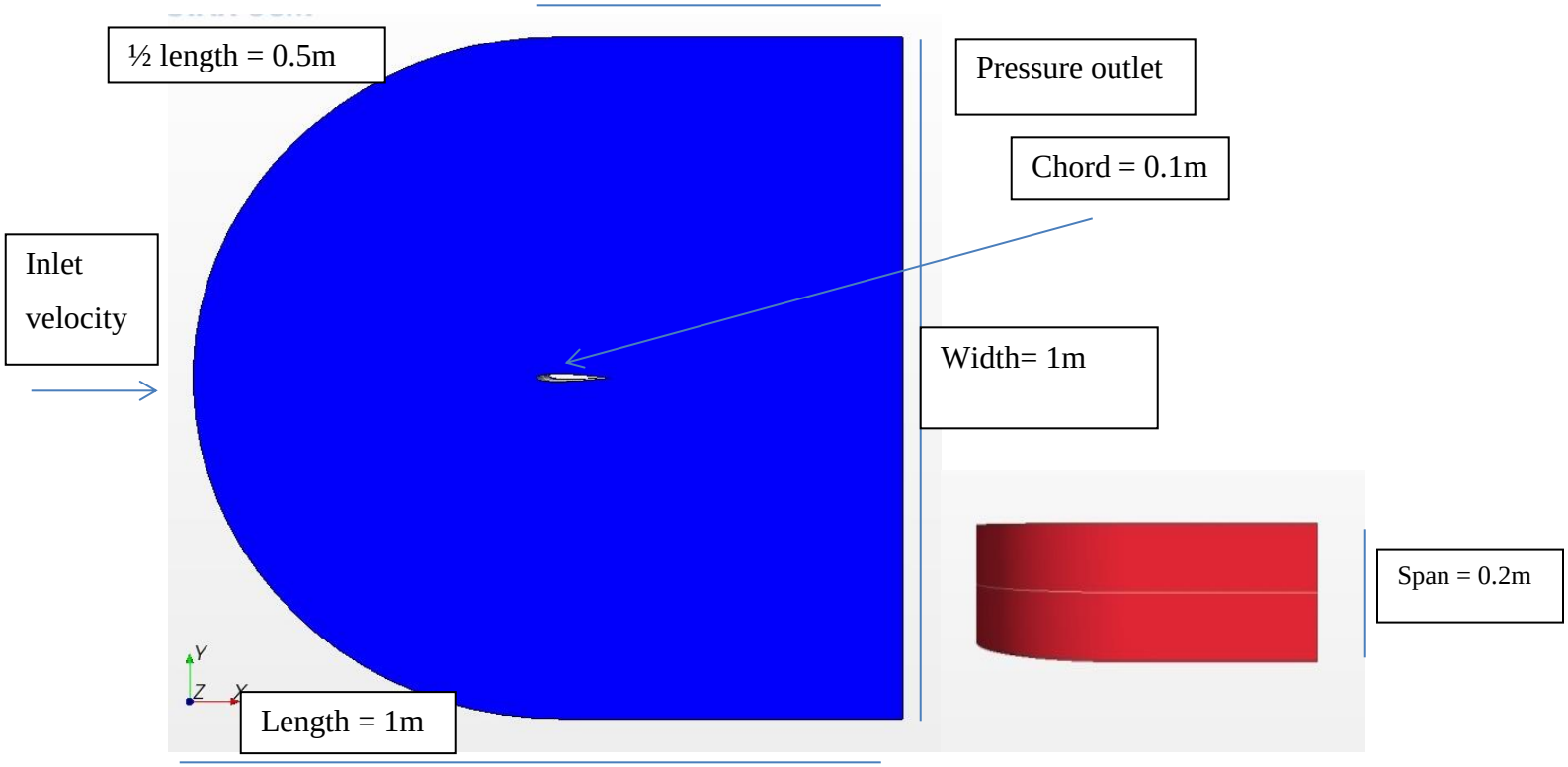

Figure 38: Initial geometry of NACA 0012 simulation.

7.4.2 Boundary Conditions:

Once the geometry of the above has been defined boundary conditions must be applied to each surface. Firstly in StarCCM+ the surfaces must be converted into regions to accurately define each boundary. The important regions include the inlet velocity region, which can be specified at an angle and speed relative to the model reference frame. The inlet velocity surface is shown in the figure 38 above.

The foil is defined as a wall boundary, and in the initial simulations a stationary wall boundary.

The pressure outlet boundary is defined behind the blade trailing edge and all other surfaces are defined as symmetrical planes.

7.4.3 Mesh

Once the geometry and boundary conditions have been defined the domain must be discretised. Thus changed from the continuous domain to a discretised domain. The domain is divided into a grid and equations are solved at each grid point. Grid points are connected together by what is called a mesh. The finite volume method of discretisation is the most common for use over a turbine blade and will be used in this study using the CFD simulation program StarCCM+.

The volume mesh in a simulation is the mathematical description of the space (geometry) of the problem being solved. It is constructed of the following mesh entities:

- Vertices
- Faces
- cells

The number of grid points and size of the mesh is very important in finding a balance between solution accuracy and acceptable computer time and storage capacity. As the smaller the grid the greater the accuracy, but more computer time and space is needed. Thus the solution must converge to an acceptable level of tolerance within an acceptable time period.

Using STARCCM+ the advanced layer mesher was used to create a mesh and also the surface remesher model. These two models where considered appropriate to mesh the complex geometry and provide assessment points for the complex flow created by the use of an aero foil.

The most important areas to assess the flow are the regions close to the foil surface. Using the advanced layer mesher we can define a prism layer closer to the foil surface; which is a layer of prismatic cells around the surface of the foil region and then the remainder of the flow region can be defined with polyhedral cells.

The mesher first generates a polygonal surface mesh and then advances this mesh into the region volume to form cell layers. Some advantages of this approach are a conformal match on either side of the foil and the ability to perform thicker and more uniform cell layers.

The prismatic cell layers help capture the boundary layer and in particular turbulence effects near wall boundaries.

In using the advanced layer mesher it is very important to accurately define the meshing properties suitable to the application. This is sometimes a trial and error process but the importance of a suitable mesh for the application to obtain solution accuracy & convergence of the navier stokes equations in an acceptable time is paramount.

Some important initial parameters for determining mesh size are contained below:

- It was considered important to accurately define the number of prism layers, the prism layer thickness, prism layer stretching, prism layer surface size(absolute) and absolute surface size to obtain an accurate transition from the prism layer to the polyhedral cell region.

- Also by using the surface curvature function the size of the cells around the curved section can be more easily controlled.
- Areas of concern where meshing a foil include the transition from prism layer to polyhedral cell region, blade trailing edge, blade leading edge and y+ value.

Some basic guidance on parameters to adjust for each area is contained below:

Transition from prism layer to polyhedral cell: prism layer stretching, prism layer thickness, number of prism layers and absolute maximum and minimum size of prism layer cells & absolute Maximum and Minimum surface size.

Blade trailing edge: To minimise the size of the x+ in this region, it is important to define a Minimum & Maximum value of the surface size on the prism layer. This will avoid long narrow cells. A section view of the blade trailing edge mesh configuration is contained Figure 39.

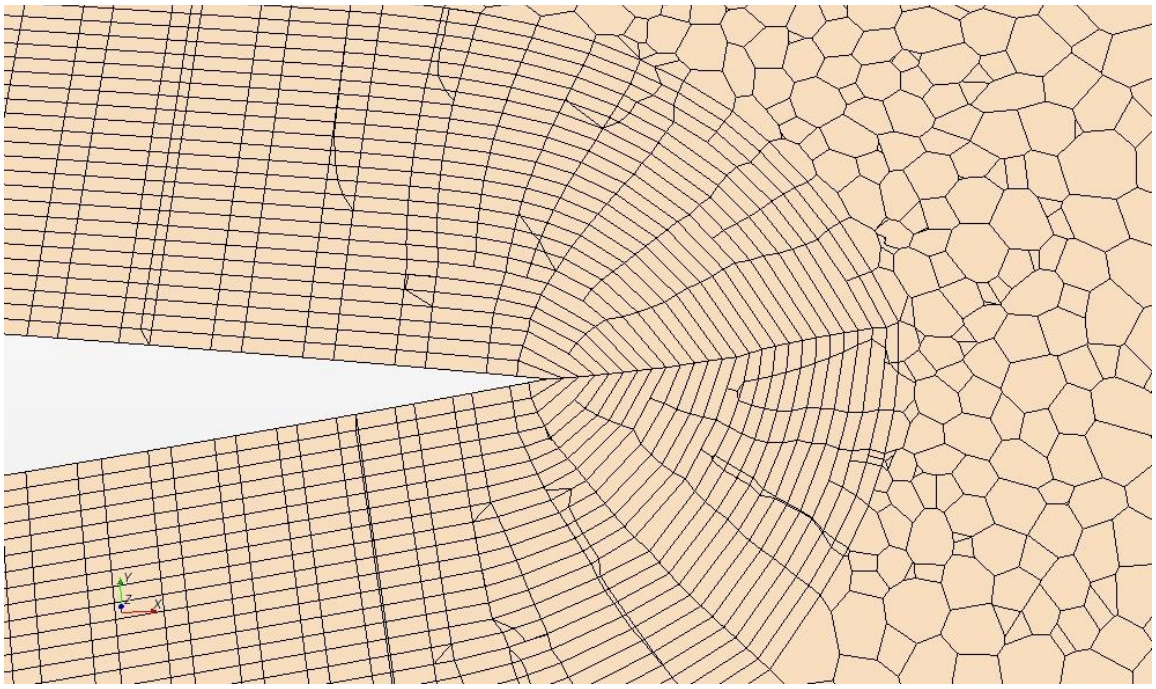

Figure 39: Blade trailing edge mesh

Blade leading edge: To accurately model the surface curvature the surface curvature function must be used to define the number of surface points on the curved face. A section of the blade leading edge mesh is shown in Figure 40.

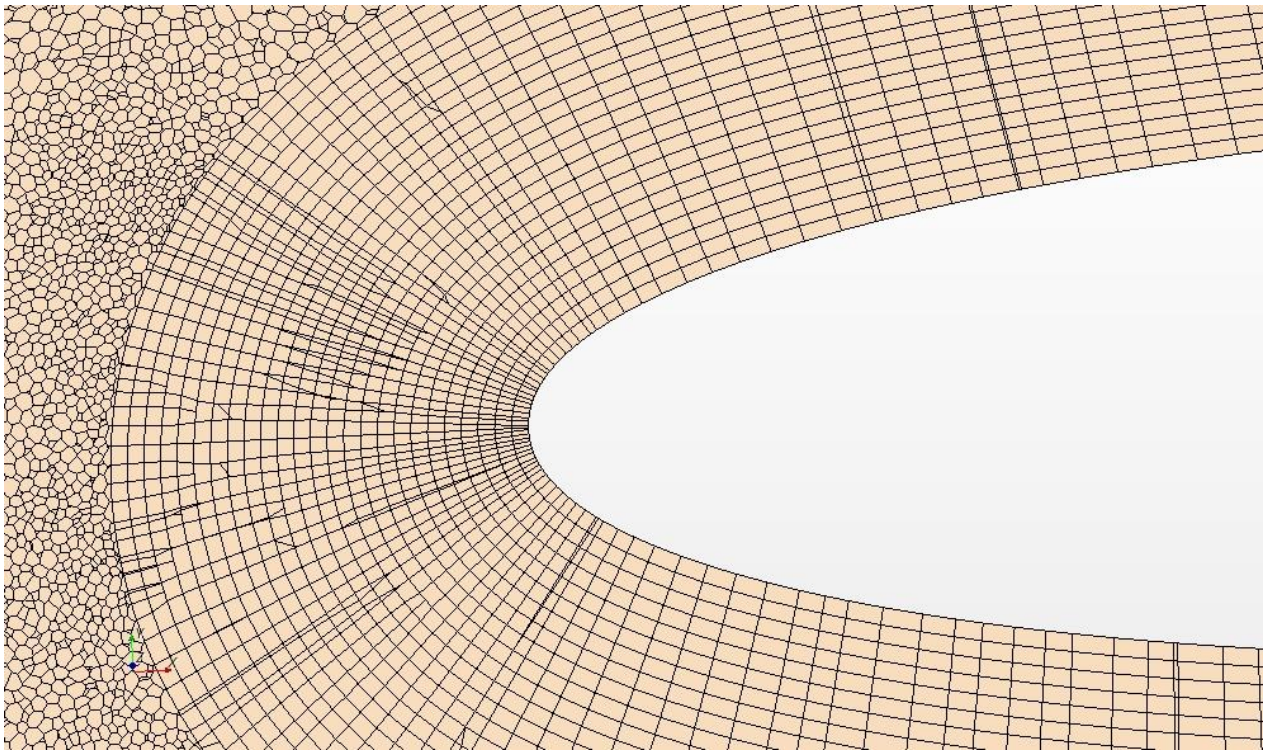

Figure 40: Blade leading edge mesh.

To obtain an optimum mesh it was a trial and error process in which several mesh arrangements were created and a simulation was run. Initially to save time a steady simulation was conducted to determine if convergence could be generated. By using a steady simulation and obtaining convergence was a good indication that the mesh parameters were close to optimal.

Some initial mesh values were based on previous studies and experience in ICAM modelling the same geometry and in particular knowledge from Mr. Jean-François Largeau. Also the article previously referenced from Kitsios provided some guidance on mesh sizing. For instance the cell spacing along the airfoil was recommended to be $\Delta C/c=1.875x10^{-4}$ to a maximum of 9.6×10^{3}. Normal to the airfoil and in the span wise (y+) direction are $\Delta N/c=1.2x10^{3}$ & $\Delta Z/c=5x10^{-2}$.

Some initial mesh dimensions trialed in various simulations are shown in the Table 4.

mesh details	1	2	3	4	5
base value (m)	0,1	0,05	0,05		0,05
number of prism layers	25	25	30	25	25
prism layer stretching	1	1	1,1	1	1
prism layer thickness (m)	0,04	0,035	0,03	0,085	0,009
surface curvature (pts./circle)	100	100	100	100	100
curvature deviation	200	200	200	200	200
curvature deviation distance (m)	0,01	0,01	0,01	0,01	0,01
surface growth rate	1,3	1,3	1,3	1,3	1,3
surface proximity (points in gap)	2	2	2	2	2
absolute surface size					
min. (m)	0,025	0,001	0,001	0,001	0,001
Max. (m)	0,1	0,1	0,1	0,1	0,05
Regions					
faces: min. (m)	0,0005	0,001	0,001	0,001	0,0001
Max. (m)	0,005	0,005	0,005	0,005	0,001

Table 4: Initial mesh values trialed in simulations.

For such a study a span of 0.1m was used to reduce the size and computation time. Accuracy was not the primary purpose of such a study, but solution convergence and time for convergence. The initial mesh used in the convergence study is shown in Figure 41.

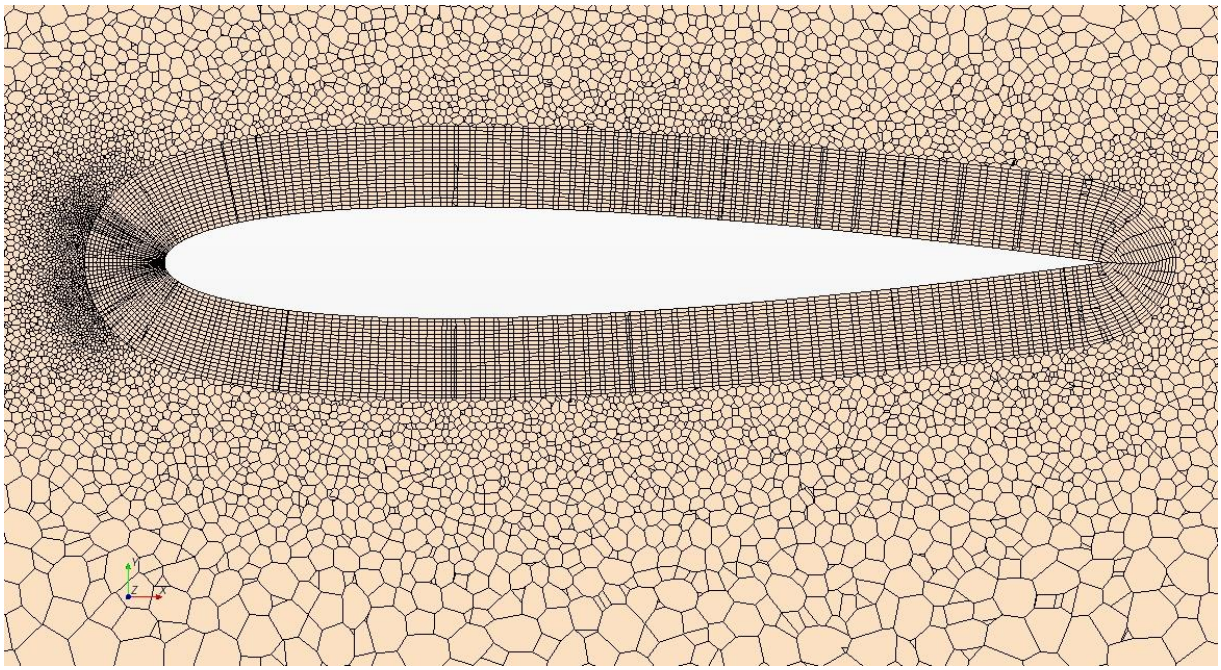

Base size: 0.05m
Number of prism layer: 25
Prism layer stretching: 1
Prism layer thickness: 0.009m

Absolute surface size:
Min:0.001m
Max:0.05m

Prism layer surface size:
Min: 0.0001m
Max: 0.001m

Figure 41: Initial mesh around a NACA 0012 foil.

7.4.4 Steady simulation:

A steady simulation was initially calculated as it is quicker and easier to quickly assess the convergence of various mesh and turbulence models. This was undertaken comparing the Spalart-Allmaras and the k-epsilon turbulence models.

The best turbulence model between the standard Spalart-Allmaras, k-epsilon and the Spalart-Allmaras High Reynolds number for the same mesh for convergence was found to be the High Reynolds Spalart-Allmaras model; for a steady flow simulation. Convergence was reached across all 3 angles and with a quicker convergence time.

It should be noted convergence was considered met when all the residuals were below a value of $1x10^{-4}$. A Reynolds number of $1.35x10^{5}$ was used to easily compare with articles and ICAM wind tunnel results.

Results are shown in Table 5.

RANS/LES	RANS	RANS	RANS	RANS	RANS	RANS	RANS	RANS	RANS	RANS
Turbulence model	SA (Stan.)	SA (Stan.)	SA (Stan.)	SA (Stan.)	k-e	k-e	k-e	k-e	SA(HR)	SA(HR)
steady/unsteady	steady	steady	steady	steady	steady	steady	steady	steady	steady	steady
Angle (Deg.)	0	5	10	15	0	5	10	15	10	15
Convergence	yes	yes	no	no	yes	yes	yes	no	yes	yes
Y+ value	30	30	30	30	30	30	30	30	30	30
Mesh type	1	1	2	2	2	2	2	2	2	2
Time (iterations)	200	600	1000 runs	1000 runs	300	650	800	1000 runs	500	600

Table 5: Initial mesh convergence study.

It was then proposed to use the high Reynolds number Spalart-Allmaras turbulence model in further implicit simulations.

7.4.5 Unsteady simulation:

When setting up an implicit linear system an important parameter is the time step. This is the time between numerical calculations. If the value is too large the simulation will not capture all flow properties and if it's too small then the solution will take too long to converge. Thus a balance needs to be made between number of iterations and time step.

It was also found that the maximum number of inner iterations was an important parameter. If value is too low, the solution does not converge within a time step, if it's too high the solution takes a long time to complete.

It was recommended by StarCCM+ to have a courant number less than 1; for decreased oscillations, improved accuracy and decreased numerical dispersion. The courant number is dependent on the x+ value, velocity and the time step. A maximum courant number of 1.6 along the blade was achieved, with the majority of the cells giving a courant number below 1.

Some further analysis of the lift and drag coefficients using the Spalart-Allmaras turbulence model in a linear system is contained in Table 6.

Steady/unsteady	unsteady	unsteady	unsteady	unsteady
Turbulence model	Spalart - Allmaras	Spalart- Allmaras	Spalart - Allmaras	Spalart - Allmaras
Angle (Deg)	5	10	15	20
Cd	-0,0504	-0,1479	-0,183	-0,04
Cl	0,647	1	1,05	0,8329
Lift (N)	1,532	2,38	2,5	1,9724
Drag (N)	-0,119	-0,35	-0,43	-0,095
Time	1 hr.	3hrs	3 hrs.	5-6hrs

Table 6: RANS Spalart-Allmaras simulation results.

It was noted that lift coefficients were some 20% higher than the articled results. This was using a wall function and a y+ of approx. 30. Attempts were made to run a simulation with a much smaller y+ value of 1 and using no wall function. The mesh is shown in Figure 42.

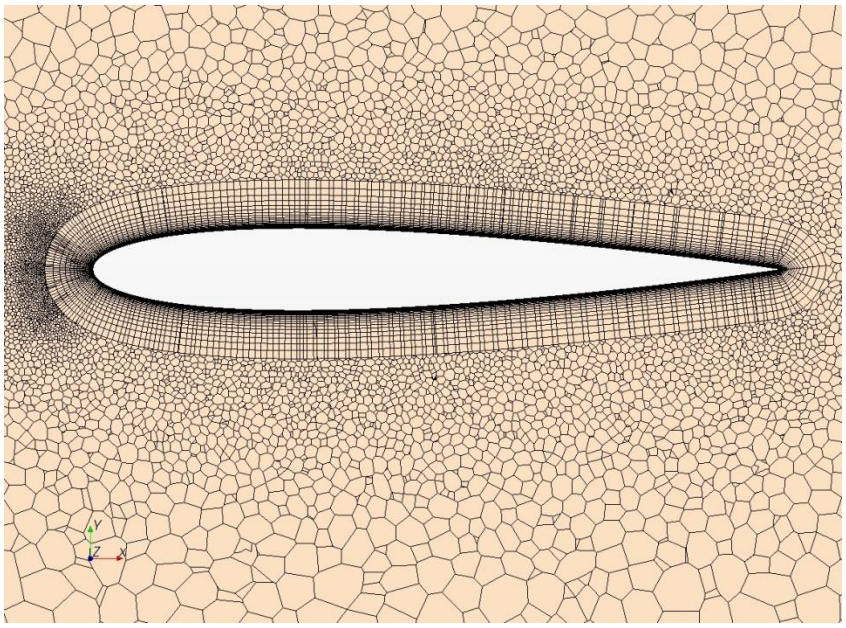

Figure 42: Mesh with a y+ of 1

For such a mesh convergence became difficult with a floating point exception occurring often.

It soon became apparent however that a RANS simulation is not appropriate for the purpose of simulating flow around a VAWT.

As explained earlier in the theory section of VAWT's it is very important to understand the flow over a VAWT to predict possible interference effects. As multiple turbine blades will be passing the wake created by the previous blade and also each blade will pass the free stream twice. Thus understanding the velocity and the direction of the flow over an airfoil in a CFD simulation is very important. This is an area of weakness of the RANS equations. As shown by results and supported by theory the RANS equations do not provide an accurate representation of the velocity vector over a turbine blade; particularly in the wake and turbulent regions. This is shown by the velocity vectors shown below in Figure 43.

As the real flow over a turbine blade will have circular eddy viscosity vectors, these need to be simulated more accurately to obtain a better representation of the real flow over a turbine.

This led to further investigations using a Large Eddy Simulation.

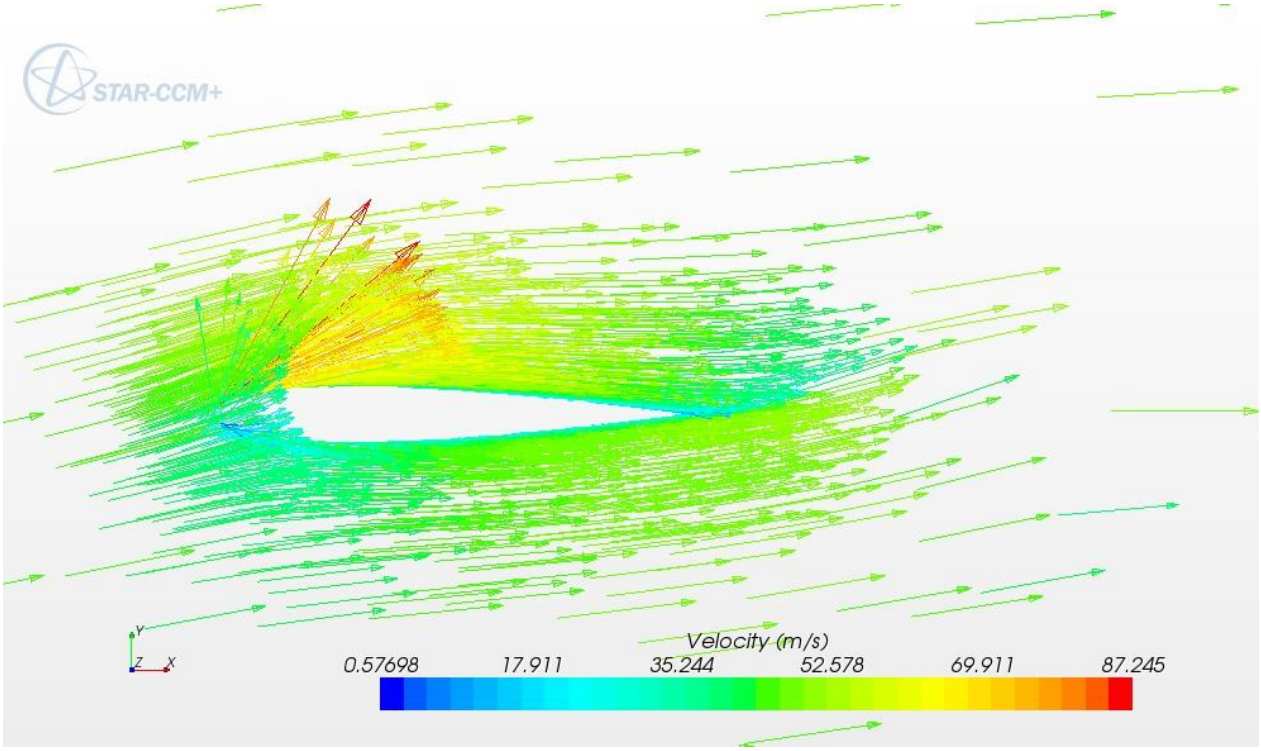

Figure 43: RANS Spalart-Allmaras NACA 0012 20 degree vector diagram.

7.5 LARGE EDDY SIMULATION

RANS equations fail to distinguish between large and small eddies. They only resolve the mean flow and provide an average of turbulent fluctuations.

Turbulence flow is known to be both 3 dimensional and rotational. Such rotational flow or swirling is often termed ‘eddies’ and can be broken down into two types. Smaller eddies and larger eddies.

The larger eddies interact and extract energy from the mean flow, are anisotropic and their behavior is determined by the geometry of the problem domain, the boundary conditions and the body forces. While smaller eddies are nearly isotropic and found have a more predictable behavior. However such behavior is more predictable at higher Reynolds numbers which will be discussed further.

A different method for the simulation of such turbulent flow accepts that the larger eddies need to be computed for each problem with a time-dependent simulation, while the smaller eddies can be simulated with a compact model. This is the essence of the Large Eddy Simulation (LES) approach to the numerical treatment of turbulence.

Instead of time averaging (RANS), LES uses a spatial filtering operation to separate the larger and smaller eddies. The method starts with the selection of filtering function and predetermined cutoff width with the aim of resolving in an unsteady flow computation all those eddies with a length scale greater than the cutoff width.

The disadvantage of LES compared with RANS is the computational expense, which although less than direct numerical simulation, is still excessive.

The equations that are solved for large eddy simulation are obtained by a filtering rather than an averaging process. The filtered equations may be rearranged into a form that looks identical to unsteady RANS equations. However, the turbulent stress tensor now represents the sub-grid scale stresses. Recent advances in computational technology have made LES more viable and affordable for industrial studies of turbulence.[45]

One of the difficulties in large eddy simulations is representing the flow upstream of the flow domain, as an inadequate amount of information introduces sources of error. In StarCCM+ the Synthetic Eddy Method is implemented to automatically provide turbulent eddies across inflow boundaries and provide an initial perturbated flow field.

7.5.1 Working with Sub-grid Kinetic Energy

When running an LES simulation in StarCCm+ sub-grid kinetic energy is a physical by-product.

LES always uses a sub-grid scale model—Smagorinsky or WALE—which in turn directly computes turbulent viscosity.

The values for sub-grid kinetic energy are affected by the parameter in the Smagorinsky expert properties or WALE expert properties. Both these methods are explained below with description and information coming from the StarCCM+ online uses manual.

Currently, two sub-grid scale models are available in STAR-CCM+:

Smagorinsky Sub-grid Scale model: This is the original and most basic sub-grid scale model, upon which many more advanced models are based. One weakness of this model is that an ad hoc Van Driest damping function is required for proper results in wall-bounded flows. The algorithm that is used to implement the Van Driest damping has the potential to incur a significant parallel overhead (both memory and communication) when the geometry is complex. Therefore, this model should be avoided for large-scale computations on complex geometries. It is, however,

[45] Gaitonde U; *Quality Criteria for Large Eddy Simulation*: University of Manchester, school of MACE, May 2008.

useful for reference simulations, since it is the original algebraic sub-grid scale model formulation.

Dynamic Smagorinsky Sub-grid Scale model: This model computes a local time-varying constant. This dynamic variation of the constant allows the model to obtain the correct result for wall-bounded flows without the use of damping functions.

WALE Sub-grid Scale model: This is a more modern sub-grid scale model that uses a novel form of the velocity gradient tensor in its formulation. Its advantage is that it does not require any form of near-wall damping, so it is more suited to large-scale parallel computation on complex geometries. Experience within STAR-CCM+ has shown this model to be reasonably insensitive to the value of the model coefficient. It is, therefore, the recommended sub-grid scale model in STARCCM+. However all models have been tried for comparison.

Some important advice on running LES simulations was found in Gaitonde's[46] document on 'Quality Criteria for Large Eddy Simulations'. One suggestion was the finest of the grid needed, as for a successful LES simulation an extremely fine grid is necessary.

Some changes were needed to the mesh to obtain convergence using the LES method. The final mesh configuration is contained below.

Base size: 0.05m **Number of prism layer**: 25 **Prism layer stretching:** 1.2 **Prism layer thickness**: 0.007m	**Absolute surface size**: Min:0.001m Max:0.05m	**Prism layer surface size**: Min: 0.0001m Max: 0.001m

Cells: 4656078	**Faces:** 22618610	**Vertices:** 14783318	**Memory**: 3607MB

Table 7: Final mesh configuration.

Initial results using LES clearly show a better representation of the flow topology, especially in the stall condition at higher blade angle of attacks. An example of a velocity vector diagram at 15 deg. is contained in Figure 44.

[46] Gaitonde U; *Quality Criteria for Large Eddy Simulations*, University of Manchester, May 2008.

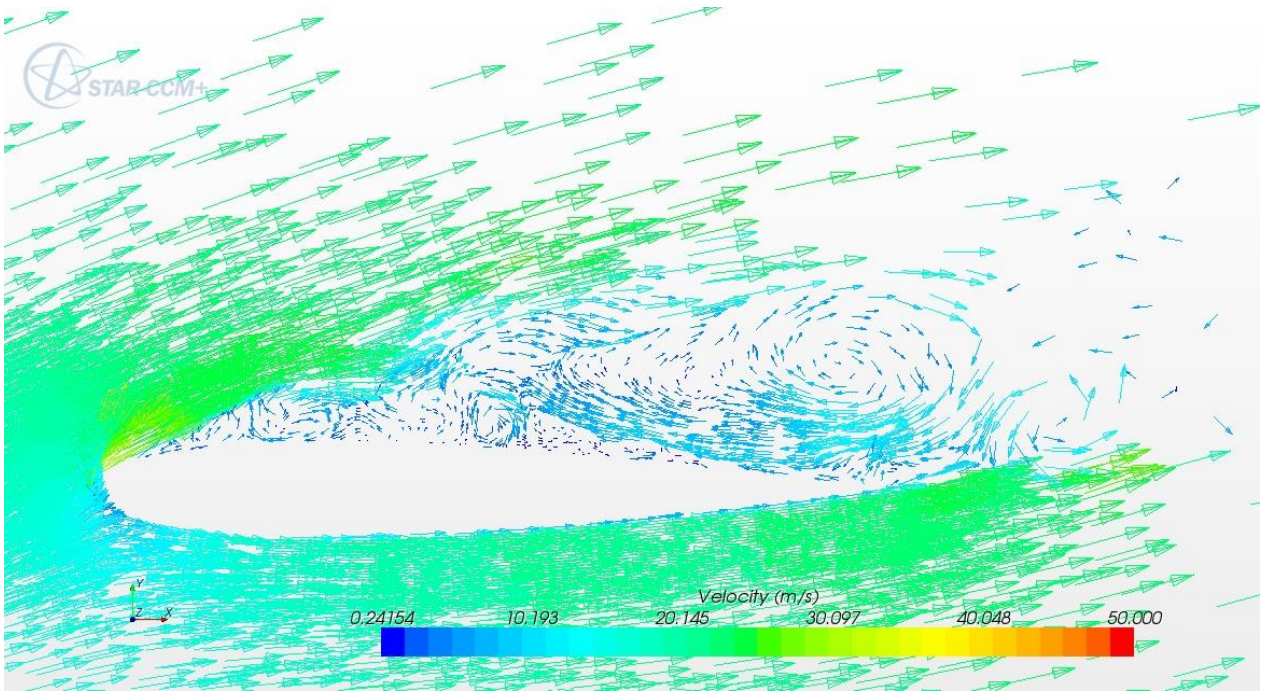

Figure 44: LES vector diagram at 15 deg.

However the disadvantage of LES is the computation time. Convergence of the lift coefficient was reached after on average 8-10000 simulations; which equated to approximately 1 week using a 12 core processer.

A comparison of the lift coefficient computed using both the LES WALE sub-grid model and the Smagorinski both standard and dynamic model are contained in Figure 45. It is clear from the results the most appropriate subgrade model using LES is the Smagorinski model, with the dynamic Smagorinski model providing slightly more accurate results.

However it should be noted the WALE sub-grid model provided more accurate results post stall, however could not accurately predict the lift coefficient in the pre stall condition.

The aim of using the models is too eventually use 1 model in a VAWT simulation, thus it was not tried or recommended to use a combination of LES WALE sub-grid post stall and dynamic Smagorinski pre-stall as the results suggest may be the most appropriate conclusion.

The Dynamic Smagorinski model was then used for further static simulations and a dynamic VAWT simulation also was set-up.

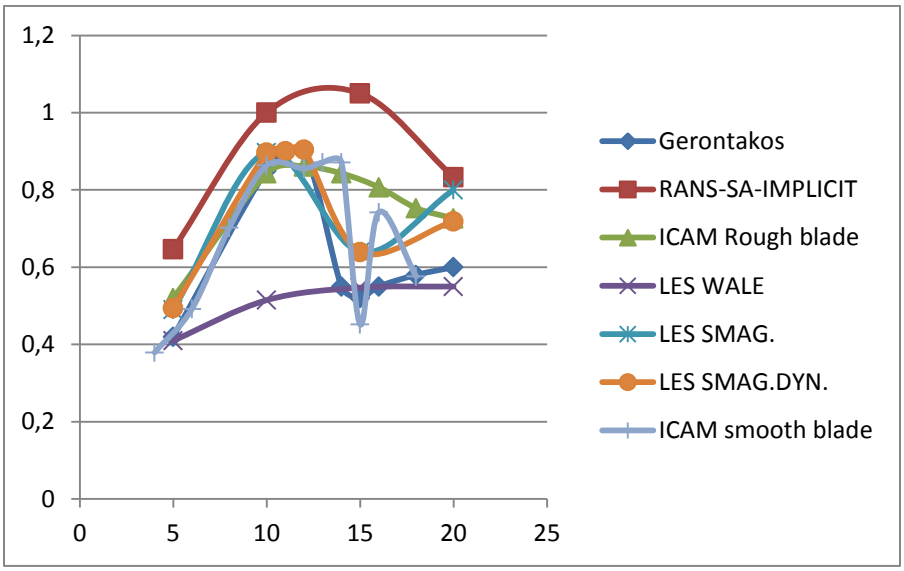

Figure 45: Comparison of lift coefficients over a range of methods; CFD – experimental.

Not only were the lift and drag coefficients found using LES Smagorinski dynamic model more accurate but the representation of the flow was very similar to that presented in Lee & Gerontakos. The comparison at key flow points along the low pressure surface is shown in figure Figure 46.

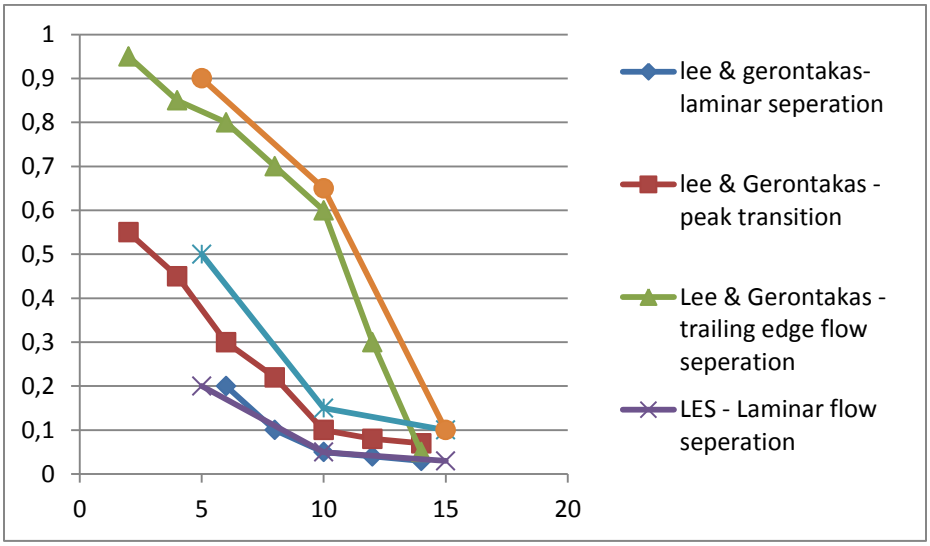

Figure 46: Boundary layer events comparison with LES.

Some observations from the results contained in figure 45 & 46 include:

- RANS simulations showed some trend of lift coefficient with the validated values; however the result was considered to high an error to be considered a reliable tool for

prediction. It could simply be used to possibly compare different blade lift coefficients. However real values are not considered reliable.

- Experimental results showed good resemblance with real values up until the static stall angle. Over this value it over predicted results by a factor of (30%). Although the stall angle was noticeable in results.
- LES Wale sub-grid did not adequately map results up until the static stall angle. After this angle it showed a good representation of the validated result.
- LES SMAG-Dynamic was the most accurate model in both the pre-stall and post-stall condition.
- LES models can accurately define the topology of the flow over the low pressure side of a turbine blade from 0 – 20 degrees.

A comparison of velocity scalar scenes over a range of blade angle of attacks from 0 to 20 degrees showed a large difference in the blade wake in pre-stall and post-stall conditions.

The stall condition has a huge influence on the wake of the flow. A comparison showing the size of the effected wake from pre-stall to post stall in increments of 5 degrees is contained in the figures below.

It is recommended to visualise such flow in a VAWT configuration. Designing to avoid interference effects and accurately predict flow throughout the turbine would be much simpler if the turbine was operated in the pre-stall condition.

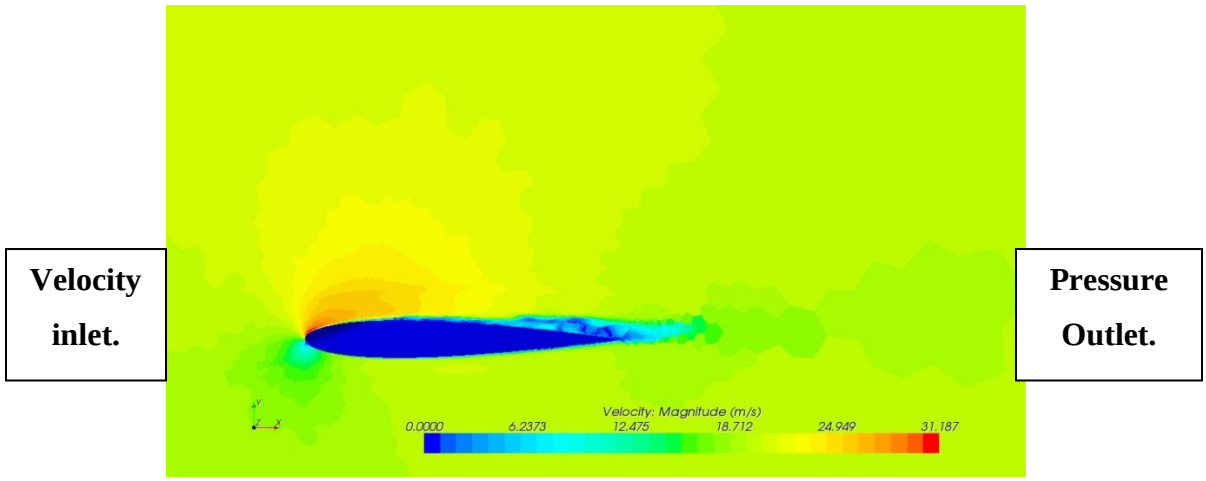

Figure 47: LES 5 degree angle of attack.

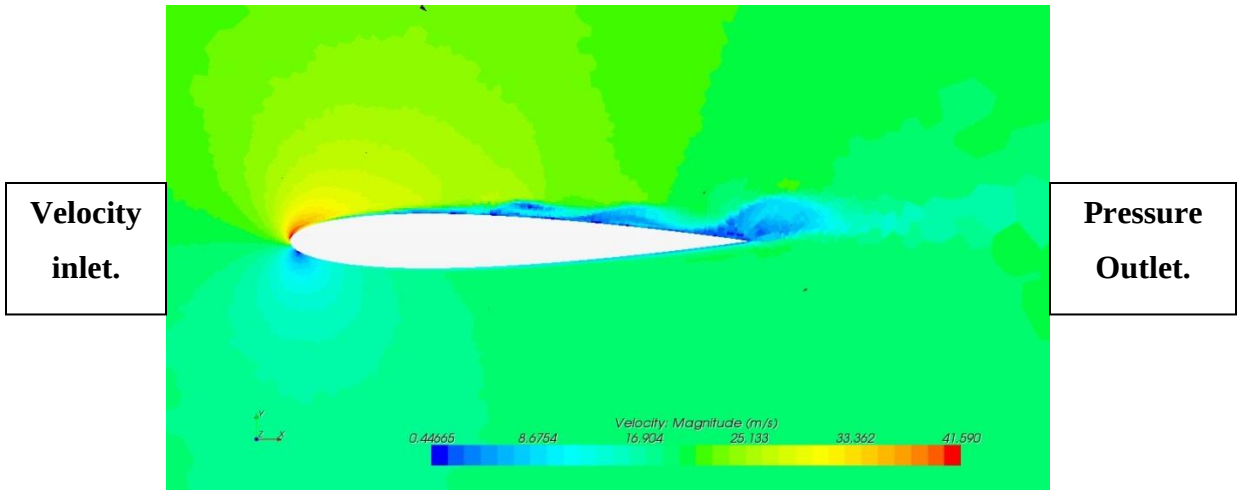

Figure 48: LES 10 degree angle of attack.

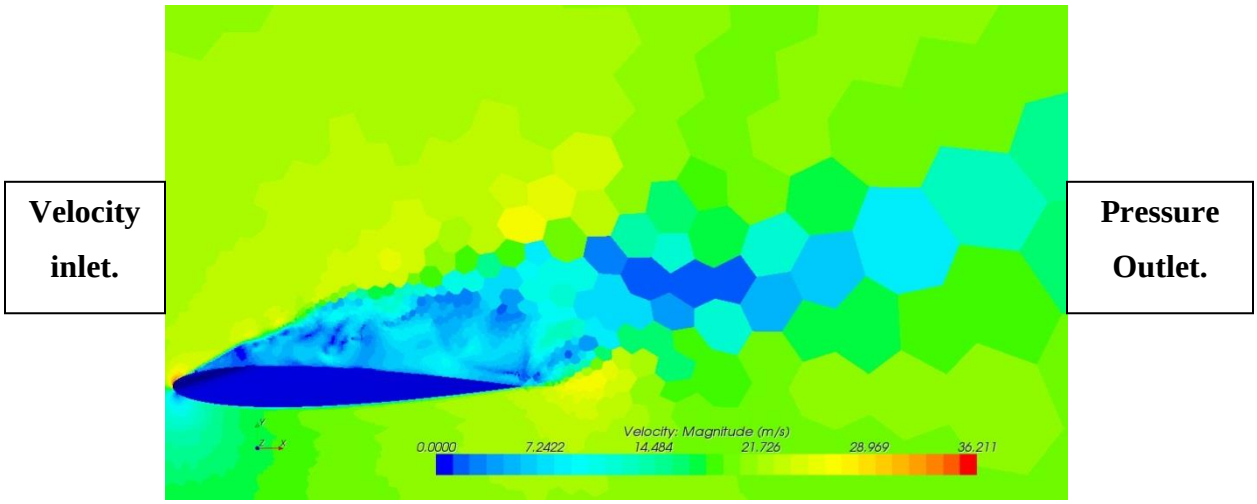

Figure 49: LES 15 degree angle of attack.

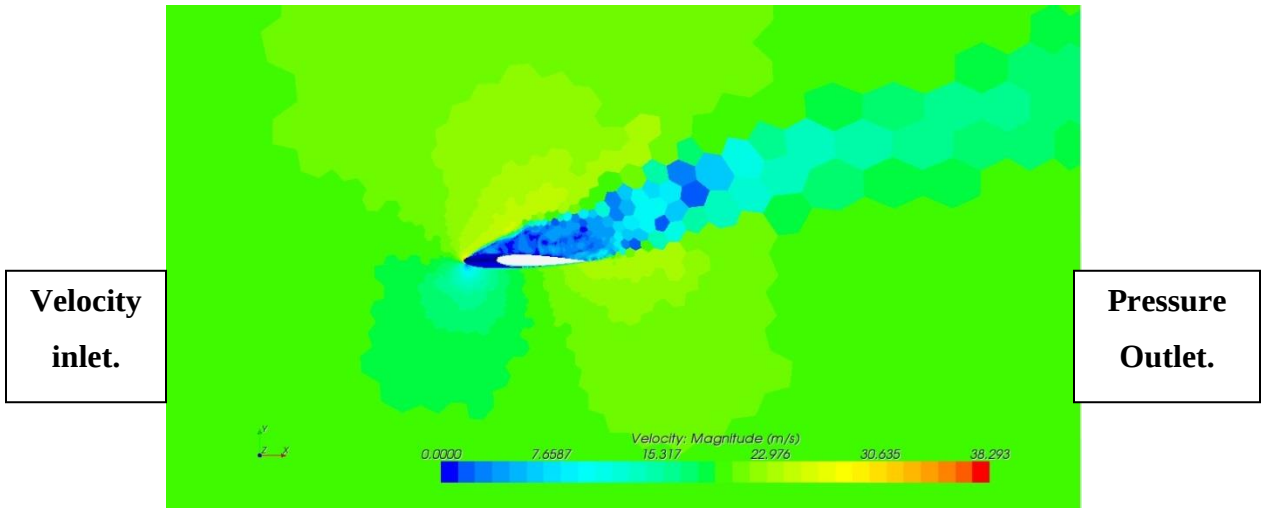

Figure 50: LES 20 degree angle of attack.

The effected zone in the post stall condition is at least 3 to 4 times the length of the chord at an instant in time. To add to this the flow is unsteady, highly turbulent with vortices as shown in the vector scene in Figure 51.

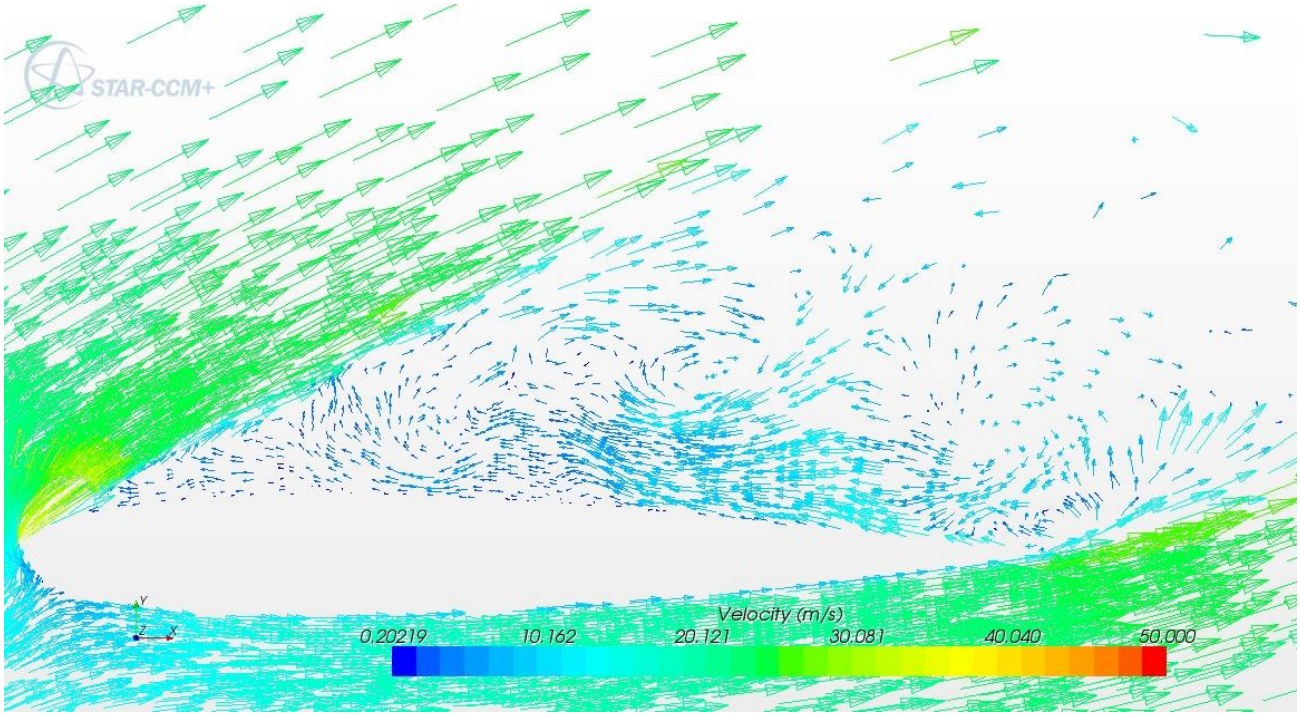

Figure 51: Vector scene LES 20 degrees flow.

If the angle of attack is below the stall angle, then the size of the mesh and consequently the simulation time can be significantly reduced also.

7.5.2 LES & Reynolds numbers:

Although a good comparison between various LES methods, model tests and articles was obtained, it should be noted this was at a fixed Reynolds number. A real VAWT is operating over a range of Reynolds numbers. It seemed knowledge of the effects of lift and drag coefficients over a range of Reynolds number (somewhat lower than previously studied in the aeronautical industry) was not readily available; as was and also the knowledge of the ability of an LES simulation to accurately predict the flow over a range of Reynolds numbers.

This is why it was planned to run experimental model tests over a range of Reynolds numbers, and equally test an LES simulation over a range of Reynolds numbers. Running LES especially at

a lower Reynolds number was desired to determine if a predetermined model of the smaller scale eddies (such as LES) is still reliable and accurate in predicting flow. Time was a key driver in LES simulations, but to obtain a lift and drag coefficients over a range of applicable Reynolds numbers would be a useful study in the future.

7.5.3 VAWT rotation simulation:

Results for a single static blade 3 dimension CFD simulation at a fixed angle of attack using the LES method predicted reasonable lift coefficients and accurately represented the real flow field behind an air foil. However the simulation time compared with the current ICAM hardware capacity was considered excessive; taking an average of 1 week for convergence of the lift coefficients. Thus it seemed unrealistic to continue attempting to simulate a 3 dimension flow with a rotating VAWT using a sliding mesh rigid body motion function in StarCCM+.

However for the purpose of the study it was attempted. A very simple geometry was set up in StarCCM+ with just 1 blade and a sliding mesh simulation was tried.

A summary of the process of setting up a sliding mesh rigid body analysis in StarCCM+ is contained in Annex E.

StarCCM+ provides the option of moving the mesh vertices of a region during a transient analysis. The rotational mesh was set up with a circular region of rotation inside the domain space. The foil will rotate around the centre of this region of rotation.

The geometry is shown in Figure 52.

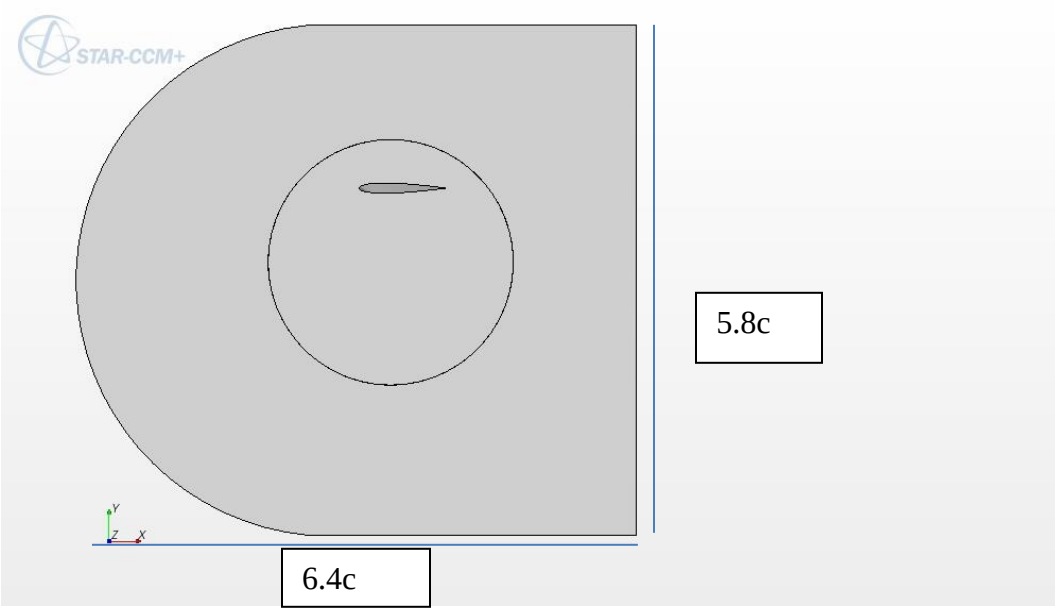

Figure 52: Initial geometry of rotational simulation.

The chord length above was maintained at 0.1m; however the domain space was reduced to try and reduce the simulation space with the aim of providing a solution. Thus the radius of rotation was just 0.1m and the rotational space had a diameter of 0.28m.

The problem with such a simulation was the floating point exception. The number of iterations was altered from 5,10,20,40 and 70 but this did not rectify the problem. Convergence was not possible – and divergence occurred.

An overview of the procedure and methodology is contained in annex E, however more computer hardware is needed to accurately obtain convergence and model a dynamic simulation.

Different speeds were trialled from 5 to 1200 rpm to try and find a solution however convergence was not reached.

There was however a weakness in the above model and observed throughout the simulation process. By attempting to simplify the domain space and size, the model has become a poor representation of the real case. Having a chord length the same size as the radius of flow is not realistic and will add further complications to results in terms of interference. To obtain the correct Reynolds number range a rotational velocity in the order of 2000 rpm is needed and a simulation time space of 8.3×10^{-5} to obtain a reading every 1 degree.

Thus it is recommended to model more closely the real case scenario.

A model and 3d simulation had been previously set up and tested in ICAM, however using the RANS equations for turbulent flow representation. To obtain a comparison of relative simulation

time in using an LES simulation this model was used but simulated using LES. The simulation model is contained in Figure 53 . A rotational speed of 30 rad/s was used and a wind speed of 5 m/s. Although the mesh was not optimised for LES the same problem of divergence occurred as shown in Figure 54.

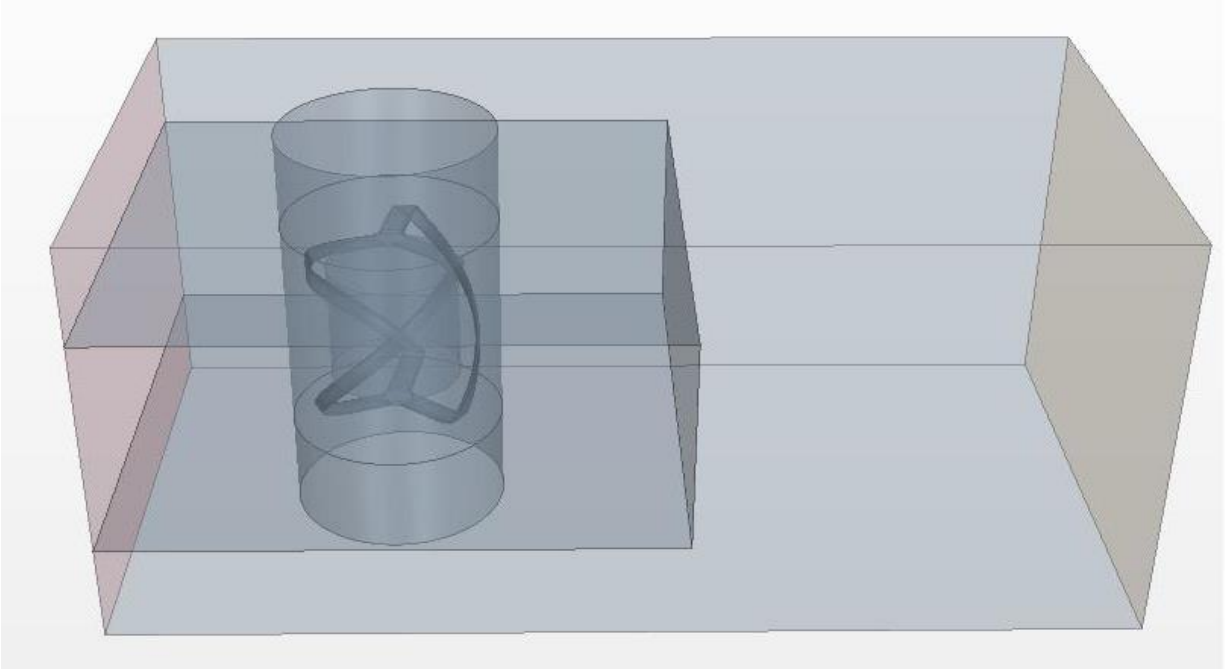

Figure 53: Previous ICAM 3D simulation model.

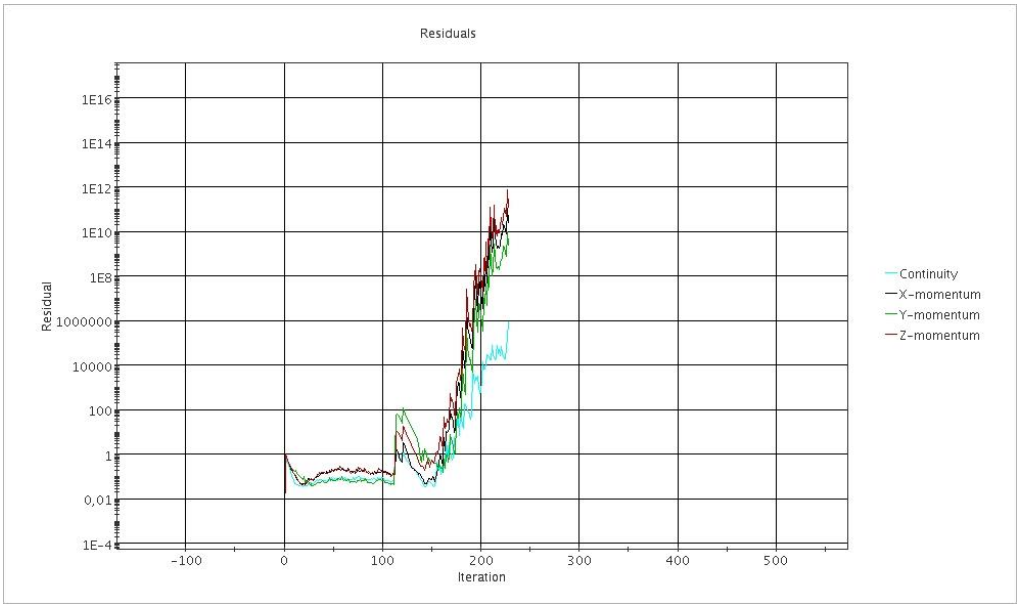

Figure 54: Residual divergence of an LES dynamic simulation.

No successful 3D rotating simulation was set up in StarCCM+ using the LES method of flow prediction. A floating point exception was always present after at most 200 iterations. This means the result is diverging rather than converging on a solution.

Solution divergence could be due to one of 2 reasons:

1. Due to the complications of a difficult physical solution Initial conditions are not correct
2. A problem is present with the set-up of physical properties, such as mesh quality, boundary conditions or solution parameters.

This is an area that needs much further investigation when running sliding mesh rigid body motion analysis in the future using LES.

Unfortunately time prevented further analysis on this matter.

7.6 SUMMARY CFD

In summary it has not been possible to accurately simulate a 3D rotating VAWT using CFD tools.

The most common and quickest CFD simulation tool is using the RANS approach of averaging the vector result of the large and small eddies in both magnitude and direction over a foil surface. However velocity magnitude and direction of a blade wake are very important factors in a VAWT design as there is a large amount of interference effects between blades. The RANS approach does not accurately represent blade wake and is not recommended for future use.

Also 2D simulations have been found to not accurately represent the real case, as the flow is 3 dimensional and you will have a large amount of span wise flow. This is particularly the case for helicoidal blades, as at each instant in time there is a blade section operating with stall phenomena.

Using CFD and using the LES method separating the large and small eddies we can more accurately represent the real flow over an air foil blade. This is particularly critical in the stall condition. By using a combination of LES and experimental measurements in the ICAM wind tunnel this methodology can be more accurately confirmed.

It was found that the LES smagorinsky dynamic sub-grid scale model was the most accurate model predicting the flow over a 20 degree angle of attack. However at post-stall angles the Wale

sub-grid scale model was closer to the published article result; however this model showed poor results in the pre-stall condition.

8. TURBINE MODEL

8.1 ANALYSIS

From the preceding analyse and results it would seem that a simple model for predicting power, forces and torque for a vertical axis wind turbine is too difficult. The flow is too non-linear and takes too many resources in the form of CFD (power and time) and that of model testing.

However there is a way of simplifying the problem aerodynamically. The condition of static and dynamic stall must be avoided. The blade tip speed ratio needs to be high enough to avoid such occurrences. This number will depend on the exact characteristics of the foil but a blade tip speed ratio above 4 creates an incident angle of attack below static stall with most foils analysed.

To achieve this however thorough 3 dimension analysis needs to be undertaken to understand the stall angles of the blade proposed, at the operating Reynolds number.

Once this is achieved then the turbine must be dimensioned to extract as much energy from the incoming wind and avoid interference effects. Thus at each angle of attack and in particular the maximum angle of attack (which will occur at the first encounter point with the wind – and cause most interference effects) the blade wake needs to be understood.

Such a turbine needs to be designed to provide as much free stream contact with the rotating air foil blade as possible, yet also avoid the occurrence where free stream wind is passing through the turbine not being utilised.

Factors affecting the occurrence of interference include:

- Blade Chord length.
- Turbine radius.
- Turbine angular speed.
- Optimum free stream wind speed.
- Blade geometry and angle of stall.
- Reynolds number.

Off course the angle of attack is important but this is a function of the blade tip speed ratio which can be derived from radius, angular speed and free stream wind speed.

A diagram of one complete revolution of a VAWT is contained below. It contains forces over the blade at each quadrant in a full revolution. The flow; as been explained will greatly depend on the

blade tip speed ratio which will govern the angle of attack. Flow however generally flows from high pressure side to low pressure side and will closely follow the drag force direction.

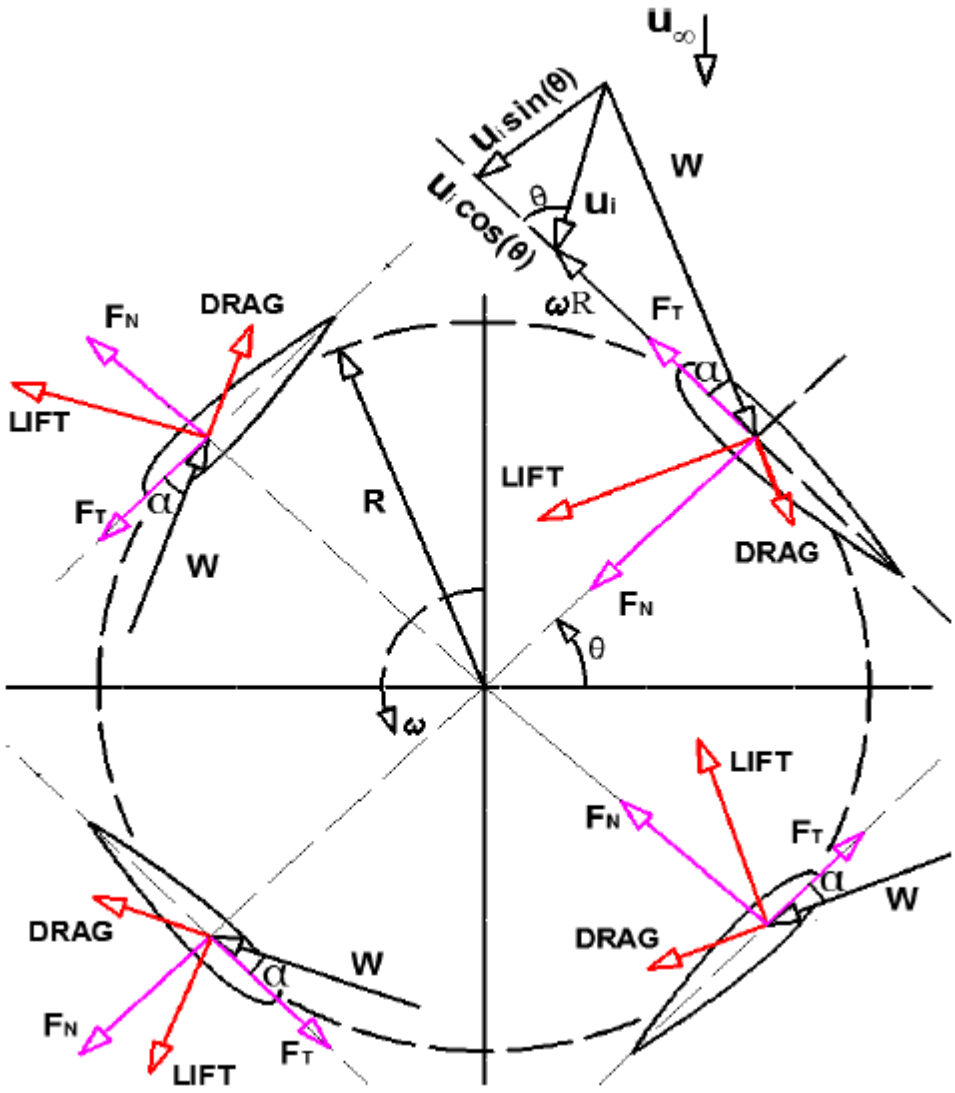

Figure 55: Overview of forces for a complete blade revolution.

It is important to note also that the definition previously defined on the blade tip speed ratio was actually the wind speed divided by the induction speed Va, which is an optimum but averaged speed of encounter over a 360 degrees rotation. It is important to design for the maximum possible free stream speed; which will be the wind speed and will occur at the first encounter point with the blade. At this point also is the maximum possible angle of attack. So defining the blade tip speed ratio as the blade tip speed divided by the free stream wind speed seems more appropriate for designing to avoid interference and avoid stall.

8.1.1 Avoiding stall:

The two Static stall angles for the NACA 0012 and 2415 blades are contained below, coupled with their respective minimum blade tip speed ratio.

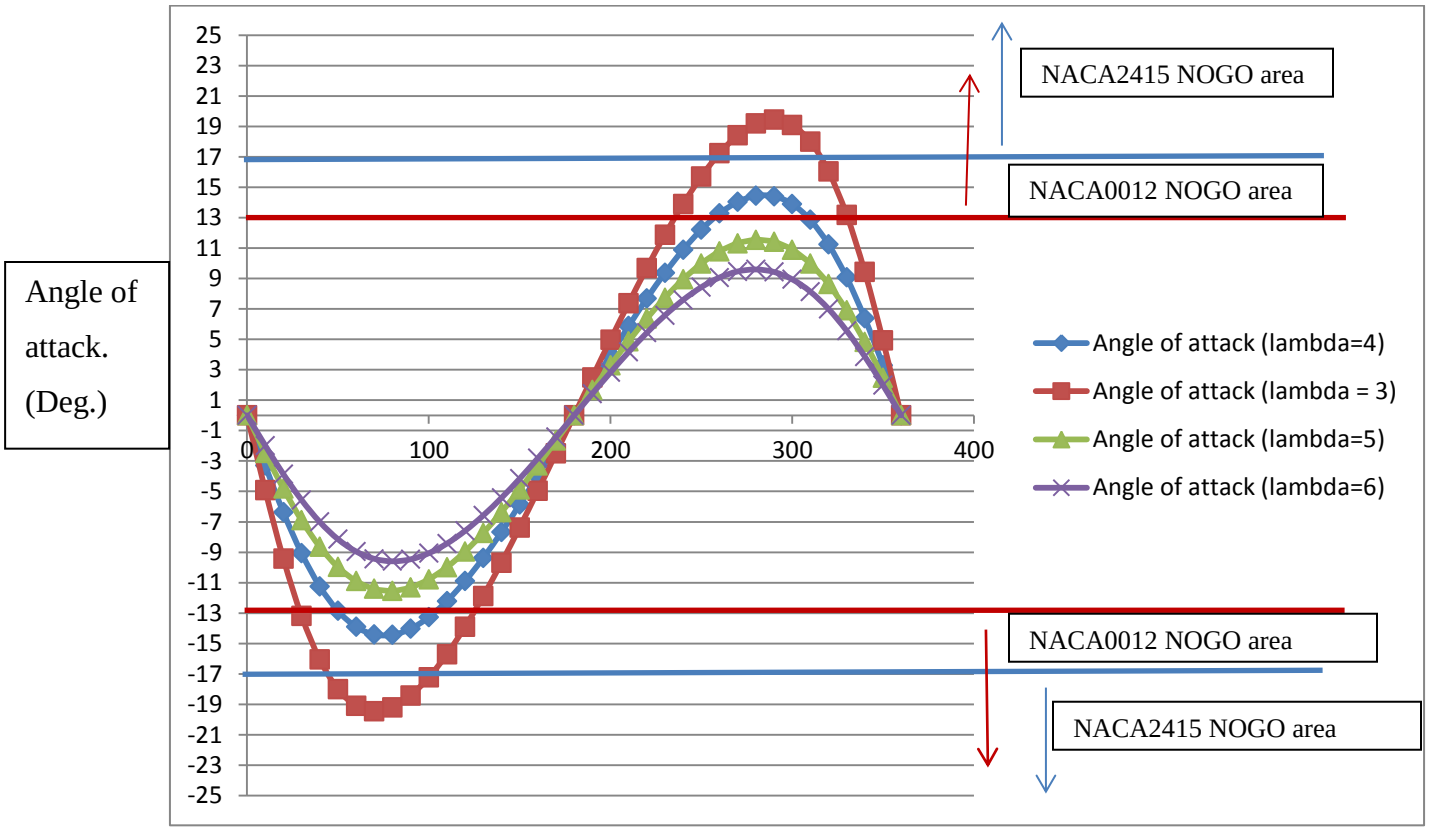

Figure 56: Azimuth angle vs Angle of attack for various blade tip speed ratios.

However this minimum blade tip speed ratio should be designed for maximum possible encounter to avoid stall. The blade tip speed ratio previously defined is using an induction velocity based on an average velocity of encounter defined by Betz. Thus using an **a** value of 1/3 defined in equation 3.1 the actual minimum blade tip speed ratios will be higher by a factor of 1.5 as shown below.

$$Va = \left(\frac{2}{3}\right) V\infty \qquad 8.1$$

$$\lambda = (3Vt)/(2V\infty) \qquad 8.2$$

Thus it is important that the blade tip speed ratio is defined correctly as this could be an area of confusion. Table 8 summarises the minimum acceptable blade tip speed ratio for the NACA 2415 and NACA0012 foils to avoid stall. The ratio is given based on values defining λ as a function of the induction velocity and λ as a function of the wind velocity.

	Stall angle	λa	λ∞
NACA2415	17	5.25	3.5
NACA0012	13	6.75	4.5

Table 8: Minimum acceptable blade tip speed ratios

To avoid confusion it is important that the method of defining blade tip speed ratio is consistent.

8.1.2 Avoiding interference:

The next step is a simple model to avoid excessive interference. This can be defined as a factor of the number of blades, the chord length, the radius and the rpm.

Firstly as previously described in equations 3.14 and 3.15 the time taken for the disturbed wind to reestablish itself (t_w) and the time required for the next blade to move into the zone of the previous blade (t_s) should be calculated.

These times are as follows:

$$t_s = \frac{2\pi}{n\omega}[\text{sec}] \quad 8.3$$

$$t_w = \frac{s}{V}[\text{sec}] \quad 8.4$$

V is the wind speed, s is the length of the disturbed wind speed, ω is the angular velocity and n is the number of blades.

From experimental results and CFD analysis we have an estimate of the size of the disturbed wind speed.as a function of chord length. At the first encounter with the wind (where interference is most critical) will be the maximum which has been calculated as 1x chord length.

Thus the length of the disturbed wind is 2C, where C=the chord length.

To allow some free stream wind through for the 2nd blade encounter and allow also some margin in avoiding interference some extra time is calculated to allow some free stream wind through.

This is given as 2 times the time of the disturbed wind.

Thus: $$tw = \frac{2C}{Vr} + \frac{2C}{V\infty} \quad 8.5$$

Letting $t_s = t_w$

$$\frac{2pi}{nw} = \frac{2C}{Vr} + \frac{2C}{V\infty} \quad 8.6$$

Therefore the optimal rotational speed is given as:

$$w(optimal) = (piVrV\infty)/(Cn(Vr + V\infty)) \quad 8.7$$

To provide a maximum allowable rpm to avoid interference at the first encounter we can just calculate w above but by using a time of 2C/V.

$$w(max.) = (2piV)/(2Cn) \quad 8.8$$

Using such a model and initially not accounting for stall effects we can find an optimum rpm, based on a fixed blade tip speed ratio, turbine radius and number of blades.

Comparing results with the 3 bladed model used in the Jules Verne Wind tunnel, with a radius of 0.7m, wind speed 10m/s and a chord length of 0.2 is below.

By introducing stall effects into the equation we will increase the size of the effected zone, by a factor of 4 times the chord length. The reduction of the optimal speed due to stall effects on the wake is also shown in the figure 57 .

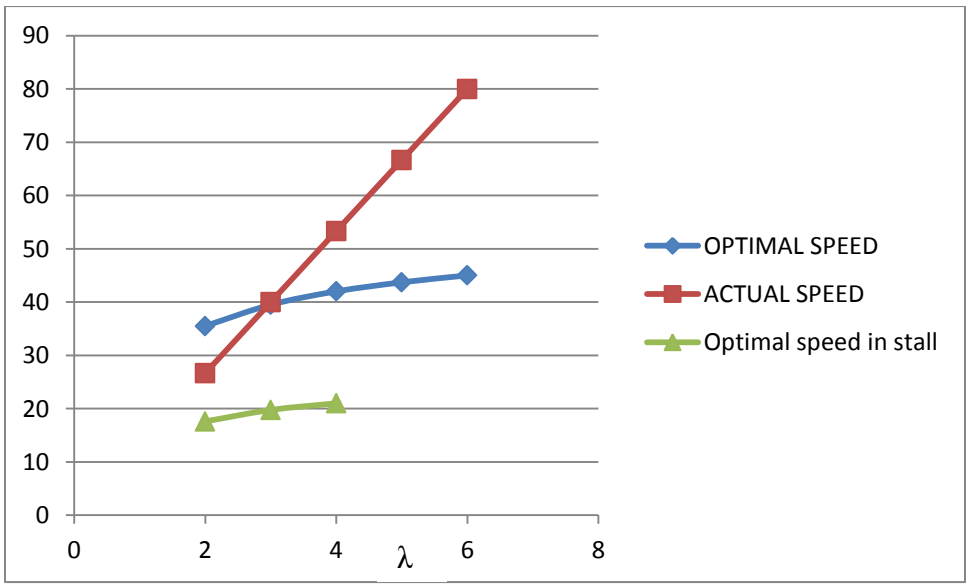

Figure 57: Optimal turbine speed calculation, R=0.7m.

It is seen from the above calculation that the optimal speed is actually a similar speed to the blade tip speed ratio used of 3. However it will be operating in the stalled condition. Thus to increase

such a speed within such a model to operate outside stall the radius of the turbine must be increased.

By increasing the radius to 1 we have moved the optimal rpm to give a higher blade tip speed ratio (approx. 4) which is outside the stall condition for the NACA 2415 blade. This is shown in figure 58.

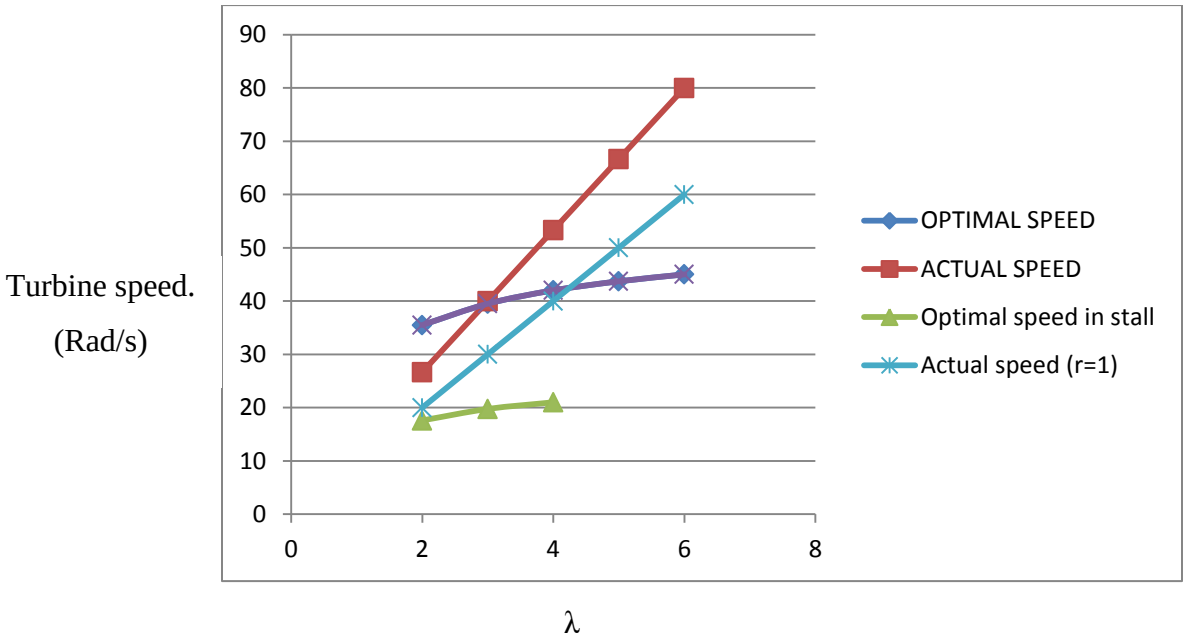

Figure 58: Optimal turbine speed calculation, R=0.7m

Thus an increase in radius can be an effective way to avoid interference effects and operate outside the stall condition.

Such a model could be further developed a better understanding of blade aerodynamics and wake analysis using a combination of small scale model testing, LES CFD analysis and full scale model testing for verification. An interference factor can be incorporated into a VAWT analysis model based on such results. This led to the discovery of the open source calculation tool; Q-blade, based on Blade Element Momentum (BEM) methods previously discussed but with more analysis and research on interference incorporated into the model.

8.2. Q BLADE.

Qblade is an open source wind turbine calculation software tool that has a feature added specifically to analyse VAWT's. The software project was developed as part of a wind energy group at the Berlin Technical University Department of Experimental Fluid Mechanics.

It is a simple design tool based on Blade Element Momentum (BEM) methods. It is a 2 dimensional model extrapolated into the 3rd dimension, however incorporates known knowledge of the real performance of a turbine blade in operation. It applies semi-empirical corrections, derived from testing and CFD to account for 3 dimensional effects.

Its aim is to conduct rapid design analysis of various turbine configurations with simplicity and low cost.

Qblade contains 3 simple sections:

- blade design and optimisation
- rotor simulation
- turbine definition and simulation

The software is very simple and user friendly. An example of a 3D Helicoidal NACA2415 blade developed is contained below.

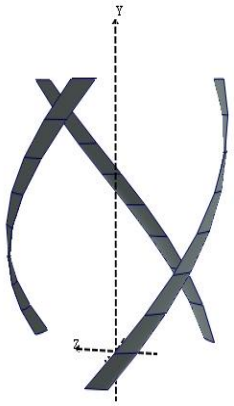

Figure 59: Q-blade helicoidal blade model.

Some simulations were conducted of the designed VAWT and compared with model test results.

The original helicoidal blade design was modelled and simulated under 3 different conditions in Q-blade.

- Ideal conditions with some interference factor.
- A more advanced interference factor is added.
- Tip speed losses are also taken into account.

This was also compared with a model with an increased turbine radius of both 1 m and 1.25m. The results are contained in figures 60, 61 & 62 below.

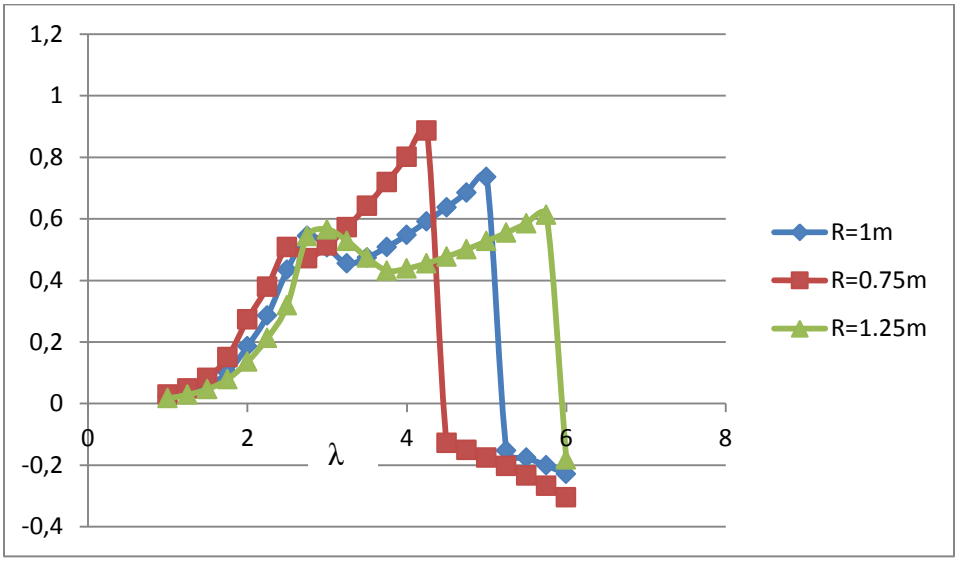

Figure 60: Q-blade analysis ideal conditions.

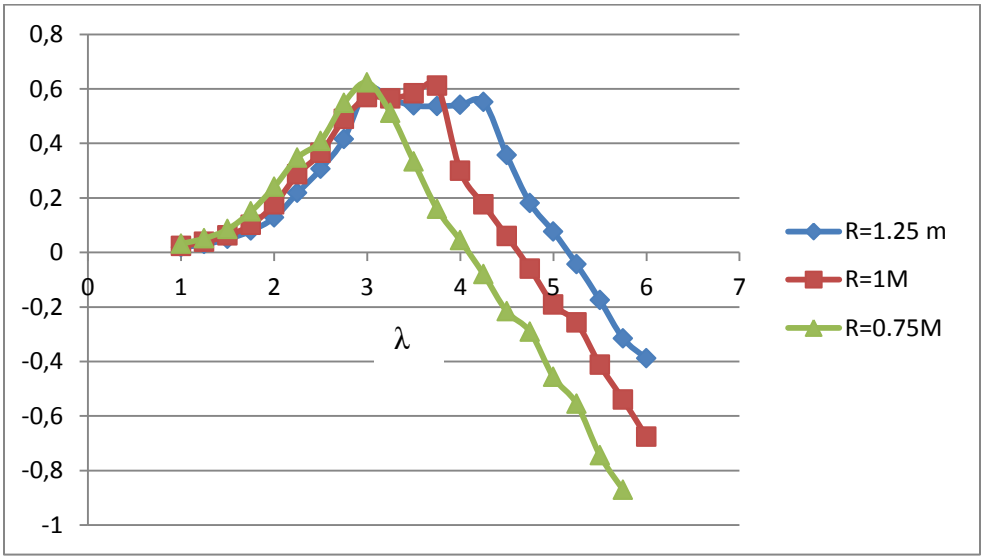

Figure 61: Q-blade analysis with additional interference factor.

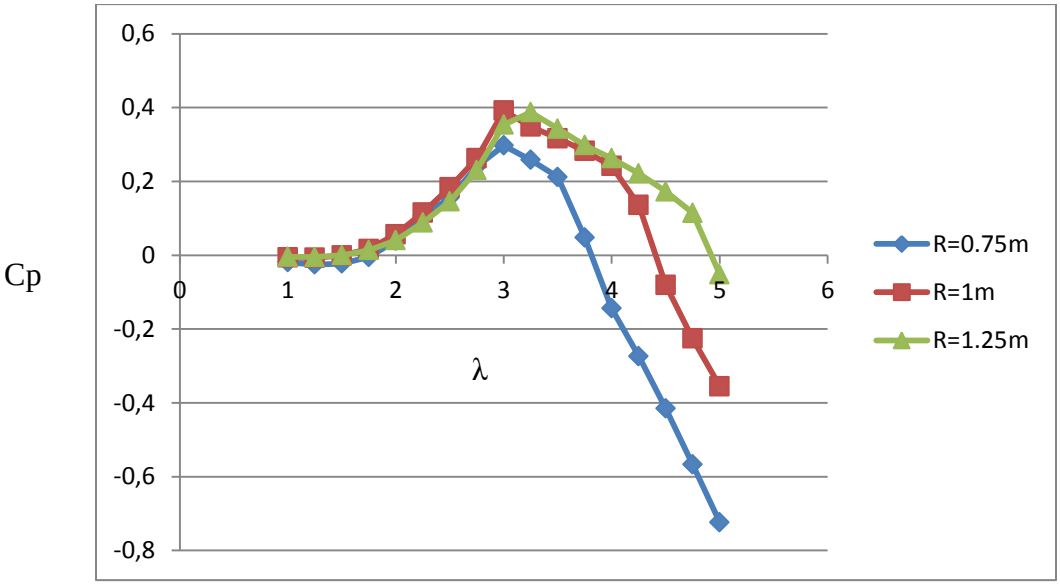

Figure 62: Q-blade analysis with tip speed losses.

Some observations of results using Q-blade include:

- Interference and tip speed losses have conflicting blade tip speed ratios for optimal power extraction than that in ideal conditions with minimal interference.
- A higher tip speed ratio is desired in ideal conditions, but when factoring in blade tip speed losses and further real interference effects a slightly lower blade tip speed ratio is desired.
- A larger radius is desired for a larger range of blade tip speed ratios where maximum power can be extracted. Also a larger radius minimises interference and maximum power occurs outside stall.

With such simple software it is easy to get a good understanding of important design parameters for optimal power extraction. Specifically the importance on blade tip speed ratio, number of blades and rotor radius to account for interference.

Also Q-blade provides a function to import your own blade data into the program. So if detailed foil data is obtained, then this can be used in the simulation and extrapolated into the VAWT model.

The Two additional features incorporated in the design of Q-blade were corrections for tip-speed losses and interference.

Tip speed losses include a tip loss factor due to the pressure difference between the upper and lower surface of the air foils and a span wise velocity component observed regarding the real blade. Such a factor would be considered important when simulating a helicoidal blade as there are multiple blade velocity angles of attack at any one time occurring on a single blade span. Thus span wise pressure differentials would be high.

Interference factors are taken into account in the model; however a separate interference factor is added to account for variable interference. As the effect of interference will actually depend on the blade azimuth angle location relative to the incoming wind.

Other effects, especially from the rotor and appendices are not accounted for in the simulation.

.

9. ELECTRICAL POWER GENERATION:

A small section has been proposed on electrical power generation, as we are designing a turbine to extract electrical power. Thus blade aerodynamics are aimed at creating lift on the air foil blade to create a working torque. This working torque must be both:

- Useable by the load carrying device to generate electricity.
- Controllable; to be easily predicted and used with reliability in a distribution network.

When designing such a turbine for electrical power generation it is important to understand the load requirements and incorporate them into the design. If the turbine is designed for small scale residential use to be connected to a battery charge through a DC generator, then speed of turbine rotation is not so important.

However for use as an Alternating Current electricity generator, the speed of the turbine becomes fundamentally important. For electrical generators and in particular large 3 phase electrical generators rotation speed will determine the size of the generator. In the past rotation speed was paramount as it determined AC electricity production at a fixed frequency, however these days frequency convertors are available to alter the frequency output for a range of rpm's. However power electronics such as frequency converters will add to the cost of a system and have a limited range where efficient electric power can be produced. The use of a frequency convertor may add to the overall electrical generation efficiency; however there will be a minimum rpm where their losses are far greater than any system efficiency gain and there use is not feasible.

Some common electrical configurations are contained below.

- DC generator, Battery charger – invertor is needed for AC current.
- AC Generator – fixed rpm
- AC Generator + frequency converter – variable rpm

9.1 USEABLE POWER:

In predicting power and specifying an electrical generator it is important to note the available electrical power at any one time is dependent on the wind speed. If there is no wind; then no electrical power is available.

Wind speed also is not fixed, its value will fluctuate in any one day and thus the available electrical generator capacity will also fluctuate. A generator must be specified for the maximum power output, thus depending on the type of generator used, its efficiency will reduce as the available power from the wind moves below the design point. Also it will be inherently expensive, as you are buying an item that has its power de-rated for a large part of its operational life.

Below is a Weibull distribution estimation of the available wind energy in the Nantes region.[47] Weibull distributions have their errors but they are a common industry tool for assessing wind conditions in a region.

Within the Aérojoules projects electrical generators have been specified initially for a wind speed of 7 m/s and 10 m/s. These two speeds account for an estimated operational time of just 6% and 2% respectively. The remainder of the time the generator is operating outside its design point and it has been over specified for its use.

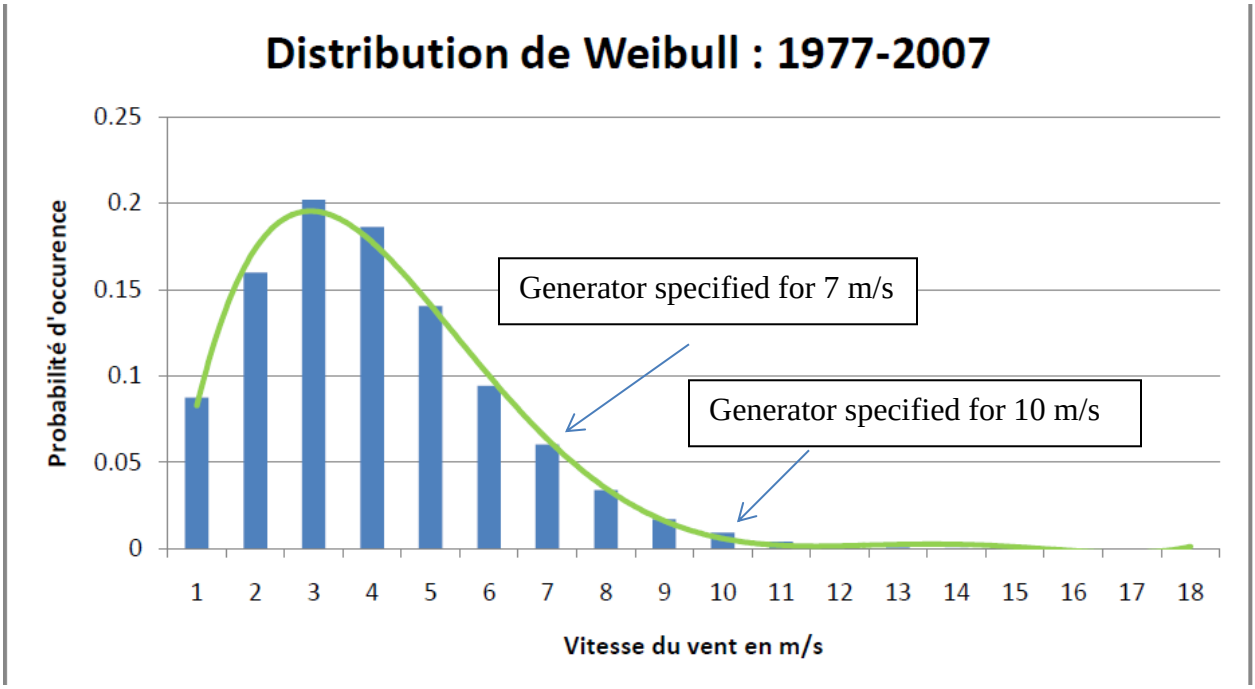

Figure 63: Weibull distribution of the wind speed in the Nantes region.

It is acknowledged that generators can be specified to have a relatively flat efficiency curve to minimise efficiency losses at lower power output, however this does add considerable cost to the

[47] Visonneau V, Funck J : Project Aérojoules – Rapport phase A1; ICAM, Rapport de mémoire Scientifique, 2013.

system. Also a frequency convertor is needed which will be specified at the maximum power, but rarely operate close to this. This further adds efficiency losses and a high initial cost.

More will be said on useable electrical power in section 12. As wind turbines really are dependent on the amount of wind energy available. This report has been focused on optimising aerodynamics to obtain a high power coefficient to extract as much useable energy from the wind. But the amount of useable energy that can be extracted is dependent on climatic conditions.

9.2 CONTROLLABLE POWER:

Also to adequately extract mechanical power from the wind and convert this power to electrical power and distribute it too a network, it must be easily controlled.

The electrical control device used is a simple Maximum Power Point Tracking (MPPT) system. This is also a research project conducted at ICAM, which is the design of the electrical control system. By using the MPPT system Aubrée's[48] initial predictions of maximum generator power output are not obtained at the same speeds as those predictions of maximum mechanical power output. This emphasizes the need to incorporate the electrical system in a 'total system approach' design analysis. As it is only the electrical power output that is 'useful power' from the wind.

Efficiency of a system needs also to factor in the generator, as previous efficiency analysis has only focussed on the mechanical losses in converting wind energy into mechanical energy. There will be further electrical losses present that need to be factored into a total system efficiency calculation.

Such electrical losses are often associated with the amount of control you have on the mechanical generating device, as if it responds slowly or inaccurately to a load change from the generator then there will be associated power losses caused by harmonics in the system. These harmonics will generate in the frequency convertor from sudden changes in rpm and will be distributed to the electrical system and will affect the quality of power supply. Such an affect on power quality may also limit the type of equipment the electricity can provide too.

[48] Aubrée R, Auger F, Dai P : *A new low-cost sensorless MPPT algorithm for small wind turbines*: LUNAM Université, IREENA, Saint-Nazaire, France, LUNAM Université, ICAM, Nantes, France

It is not the intention to discuss in detail losses in frequency convertors, harmonics and the quality of power supply. Just that they should be factored into a design analysis of a turbine. As often the best mechanical design point will be different to the optimum electrical.

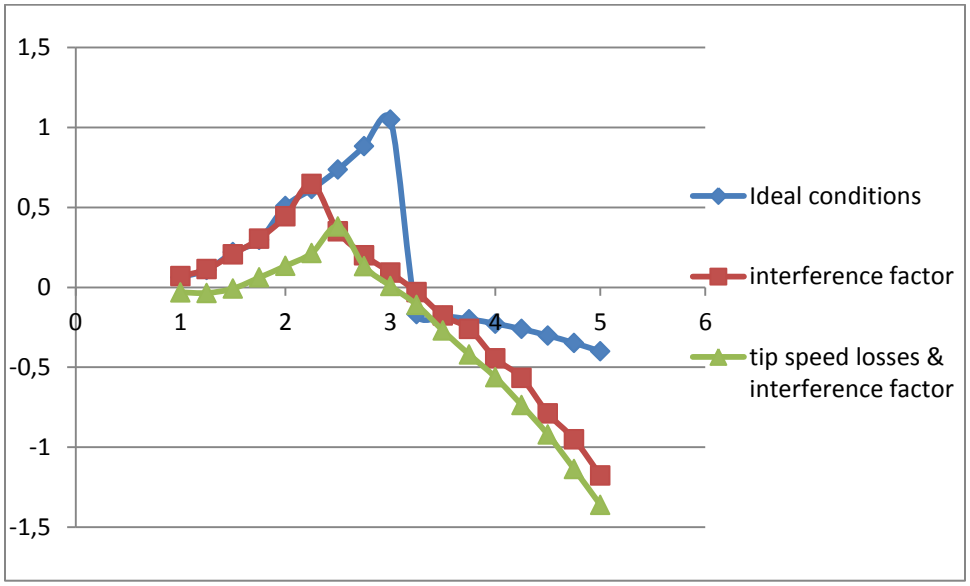

10. AÉROJOULES DESIGN

The current Aérojoules design is innovative; and may benefit from some aerodynamic optimisation. Such a design does encounter complicated aerodynamic flow that is difficult to predict.

The blades are operating in the stall condition, with non-linear erratic flow at each angle of rotation in a revolution. The key feature of the designed turbine is its starting ability, as it can be started from all wind directions, due to the helicoidal nature of the blades. This is true and optimum torque is also available at each moment in time. However its designed rpm is below the maximum rpm to avoid stall, and as such will have one part of a blade operating in stall at any one time. With the knowledge of the magnitude and influence of the non-linear flow it is difficult to foresee that the positives of obtaining a favorable lift coefficient at all azimuth angles will outweigh the negatives of having a blade in stall at the same time.

At each instant on a rotation the turbine contains the optimum and the least desired aerodynamic flow. Unfortunately the least desired flow is so non-linear and erratic and it can affect the flow phenomenon of other blade angles along the chord. Particularly shown by the ink droplet testing and the need for 3 dimensional CFD testing for accurate results; flow in the stall condition is erratic and flow will travel along the foil span and effect the flow of adjacent foil sections.

At speeds of a blade tip speed ratio of above approx. 2.6 and up to 3 the efficiency of the turbine is decreasing as shown by real scale model tests. This is seen as a combination of both stall and interference effects between turbine blades. Thus it seems difficult to foresee the turbine creating enough torque from the wind to move into an operating speed giving an acceptable blade angle of attack to avoid stall; without an external power source.

Operating in the stalled condition provides aerodynamic complexities in predicting flow not just from a design perspective but also controlling the turbine via the governor of a permanent magnet motor for electrical production. Such quality of control issues will affect the quality level of the electrical energy generated and may limit its effective use to heating and resistive circuits.

Such blade vortices and non-linearity will create excess noise and vibration from the turbine. It is unclear of the specific breakdown of total airborne noise generated from dissipated energy loss and vibration from both static and dynamic stall effects; as compared with increased noise generated from higher blade tip speeds. More analysis is needed in this area.

The designed turbine rpm needs to be increased to operate outside the stall condition. It is understood that the turbine is structurally designed for a lower blade tip speed ratio and increasing the blade tip speed will increase radial loads on the turbine; however aerodynamic efficiency is being compromised and maximum power coefficients can theoretically be obtained at a higher blade tip speed ratio. From initial Q-Blade analysis by increasing the radius of the turbine the effects of stall and interference can provide an optimum power coefficient at an acceptable blade tip speed ratio for a NACA 2415 air foil.

How do we know what the real loads are on the blades at various tip speed ratios? It is proposed during the model test to run an electric motor (with a flat power coefficient) up to a desired blade tip speed and measure the power and torque loads and noise on the turbine. If extra power is needed to operate through beyond the stall condition this can be identified and then be calculated.

An extra power source may be needed in getting the turbine to operate with a higher blade tip speed ratio and maintain this ratio when under load, as it appears with the erratic flow the turbine can start but it cannot move through the static stall condition and into a higher rpm range needed, and further maintain this rpm when operating under load. Possibly a more reliable torque is needed to counteract the non-linear flow when operating in stall.

10.1 COMBINATION SALVONIUS – DARRIEUS TURBINE:

One means of providing starting capability and also aiding in moving the turbine through to an acceptable rotational speed operating condition is the Salvonius turbine. Such a turbine is featured on the figure 3 list of different types of VAWT's

The Salvonius turbine is characterised by high efficiency but much lower blade tip speed ratios (optimally 1 as shown in figure 7), however by designing with a much lower radius to operate efficiently within the same rotor this is possible.

Some examples of combination Darrius/salvonius available on the market is contained in Figure 64.

Paraschivoiu[49] estimated that a power coefficient of 30% is possible with a salvonius rotor. He proposed some simple models for estimating power and sizing, which are contained in 19.6. These turbines are generally not viable when compared to standard wind turbines as they require up to 30 times more surface area for the same power. Thus not being weight/cost/power effective. They are limited to small power applications, and such an application such as providing some boost power to stabilise the Darrius turbine and allow it to run through the stall condition is worth considering.

The design in Figure 64 will affect the flow captured in the downstream rotation cycle and this effect needs careful consideration also. Possibly a salvonius turbine could be placed above the top of the rotor of the Aérojoules design, however sizing can only be determined after knowledge of the additional power needed from the salvonius turbine is obtained.

Figure 64: Combination Darrius/Salvonius VAWT provided by HIVAWT[50]

[49] Paraschivoiu I, *Wind Turbine Design – With Emphasis on Darrieus Concept*, Presses internationals Polytechnique, Québec, Canada, 2009, page 16.

[50] Chen J: 'Vertical Axis Small Wind Turbine Breakthrough and Small Wind Turbine Application Limit'; HIVAWT, 2009 US-Taiwan High Technology Forum | Clean Energy conference, 2009.

11. PITCH CONTROL:

The option of pitch control needs further investigation. By controlling the pitch of each blade complex aerodynamics can be potentially simplified and the lift coefficient maximised at each degree of rotation providing a potentially much higher lift coefficient, generated torque and power efficiency.

The concept of controlling the pitch of a Vertical Axis Turbine has been used in the marine industry for years, pioneered by the well-known marine propulsion provider Voith Turbo Schneider Propulsion of Heidenheim, Germany. Such a device is used to provide not electrical energy but ship propulsion in the form of thrust; however directional thrust is controlled by the use of pitch control of the blades. It is characterised by its high torque and thrust at low speeds and due to the pitch control device its superior maneuverability.

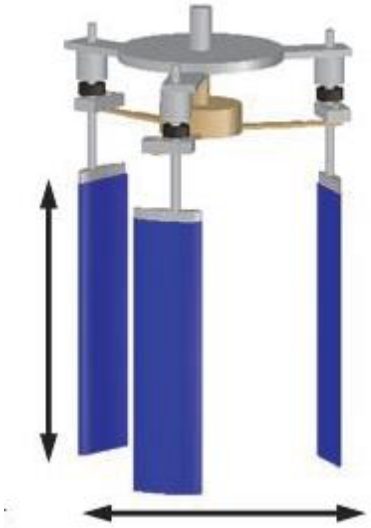

Figure 65: Model blade pitching mechanism used in the marine industry.

If such a device could be used on a VAWT then potentially complex aerodynamics and large load fluctuations could be eliminated and power could be more easily controlled and predicted. However it is acknowledged that speeds and loads of wind turbines are much different to that of water turbines, so more analysis is needed.

A theoretical model was developed based on analysis of equations set out in chapter 3. It is a simple 2 dimensional model based on ideal conditions, however gives an indication of the possibility of controlling the turbine angle of attack to better control the turbine aerodynamics.
Using the NACA 0012 airfoil to start with and optimising for maximum torque of a 13 degrees angle of attack at each azimuth angle.
A simulation below contains the change in angle needed from the fixed angle over a blade tip speed ratio of 3. The period of pitch rotation of a cycle is 0.21 seconds.

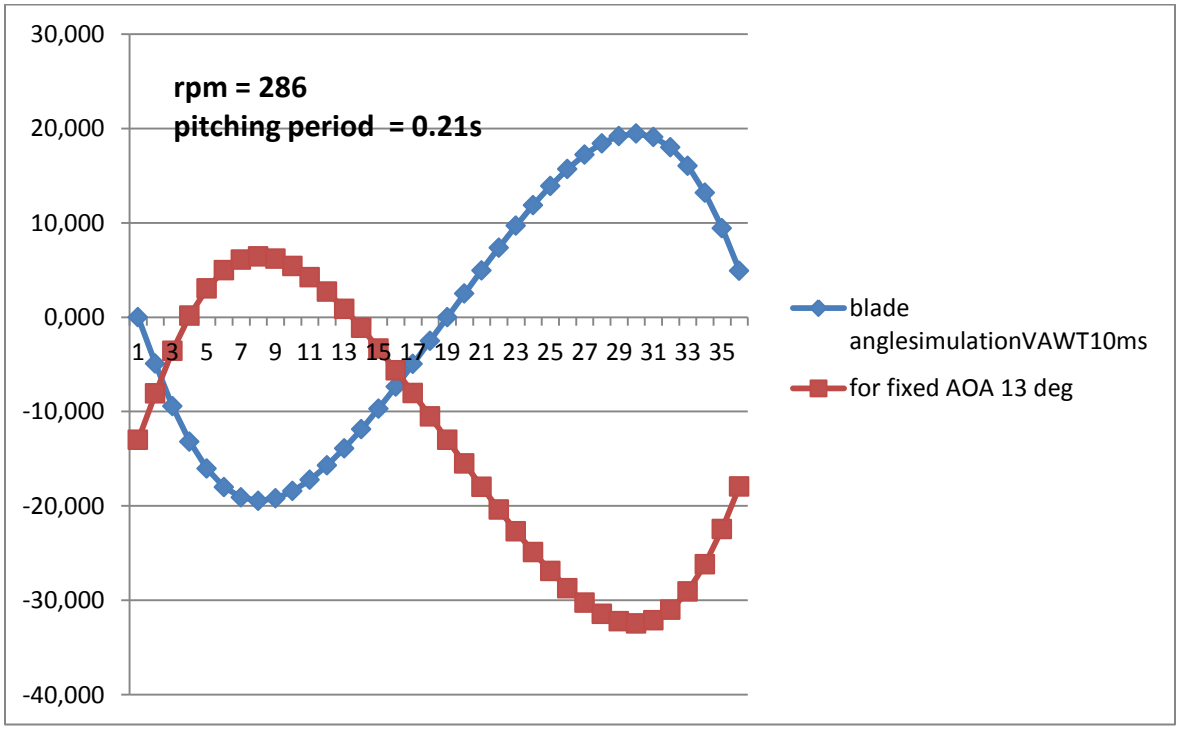

Figure 66: Comparison of blade pitch angles between a fixed pitch and Controllable pitch VAWT.

A comparison between ideal condition power coefficients between a fixed blade and a pitching blade is contained in figure 67.
The model does not contain an interference factor so such high power coefficients for a high blade tip speed ratio are not realistic, but the potential for increased power efficiency is evident.
This is especially evident at lower tip speed ratios, the negatives of stall can be avoided and interference minimised.

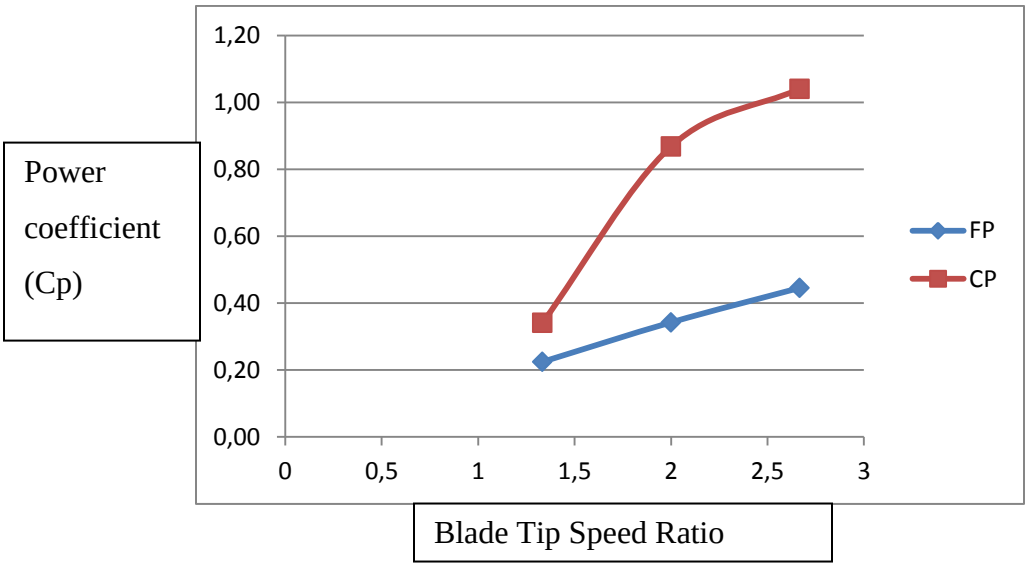

Figure 67: Comparison fixed pitch vs Controllable pitch

There are many unknowns however with this bold prediction of power increase, and off course any power increase must be offset by the energy consumed in changing the pitch angle. However by applying an experimental set up in a wind tunnel as proposed in chapter 4 we can test the power consumed by a stepper motor in changing the pitch angle.

Such a concept has been studied and tested by Miau[51] of the National Cheng Kung University, Taiwan in 2012 with favorable results using a stepper motor. While an experimental and computational approach using a mechanical four bar linkage system was conducted by Benedict[52] of the Alfred Gessow Rotorcraft Center, University of Maryland.

[51] Miau j, Liang S, Yu R, Hu C, Leu T, Cheng J, Chen S: *Design and Test of a Vertical-Axis Wind Turbine with Pitch Control:* National Cheng Kung University, Taiwan; Trans Tech Publications, Switzerland 2012.
[52] Benedict M, Lakshminarayan V, Pino J, Chopra I: *Fundamental Understanding of the Physics of a Small-Scale Vertical Axis Wind Turbine with Dynamic Blade Pitching: An Experimental and Computational Approach,* Alfred Gessow Rotorcraft Center, University of Maryland, American Institute of Aeronautics and Astronautics, Inc, 2013.

12. WIND ENERGY AVAILABLE:

In specifying a wind turbine there must be a reliable source of wind energy available in a particular region. If not then the turbine will only be available for a small period of time. Also the wind speed available should be within a small range, as this will allow an electrical generator to be specified correctly; thus reducing unnecessary large initial costs of the system and minimising large electrical losses in operation.

Thus a Weibull distribution needed which would provide favorable conditions for an efficient wind turbine would include the following:

- A high probability of occurrence within a small range of wind speeds. (the Weibull curve is tall and narrow)
- Such wind speeds are high enough to provide enough power to be useful electrical energy. (The curve is further to the right in the higher electrical energy range).

The term used in the electrical power generation domain is the 'capacity factor'[53], which is the percentage of time that a wind energy park or turbine produces electricity during a typical year. Operating at the turbines nominal generation capacity Yasseri[49] recommended a load factor of 34-37% as acceptable.

Using the Weibull distribution in figure 63 of wind energy in the Nantes region and using a nominal wind speed of 5m/s the load factor for electrical energy produced will be roughly 14%. Well below the recommended value.

However as will be further explained in chapter 11, a new possible market and region has been proposed where favorable conditions are present and efficient, reliable electrical energy can be provided from the wind. Such energy is offshore and potentially on board a cargo ship.

Firstly why offshore; as this is definitely an industry trend, winds can be higher per unit area, unobstructed space is more easily available and any visual or noise impact on the population is reduced[54]. 71% of the world's land mass is offshore covered by oceans[55]. Ocean data has been mapped for many years with sources coming from satellites, ships and buoys. A map of a mean

[53] Yasseri S: *Economic profiling of wind energy*; Safe Sight technology, UK, RINA 2012.
[54] X Chen, Q Yu *DESIGN REQUIREMENTS FOR FLOATING OFFSHORE WIND TURBINES;* OMAE conference 2013, Nantes
[55] Ecole Centrale Nantes; Water, waves and sea state models part 1, lecture notes, 2013.

annual wind speed and surface pressure distribution plot was provided in Stewart's[56] publication in 2008 and is contained in figure 68 below.

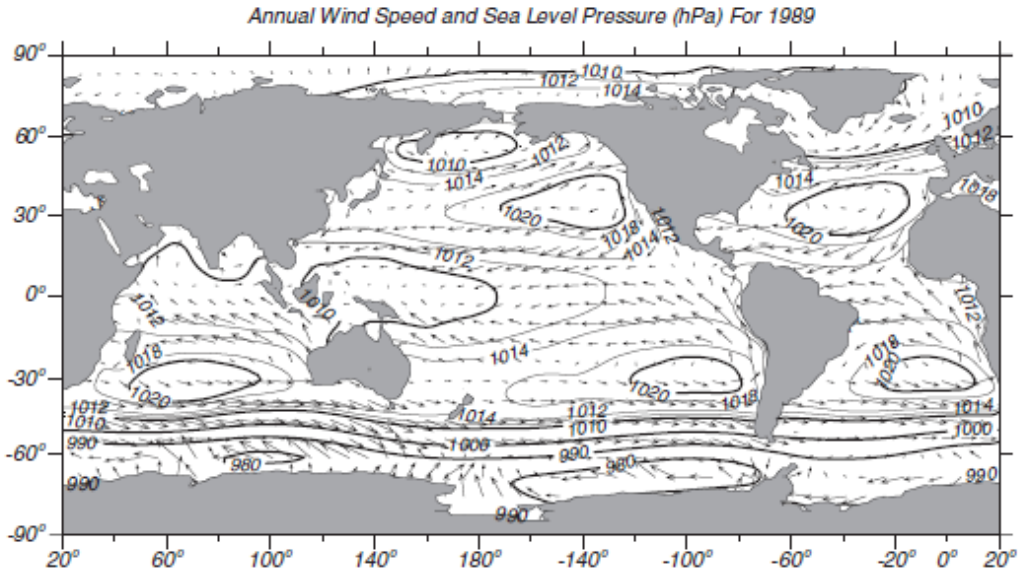

Figure 4.2 Map of mean annual wind velocity calculated from Trenberth et al. (1990) and sea-level pressure for 1989 from the NASA Goddard Space Flight Center's Data Assimilation Office (Schubert et al. 1993). The winds near 140°W in the equatorial Pacific are about 8 m/s.

Figure 68: 1989 world annual wind speed and sea level pressure calculation.

Actual specific wind velocity data will depend on the region but a mean value of wind over the ocean was estimated by Wentz[57] to be 7.4m/s.

From the brief analysis of references it can be concluded that available wind energy offshore is usually more predictable, constant and available at higher velocities than that of wind energy ashore.

The difficulty from industry has been in implementing fixed and floating platforms offshore and successfully transporting the energy to a grid distribution network ashore. However electrical power distribution of cargo ships does not contain such electrical transport and distribution problems.

Merchant shipping is often considered the lifeblood of the world economy, carrying some 90% of international trade[58] with the amount of trade carried increasing as quoted by the renowned world

[56] Stewart R: 'Introduction to physical oceanography'; Dept. of Oceanography, Texas A & M University, Sept. 2008.
[57] Wentz P, Peteherych S, Thomas L:' A model function for ocean radar cross sections at 14.6 GHz'. Journal of Geophysical Research 89 (C3): 3689–3704. 1984.
[58] Maribus; World ocean view; Hamburg; http://worldoceanreview.com/en/wor-1/transport/global-shipping/, site accessed Dec 2012.

ocean view magazine[59] by an average of 5.4% from 2000-2008, which led to a further drive in ship builds. The increase in large cargo ships built is shown in figure 69 below.

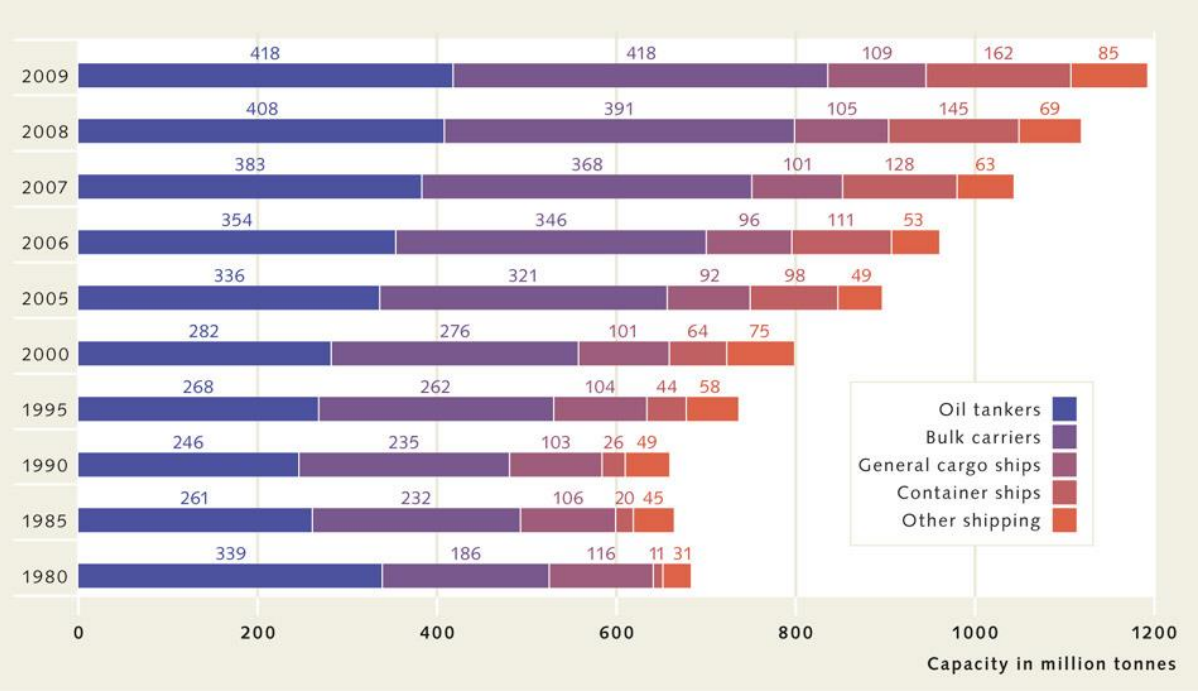

Figure 69: The growth of the world merchant fleet according to vessel type.

Not only does the shipping industry present such an important one in connecting the world economy, but it presents an operational profile that is very favorable for wind energy generation.
Large cargo ships travel at a constant designed speed often from a predetermined route from A to B. Thus the operational profile of a typical cargo ship involves cargo transportation, loading or unloading and a return route. A study of ships operational profiles conducted by Banks[59] in 2013 showed bulk carriers spend on average 75% of their time at sea, tankers 60-70% and container ships approx. 75%.
Thus the majority of the time the ships are at sea and while the ships are at sea the ships are moving at a speed into the wind. If no wind is available, then the air resistance over the ship's hull above the waterline and superstructure will be that of the ship speed. This could be classified as a constant wind speed for wind turbine generation.
This concept will be further analysed in chapter 13.

[59] Banks C, Turan O, Incoik A: *Understanding ship operating profiles with an aim to improve energy efficient ship operations;* Low carbon shipping conference, London, 2013; University of Strathclyde, UK.

13. SHIPPING INDUSTRY:

Wind turbine design starts with the wind. Wind energy needs to be available and available often enough to provide a reliable source of electrical energy with minimal efficiency losses.
In the theme of the EMSHIPS program; 'Advanced masters in ship design' there is a requirement to provide advanced competence related to the field of designing, building, operation and repairing of ships[60], the option of using a small VAWT on cargo ships to increase the ships energy efficiency was studied.

13.1 CONCEPT DESIGN STUDY:

Based on tools developed and knowledge gained on the limitations and capacities of a Darrieus type VAWT, a small study was conducted on the viability of using such turbines on cargo ships.
Four main cargo ship types were studied for wind turbine applications. These included the **Tanker,** the **Bulk carrier**, the **Container ship** and the **Ro-Ro ship**. Each was studied in terms of ship speed and available energy, hull design and general arrangements & electrical generator capacity and load. A brief overview of each ship type and reference material is contained in Annex G.
The aim of the wind turbine was to be used as a means of electrical power generation, so ships generators can be shut-down, reduced or installed capacity needed can be minimised so wind energy can provide some ships hotel load while on transit.
For each ship type an estimate of hotel load while on transit and total installed load was provided. Also an estimate of total wind energy available based on design ship speed and a wind allowance factor of 5m/s was calculated.
Note: Such an allowance factor was considered conservative considering the average at sea wind speed was found in section 11 to be 7.4m/s. However wind direction is also important and a specific figure will depend on local conditions and the ships route.

[60] Rigo P; *The thesis developed in the EMSHIP Program*: Distributed as part of the Erasmus Mundus program, EMSHIPS: Advanced Masters in Naval architecture, University of Liége, Belgium, 2014.

The assumptions made on design characteristics of the ship types studied are contained in Table 9.

Ship type	Size(Length)	Design Speed (kn)	Available wind (m/s)	With ocean allowance factor (5 m/s)	Sea hotel load (KWe)	Total installed capacity (KWe)
Tanker	180-300+ m	16,00	8,23	13,23	400,00	4000,00
Bulk carrier	115-300+m	15,00	7,72	12,72	300,00	2000,00
Container ship	150-350m	25,00	12,86	17,86	12000,00	15000,00
Ro-Ro ship (conventional)	150-200m	20,00	10,29	15,29	500,00	4000,00
Ro-Ro Catamaran.	130m	45,00	23,15	28,15	300,00	1500,00

Table 9: Design characteristics of various cargo ships

Data from table 9 came from a variety of sources. Ship speed data came from an online MAN Diesel publication[61], General arrangements and electrical information predominately was found in Taggarts[62] well known publication 'ship design and construction'. More specific electrical analysis of hotel loads of large reefer container ships came from Nielsen's[63] publication on 'Green ships of the future'.

Table 9 above provides a wind turbine designer with a nominal wind speed to design too; being the wind speed with the ocean allowance factor. Also an indication of electrical load and installed power in which the wind turbine will connect too is provided.

The study then involved an overview of the general arrangements of each ship type. The available deck space of each ship type was assessed and an estimate of the maximum size of a VAWT that could possibly be installed in front of the ships superstructure was provided.

Due to the side thrust developed by a VAWT it was proposed that a turbine must be installed in pairs so any side thrust developed will not impact on the ships steering, and to maintain ship symmetry. Also larger diameters were less desirable.

[61] MAN Diesel Propulsion trends in tankers; bulk carriers; container vessels; http//www.mandieselturbo.com/files/news/filesof11535/propulsion%20trends%20in%20tankers.htm.pdf. Accessed 20th Dec. 2013.
[62] Taggart R: Ship Design and Construction; the Society of Naval Architects & Marine Engineers, New York 1980.
[63] Nielsen B: *Green ship of the future*; 8500TEU Container ship green ship of the future concept study; Odense Steel Shipyard Ltd 2009.

Then using the program Q-blade an estimate was provided of the maximum power that could be generated from such a turbine. The results were then compared with the installed generator and hotel load information for each ship type.

An overview of the general arrangements of each ship type is contained in Annex F with some typical General Arrangements. Cargo ships are relatively slow speed displacement vessels. Weight influence of the installed turbine was neglected and ships motion on turbine performance was also neglected in the study.

Table 10 provides the results of the study with the maximum size of each turbine that could be installed and its generator capacity.

Ship type	Max. size possible	Location	Electrical power available (KW)	% of installed power	% of Hotel load
Tanker	2x D=2m, H=3m	Forecastle	6,00	**0,15**	1,50
Bulk carrier	2x D=5m, H=8m, 2x D=2m, H=3m	Amidships above ballast tanks & Forecastle	46,00	**2,30**	15,33
Container ship	2 x D=1,5, H=2,75	Forecastle	10,00	**0,07**	0,08
Ro-Ro ship (conventional)	2x D=1,5, H=2,75	Forecastle	6,00	**0,20**	1,20
Ro-Ro Catamaran.	2x D=2m, H=3m	Forecastle	56,00	**2,80**	18,67

Table 10: Overview of Wind turbine generator sizing and capacity per ship type.

It is acknowledged that such a study has concluded that by using a small wind turbine on cargo ships will not contribute to reducing the size of installed electrical generators. For all ship types the % of power available compared to the installed power is well below 5%.

This is the case for hotel load also. In all cases the wind turbine load available is below 20% of total hotel load There is potential for Bulk carriers and high speed Ro-Ro Catamarans to reduce some fuel consumption by using wind turbines, but it will never replace or supplement the majority of load taken by generators.

14. SHIPS WIND RESISTANCE:

As been discussed there is a large amount of known and predictable wind energy available at sea. The report has so far focused on using a VAWT to extract such energy into mechanical and then electrical power. However the study now focusses on flow interference, and using a turbine placed on a cargo ship to alter the wind flow and dissipate the energy away from a ships external hull surface to reduce a ships wind component of resistance and ultimately the fuel consumption of the vessel.

It was found that using small VAWT's as a means of electrical power generation while ships are on transit provided negligible net benefits to the ships operation. However the concept of reducing a ships wind resistance while at sea could provide more positive benefits.

The use of a small VAWT could be used to minimise ships wind resistance by pushing the wind energy away from the superstructure, reducing its velocity of impact on the superstructure and also potentially increasing the amount of turbulence flow in contact with the ships superstructure, which at the same Reynolds number actually will reduce frictional resistance.

The current designed VAWT contains a lot of turbulent flow. It is operating in the stall condition for 100% of its operation, and it will have a high level of blade tip losses and span wise flow due to the nature of flow of helicoidal Darrieus turbine blades. If placed in front of the ships superstructure the velocity flow over the ships superstructure would be disturbed.

The amount of such disturbance and its impact on ship's hull wind resistance, total ships resistance and eventually ships full consumption needs further investigation.

14.1 SHIPS WIND RESISTANCE STUDY:

Continuing the previous study in chapter 12 with the same ship types, we now consider the same turbines but their ability to reduce the wind resistance of the ships.

As discussed in chapter 12 there is a large amount of known wind energy available offshore. Predicting the impact of such energy on the resistance of ships is often a neglected task. Ships are

often designed for ideal conditions, and then a margin is added to account for high winds and heavy sea conditions. The margin added however usually adds to total ship installed power.
Wind resistance on ships can do 2 things.

- Increase the amount of power consumed by the main engine to maintain a speed profile.
- Reduce the ships speed and reduce the schedule arrival time.

Often it may actually do a combination of both, but this will depend on the particular ship type and how its propulsion was designed, how it is being operated and the priorities of the ship owner.

14.2 WIND ENERGY RESISTANCE PREDICTION:

Predicting the amount of extra resistance created by wind on a ships exterior hull and then translated into additional power needed on the main engine to maintain speed will depend on the following.

- Ships superstructure and area in contact with the wind;
- Wind speed and direction.
- Ships speed.

A numerical prediction model based on experimental results was published by Isherwood[64] in 1972 for discussion in the Royal Institute of Naval Architects magazine.
The paper provided a quick numerical method of predicting wind resistance depending on ship type and particulars, ship speed and wind direction relative to the ship.
The equations were intended to provide estimates of the wind forces and moments on a ship for use in trials and voyage analysis where no wind tunnel results are available. They are also broken down into the following ship types in table 11.

[64] Isherwood R : *Wind Resistance of Merchant Ships* ; Royal Institute of Naval Architects, 1972

1	Passenger ships and ferries
2	Cargo ships with engines amidships
3	Cargo ships with engines amidships, ballast
4	Cargo ships with engines aft, loaded
5	Cargo ships with engines aft, ballast.
6	Tankers and ore carriers with bridge amidships, loaded.
7	Tankers and ore carriers with bridge amidships, ballast.
8	Tankers and ore carriers with bridge aft, loaded.
9	Tankers and ore carriers with bridge aft, loaded.
10	Stern trawlers
11	Tugs

Table 11: Classification of ship types.

Equations and variables are contained in Annex F for reference. For the purposes of the study the mean value of independent variables was taken for each ship type.

Results were also taken with the wind at 0 degrees heading to the ship, so a worst case scenario.

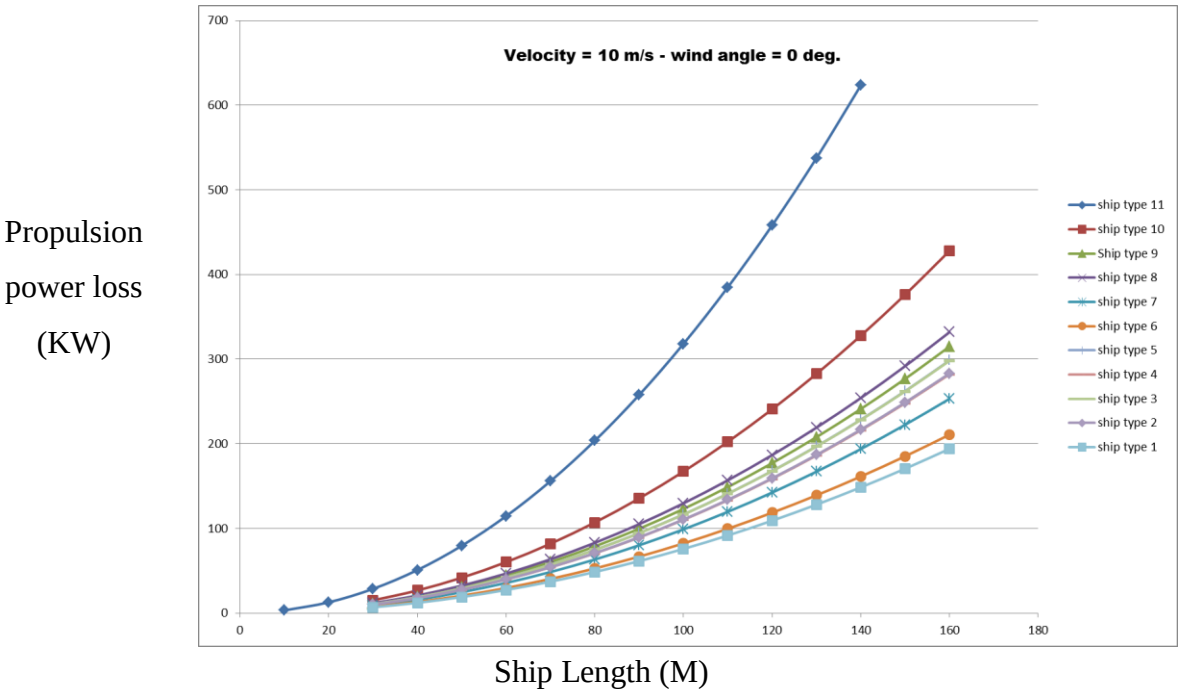

Figure 70: Power loss due to wind resistance – wind angle 0 degrees, relative wind velocity = 10m/s

Ship types 1, 4 and 8 were studied further at relative wind speeds of 15 & 20 m/s.

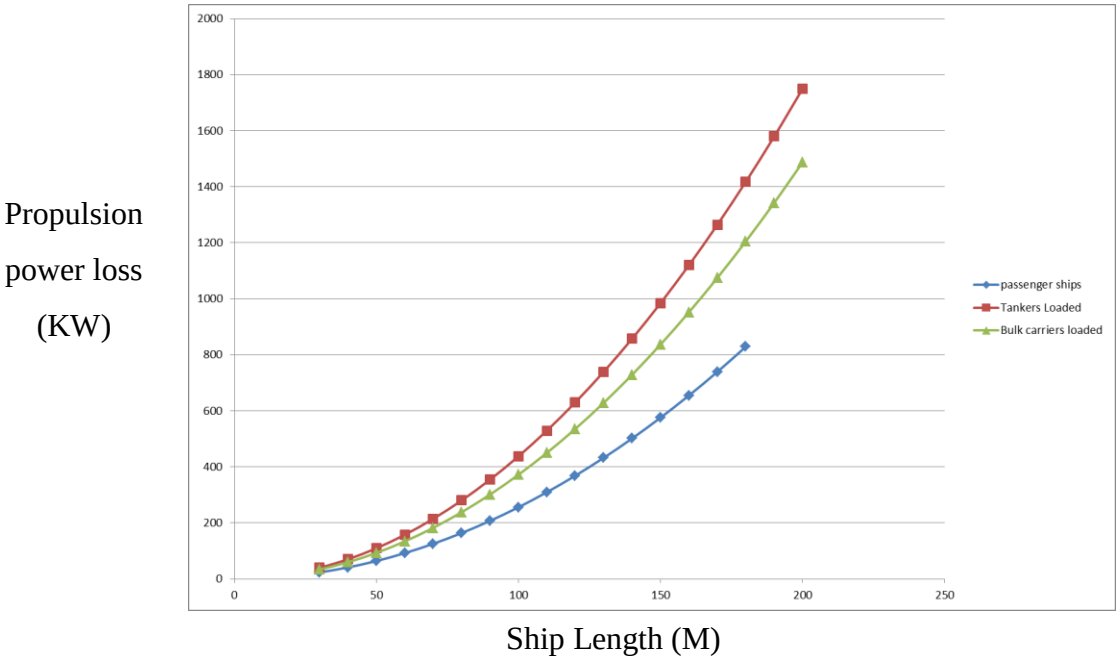

Figure 71: Power loss due to wind resistance – wind angle 0 degrees, relative wind velocity = 15m/s

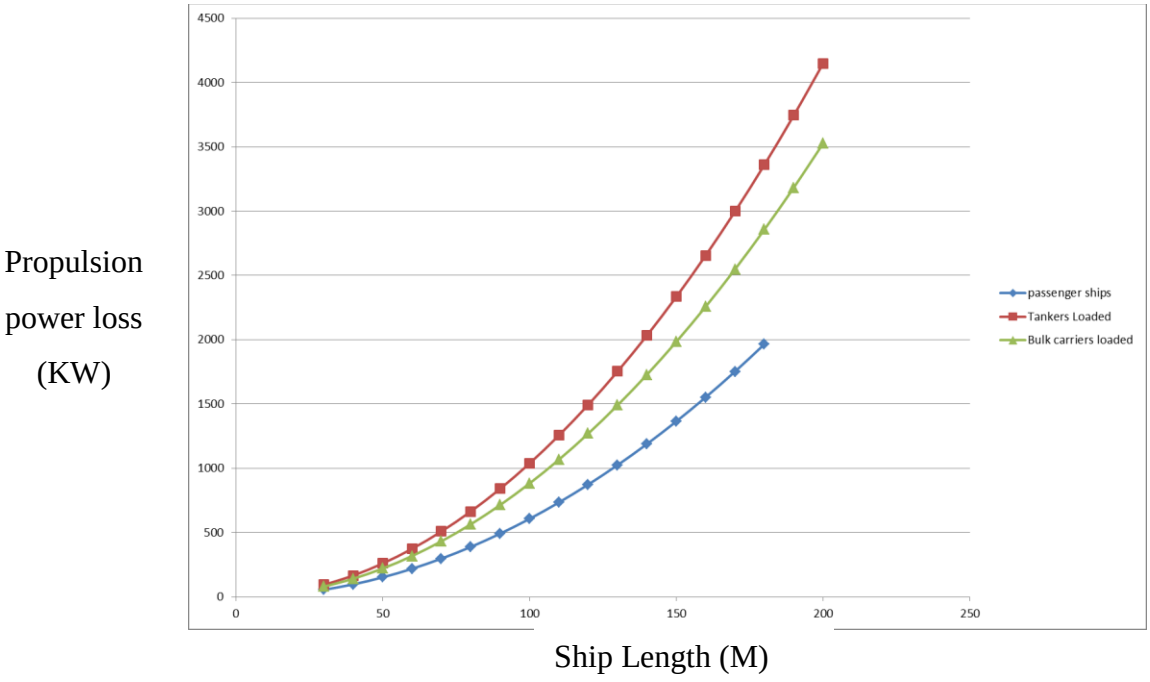

Figure 72: Power loss due to wind resistance – wind angle 0 degrees, relative wind velocity = 20m/s

The above study is based on a published numerical wind resistance tool that can be applied to a broad range of merchant ships. Values will differ for specific ships, but it provides a good order of magnitude of the amount of wind resistance a ship type may experience.

Worst case scenario in the head wind condition and a relative velocity of 20m/s is a propulsion power loss of 4000KW for tankers, 3500KW for bulk carriers and 2000KW for passenger ships. At a relative wind velocity of 10m/s which would be more common the power loss is 300KW, 250KW and 200KW. A considerable amount of power.

14.3 USING A VAWT TO REDUCE SHIP WIND RESISTANCE

The above analysis predicts the order of magnitude of the extra wind resistance on the ships exterior hull at a 0 degree heading angle with the wind. Results have then been converted to additional propulsion power needed to maintain the same speed and presented in figures 70, 71 & 72. A total propulsive loss of 55% was taken in converting thrust from the propeller load on the main engine.

The next step is to estimate the effect on such ship resistance by placing a small VAWT in front of the ships superstructure into the wind.

As an example if wind speed in the previous model is reduced to 5 m/s the amount of ship wind resistance is significantly reduced. This reduction is shown in figure 73 to be by a factor of 5-7 times for each ship type from 10m/s to 5/s. So for passenger ships a reduction from 200KW to 30KW; a 170KW reduction in propulsion power needed to maintain a ship speed.

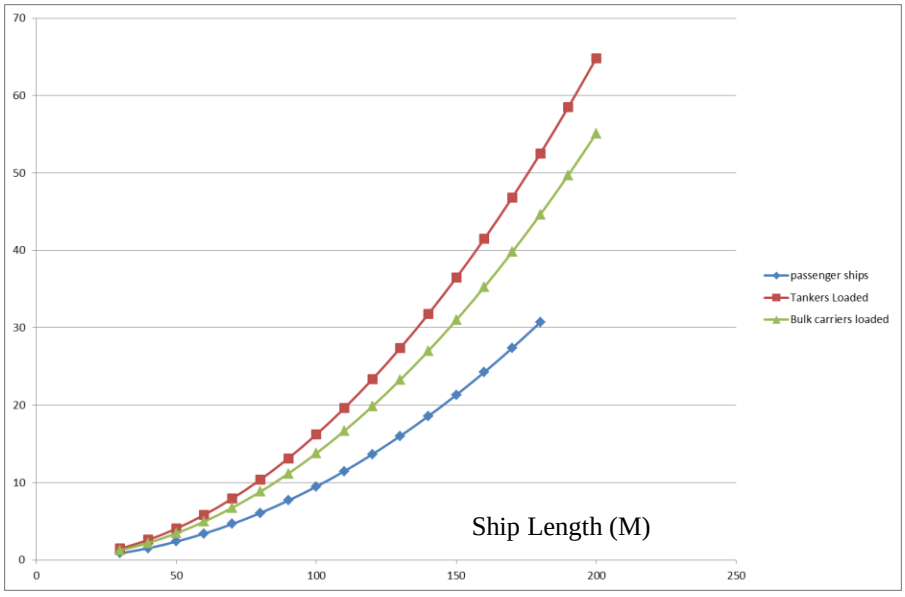

Figure 73: Power loss due to wind resistance – wind angle 0 degrees, relative wind velocity = 20m/s

This model is too simplistic for clear conclusions but this is an area for further investigation. It was intended from detailed model testing the loss in wind energy from a VAWT downstream of the turbine could be calculated. However model testing occurred to late in the project and the analysis was not possible.

The investigation however is certainly recommended for future work.

Already StenaLines is trialing this very concept; both to reduce ship resistance and to generate a small amount of electricity while the ship is under way.[65]

Figure 74: VAWT placed in the front of the superstructure to reduce air resistance & for power generation.

[65] Todd T, *Stena hopes for wind turbines pay-off*, Maritime Journal, July 2011, articehttp://www.maritimejournal.com/news101/vessel-build-and-maintenance/vessel-repair-and-maintenance/stena-hopes-for-wind-turbines-pay-off

15. CONCLUSIONS:

There is no doubt aerodynamic flow over a VAWT is complicated and difficult to predict. A good understanding of the flow phenomena, prediction tools and design drivers has been developed, predominately aimed at aerodynamic optimisation

15.1 AERODYNAMICS AND AEROJOULES:

Understanding such aerodynamics is crucial to optimising a design. Maximum power coefficients can be achievable and areas of potential unsteady flow can be avoided. Designing to operate in regions inside the stall angle of attack (avoiding stall phenomena) is optimal for power extraction, and will help avoid unsteady structural loading and allow the generator to obtain a more reliable and predictable flow of power.

In designing a VAWT it is critical to understand the aerodynamic theory of blade foils. Two simple phenomena need to be managed for optimal aerodynamic flow and turbine dimensioning.

- Blade tip speed ratio needs to be high enough to avoid stall phenomena occurring on the blades.
- Interference effects between blades needs to be managed with a good understanding of the blade wake, turbine radius and rpm.

Often these two values are conflicting with the need for a higher blade tip ratios to avoid stall and a lower blade tip speed ratio to avoid interference. Other effects such as tip speed losses due to span wise pressure differentials need to be considered also; in particular for a helicoidal VAWT such as Aérojoules.

Helicoidal blades in a VAWT do provide complications in flow dynamics, with differing angles of attack along the span of a blade and stall phenomena occurring at any instant in time. For such a VAWT design it seems critical to operate at a blade tip speed ratio avoiding stall.

15.2 PREDICTION TOOLS:

A good understanding of current VAWT aerodynamic prediction tools has been developed.

The use of empirical methods such as the Blade Element Momentum method presented provide simple assessment, allowed a good understanding of the turbine wind interaction and provided

rapid assessment to optimise a turbine design. If such simple methods could be coupled with more detailed assessments of foil blade wake and its interaction between turbine blades, and tip speed losses and incorporated into the model then an accurate, quick and low cost means of turbine assessment is available.

The use of Q-blade which is such a tool designed for rapid assessment based on simple input design criteria, seems to incorporate such methods; with the ability to input individual blade data into the program, based on experimental or CFD results.

The next step is too incorporate such tools in other areas of the turbine design. Such as vibration analysis, noise assessment and structural analysis.

CFD analysis on a VAWT design must be conducted in 3D. Flow phenomena is often unsteady and 2D results have been proven to be unreliable.

In performing a CFD calculation the use of Reynolds Averaged Navier Stokes (RANS) equations in averaging the large and small eddies in the flow is also not appropriate. The RANS method does not accurately represent the wake of a turbine blade, which is critical to understanding interference effects between blades.

Performing a Large Eddy Simulation on a simple static airfoil did provide a good representation of the flow phenomena with both experimental results and published articles. It seems LES can accurately predict air foil wake, and could be a useful tool in the future for VAWT blade analysis. LES however needs a lot of computer hardware and simulation time. Its use was restricted to simple static foil calculations, and simulation time was excessive.

The use of LES combined with simple experimental results in the ICAM wind tunnel for validation of various air foil blades is an area for study in the future.

15.3 FUTURE EXPERIMENTAL WORK:

The ICAM wind tunnel could be used to simulate the rotational flow of a VAWT in the static condition, by altering the blade angle of attack by the use of a stepper motor. By the use of a frequency convertor a VAWT blade can be simulated statically with varying speed and also angle of attack. By the use of a stepper motor the blade angle of attack change can occur in real time.

This will also allow an understanding of dynamic stall, and an assessment of power loss in changing the blade pitch angle of a turbine.

As theoretical predictions confirm that by controlling the blade pitch angle over a rotation could potentially increase the operating speed range of a VAWT and also its power coefficient. Further investigation is desired.

In the real scale test it is recommended to attempt to operate the turbine at a higher rpm, by the use of an electric motor. By monitoring the load on the motor over a speed profile may provide a good insight into the VAWT aerodynamics. As potentially the turbine needs a power device to operate through the stall condition, then post stall its aerodynamics may be more favorable. However the effects of interference between blades may prevent such an occurrence.

A good comparison between the model test and the prediction tool Q-blade is also desirable.

15.4 FUTURE STUDIES:

Some future studies have been proposed relating to both the Aérojoules project and the wider marine industry.

Firstly a thorough real scale model test being conducted in Jan 2014 will provide some further insight into the turbine performance. By applying load on the turbine and studying the loads up to a blade tip speed ratio above stall then a good understanding of the effects of stall and interference can be assessed. Potentially the turbine needs an extra power source to move through the static stall angle. A salvonius turbine is proposed but this will depend on the additional power needed.

A good understanding of the effects of stall and blade encountered vibration and noise dissipation need further assessment. As to decrease stall encounter, blade tip speeds need to increase for a given diameter. It is unclear which is more prominent tip speed or stall phenomena for turbine noise and vibration.

Also a small study was conducted on the merits of using such a turbine on board various cargo ships whilst underway. The turbine was assessed as an electrical generator and as a means to reduce the ships wind resistance. Its seems there is great potential to use such a device to reduce a cargo ships wind resistance and subsequent fuel consumption. Further analysis is recommended.

16. DECLARATION OF AUTHORSHIP

Declaration of Authorship

I declare that this thesis and the work presented in it are my own and have been generated by me as the result of my own original research.

Where I have consulted the published work of others, this is always clearly attributed.

Where I have quoted from the work of others, the source is always given. With the exception of such quotations, this thesis is entirely my own work.

I have acknowledged all main sources of help.

Where the thesis is based on work done by myself jointly with others, I have made clear exactly what was done by others and what I have contributed myself.

This thesis contains no material that has been submitted previously, in whole or in part, for the award of any other academic degree or diploma.

I cede copyright of the thesis in favour of l'Institut Catholique d'Arts et Métiers (ICAM), Nantes.

Date: ***20/01/2014*** *Signature:* ***Michael O'Connor***

17. ACKNOWLEDEGEMENTS:

This thesis was developed in the frame of the European Master Course in “Integrated Advanced Ship Design” named “EMSHIP” for “European Education in Advanced Ship Design”, Ref.: 159652-1-2009-1-BE-ERA MUNDUS-EMMC.

I would like to acknowledge the EMSHIP programme and the opportunity to participate in such a diverse program. I have met many friends and industry contacts that I’m sure I will maintain for life. Also bringing together a network of international knowledge focussed on the marine industry is impressive and great to be a part of.

I thank the ICAM staff for their professionalism and friendliness. In particular to professor Le Sourne for the opportunity to study at ICAM and my supervisor Mr Jean François Largeau; your advice and input especially when needed most; when presenting results and concluding this report was appreciated.

Jose & Andreas; it was a pleasure to study with you in Nantes.

To Hélène; thanks for bringing me to France. It has been a wonderful experience.

18. REFERENCES:

1. Sutherland H, Berg D, Ashwill T; A *Retrospective of VAWT Technology,* Sandia National Laboratories, New Mexico, 2012.
2. Paraschivoiu I, *Wind Turbine Design – With Emphasis on Darrieus Concept,* Presses internationals Polytechnique, Québec, Canada,2009.
3. Bottero C , *Aérojoules project: Vertical Axis Wind Turbine;* Master's Thesis; 'EMSHIP' program in 'Integrated Advanced Ship Design', West Pomeranian University of Technology, Szczecin, 2011.
4. Breluzeau J, *Projet collaboratif Aérojoules : une éolienne 300 W sur le marché en 2012...*, Océan Vital Fondation, 11/04/2012, http://www.fondationoceanvital.com/Actualites/Projet-collaboratif-Aerojoules-une-eolienne-300-W-sur-le-marche-en-2012. (Accessed 26 June 2013).
5. J Auxiette, *The tide is turning for marine renewable energy in the French region pays de la Loire*; http://www.mre-paysdelaloire.com/presentation/ , Pay de la Loire regional council, June 2013. (Accessed June 26 2013).
6. ADEMA, '*French know how in the field of RENEWABLE ENERGIES'*, French Environment and Energy Management Agency, Angers, April 2012, pg. 2. (Accessed 26 June 2013).
7. Georgescu A, *'Introductory course to offshore wind turbines'*, University of Liege, 10th December 2012, Liège, slide 3
8. Manwell J, McGowen J, Roger A; *Wind energy explained: Theory, design & application*, 2nd edition, John Wiley & sons ltd, 2009,pg 1,2
9. Paraschivoiu I; *Wind Turbine Design – With Emphasis on Darrieus Concept*, Presses internationales Polytechnique, 2009, Canada, pg. 1,2
10. Ashwill T, Berg D, Sutherland H ; *A retrospective of VAWT technology*, SANDIA report, SAND2012-0304, Sandia National laboratories, California, USA, Jan 2012, pg. 13
11. Ashwill T, Berg D, Sutherland H ; *A retrospective of VAWT technology*, SANDIA report, SAND2012-0304, Sandia National laboratories, California, USA, Jan 2012, pg. 13
12. Manwell J, McGowen J, Roger A; *Wind energy explained: Theory, design & application*, 2nd edition, John Wiley & sons ltd, 2009,pg 10

13. G.J.M. Darrieus, Turbine Having Its Rotating Shaft Transverse to the Flow of Current, U.S. Patent #1834018, December, 1931.
14. Sutherland H, Berg D, Ashwill T; A Retrospective of VAWT Technology, Sandia National Laboratories, New Mexico, 2012,pg 14.
15. Johnson G; Wind Energy Systems, electronic edition, Manhatton KS, May 2005, pg. 26.
16. Worstell, M. H.: *Aerodynamic Performance of the 17- Metre-Diameter Darrieus Wind Turbine*, Sandia Laboratories Report SAND78-1737, January 1979.
17. Johnson G; Wind Energy Systems, electronic edition, Manhatton KS, May 2005, pg. 26
18. Paraschivoiu I; *Wind Turbine Design – With Emphasis on Darrieus Concept*, Presses internationales Polytechnique, 2009, Canada, pg. 29.
19. Sutherland H, Berg D, Ashwill T; *A Retrospective of VAWT Technology,* Sandia National Laboratories, New Mexico, 2012,pg 14.
20. Manwell J, McGowen J, Roger A; *Wind energy explained: Theory, design & application*, 2nd edition, John Wiley & sons ltd, 2009, pg. 20.
21. Bottero C **,** *Aérojoules project: Vertical Axis Wind Turbine;* Master's Thesis; 'EMSHIP' program in 'Integrated Advanced Ship Design', West Pomeranian University of Technology, Szczecin, 2011. Pg. 76
22. Klimas P, *Darrieus Rotor Aerodynamics*, Sandia National Laboratories, Advanced Energy Projects Division, Albuquerque, USA
23. Beri H, Yao Y**:** *Double Multiple Stream Tube Model and Numerical Analysis of Vertical Axis Wind Turbine* ; Department of Manufacturing and Automation, Harbin Institute of Technology, Harbin, China, published May 2011, (http://www.SciRP.org/journal/epe)
24. Ragheb M, Ragheb A:*Wind Turbines Theory - The Betz Equation and Optimal Rotor Tip Speed Ratio, Fundamental and Advanced Topics in Wind Powe*r, Dr. Rupp Carriveau (Ed.), ISBN: 978-953-307-508-2,2011; InTech, Available from: http://www.intechopen.com/books/fundamental-and-advanced-topicsin-wind-power/wind-turbines-theory-the-betz-equation-and-optimal-rotor-tip-speed-ratio
25. Gerontakos P, Lee T: *Investigation of flow over an oscillating airfoil;* Department of Mechanical Engineering, McGill University, Montreal, Canada. J. Fluid Mech. (2004), vol. 512, pp. 313–341. 2004 Cambridge University Press

26. Gerontakos P, Lee T: *Investigation of flow over an oscillating airfoil;* Department of Mechanical Engineering, McGill University, Montreal, Canada. J. Fluid Mech. (2004), vol. 512, pp. 313–341. 2004 Cambridge University Press
27. Wang S, Ingham D, Ma L, Pourkashanian M, Tao Z: *Turbulence modelling of deep dynamic stall at relatively low Reynolds number:* Journal of fluids and structures, science direct, 2012 Elsevier Ltd.
28. Fujisawa N, Shibuya S; *Observations of dynamic stall on darrieus wind turbine blades*. Journal of Wind Engineering and industrial Aerodynamics, 2001, pg. 201-214.
29. Ghods M: *THEORY OF WINGS AND WIND TUNNEL TESTING OF A NACA 2415 AIRFOIL:* Technical Communication for Engineers, University of British Columbia, July 2001. http://www.ewp.rpi.edu/hartford/~ferraj7/ET/Other/References/Ghods2001.PDF; accessed Dec 14, 2013.
30. Gerontakos P, Lee T: *Investigation of flow over an oscillating airfoil;* Department of Mechanical Engineering, McGill University, Montreal, Canada. J. Fluid Mech. (2004), vol. 512, pp. 313–341. 2004 Cambridge University Press
31. Visonneau V, Funck J : Project Aérojoules – Rapport phase A1; ICAM, Rapport de mémoire Scientifique,2013.
32. Chung T, *Computational Fluid Dynamics*, Cambridge University Press 2002
33. Le Touzé D; *An intro to Computational Fluid Dynamics*, 2013 EMSHIPS course notes, Ecole Centrale Nantes, France
34. Launder B, Spalding D; *The numerical computation of turbulent flows: Computer methods in applied mechanics and Engineering*, Imperial College of Science & Technology, London, 1974.
35. Ferziger J, Peric M*; Computational Methods of Fluid Dynamics*, 3rd edition, Springer, 2002.
36. Wilcox D; *Turbulence modeling for CFD*, DCW Industries Inc, California, 2006.
37. DeGennero M*; Computational Fluid Dynamics and Computational Aeroacoustics for Turbomachinery Applications with emphasis on High-Speed Propellers and Vertical Axis Wind Turbines*, Universita Degli Studi Di Napoli Federico II, 2010.

38. Shih T, Liou W, Shabbir A, Yang Z, Zhu J*; A new k-epsilon eddy viscosity model for high Reynolds number turbulent flows: model development and validation. Computers & Fluids*, USA National Aeronautics & Space Administration, 1994. Pg. 227-238.
39. Spalart P, Allmaras S; *A one-equation turbulence model for aerodynamic flows*, AIAA Paper 92-0439.
40. Ribeiro A, Awruch A, Gomes H: *An airfoil optimization technique for wind turbines*, Graduate Program in Mechanical Engineering, Federal University of Rio Grande do Sul, Brazil. SciVerse, science direct, 30 Dec 2011.
41. Baillergeau D; *Vertical Axis Wind Turbines: Aérojoules project*. ICAM, Nantes, France, 04/07/2013.
42. Paraschivoiu I, *Wind Turbine Design – With Emphasis on Darrieus Concept,* Presses internationals Polytechnique, Québec, Canada,2009. Pg. 35.
43. Chung T, *Computational Fluid Dynamics*, Cambridge University Press 2002.
44. V. Kitsios, R. k. Numerical simulation of lift enhancement on a NACA airfoil using ZNMF jets. *Center forTurbulence Research proceedings of the summer program,* 2006.
45. Gaitonde U; *Quality Criteria for Large Eddy Simulation*: University of Manchester, school of MACE, May 2008.
46. Gaitonde U; *Quality Criteria for Large Eddy Simulations*, University of Manchester, May 2008.
47. Visonneau V, Funck J : Project Aérojoules – Rapport phase A1; ICAM, Rapport de mémoire Scientifique,2013.
48. Aubrée R, Auger F, Dai P : *A new low-cost sensorless MPPT algorithm for small wind turbines*: LUNAM Université, IREENA, Saint-Nazaire, France, LUNAM Université, ICAM, Nantes, France
49. Paraschivoiu I, *Wind Turbine Design – With Emphasis on Darrieus Concept,* Presses internationals Polytechnique, Québec, Canada,2009, page 16.
50. Chen J: 'Vertical Axis Small Wind Turbine Breakthrough and Small Wind Turbine Application Limit'; HIVAWT, 2009 US-Taiwan High Technology Forum | Clean Energy conference, 2009.

51. Miau j, Liang S, Yu R, Hu C, Leu T, Cheng J, Chen S: *Design and Test of a Vertical-Axis Wind Turbine with Pitch Control:* National Cheng Kung University, Taiwan; Trans Tech Publications, Switzerland 2012.
52. Benerdict M, Lakshminarayan V, Pino J, Chopra I: *Fundamental Understanding of the Physics of a Small-Scale Vertical Axis Wind Turbine with Dynamic Blade Pitching: An Experimental and Computational Approach,* Alfred Gessow Rotorcraft Center, University of Maryland, American Institute of Aeronautics and Astronautics, Inc, 2013.
53. Yasseri S : *Economic profiling of wind energy*; Safe Sight technology, UK, RINA 2012.
54. X Chen, Q Yu *DESIGN REQUIREMENTS FOR FLOATING OFFSHORE WIND TURBINES;* OMAE conference 2013, Nantes
55. Ecole Centrale Nantes; Water, waves and sea state models part 1, lecture notes, 2013.
56. Stewart R: 'Introduction to physical oceanography'; Dept. of Oceanography, Texas A & M University, Sept. 2008.
57. Wentz P, Peteherych S, Thomas L:' A model function for ocean radar cross sections at 14.6 GHz'. Journal of Geophysical Research 89 (C3): 3689–3704. 1984.
58. Maribus; World ocean view; Hamburg; http://worldoceanreview.com/en/wor-1/transport/global-shipping/, site accessed Dec 2012.
59. Banks C, Turan O, Incoik A: *Understanding ship operating profiles with an aim to improve energy efficient ship operations;* Low carbon shipping conference, London, 2013;University of Strathclyde,UK.
60. Rigo P; *The thesis developed in the EMSHIP Programme*: Distributed as part of the Erasmus Mundus program, EMSHIPS: Advanced Masters in Naval architecture, University of Liége, Belgium, 2014.
61. MAN Diesel Propulsion trends in tankers; bulk carriers; container vessels;http//www.mandieselturbo.com/files/news/filesof11535/propulsion%20trends%20in%20tankers.htm.pdf. Accessed 20th Dec. 2013.
62. Taggart R: Ship Design and Construction; the Society of Naval Architects & Marine Engineers, New York 1980.
63. Nielsen B: *Green ship of the future*; 8500TEU Container ship green ship of the future concept study; Odense Steel Shipyard Ltd 2009.

64. Isherwood R: *Wind Resistance of Merchant Ships*; Royal Institute of Naval Architects, 1972.
65. Todd T, *Stena hopes for wind turbines pay-off*, Maritime Journal, July 2011, articehttp://www.maritimejournal.com/news101/vessel-build-and-maintenance/vessel-repair-and-maintenance/stena-hopes-for-wind-turbines-pay-off

19. APPENDICES

19.1 ANNEX A: EXPERIMENTAL RESULTS.

Tools:

A wind tunnel is used in a horizontal direction which ensures a constant velocity around the cylinder. A maximum velocity of 40m/s can be obtained. It contains a 2 speed motor, where speeds of 20 m/s and 40 m/s are desired.

The wind tunnel contains:

- A 2 speed electric motor providing wind speeds of approx. 20m/s & 40 m/s.
- A glass tunnel area for testing and visualization of flow with an area of 0.2x0.2m.
- A Pitot tube connected to a differential manometer gives a measurement of :
    - $P_{A'}-P_{\infty} = P_A-P_{\infty}$
- The static pressure probe S of the Pitot tube (measuring P_{∞}) and pressure probe M of the cylinder (measuring P) are connected to another differential manometer giving ($P - P_{\infty}$)
- The differential manometers give a pressure difference in mm WC.
- The static pressure probe S of the Pitot tube (measuring P_{∞}) and pressure probe M of the cylinder (measuring P) are connected to another differential manometer giving ($P - P_{\infty}$)
- Strain gauge: delta lab 38340 strain gauge balance conditioner. By using the resistance measurement in a Wheatstone bridge arrangement, lift and drag forces can be calculated.

19.1.1 Experiment 1: Obtain lift & drag coefficients.

Density	1,2041	kg/m
Temperature	20	deg
Foil span	0,022	m
Target wind velocity	20	m/s

Table 12: Initial conditions

Devices:

- Delta lab 38340 strain gauge balance conditioner.
- 0.2mx0.2m - 20 m/s wind tunnel

Blade 0012 results:

Blade 1: **Rough surface**

Test 1:

Angle (deg.)	5	10	15	20	0
Lift (N)	-4,62	-6	-5	-4,6	-0,72
Drag (N)	0,35	1	1,6	2,05	0
Cl	0,74	1,00	0,81	0,73	
Cd	0,07	0,19	0,30	0,39	0,00

Table 13: NACA0012 rough surface foil – lift and drag coefficients test 1.

initial values no wind	
Drag (N)	0
Lift (N)	-0,72

Table 14: Initial strain gauge readings.

Test 2:

Angle (deg)	5	10	12	14	16	18	20	0
Lift (N)	2,7	4,5	4,6	4,5	4,3	4	3,85	-0,2
Drag (N)	0,03	0,5	0,65	0,98	1,2	1,4	1,6	0
Cl	0,55	0,89	0,91	0,89	0,85	0,79	0,76	0,00
Cd	0,01	0,09	0,12	0,18	0,23	0,26	0,30	0,00

Table 15: NACA0012 rough surface foil – lift and drag coefficients test 2.

initial values no wind	
Drag (N)	0
Lift (N)	-0,2

Table 16: Initial strain gauge readings.

Test 3:

angle	0	0	5	10	13	15	13
Lift (N)	-3,45	-0,22	3,35	4,95	5,15	4,95	5,05
Drag (N)	0	0,17	0,14	0,2	0,55	0,9	0,9
Cl	-0,61	0,00	0,67	0,97	1,01	0,97	0,99
Cd	0,00	0,03	0,03	0,04	0,10	0,17	0,17

Table 17: NACA0012 rough surface foil – lift and drag coefficients test 3.

Test 4: Attempt at 40m/s

angle	13
Lift (N)	20,95
Drag (N)	2,8
Cl	3,99
Cd	0,53

Table 18: NACA0012 rough surface foil – lift and drag coefficients at 40m/s.

initial values no wind	
drag	0
Lift	-0,2

Table 19: Initial strain gauge readings.

Notes:

- At a wind speed of 40m/s there was too much vibration on the blade to have an accurate result. Also interference effects are likely.
- Very erratic results were obtained at lift coefficients in the stall condition (above 13 degrees). The lift and drag forces are constantly fluctuating.

Blade 2**: Smooth surface:**

pressure	30,00	30,00	29,50	29,00	29,00	29,00	28,00	27,50	27,00	27,00	27,00	25,00	24,00
angle	0,00	2,00	4,00	6,00	8,00	10,00	12,00	13,00	14,00	15,00	16,00	18,00	20,00
lift	-2,41	-1,41	-0,70	1,55	2,25	3,55	4,55	4,50	4,60	4,60	2,00	3,80	2,77
drag	0,00	0,27	0,29	0,28	0,32	0,35	0,40	0,45	0,50	0,56	0,64	0,98	1,10
Cl	-0,32	-0,13	0,00	0,43	0,56	0,81	0,99	0,99	1,00	1,00	0,51	0,85	0,66
Cd	0,00	0,05	0,05	0,05	0,06	0,07	0,08	0,08	0,09	0,11	0,12	0,18	0,21
V(pitot tube)m/s	22,32	22,32	22,14	21,95	21,95	21,95	21,57	21,37	21,18	21,18	21,18	20,38	19,97

Table 20: NACA0012 smooth surface foil – lift and drag coefficients test 1.

initial values no wind	
Drag(N)	0
Lift (N)	-0,2

Table 21: Initial strain gauge readings.

Blade 3: **Blade 2415 results.**

Pitot tube reading.	30,00	29,00	29,00	29,00	29,00	28,50	28,00	27,50	26,00	25,00	24,00
Angle (Deg.)	0,00	2,00	4,00	6,00	8,00	10,00	12,00	14,00	16,00	18,00	20,00
Lift (N)	-1,50	-0,75	-0,30	2,40	3,40	4,00	4,62	4,80	4,60	2,95	3,10
Drag (N)	0,18	0,18	0,19	0,21	0,23	0,32	0,41	0,50	1,00	1,50	1,80
Cl	0,08	0,20	0,27	0,69	0,85	0,96	1,08	1,13	1,16	0,90	0,97
Cd	0,03	0,03	0,03	0,03	0,04	0,05	0,07	0,08	0,17	0,27	0,34
V (m/s)	22,32	21,95	21,95	21,95	21,95	21,76	21,57	21,37	20,78	20,38	19,97

Table 22: NACA2415 smooth surface foil – lift and drag coefficients test 1.

initial values of strain gauge (no wind)	
Drag (N)	0
Lift (N)	-2,02

Table 23: Initial strain gauge readings.

Notes:

- Very erratic results were obtained at lift coefficients in the stall condition (above 13 degrees). The lift and drag forces are constantly fluctuating.
- The smooth blade surface tended to over predict the lift coefficient between 12 and 16 degrees.
- The smooth blade also increased the stall angle.

19.1.2 Experiment 2: Obtain turbine flow characteristics:

The following two methods were utilised to understand better the turbine flow characteristics, especially the turbine wake and turbulence regions. A NACA 0012 airfoil was utilized.

String method:

- It is proposed to use string on the low pressure side of a fixed turbine blade at various chord lengths along the blade to better understand the flow conditions.
- Also string was used on a steel rod at various horizontal and vertical distances from foil to obtain a flow direction at a set distance from the foil blade.

Hot-wire anemometry

- To better understand the speed of the flow a test 490 manual hot-wire anemometer was used at various horizontal and vertical distances from the foil.

Ink:

- Ink droplets were utilized over the blade low pressure surface to better understand the vortex bubble created at various angle of attacks along the blade.

String method:

Predicting Surface flow:

String was initially trialed as shown in the figure 75 below to better understand the surface flow at various points on the blade. It became difficult to accurately stick the string to the blade surface and interference became apparent between the strings. Good predictions were obtained at angles of 0 and 2 degrees. But 4 degrees and above the flow is too erratic. As shown in the proceeding results, a better method for predicting surface flow was using ink droplets and using a piece of string on a steel rod.

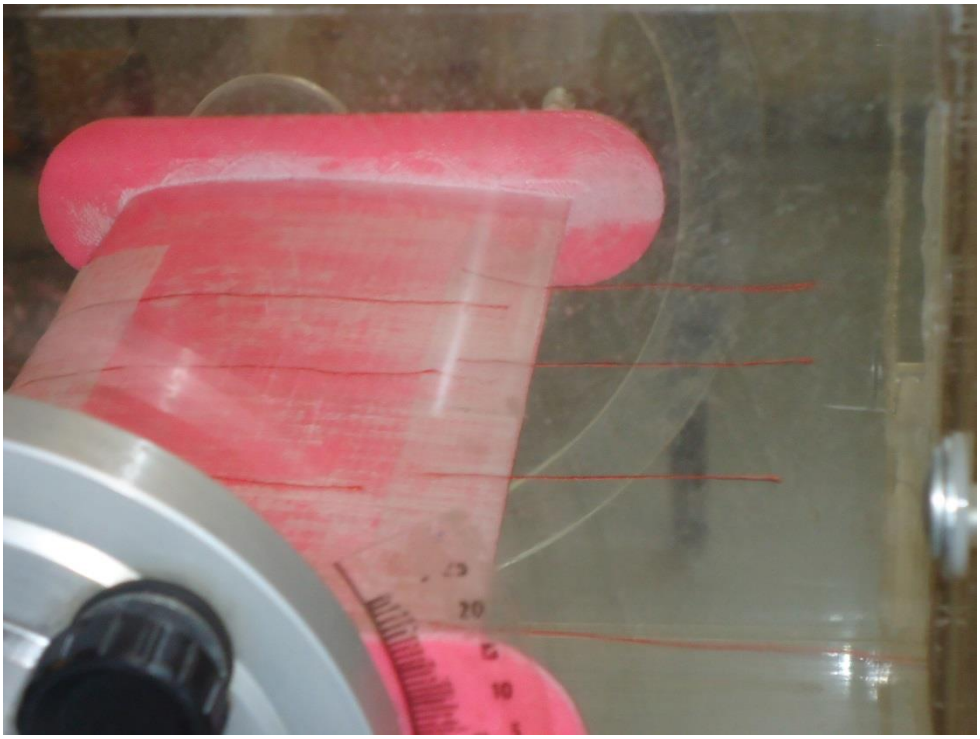

Figure 75: Straight flow: 2 degree angle of attack.

String was placed on a metal rod and put in the slipstream as shown in the figure 76. Using this method the string could be easily moved a distance from the blade to understand the flow direction at various distances along the blade and heights above the low pressure surface.

This method could provide a much quicker representation of the flow at various angles of attack and at various flow points in the spatial domain.

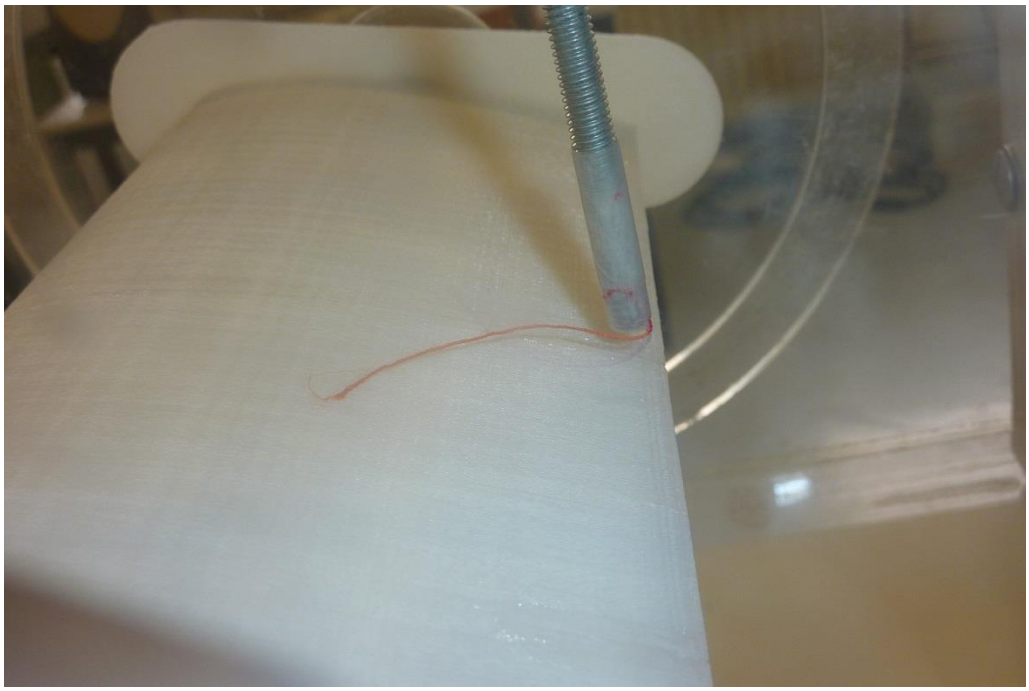

Figure 76: Steel rod method.

Angle of attack	pita tube pressure	Flow point 3	Flow point 4	flow point 4
0	30			straight - slightly up- (5 degrees)
2	30	5 - 10 degrees - straight flow.	on blade to 3cm above blade - very turbulent - velocity in other direction ; above 3 cm - mean of 10 degrees	2cm below blade is vibrating with a mean angle of 10 deg ; 1cm below blade - 2 cm above blade - is perfectly straight ; 2-4cm above blade, is vibrating at 45degrees : above 4cm - vibrating with a mean angle of 10 deg
4	**29,5**	10 degrees - some vibration at the tip	0-1 cm cotton straight - 1-6cm heavy vibration - turbulence- above 6 cm - 15 degree flow.	3 cm above blade - turbulence vibration. Quite straight until 2 cm below blade - 10 degrees - some vibration.
6	29	20 degrees - tip vibration - similar the distance above the blade	0-4cm large turbulence - negative velocity - above 4 cm : 20 degrees flow.	1 cm below blade - tip vibration - between 1 - 5 cm the thread is quite straight - excessive vibration above 5 cm
8	29	Tip vibration above blade. above 3 cm angle of 30 degrees with most tip vibration.	1 cm above excessive vibration and negative velocity. 2 cm above 30 degree angle and tip vibration.	Excessive vibration from 4cm below up to 6 cm above blade.

10	29	Excessive turbulence - reverse velocity 0-1cm. Above 1 cm tip vibration but not excessive.	45 degrees and excessive tip vibration all the way.	Tip vibration all the way but not excessive
12	28	Excessive turbulence - reverse velocity 0-1cm. Above 1 cm tip vibration but not excessive.	0-4cm above blade - turbulence - reverse flow. 4 cm above - 20 degrees - tip vibration	Excessive vibration 5 cm above blade - also 5 cm below blade - interference effects I think. Tip vibration between 5 - -5.
14	27	0-2cm turbulence - above 2 cm - just tip vibration.	0-4cm above blade - turbulence - reverse flow. 4 cm above - 20 degrees - tip vibration	10 degrees - some tip vibration but minimum. Interference effects above and below 5cm.
16	27	turbulence at blade- gradually less turbulence until at 4 cm 45 degrees and tip vibration	Reverse flow at 0-2cm. After 15 degrees and high tip velocity	Excessive tip vibration. At 3-4cm above the blade - excessive turbulence and reverse flow.
18	25	0-1cm- turbulence- some reverse flow. Above 1 cm - 10 degrees minimal tip vibration.	0-3cm reverse flow and turbulence- above 3 cm- just tip vibration.	Tip vibration all the way but not excessive
20	24	0-1cm - reverse flow turbulence. Above 1cm - 20 degrees minimal tip vibration	0-2cm reverse flow and excessive turbulence. Above 2 cm - excessive vibration - 45 degrees. Above 6cm - tip vibration	0-4cm-reverse flow turbulence. Above 4cm excessive vibration 45degrees, below tip - excessive vibration 45 degrees. At zero relatively small tip vibration.

Table 24: Results of the metal rod string method on the NACA 0012 rough blade

Angle of attack	**pita tube pressure**	**Flow point 3**	**Flow point 4**	**flow point 5**
	0			
0	30			
2	30	straight with excessive tip vibration	0-1cm above - tip vibration, 1-5cm = excessive vibration with fluctuations of 90 degrees, above 5 cm, just tip vibration.	Quite straight from top to bottom.
4	**29,5**	Reverse flow on the blade, 1 cm above tip vibration.	Reverse flow and turbulence up to 5 cm above blade.	1-4cm above blade excessive vibration and reverse flow. All other regions are straight flow.

6	29	Reverse flow on the blade, 1 cm above tip vibration.	reverse flow on the blade, excessive tip vibration above the blade	1-4cm above blade excessive vibration and reverse flow. All other regions are straight flow.
8	29	Reverse flow on the blade. Above the blade-tip vibration.	0-3 cm - reverse flow. Above 3 - tip vibration up to 45 degrees.	Directly behind - just tip vibration. 1-5cm above - vibration up to 45 degrees. 1-4cm below - vibration up to 45 degrees.
10	29	On the blade reverse flow. Above the blade just excessive tip vibration.	0-2 reverse flow. 2-'4 excessive vibration. Above 4 just tip vibration.	0-2 cm above- tip vibration, 2-5 cm above - excessive vibration with reverse flow. Below blade, straight flow.
12	28	On the blade; reverse flow. Up to 4 cm vibration and 45 degree flow. Above 4 cm excessive vibration.	0-3 cm - 45 degree flow and excessive vibration. 3-5 cm = reverse flow and turbulence. Above 5 cm = excessive vibration.	Tip vibration. Excessive vibration between 4-5 cm above the blade.
14	27	0-1 cm = reverse flow. Above 1 cm = excessive vibration up to 30 degrees.	Reverse flow on the tip. 0-2 cm excessive vibration up to 45 degrees. 2-5 cm excessive vibration up to 90 degrees. Above: tip vibration.	0-2 cm above blade= tip vibration. 2-4cm above blade = excessive vibration up to 30 degrees. 4-6 cm above blade = excessive vibration up to 60 degrees. Below the blade = tip vibration.
16	27	0-1 cm = reverse flow. Above 1 cm = excessive vibration up to 30 degrees.	0-2 cm: reverse flow. Above 2 cm = excessive vibration up to 30 degrees.	Excessive tip vibration the entire section.
18	25	0-1cm = reverse flow. Above is excessive tip vibration at 45 degrees.	0-3cm reverse flow. Above 3 cm: excessive tip vibration.	2-5cm = excessive vibration and some reverse flow. Other areas just excessive vibration.
20	24	0-1cm = reverse flow. Above 1 cm = tip vibration, 30 degrees	0-3 cm reverse flow(very turbulent). Excessive tip vibration above.	Excessive vibration and turbulence the whole section.

Table 25: Results of the metal rod string method on the NACA 0012 smooth blade

Angle of attack	pita tube pressure	Flow point 1	Flow point 2	flow point 3
0	29	straight flow	0-2cm: straight flow. 2-4cm above: turbulence and reverse flow. Above 4 cm: tip vibration.	Straight flow the entire depth.
2	30	Tip vibration, but mainly straight flow.	Excessive turbulence and reverse flow.	Excessive turbulence and reverse flow.
4	29	On blade excessive turbulence and reverse flow. 0 - 1 cm: just tip vibration. Above 1 cm: excessive turbulence and reverse flow.	0-5cm above blade: excessive turbulence and reverse flow.	Excessive turbulence and reverse flow.
6	28	Excessive turbulence above the blade. Some reverse flow also on the blade.	Above blade: excessive turbulence and reverse flow.	Straight flow with tip vibration. Some turbulence and reverse flow at 2cm above the blade.
8	28	Excessive turbulence above the blade. 0-1 cm: Some reverse flow and excessive turbulence.	Above blade: excessive turbulence and reverse flow.	Excessive turbulence and reverse flow. Straight flow 0-1 cm above blade
10	28	Excessive turbulence above the blade. 0-1 cm: just tip vibration and some turbulence above 1cm	Excessive turbulence and reverse flow.	Excessive turbulence and reverse flow.
12	26	Excessive turbulence above the blade. 0-1 cm: just tip vibration and some turbulence above 1cm	Straight flow on the blade. Excessive turbulence and reverse flow above.	Directly behind the blade, straight flow. Excessive turbulence and reverse flow elsewhere.

14	28	Excessive turbulence above the blade. 0-1 cm: just tip vibration and some turbulence above 1cm	Excessive turbulence and reverse flow above.	Excessive turbulence and reverse flow at 2cm above the blade. Elsewhere just excessive turbulence.
16	26	Excessive turbulence and reverse flow above the blade.	Excessive turbulence and reverse flow above. Especially on the blade.	Excessive turbulence and reverse flow at 2cm above the blade. Elsewhere just excessive turbulence.
18	25	Excessive turbulence and reverse flow on the blade. Excessive turbulence above.	Excessive turbulence and reverse flow above. Full reverse flow up to 2 cm above the blade.	Excessive turbulence and reverse flow.
20	24	Excessive turbulence and reverse flow 0-1cm above the blade. Excessive turbulence above.	Excessive turbulence and reverse flow above. Full reverse flow up to 3 cm above the blade.	Excessive turbulence and reverse flow. Full reverse flow 1-3 cm above the blade.

Table 26: Results of the metal rod string method on the NACA 2415 smooth blade

Angle of attack	**pita tube pressure**	**Flow point 3**	**Flow point 4**	**flow point 5**
0	119	Straight flow with tip vibration 0-1cm, vibration increases, at 3 &4 cm excessive turbulence. Above 5 cm - tip vibration.	0-5cm - excessive turbulence. Above 5 cm - just tip vibration.	0-4cm: straight flow, above 4 cm excessive turbulence.0--4cm straight flow. Below turbulence.
2	120	0-4cm: excessive turbulence. Above just tip vibration.	0-2 cm: excessive turbulence and reverse flow. Above 2cm excessive turbulence.	From -1-3cm straight flow, above 3 cm excessive turbulence and reverse flow. Below -1cm: excessive turbulence.
4	117	0-2cm tip vibration, above 2cm turbulence and reverse flow.	0-1 cm excessive tip turbulence, 1-4cm turbulence and reverse flow. Above 4 cm excessive turbulence.	0-2cm above: straight flow-tip vibration. Above 2 cm reverse flow and turbulence. Below blade, excessive tip vibration.

6	114	turbulent flow above blade	0-4cm - turbulent flow. Above 4 cm - tip vibration	

Table 27: Results of the metal rod string method on the NACA 0012 smooth blade at 40m/s

Note: At a wind speed of approx. 40m/s at 6 degrees and above it became clear that interference effects were too much and the foil vibration was also affecting the results. It was not considered appropriate to continue testing at 40m/s.

Hot-bulb/wire anemometry

To better understand the speed of the flow a testo 490 manual hot-bulb anemometer was used at various horizontal and vertical distances from the foil which can calculate wind speeds between 0.2m/s and 60m/s.Such a device can give an indication of speed only, the direction of the flow is not known. However it could be a useful device to understand the magnitude of speeds present around the foil at various angle of attacks.

Hot wire anemometers use a very fine wire (on the order of several micrometres) electrically heated up to some temperature above the ambient. Air flowing past the wire has a cooling effect on the wire. As the electrical resistance of most metals is dependent upon the temperature of the metal (tungsten is the metal), a relationship can be obtained between the resistance of the wire and the flow speed.

Hot-wire anemometers, while extremely delicate, have high frequency-response and fine spatial resolution compared to other measurement methods, and as such are almost universally employed for the detailed study of turbulent flows, or any flow in which rapid velocity fluctuations are of interest. Its use is very relevant for the current study.

One disadvantage of such a device is that is interferes with the flow to obtain a reading, which may affect the results. However it was the best device available to provide a magnitude of speed around the blade.

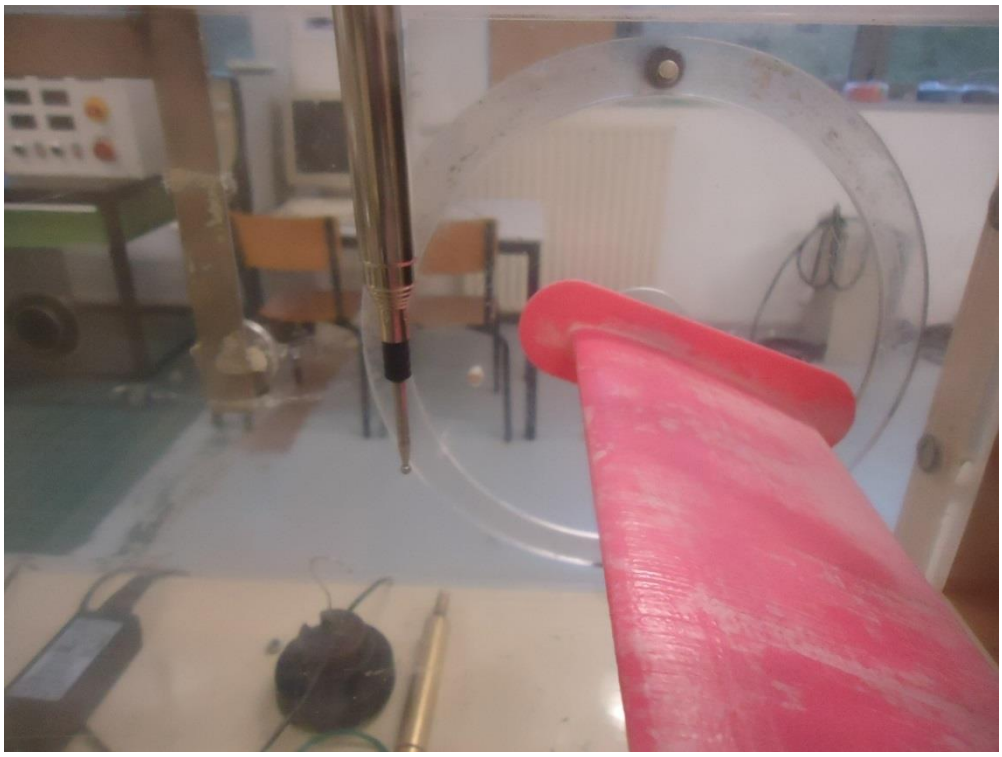

Figure 77: Use of hot bulb anemometer to measure the speed of flow

Angle of attack (deg)	**pita tube pressure**	mean velocity point 1(m/s)	mean velocity point 2 (m/s)	mean velocity point 3 (m/s)	mean velocity point 4 (m/s)	mean velocity point 5 (m/s)
2	30	18	26	17	16	26
4	**29,5**	20	27	19	16	25
6	29	22	29	19	17	25
8	29	23	30	21	17	21
10	29	20	28	21	16	22
12	28	21	29	21	18	22
14	27	19	28	20	18	19
16	27	22	28	26	11	17
18	25	22	26	25	10	16
20	24	20	27	30	8	19,5

Table 28: Anemometer readings: NACA 0012 foil (rough) at blade surface and in line with blade.

Angle of attack (deg)	**pita tube pressure**	mean velocity point 1	mean velocity point 2	mean velocity point 3	mean velocity point 4	mean velocity point 5
2	30	20	27	17	16	25
4	**29,5**	20	23	18	16	21
6	29	19	28	18	16	23
8	29	24	29	18	16	23
10	29	20	28	19	16	20
12	28	19	28	19	18	16
14	27	20	27	18	17	17
16	27	22	29	19	19	17
18	25	25	28	23	11	16
20	24	21,5	28	33,5	6,5	15

Table 29: Anemometer readings: NACA 0012 foil (rough) at 1 cm above blade surface.

Angle of attack (deg)	**pita tube pressure**	mean velocity point 1	mean velocity point 2	mean velocity point 3	mean velocity point 4	mean velocity point 5
2	30	18	24	19	16	18
4	**29,5**	20	23	18	16	19
6	29	22	28	21	16	17
8	29	22	29	20	16	17
10	29	22	28	18	17	17
12	28	20	27	22	17	18
14	27	19	28	20	17	16
16	27	22	30	21	18	18
18	25	22	28	28	20	14
20	24	19	25	31	12	13

Table 30: Anemometer readings: NACA 0012 foil (rough) at 2 cm above blade surface.

Angle of attack (deg)	**pita tube pressure**	mean velocity point 1	mean velocity point 2	mean velocity point 3	mean velocity point 4	mean velocity point 5
2	30	19	24	17	18	18
4	29,5	21	23	19	17	17
6	29	21	26	19	17	20
8	29	24	29	19	18	18
10	29	18	25	19	17	16
12	28	18	22	23	17	16
14	27	18	26	22	19	15
16	27	17	18	20	20	16
18	25	18	27	27	20	17
20	24	20	20	28	19	18

Table 31: Anemometer readings: NACA 0012 foil (rough) at 3 cm above blade surface.

Angle of attack (deg)	pita tube pressure	mean velocity point 1	mean velocity point 2	mean velocity point 3	mean velocity point 4	mean velocity point 5
2	30	22	22	23	17	19
4	29,5	19	17	17	17	23
6	29	20	19	18	17	21
8	29	20	22	19	18	18
10	29	18	25	18	17	15
12	28	18	19	19	17	16
14	27	18	19	19	18	17
16	27	16	17	20	18	16
18	25	16	22	25	18	18
20	24	20	16	21	19,5	18

Table 32: Anemometer readings: NACA 0012 foil (rough) at 4 cm above blade surface.

Angle of attack (deg)	pita tube pressure	mean velocity point 1	mean velocity point 2	mean velocity point 3	mean velocity point 4	mean velocity point 5
2	30	19	20	17	17	17
4	29,5	17	20	19	18	17
6	29	19	18	19	17	17
8	29	18	19	20	18	20
10	29	17	18	18	17	16
12	28	18	18	19	17	16
14	27	18	19	19	17	16
16	27	17	17	18	18	17
18	25	int	int	22	21	19
20	24	15	22	20	20	17

Table 33: Anemometer readings: NACA 0012 foil (rough) at 5 cm above blade surface.

Angle of attack (deg)	pita tube pressure	Velocity 1cm below blade	Velocity 2cm below blade	Velocity 3cm below blade	Velocity 4cm below blade	Velocity 5cm below blade
2	30	23	27	27	27	27
4	29,5	20	26	25	25	26
6	29	22	26	27	27	19
8	29	19	23	27	18	18
10	29	18	23	27	26	15
12	28	17	22	23	24	16
14	27	18	18	22	18	17
16	27	16	17	17	16	14
18	25	17	17	17	15,5	14
20	24	17,5	19	17	15,5	15

Table 34: Anemometer readings: NACA 0012 foil (rough) at point 5 below blade surface.

Angle of attack (deg)	pita tube pressure	mean velocity point 1	mean velocity point 2	mean velocity point 3	mean velocity point 4	mean velocity point 5
2	30	20	27	19	19	25
4	29,5	20	27	19	18	25
6	29	26	29	20	17	25
8	29	25	30	21	18	25
10	29	26	30	20	20	23
12	28	28	32	22	17	24
14	27	25	32	21	18	22
16	27	21	29	21	12	19
18	25	23	28	21	10	19
20	24	20	27	24	10	19

Table 35: Anemometer readings: NACA 0012 foil (smooth) at point on blade surface and in line.

Angle of attack (deg)	pita tube pressure	mean velocity point 1	mean velocity point 2	mean velocity point 3	mean velocity point 4	mean velocity point 5
2	30	20	28	17	17	26
4	29,5	17	27	18	16	23
6	29	22	29	17	16	23
8	29	22	30	19	16	18
10	29	26	33	19	16	20
12	28	24	32	20	16	21
14	27	24	30	20	17	20
16	27	18	30	19	16	18
18	25	20	29	20	15	16
20	24	18	27	22	10	16

Table 36: Anemometer readings: NACA 0012 foil (smooth) at point 1cm above blade surface.

Angle of attack (deg)	pita tube pressure	mean velocity point 1	mean velocity point 2	mean velocity point 3	mean velocity point 4	mean velocity point 5
2	30	18	27	18	16	16
4	29,5	19	26	18	16	20
6	29	22	28	18	16	20
8	29	21	28	19	17	18
10	29	23	31	18	16	17
12	28	24	30	17	16	15
14	27	25	27	18	17	15
16	27	17	28	19	18	18
18	25	19	28	20	18	17
20	24	18	27	21	19	15

Table 37: Anemometer readings: NACA 0012 foil (smooth) at point 2cm above blade surface.

Angle of attack (deg)	pita tube pressure	mean velocity point 1	mean velocity point 2	mean velocity point 3	mean velocity point 4	mean velocity point 5
2	30	19	25	19	20	21
4	29,5	20	23	19	18	17
6	29	21	24	18	16	17
8	29	20	25	19	18	18
10	29	22	25	19	18	19
12	28	20	25	18	16	15
14	27	20	24	18	17	16
16	27	18	23	18	17	17
18	25	17	22	19	17	16
20	24	19	22	22	18	16

Table 38: Anemometer readings: NACA 0012 foil (smooth) at point 3cm above blade surface.

Angle of attack (deg)	pita tube pressure	mean velocity point 1	mean velocity point 2	mean velocity point 3	mean velocity point 4	mean velocity point 5
2	30	20	20	17	17	17
4	29,5	20	20	20	18	16
6	29	20	21	18	17	17
8	29	20	20	19	17	18
10	29	21	21	18	18	17
12	28	19	22	18	17	18
14	27	18	20	18	17	15
16	27	17	21	18	17	17
18	25	Int.	18	19	17	16
20	24	Int.	18	20	18	16

Table 39: Anemometer readings: NACA 0012 foil (smooth) at point 4cm above blade surface.

Angle of attack (deg)	pita tube pressure	mean velocity point 1	mean velocity point 2	mean velocity point 3	mean velocity point 4	mean velocity point 5
2	30	18	19	17	17	17
4	29,5	18	19	20	17	16
6	29	20	20	18	18	18
8	29	19	19	18	17	17
10	29	19	19	19	18	16
12	28	18	20	18	17	17
14	27	19	20	18	17	18
16	27	16	18	19	16	16
18	25	Int.	16	18	17	16
20	24	Int.	Int	19	17	16

Table 40: Anemometer readings: NACA 0012 foil (smooth) at point 5cm above blade surface.

Angle of attack (deg)	pita tube pressure	Velocity 1cm below blade	Velocity 2cm below blade	Velocity 3cm below blade	Velocity 4cm below blade	Velocity 5cm below blade
2	30	23	25	27	26	21
4	29,5	23	25	25	27	20
6	29	22	26	26	24	20
8	29	25	25	25	24	21
10	29	20	26	26	25	21
12	28	19	25	26	25	23
14	27	23	26	28	23	21
16	27	20	26	23	Int.	Int.
18	25	19	20	20	Int.	Int.
20	24	20	20	17	Int.	Int.

Table 41: Anemometer readings: NACA 0012 foil (smooth) at point 5 below the blade surface.

Angle of attack (deg)	pita tube pressure	mean velocity point 1	mean velocity point 2	mean velocity point 3	mean velocity point 4	mean velocity point 5
0	30	20	24	17	21	25
2	29	18	28	18	19	22
4	29	22	31	18	23	24
6	29	23	32	19	24	22
8	28	22	30	20	18	22
10	26	19	29	19	11	18
12	26	20	30	20	11	19
14	25	23	28	11	9	18
16	24	22	27	18	8	18
18	23	21	27	10	7	19
20	21	20	27	9	7	19

Table 42: Anemometer readings: NACA 0012 white foil (smooth) at point on blade surface and in line.

Angle of attack (deg)	pita tube pressure	mean velocity point 1	mean velocity point 2	mean velocity point 3	mean velocity point 4	mean velocity point 5
0	30	18	25	17	20	24
2	29	20	28	17	18	21
4	29	22	30	17	16	21
6	29	22	30	17	16	22
8	28	21	30	20	16	22
10	26	20	29	22	17	15
12	26	21	29	20	16	16
14	25	21	27	19	10	16
16	24	18	27	29	8	14

18	23	20	27	30	7	14
20	21	18	27	30	6	14

Table 43: Anemometer readings: NACA 0012 white foil (smooth) at point 1cm above blade surface.

Angle of attack (deg)	**pita tube pressure**	mean velocity point 1	mean velocity point 2	mean velocity point 3	mean velocity point 4	mean velocity point 5
0	30	21	21	17	20	22
2	29	21	26	17	19	18
4	29	24	28	19	16	20
6	29	20	27	18	16	16
8	28	21	27	20	18	19
10	26	22	25	22	18	19
12	26	21	29	21	16	17
14	25	19	24	18	12	15
16	24	20	27	30	19	15
18	23	int	28	30	15	17
20	21	int	24	29	14	13

Table 44: Anemometer readings: NACA 0012 white foil (smooth) at point 2cm above blade surface.

Angle of attack	**pita tube**	mean velocity	mean velocity	mean velocity	mean velocity	mean velocity
0	30	20	23	17	17	21
2	29	19	24	19	16	23
4	29	20	20	18	17	16
6	29	23	26	18	18	16
8	28	20	20	19	17	17
10	26	21	25	21	18	18
12	26	20	26	19	17	15
14	25	Int.	23	21	20	18
16	24	18	24	22	17	17
18	23	Int.	22	24	18	16
20	21	Int.	Int.	25	20	14

Table 45: Anemometer readings: NACA 0012 white foil (smooth) at point 3cm above blade surface.

Angle of attack (deg)	pita tube pressure	mean velocity point 1	mean velocity point 2	mean velocity point 3	mean velocity point 4	mean velocity point 5
0	30	20	22	18	17	23
2	29	22	22	18	17	23
4	29	19	19	17	18	18
6	29	21	21	18	17	20
8	28	20	21	18	16	20
10	26	22	22	18	17	22
12	26	15	19	19	18	16
14	25	int	18	18	19	17
16	24	int	21	20	18	17
18	23	int	20	20	18	17
20	21	int	int	20	19	18

Table 46: Anemometer readings: NACA 0012 white foil (smooth) at point 4cm above blade surface.

Angle of attack (deg)	pita tube pressure	mean velocity point 1	mean velocity point 2	mean velocity point 3	mean velocity point 4	mean velocity point 5
0	30	19	20	18	17	17
2	29	20	21	19	16	18
4	29	17	18	17	17	16
6	29	22	18	18	17	17
8	28	20	20	18	17	17
10	26	17	18	19	17	17
12	26	int	18	17	17	17
14	25	int	int	17	18	16
16	24	int	int	19	17	17
18	23	int	int	int	19	17
20	21	int	int	19	20	17

Table 47: Anemometer readings: NACA 0012 white foil (smooth) at point 5cm above blade surface.

Angle of attack (deg)	pita tube pressure	Velocity 1cm below blade	Velocity 2cm below blade	Velocity 3cm below blade	Velocity 4cm below blade	Velocity 5cm below blade
0	30	25	26	26	29	Int.
2	29	24	25	27	27	Int.
4	29	24	24	26	27	Int.
6	29	22	24	26	25	Int.
8	28	20	20	25	Int.	Int.
10	26	20	20	20	Int.	Int.
12	26	19	24	24	Int.	Int.
14	25	17	17	17	Int.	Int.
16	24	19	18	Int.	Int.	Int.
18	23	18	19	Int.	Int.	Int.

20	21	19	Int.	Int.	Int.	Int.

Table 48: Anemometer readings: NACA 0012 white foil (smooth) at point 5 below the blade surface.

NACA 2415 foil:

Angle of attack (deg)	**pita tube pressure**	mean velocity point 1	mean velocity point 2	mean velocity point 3	mean velocity point 4	mean velocity point 5
0	30	17	20	18	23	22
2	30	19	26	19	20	25
4	29	19	28	19	25	26
6	28	25	28	20	17	23
8	28	24	30	21	18	24
10	28	25	31	21	19	23
12	26	26	31	21	20	23
14	28	26	30	20	17	20
16	26	22	27	18	16	22
18	25	21	27	12	10	19
20	24	20	27	20	9	18
-2	29	18	19	17	20	24

Table 49: Anemometer readings: NACA 2415 foil (smooth) at point on blade surface and in line.

Angle of attack (deg)	**pita tube pressure**	mean velocity point 1	mean velocity point 2	mean velocity point 3	mean velocity point 4	mean velocity point 5
0	30	14	24	17	17	19
2	30	19	28	18	18	20
4	29	21	28	17	22	17
6	28	25	28	18	16	19
8	28	24	30	18	16	21
10	28	24	32	18	16	19
12	26	27	31	19	16	20
14	28	26	25	19	16	17
16	26	22	29	18	14	17
18	25	20	28	22	10	15
20	24	19	28	28	8	16
-2	29	16	23	16	17	21

Table 50: Anemometer readings: NACA 2415 foil (smooth) at point 1cm above blade surface.

Angle of attack (deg)	pita tube pressure	mean velocity point 1	mean velocity point 2	mean velocity point 3	mean velocity point 4	mean velocity point 5
0	30	15	24	18	18	19
2	30	20	25	20	20	16
4	29	23	29	18	22	17
6	28	26	25	19	18	18
8	28	25	28	18	17	16
10	28	22	28	18	16	17
12	26	23	28	17	15	16
14	28	21	26	18	16	16
16	26	21	28	20	17	16
18	25	20	28	26	17	16
20	24	20	28	26	18	16
-2	29	19	23	16	22	21

Table 51: Anemometer readings: NACA 2415 foil (smooth) at point 2cm above blade surface.

Angle of attack (deg)	pita tube pressure	mean velocity point 1	mean velocity point 2	mean velocity point 3	mean velocity point 4	mean velocity point 5
0	30	16	24	19	22	21
2	30	18	24	18	19	21
4	29	20	22	18	19	19
6	28	21	22	18	17	25
8	28	19	23	19	17	19
10	28	23	25	19	19	20
12	26	22	24	18	17	16
14	28	20	23	19	17	15
16	26	int	26	20	17	17
18	25	int	24	22	20	16
20	24	int	23	23	20	16
-2	29	18	22	18	18	22

Table 52: Anemometer readings: NACA 2415 foil (smooth) at point 3cm above blade surface.

Angle of attack (deg)	pita tube pressure	mean velocity point 1	mean velocity point 2	mean velocity point 3	mean velocity point 4	mean velocity point 5
0	30	19	20	17	19	16
2	30	20	20	18	18	18
4	29	21	21	19	21	18
6	28	22	18	19	16	17
8	28	20	23	19	17	17
10	28	20	20	19	18	18
12	26	int	21	19	17	20
14	28	int	22	18	17	17
16	26	int	21	18	18	17
18	25	int	21	20	17	16
20	24	int	20	20	19	17
-2	29	19	19	18	17	17

Table 53: Anemometer readings: NACA 2415 foil (smooth) at point 4cm above blade surface.

Angle of attack (deg)	pita tube pressure	mean velocity point 1	mean velocity point 2	mean velocity point 3	mean velocity point 4	mean velocity point 5
0	30	20	18	17	17	16
2	30	20	20	18	17	18
4	29	20	20	17	20	17
6	28	20	int	18	16	16
8	28	18	20	19	17	18
10	28	int	20	18	18	17
12	26	int	19	19	17	17
14	28	int	int	int	17	17
16	26	int	18	18	18	19
18	25	int	int	int	int	16
20	24	int	int	19	18	16
-2	29	19	18	18	16	17

Table 54: Anemometer readings: NACA 2415 foil (smooth) at point 5cm above blade surface.

Angle of attack (deg)	pita tube pressure	Velocity 1cm below blade	Velocity 2cm below blade	Velocity 3cm below blade	Velocity 4cm below blade	Velocity 5cm below blade
0	30	25	25	30	int	int
2	29	24	27	28	int	int
4	29	24	27	29	int	int
6	29	19	25	27	int	int
8	28	22	25	27	int	int
10	26	22	26	25	int	int
12	26	24	24	int	int	int
14	25	21	23	int	int	int
16	24	20	int)	int		
18	23	17	18	int	int	int
20	21	18	19	int	int	int
-2	29	25	22	28	int	int

Table 55: Anemometer readings: NACA 2415 foil (smooth) at point 5 below the blade surface.

Ink droplets:

Using two or three droplets of ink on the low pressure leading edge side of the blade is a very effective way of visualizing the flow on the surface of the blade. An example is shown in figure 78 below before the wind fan is turned on.

Figure 78: 2 Droplets on leading edge low pressure face before the fan is turned on.

Angle of attack	Ink droplets:
5	Started at leading edge and jumped to trailing edge. Droplet is stagnant 1.5cm from trailing edge.
10	Started at leading edge and jumped to trailing edge. Droplet is longer at 2 cm length from trailing edge. Some ink fell over trailing edge.
15	Much slower to move aft, very erratic, jumped everywhere. Moved transversely to 5cm from centre.

20	Some of the droplet jumped aft, but also some has stayed at the leading edge. Movement is fwd. and aft, and right and left. Most of the droplet eventually moved to the trailing edge.

Table 56: Ink droplet results on the NACA 0012 smooth foil.

Angle of attack:	Ink droplets:
5	Even flow over blade. Ink gathered at trailing edge, 2cm left at trailing edge.
10	Jumped to leading edge. 3 cm on the leading edge.
15	Reverse flow: however not full reverse flow. Bubble moves to the trailing edge but slowly. Bubble moves transversely.
20	Reverse flow. Very erratic flow and messy. Bubble started at the trailing edge but moved towards the leading edge.

Table 57: Ink droplet results on the NACA 2415 smooth foil.

Comments:

The ink droplets truly demonstrate the 3 dimensional flow of the wind in the stall condition. Post stall the ink moves aft, forward and transversely in an erratic manner. It really exemplifies the complex flow present.

You also notice the reverse flow is more present as the angle of attack is increased. The separation bubble slowly moves from aft to forward of the foil pre-stall condition and then is too erratic too predict post stall.

19.2 ANNEX B: LIST OF COMMONLY USED TURBULENCE MODELS.

1. Equations Models (Algebraic Models)

- Cebeci-Smith Model
- Baldwin-Lomax Model
- Johnson-King Model
- Roughness dependent Models

2. 1-Equation Model

- Prandtl's Models
- Baldwin-Barth Model
- Spalart-Allmaras Model

3. 2-Equations Models

- Standard k-epsilon Model
- Realizable k-epsilon Model
- RNG k-epsilon_ Model
- Wilcox k-omega Model
- Menter SST k-omega Model

4. Other Models (more than two equations)

- v^2-f Model
- *zeta-f* Model
- RSM Model

19.3 ANNEX C: VARIOUS TURBULENCE MODELS - FLUENT & STARCCM+

CFD Models	K-ε (StarCCM+)	K-ω SST (Fluent-Shear Stress Transport)	Spalart-Allmaras (STARCCM+)	K-kl-ω (Fluent)
Qualities	- Robustness - Reasonable accuracy	- Accurate - Reliable	- Accurate for the prediction of the boundary layers	-Predict boundary layer development -Transition onset
Concerning	- Turbulence flows - Confined flows	- Wide class of flows	-Aerospace applications	
Limits	- Rotational flows		-General industrial flows -Free shear flows	
Numbers of equations	2	4	1	3
Y+ value	30	1 or 30	1	1

Options	- Enhanced Wall Treatment - Non-Equilibrium Wall Functions			

19.4 ANNEX D: RESULTS OF CFD LES SIMULATIONS:

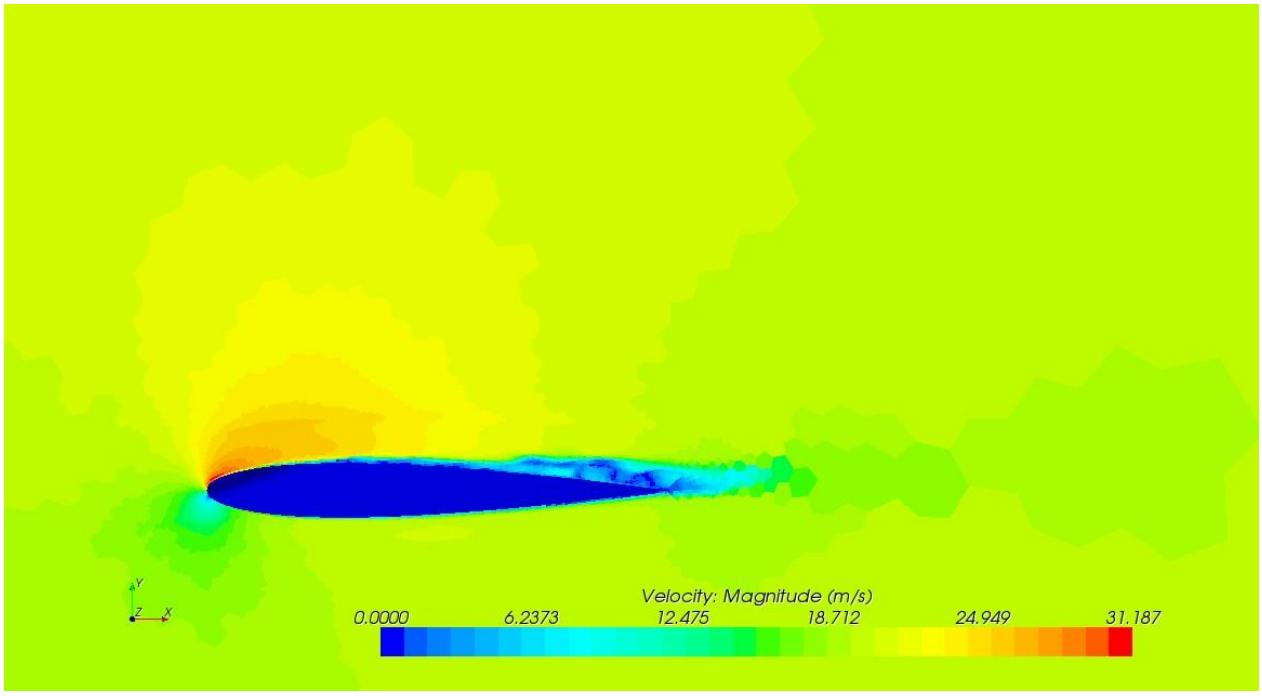

Figure 79: Scalar velocity magnitude LES 5deg.

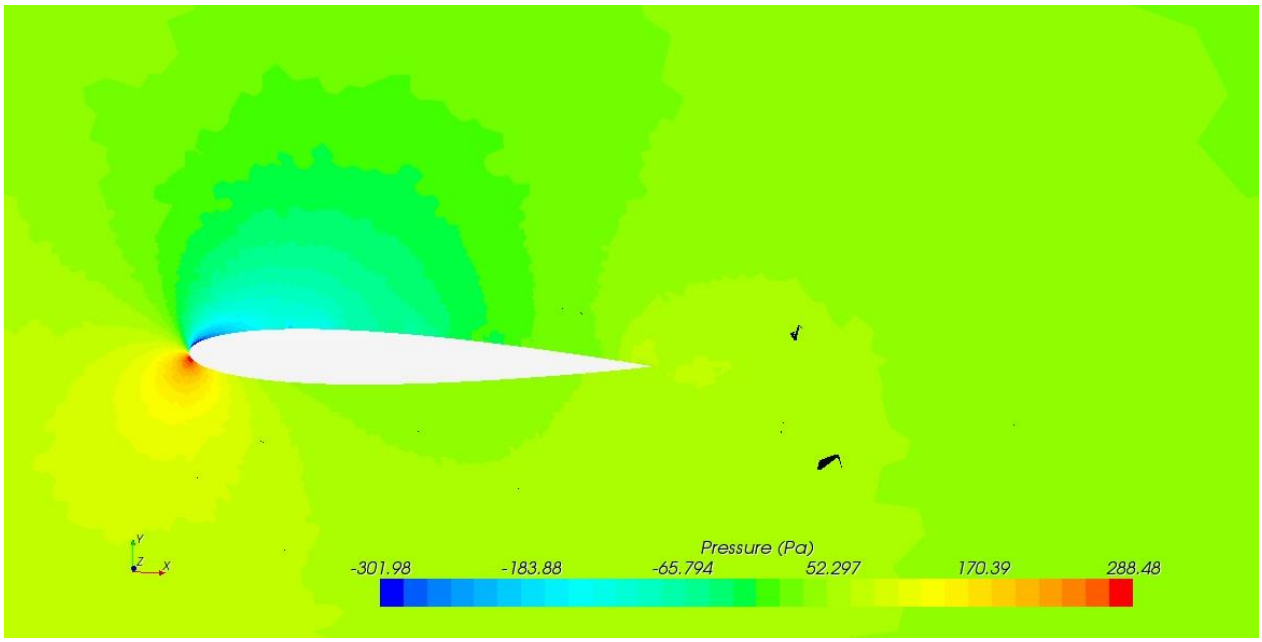

Figure 80: Scalar pressure magnitude LES 5deg.

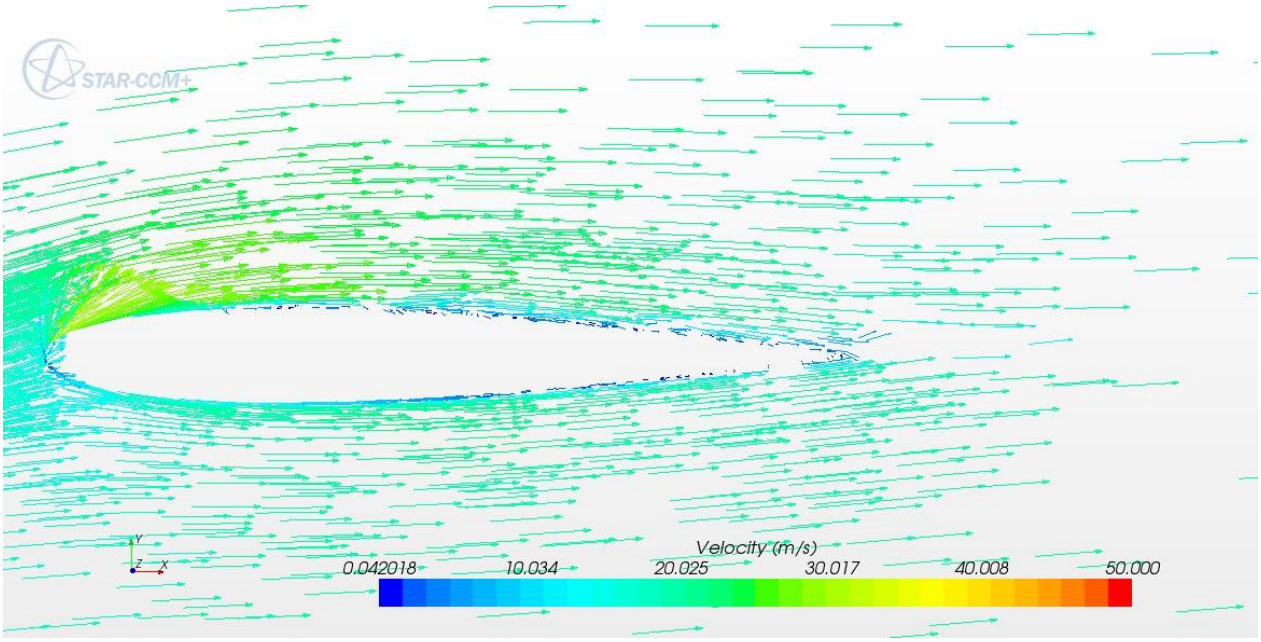

Figure 81: Velocity vector LES 5deg.

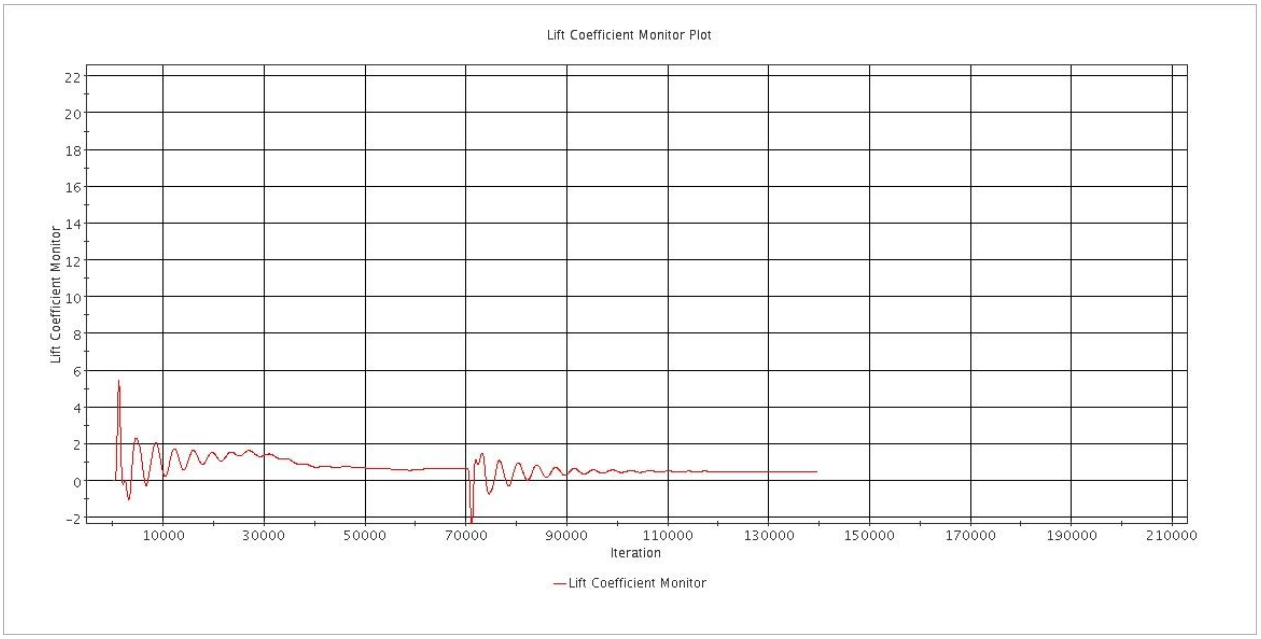

Figure 82: Lift coefficient LES 5deg.

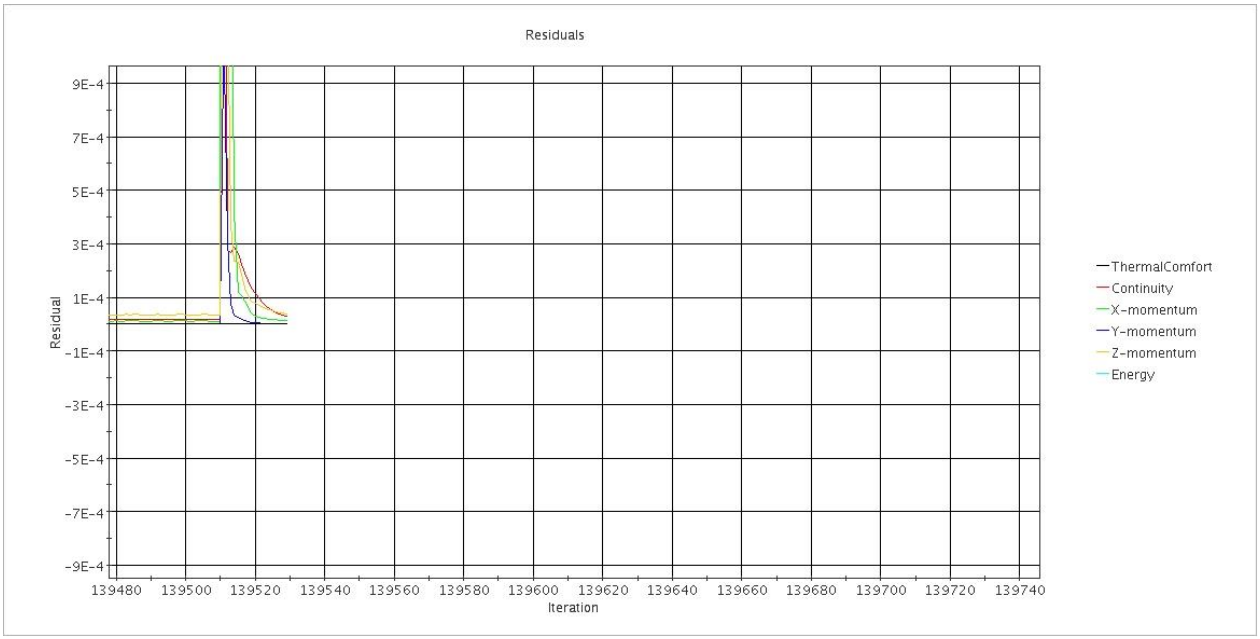

Figure 83: Residuals LES 5deg.

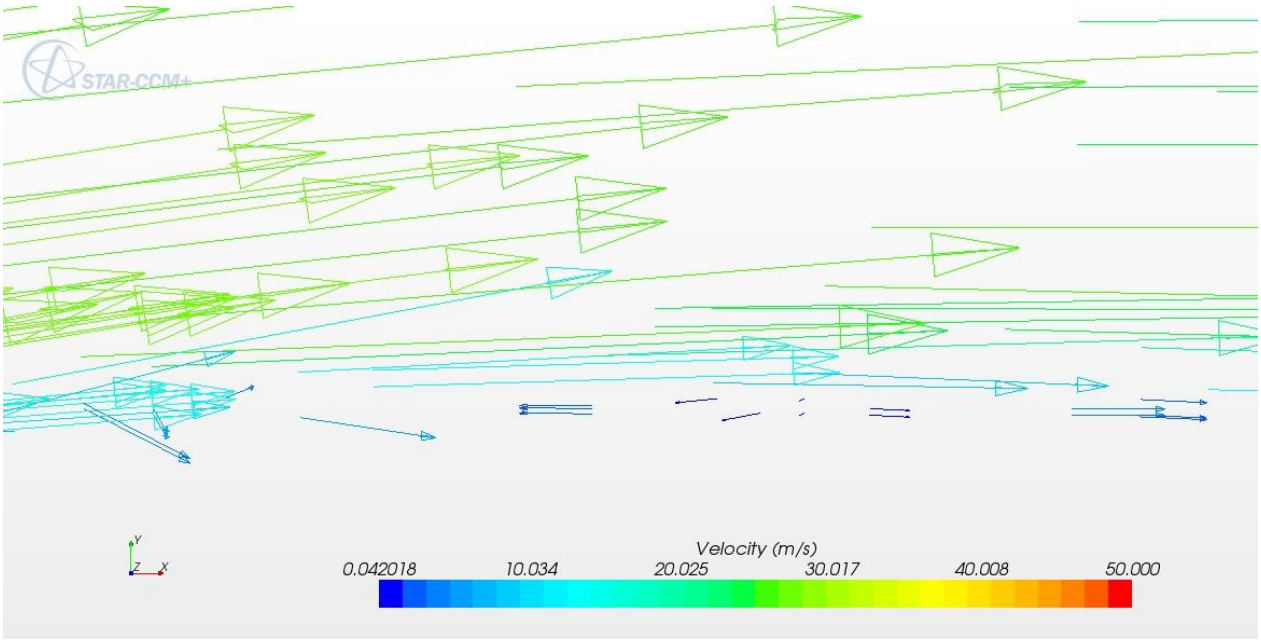

Figure 84: Start of laminar separation- 0.2L LES 5deg.

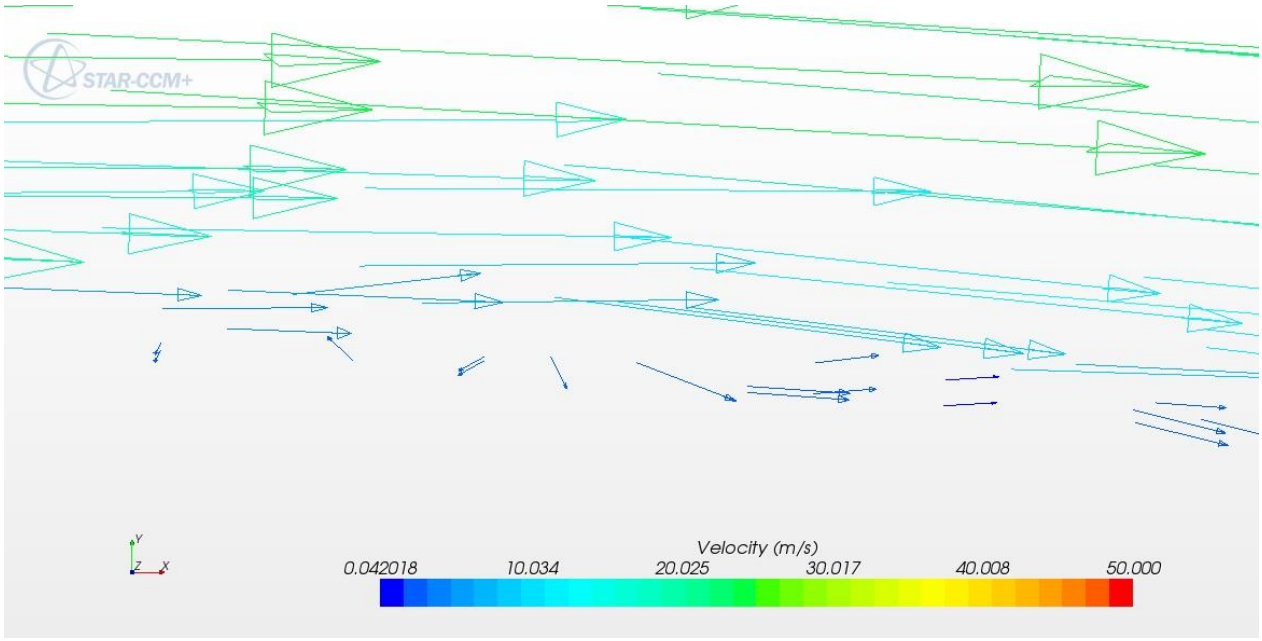

Figure 85: End of first Sep. bubble, start of 2nd bubble 0.5L.

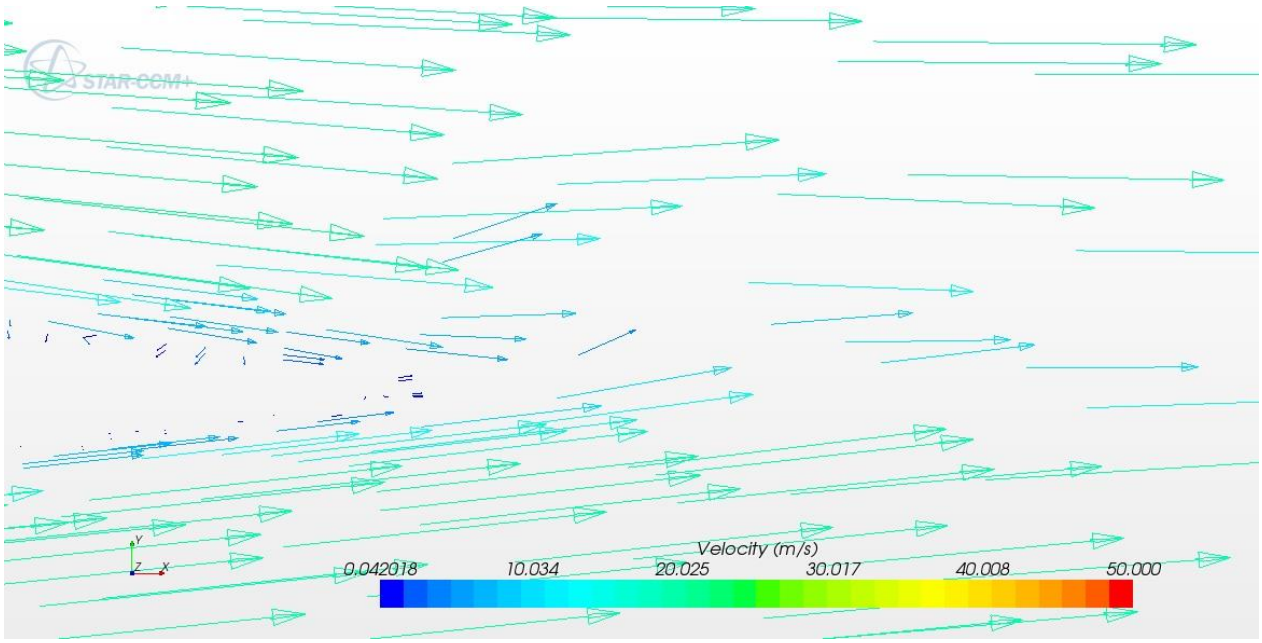

Figure 86: Trailing edge separation LES 5deg.

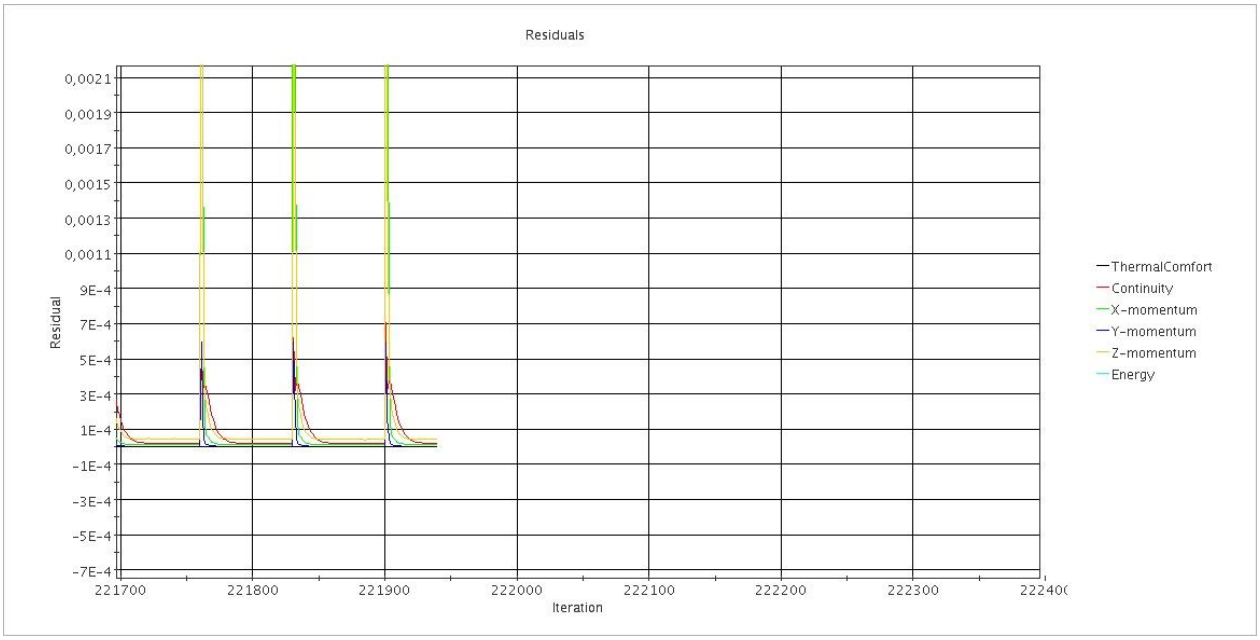

Figure 87: Residuals LES 10 deg.

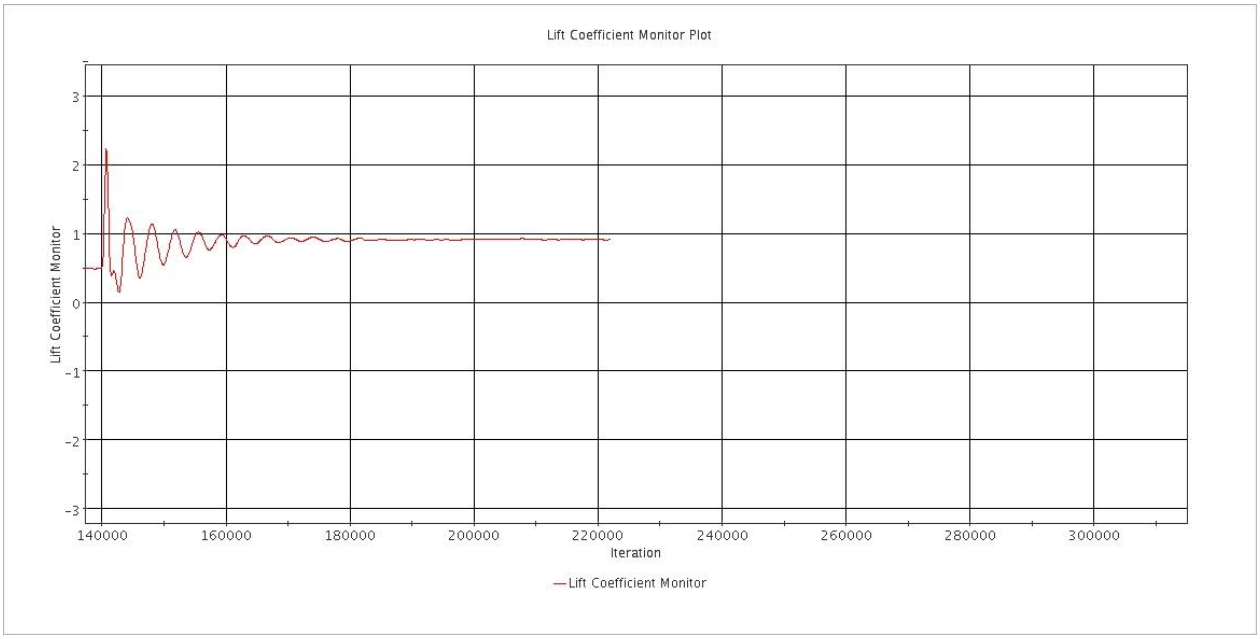

Figure 88: Lift coefficient LES 10 deg.

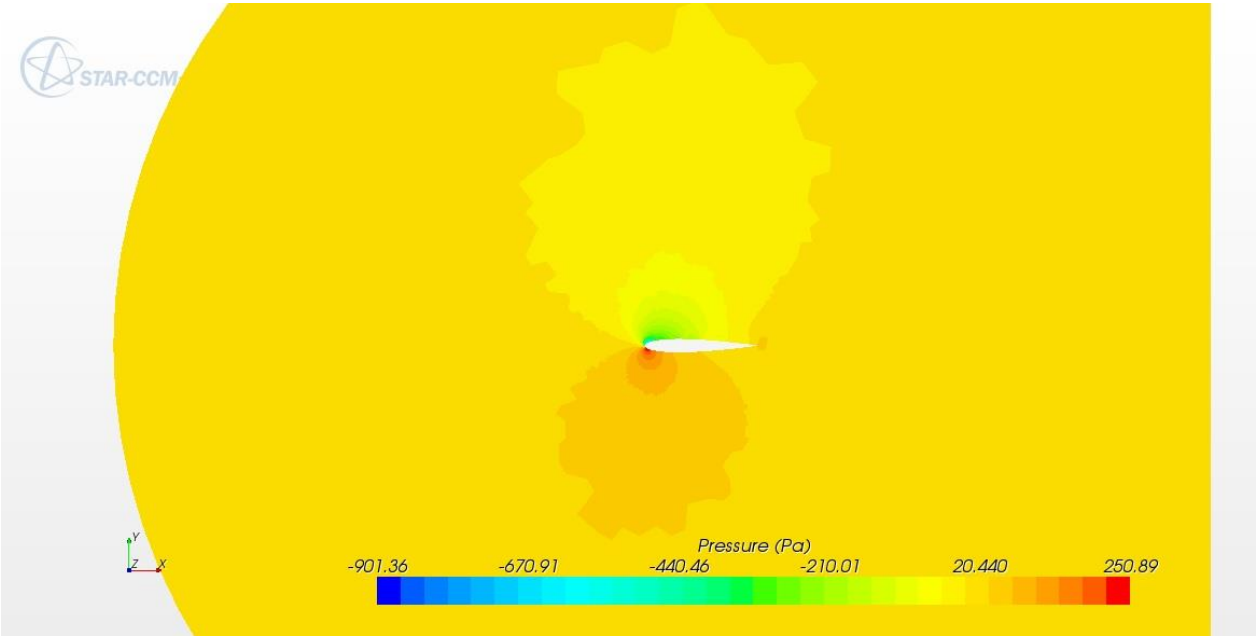

Figure 89: Pressure LES 10 deg.

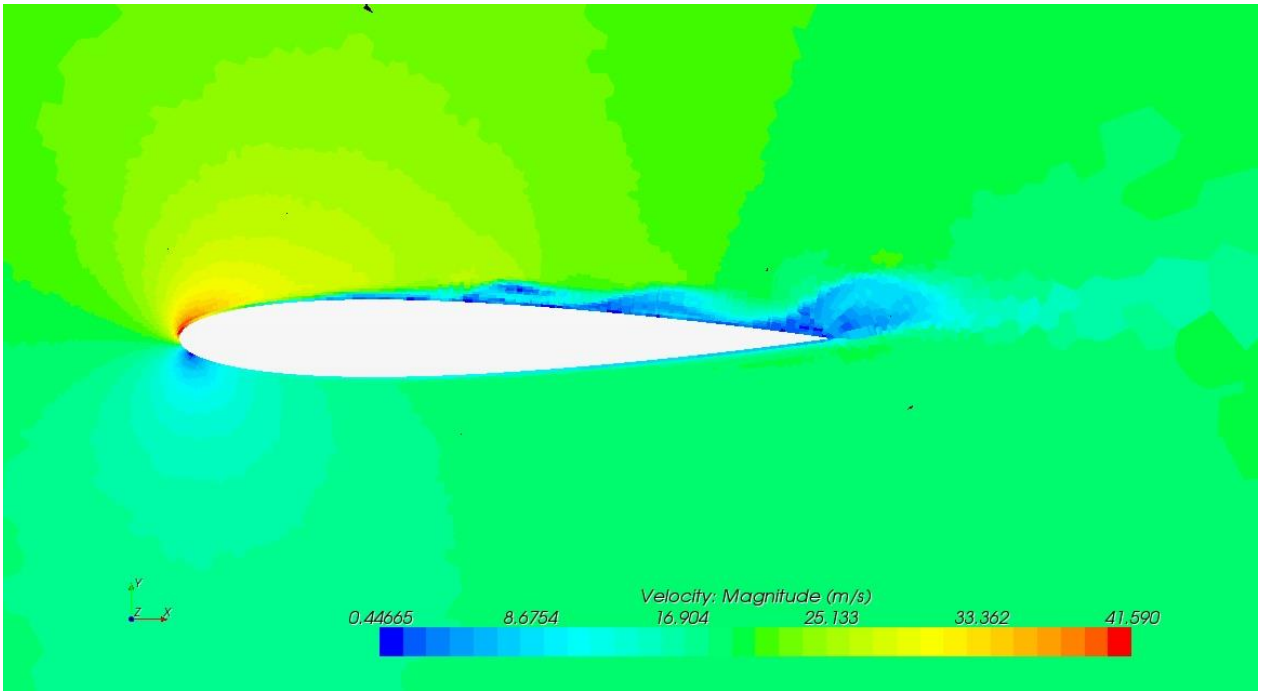

Figure 90: Scalar velocity magnitude LES 10 deg.

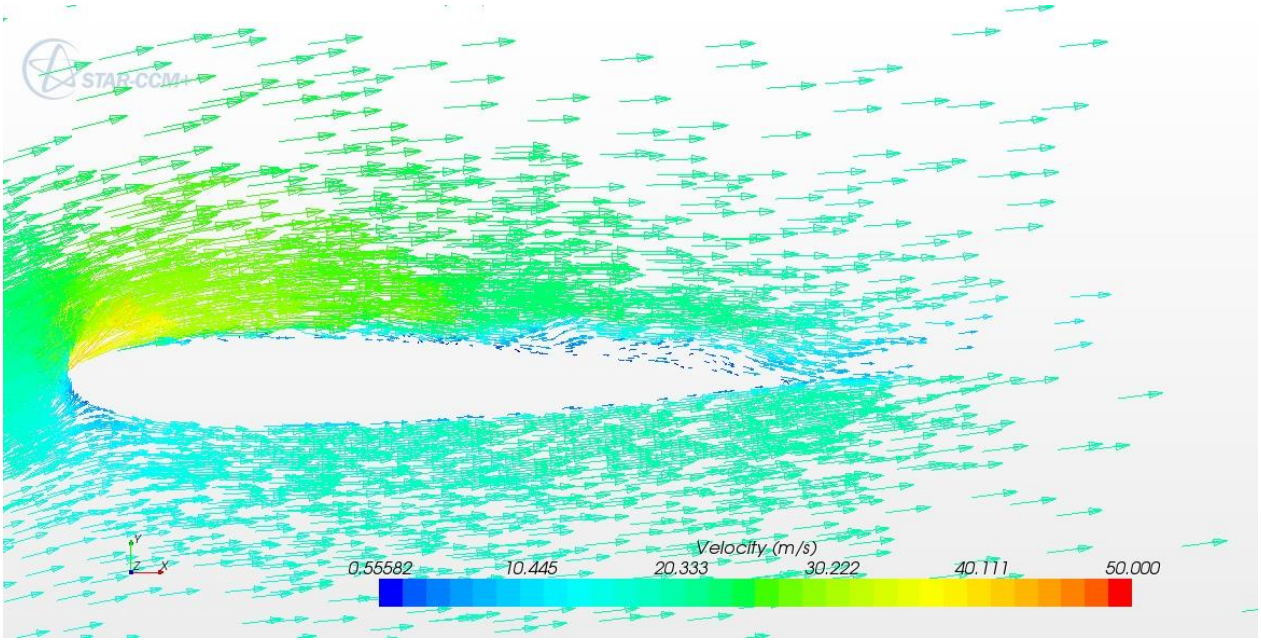

Figure 91: Velocity magnitude LES 10 deg.

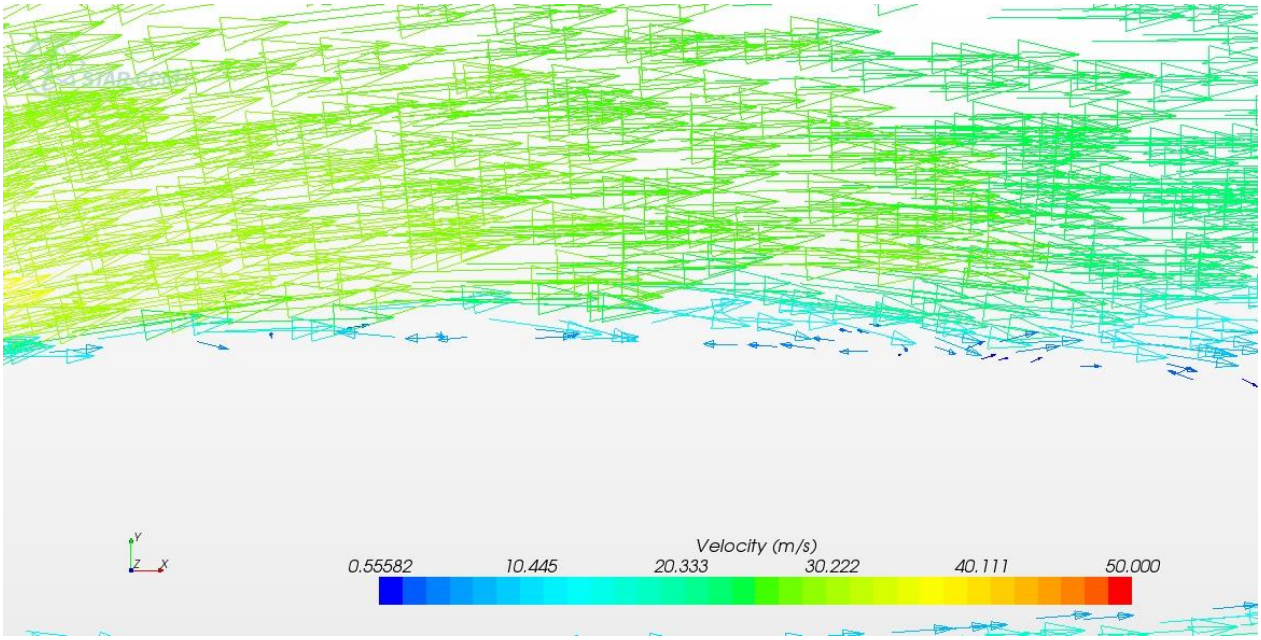

Figure 92: Velocity magnitude first separation point, 0.15L; & start of laminar separation-0,05L; LES 10 deg.

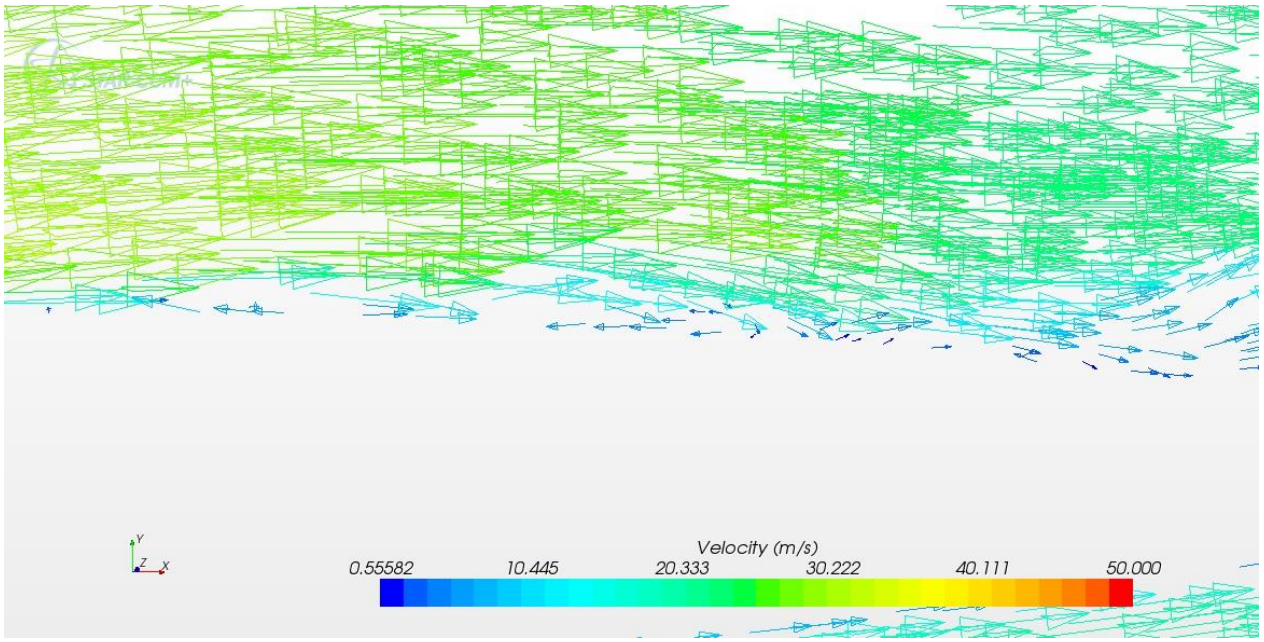

Figure 93: Velocity 2nd bubble: 0.6L: LES 10 deg.

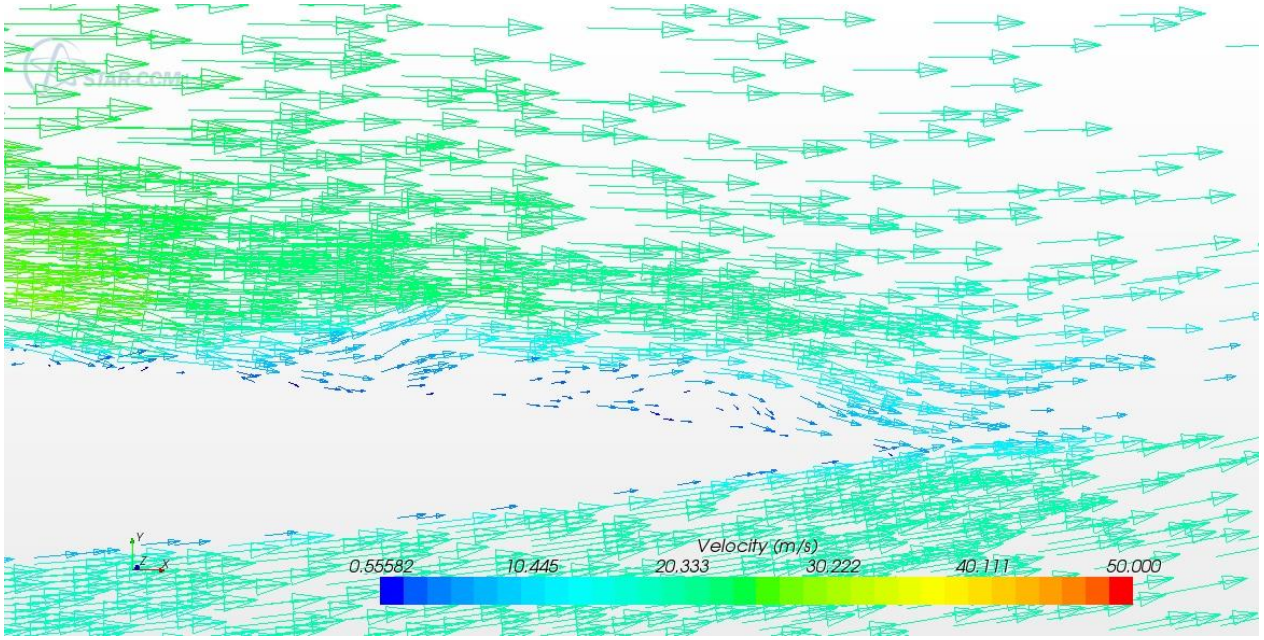

Figure 94: Trailing edge flow LES 10 deg.

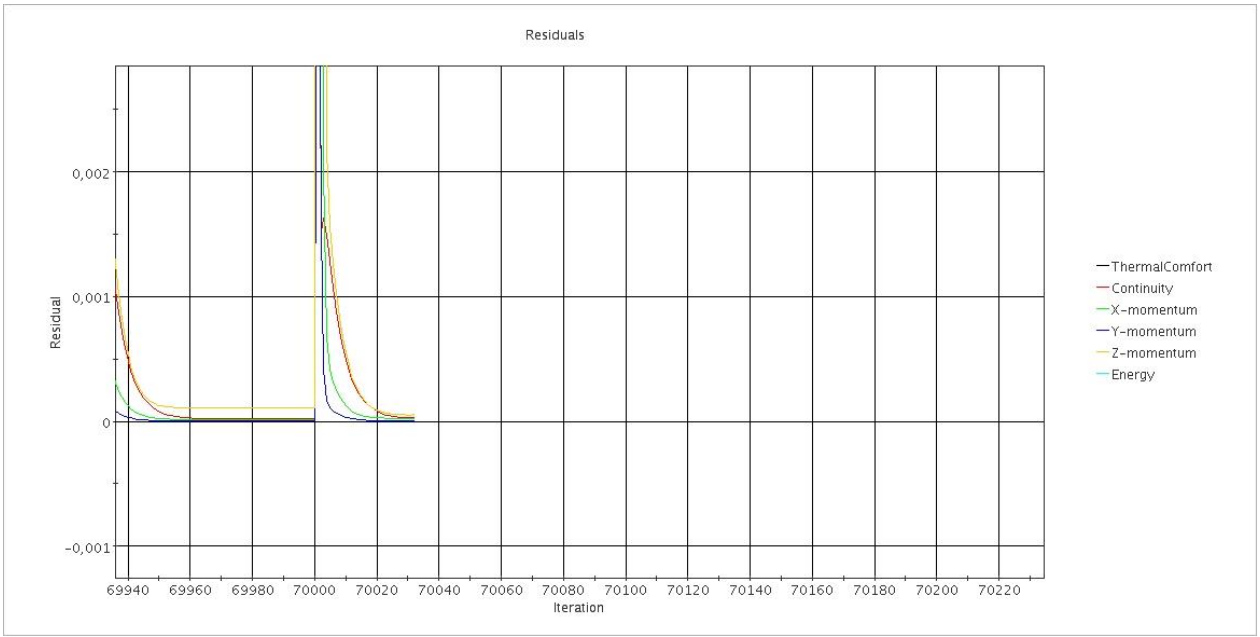

Figure 95: Residuals LES 15 deg.

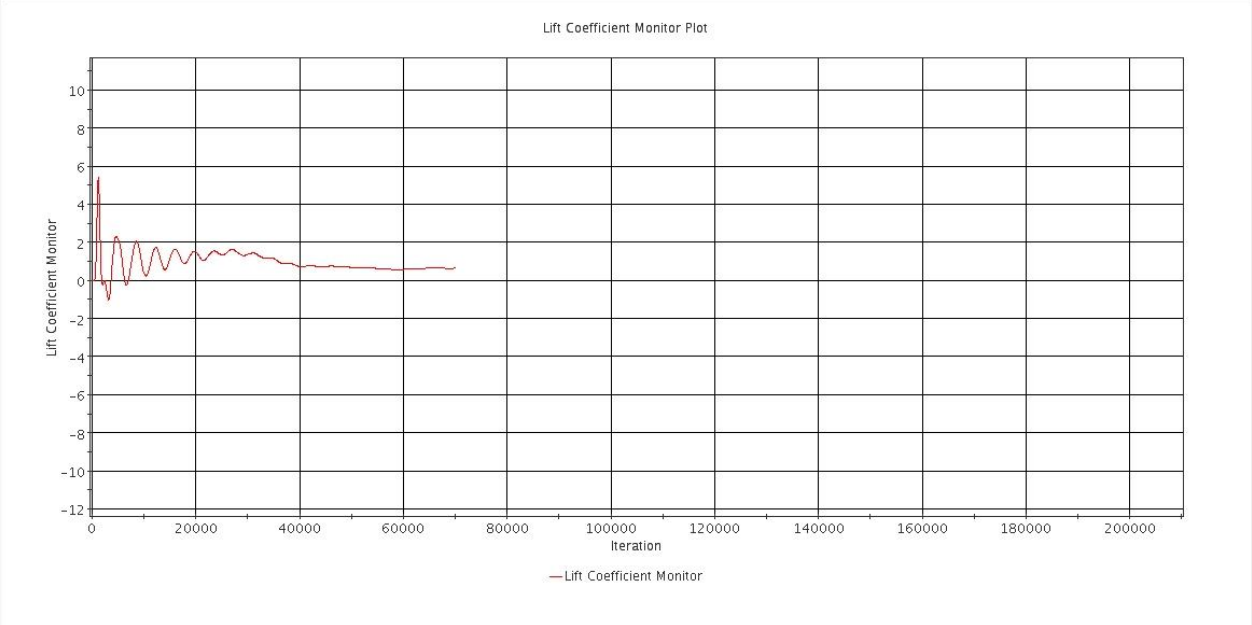

Figure 96: Lift coefficient LES 15 deg.

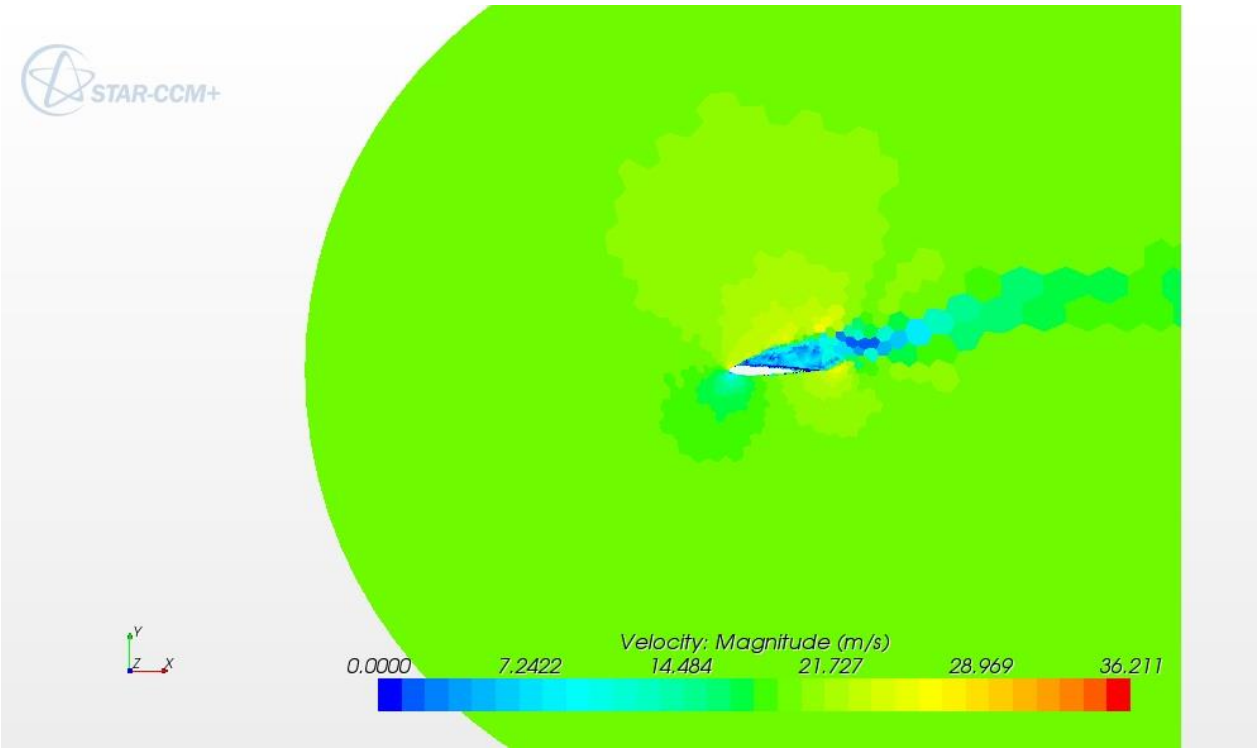

Figure 97: Scalar velocity magnitude LES 15 deg.

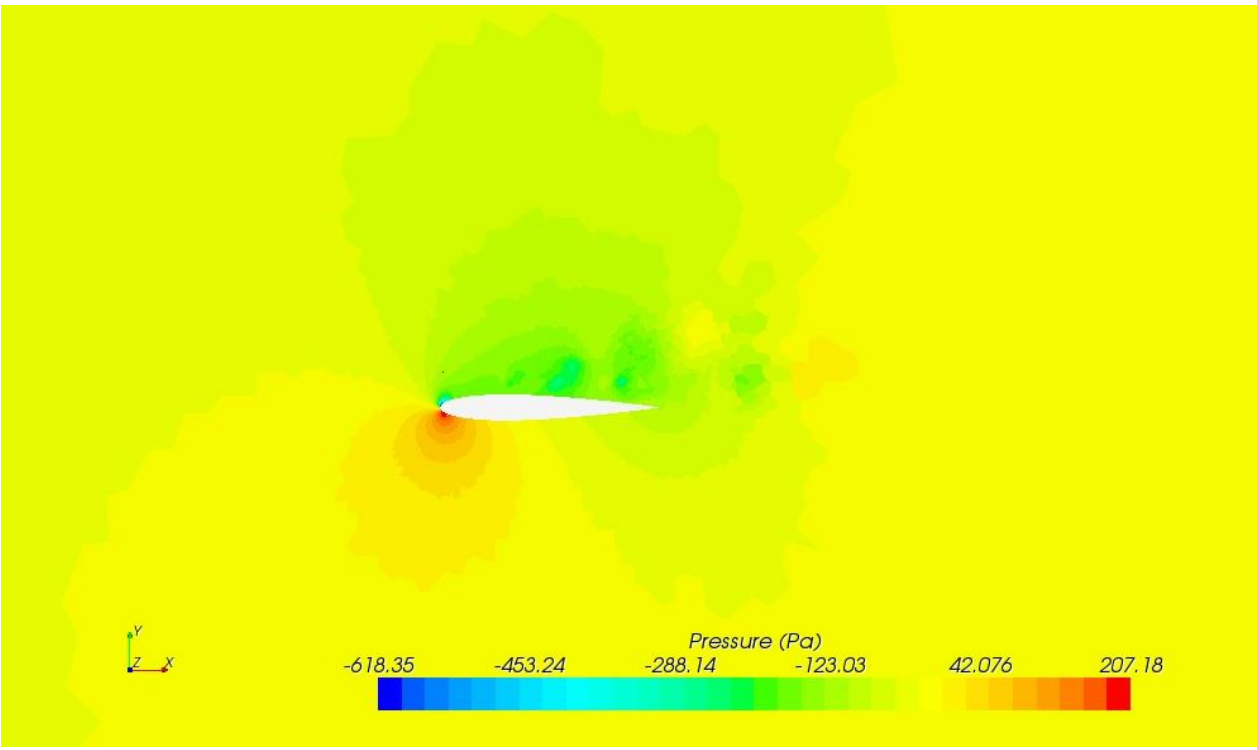

Figure 98: Pressure LES 15 deg.

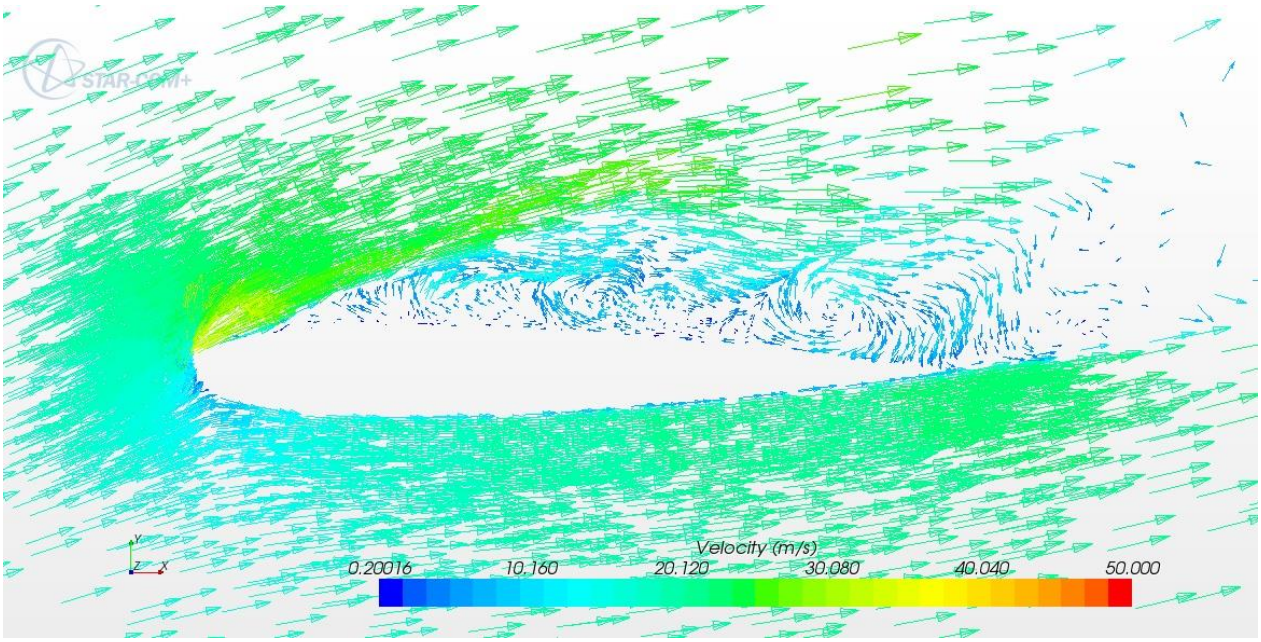

Figure 99: Velocity magnitude LES 15 deg.

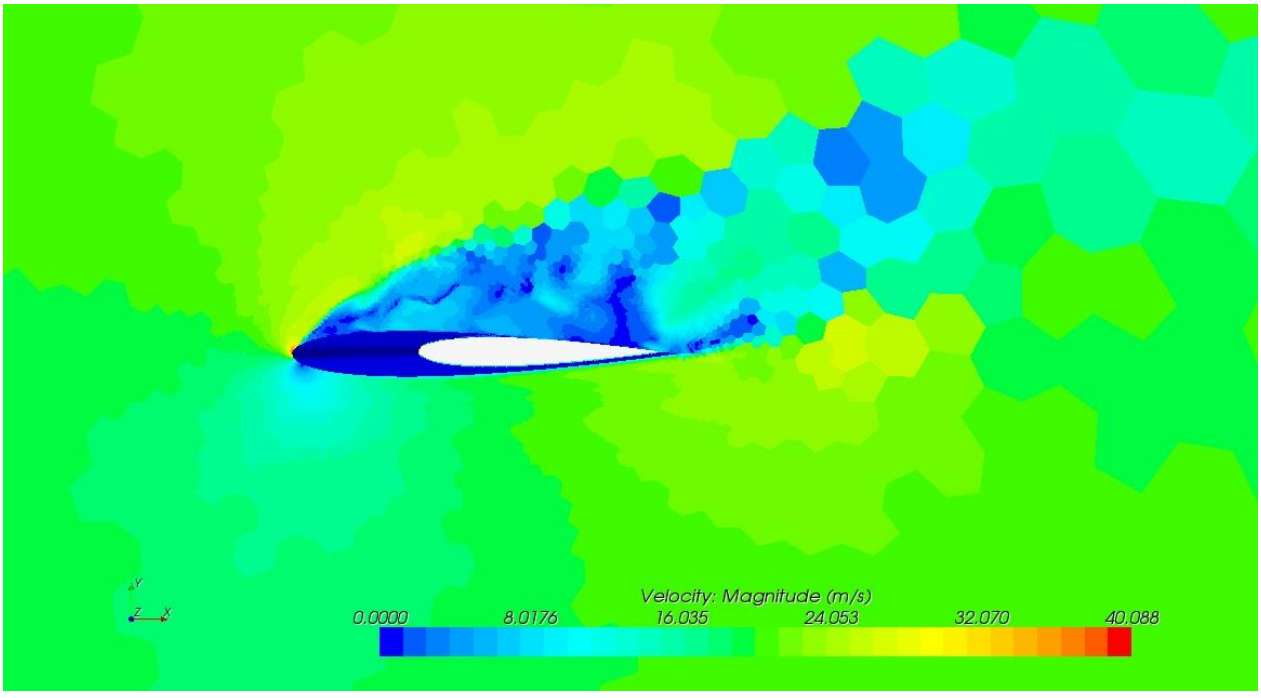

Figure 100: Velocity magnitude LES 20 deg.

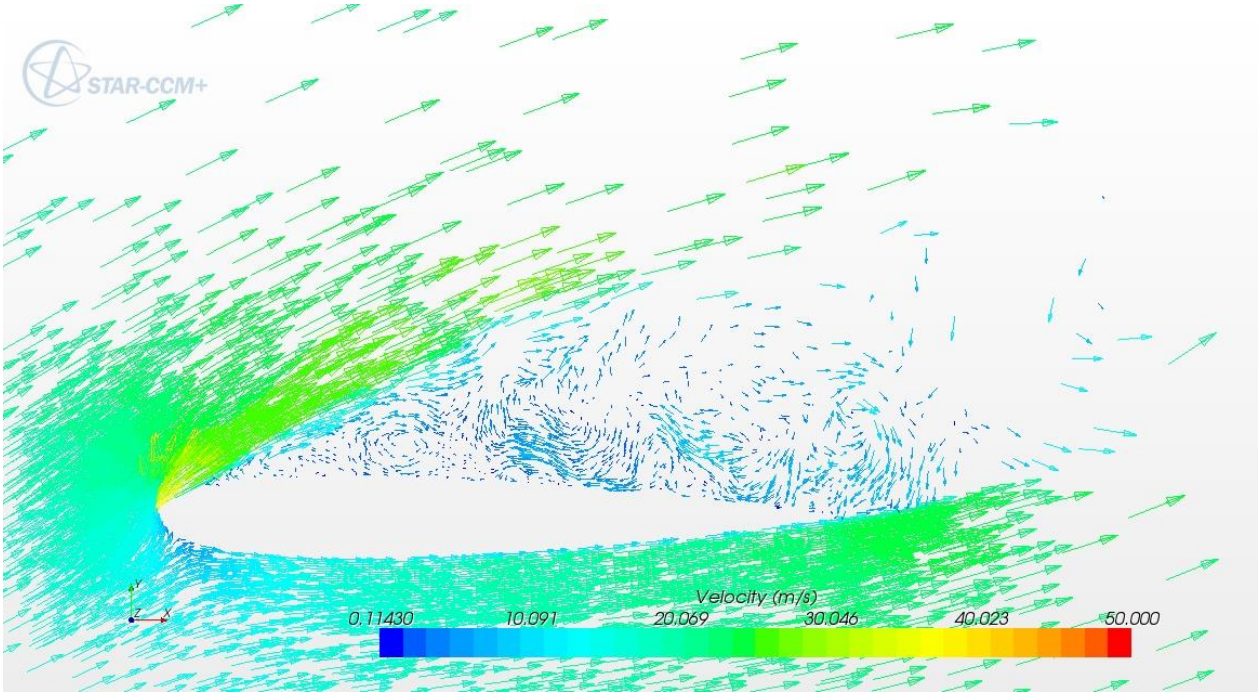

Figure 101:Velocity vector LES 20 deg.

19.5 ANNEX E: RIGID BODY MOTION ROTATION SIMULATION.

The following is the processes for setting up a rotation in StarCCM+. Data is provided from the StarCCM+ online user's guide and experience gained.

A transient rigid body motion model must be set up in StarCCM+.

- The most difficult part of such a simulation is accurately defining the mesh geometry. As different regions must be set up – some to rotate while some to remain stationary. Within the regions section an interface must be set up between the rotating region and the stationary region.
- Models are set up much the same way as a static analysis. As previously noted, only LES was considered an appropriate model to run a dynamic VAWT analysis.
- The tools menu must be used and a new motion must be created on the motion section. This new motion must be rotation. There is the option of translation also, but at this stage just rotation is necessary. The rate of rotation and the axis of rotation must be specified.
- This motion must then be applied to the rotation region. Thus the motion specification in the region must be changed to rotation and the reference frame to Lab reference frame.
- The solver parameters must then be adjusted to realistically reflect the rotation rate specified. Thus the time step for calculation must reflect the rotation rate, a time step of approx. 1 deg. per time step is recommended.

Thus for a rotation of 30 rad/s a time step of 5.8×10^{4} was used.

- For accuracy 2^{nd} order temporal discretization is recommended. This is due to the connectivity of the mesh interfaces between rotating and stationary surfaces. The solver can experience instability for LES simulations and the StarCCm+ user guide recommends this setting.
- The maximum inner iterations are also very important. Based on experience with previous LES flows, a higher value of approx. 40 is recommended. However this is contradictory in finding a fast solution. This value can be adjusted to obtain an optimum time/ solution accuracy. StarCCM+ recommends starting with a value of 7.

- StarCCM+ recommends creating a report monitor called moment1. Monitoring such a value can indicate a trend in solution convergence within a time step.

The 3 dimensional models and mesh developed and tested in LES is contained below.

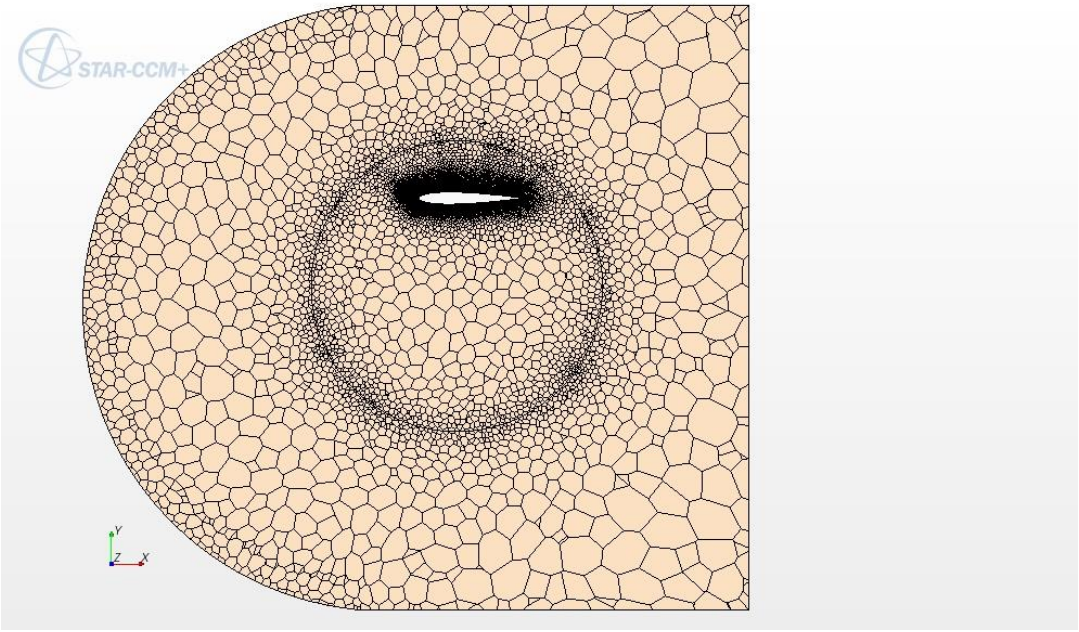

Figure 102: Initial 3D dynamic simulation – 1 blade.

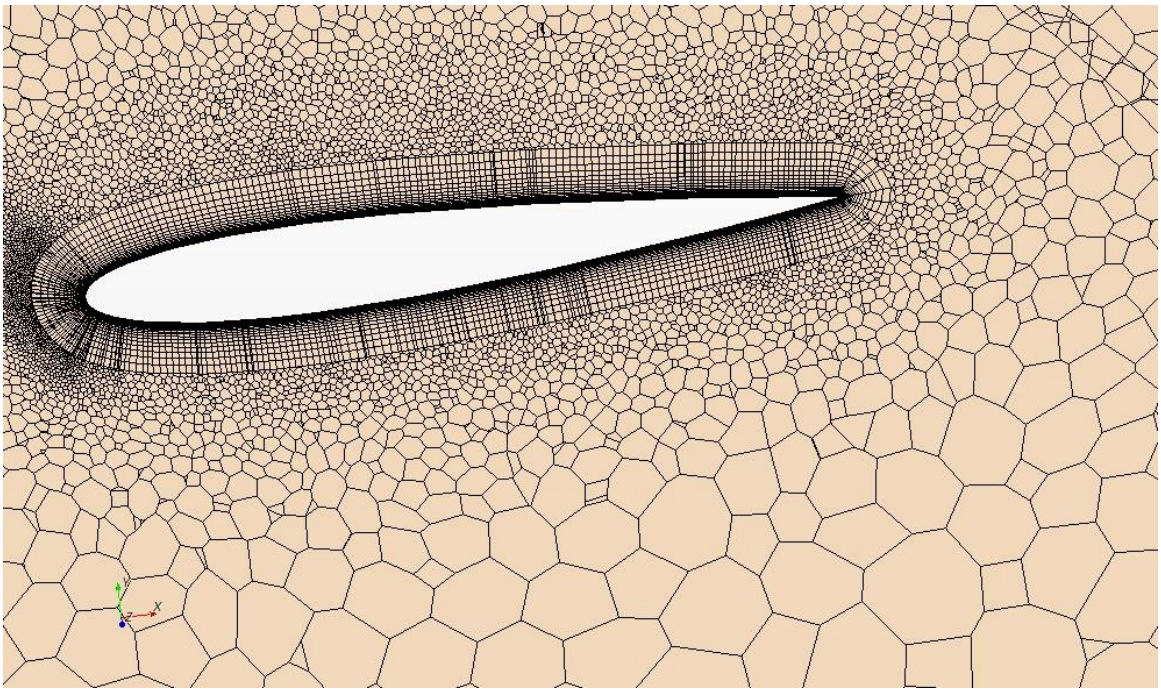

Figure 103: Initial 3D dynamic simulation prism layer mesh.

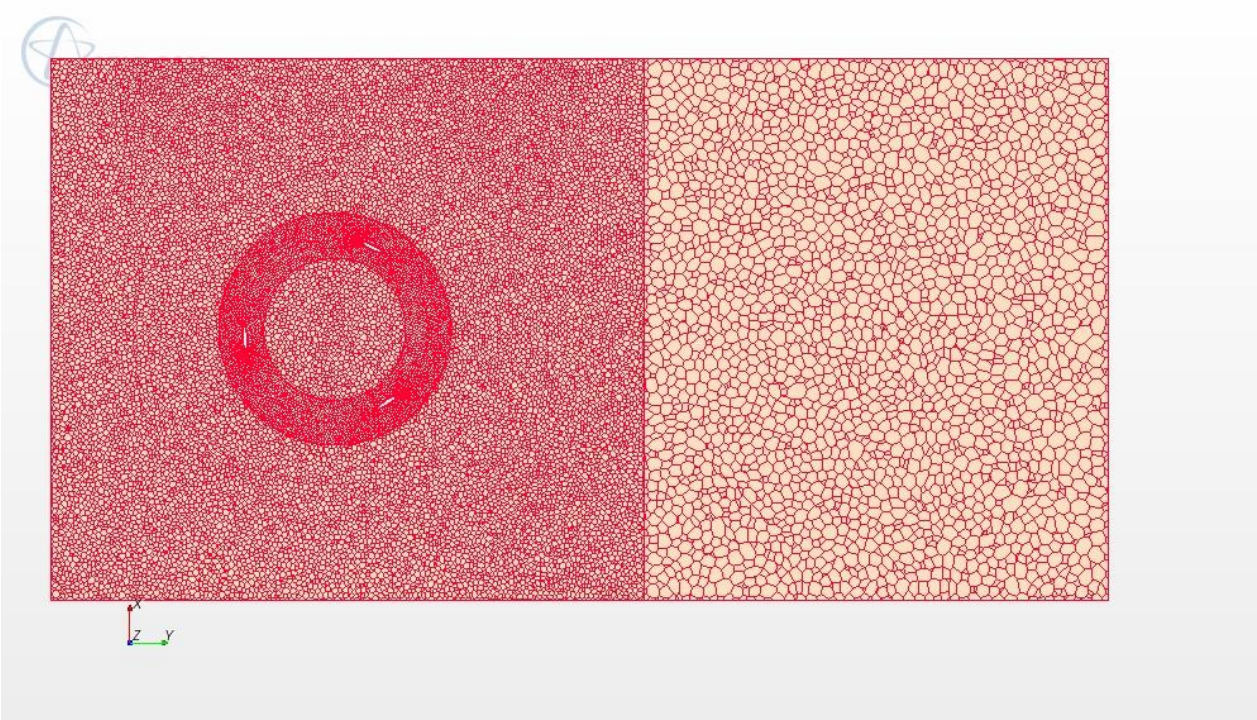

Figure 104: ICAM 3D dynamic simulation mesh.

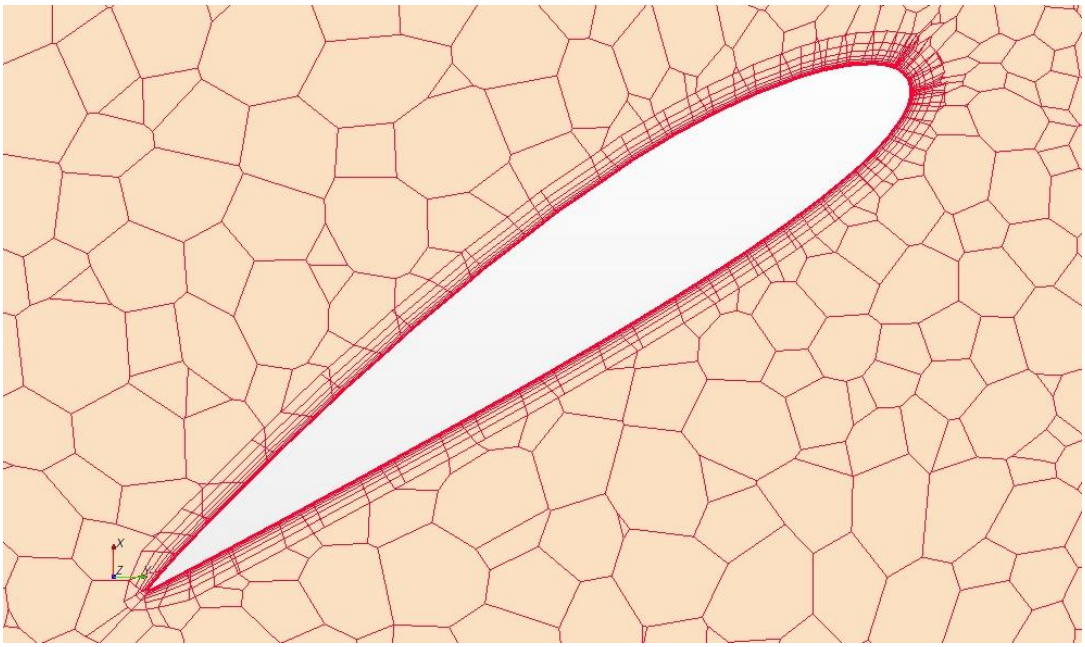

Figure 105: ICAM 3d dynamic simulation prism layer.

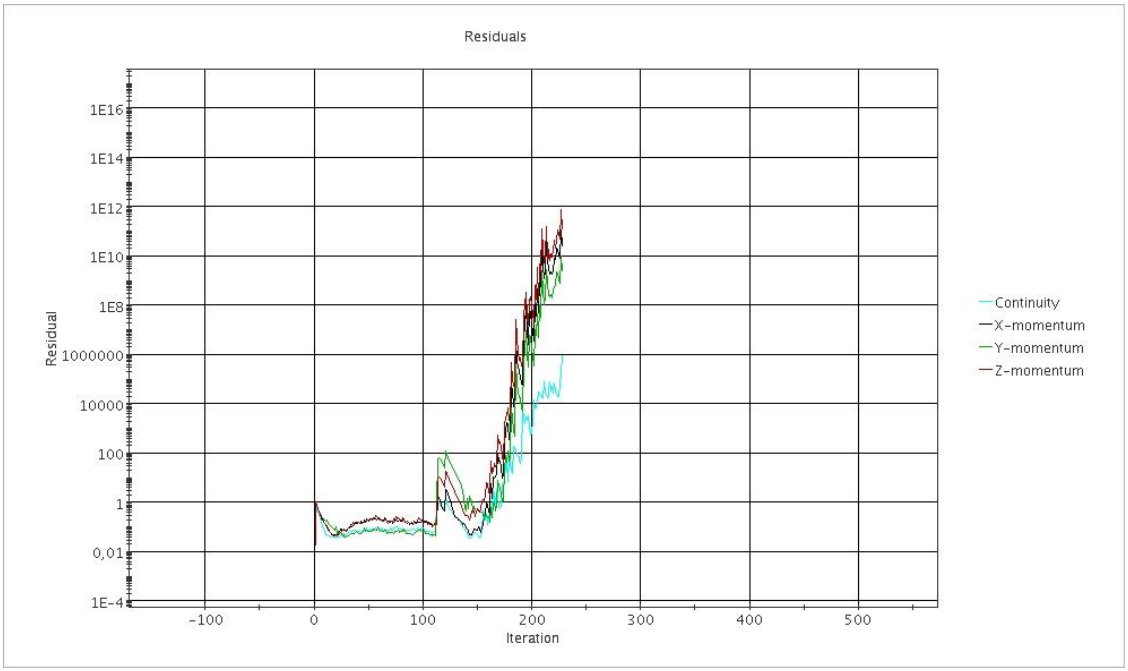

Figure 106: ICAM 3d simulation residual divergence.

19.6 ANNEX F: SAVONIUS TURBINE MATHEMATICAL MODEL.

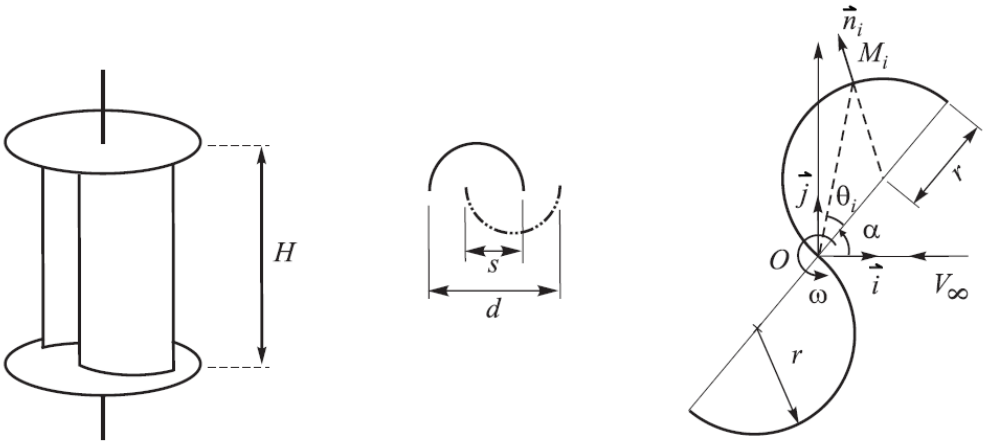

2.2.1 Mathematical Model

A mathematical model based on the pressure drop on each side of the blades was proposed by Chauvin *et al.* [2.13] to evaluate the power of a two-bucket Savonius rotor with a gap spacing $s/d = 0$. From Fig. 2.2, if $\vec{\omega} = \dot{\alpha}\vec{k}$ is the instantaneous rotation vector and, due to the symmetry of the Savonius rotor, $\dot{\alpha} = \omega =$ constant, then the torque is given by:

$$Q = \sum_i \left(\overrightarrow{OM} \times \vec{F}_i\right) \cdot \vec{k} \tag{2.1}$$

This sum has two components:

a) the first is associated with the retreating blade, a driven component, Q_M

b) the second is associated with the advancing blade, a resistant component, Q_D

$$Q = Q_M + Q_D \tag{2.2}$$

19.7 ANNEX G: OVERVIEW OF SHIP TYPES STUDIED.

The Tanker:

Tankers are normally designed to carry petroleum products ranging from crude oil to gasoline, with specific gravities ranging from 0.73 – 0.97. The normal cycle of tanker operation consists of loading, cargo voyage, unloading, ballasting, ballast voyage, tank cleaning, deballasting and then loading again. The use of a wind turbine as a means of electrical power generation is only considered on the cargo voyage and the ballast voyage.

General arrangement:

The tanker design is quite standardised. With a small superstructure aft, an array of tanks fwd. of the superstructure, oil tanks along the ships centerline and wing ballast tanks on the side. Mooring equipment fwd. of the tanks at the bow of the ship. An example of such a design is contained in figure 107.

Some possible areas where a wind turbine could be placed in front of the superstructure include.

- **In front of the oil tanks with mooring equipment,**
- **On both port and starboard side above the wing/ballast tanks.**

It was not considered appropriate from a safety point of view and a ships operation point of view to place the wind turbines above cargo tanks.

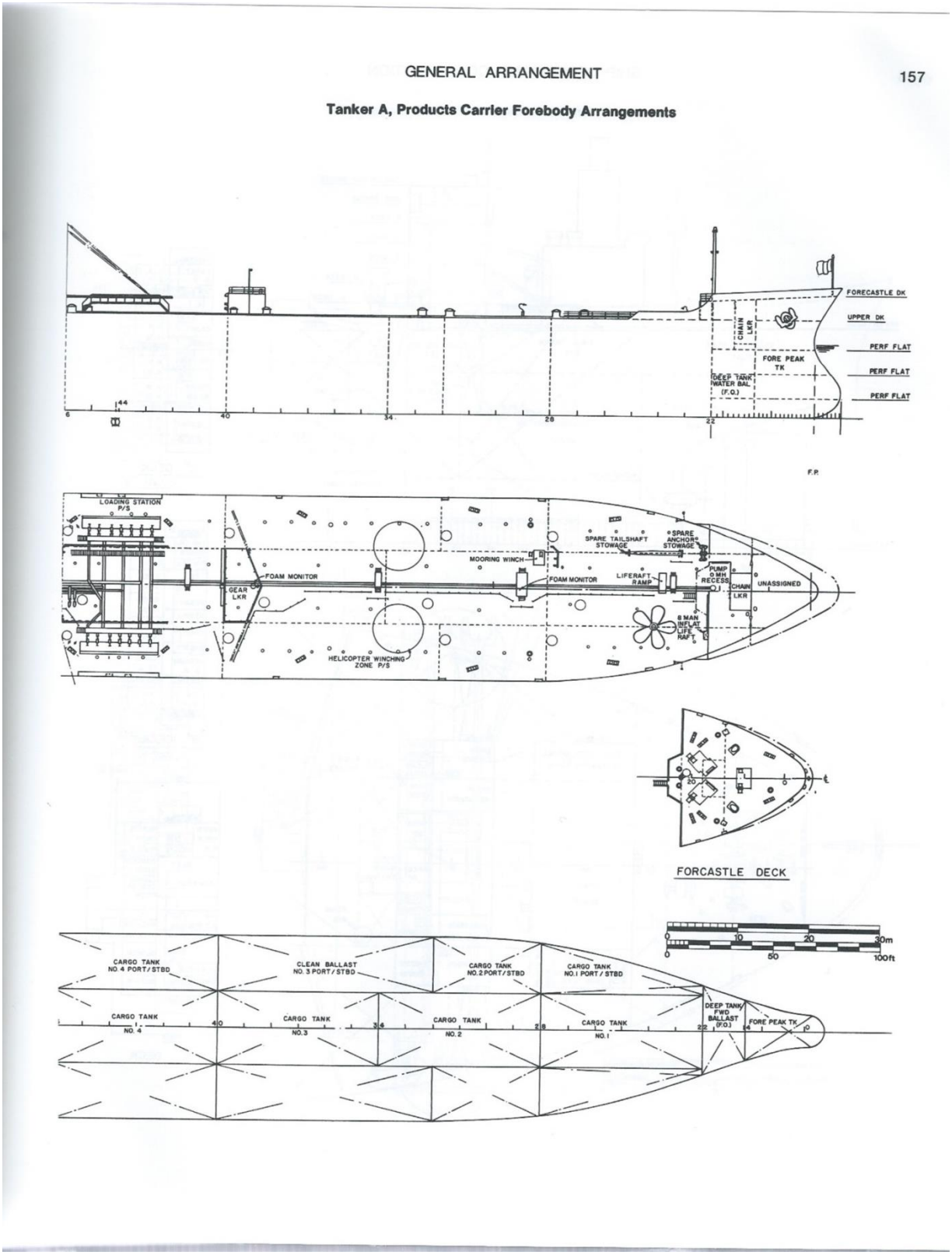

Figure 107: Tanker example GA

Dry-bulk Carriers

Dry Bulk carriers are vessels intended to carry dry bulk cargo which may vary in specific density from Iron Ore being 3.49 to grains of 0.36. Generally they are not self-discharging and will require shore based facilities to load and unload the cargo. However some bulk carriers have self-discharge cranes which will affect the vessels hotel load and main deck arrangements.

General arrangement:

The general arrangement of a bulk carrier is very standardised with cargo hatches forward of the superstructure aft. Ballast tanks are situated on both port and starboard side of the cargo tanks and a small area at the bow of the ship is reserved for mooring equipment. As there is generally no loading and unloading facilities bulk carriers don't have the associated pipework on the main deck as do tankers. Giving much greater flexibility for the placement of wind turbines on the main deck.

Some profile views and a plan view of typical bulk carrier arrangements is contained in Figure 108.

Some possible areas where a wind turbine could be placed in front of the superstructure include.

- **In front of the hatches with mooring equipment,**
- **On both port and starboard side above the wing/ballast tanks.**
- **In between hatches or in between the superstructure and the first hatch running the beam of the ship from port to starboard side.**

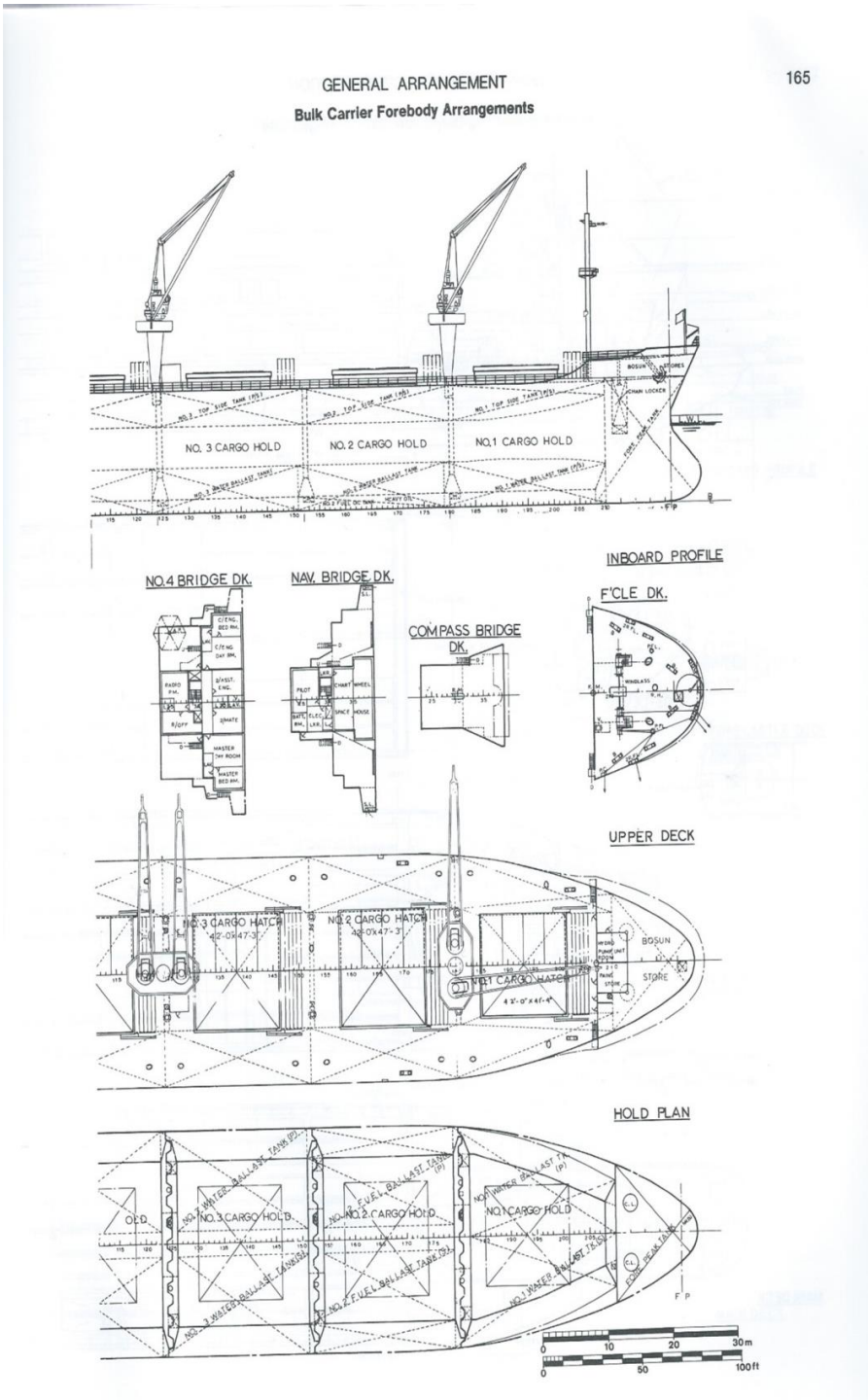

Figure 108: Bulk Carrier example GA

Container ships

A container ship refers to a ship designed specifically to carry all its cargo via containers. Most containerships these days are designed without self-loading facilities, and will rely on shore facilities for loading and unloading.

General arrangements:

Space is very limited on a modern containership with the main deck filled with as many containers as possible. A small superstructure is usually aft for crew and mooring equipment is places in front of the containers at the bow.

A typical containership specification and general arrangement is contained in figure 109 & 110.

Due to such a GA it is very difficult to find space for a VAWT. The only possible solution in modern designs is in front of containers in the bow area with the mooring equipment.

GENERAL ARRANGEMENT

Containership A

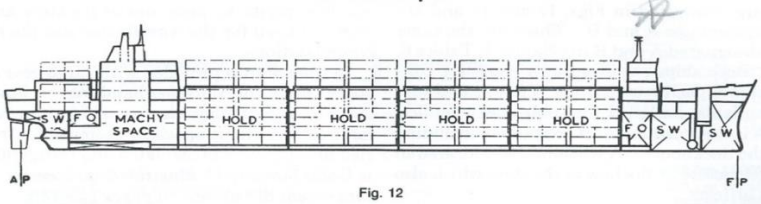

Fig. 12

Length Overall	186 m (610 ft)
Length Between Perpendiculars	177 m (580 ft)
Beam, Molded	23.8 m (78 ft)
Depth To Upper Deck At Side, Molded	16.6 m (54.5 ft)
Draft, Full Load (Scantling), Molded	9.64 m (31.5 ft)
Light Ship	7,480 Tons
Crew Effects & Stores	50 Tons
Fuel Oil	3,380 Tons
Fresh Water	230 Tons
General & Refrigerated Cargo	10,940 Tons
Total Deadweight	14,600 Tons
Displacement, Full Load (Scantling) Draft	22,080 Tons
Cargo Volume, Bales (20-ft Containers)	27,800 m^3 975,840 ft^3
Refrigerated Volume (20-ft Containers)	1,795 m^3 63,360 ft^3
Containers In Hold	612
Containers On Deck	316
Crew Accommodations	42
Shaft Horsepower, A.B.S.	17,500
Speed, Knots	200
Propeller 5 Blades, diam	6.56 m (21.5 ft)

Propelling Machinery, Cross Compound Double Reduction Geared Turbine

Containership B

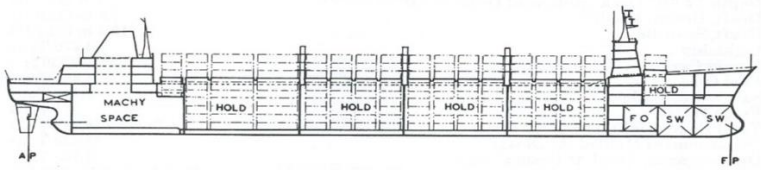

Fig. 13

Length Overall	220 m (719 ft)
Length Between Perpendiculars	206 m (677 ft)
Beam, Molded	29 m (95 ft)
Depth To Main Deck At Side, Molded	16.5 m (54 ft)
Draft, Design Molded	10.4 m (34 ft)
Lightship	14,574 Tons
Crew Effects & Stores (Bale)	1100 m^3 (38,977 ft^3)
Fuel Oil	6,943.3 Tons
Anti-Roll Tank	1,790 Tons
Fresh Water	588.7 Tons
Total Deadweight	24,126 Tons
Displacement At Design Draft	38,700 Tons
Cargo Volume, Bale (35-ft Containers)	23,100 m^3 816,340 ft^3
Cargo Volume, Bale (40-ft Containers)	14,000 m^3 484,160 ft^3
Containers In Hold (35-ft Containers)	394
Containers In Hold (40-ft Containers)	178
Containers On Deck (35-ft Containers)	165
Basic Manning	37
Crew Accommodations	39
Shaft Horsepower, ABS (Maximum)	32,000
Speed, Knots	22.8
Propeller, 6 Blades, diam	6.87 m (22.5 ft)

Propelling Machinery, Cross Compound, Double Reduction Geared Steam Turbine

Figure 109: Containership example specification

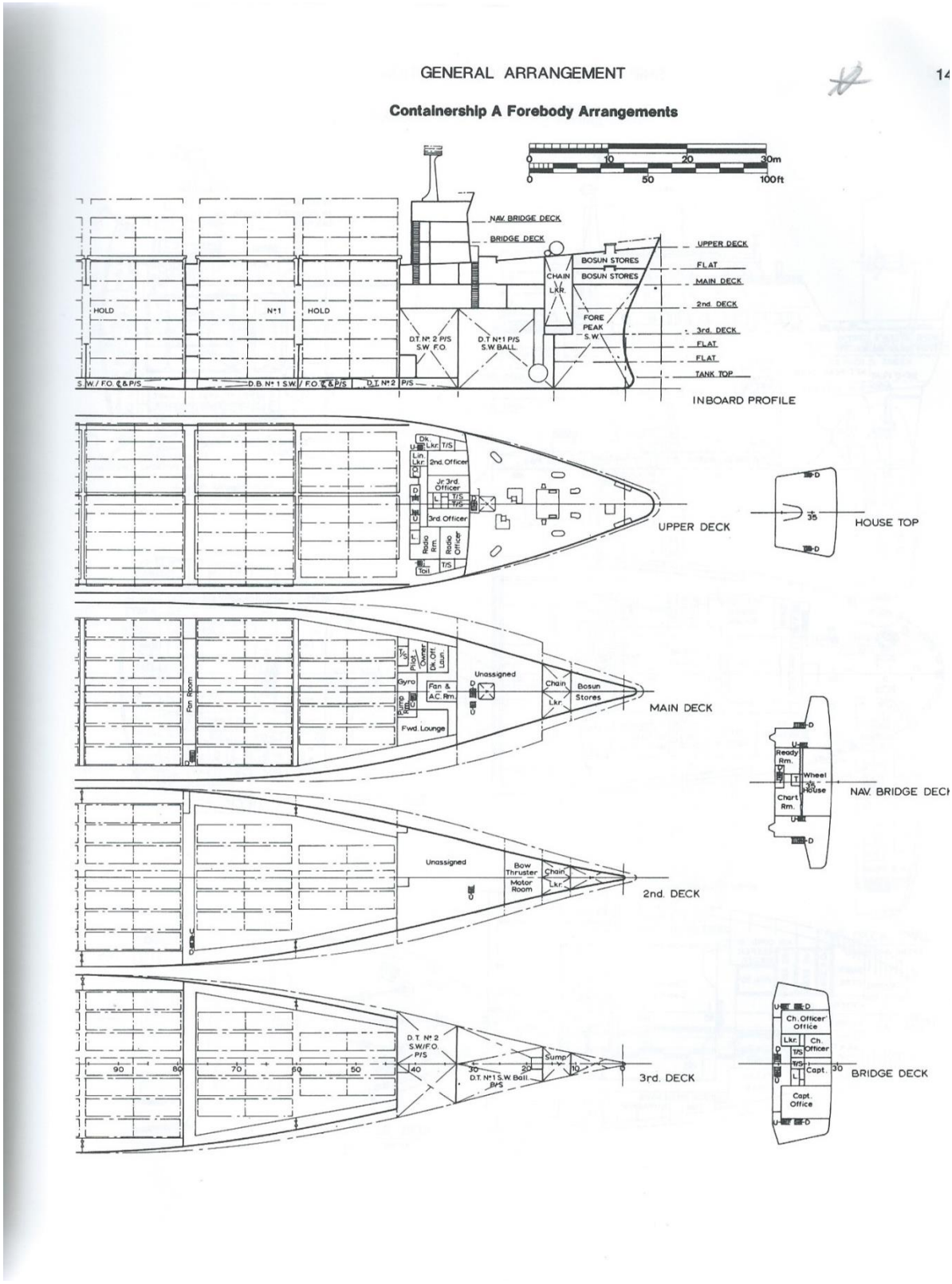

Figure 110: Containership example GA

Ro-Ro ships

This is a broad term for ships designed to carry cargo which rolls on wheels. This ship was the forerunner of the modern container ship, and these days are often designed to carry passengers also. It is usually designed to operate on short routes with quick loading and discharge times, however can also operate on longer routes in the form of car and truck carriers.

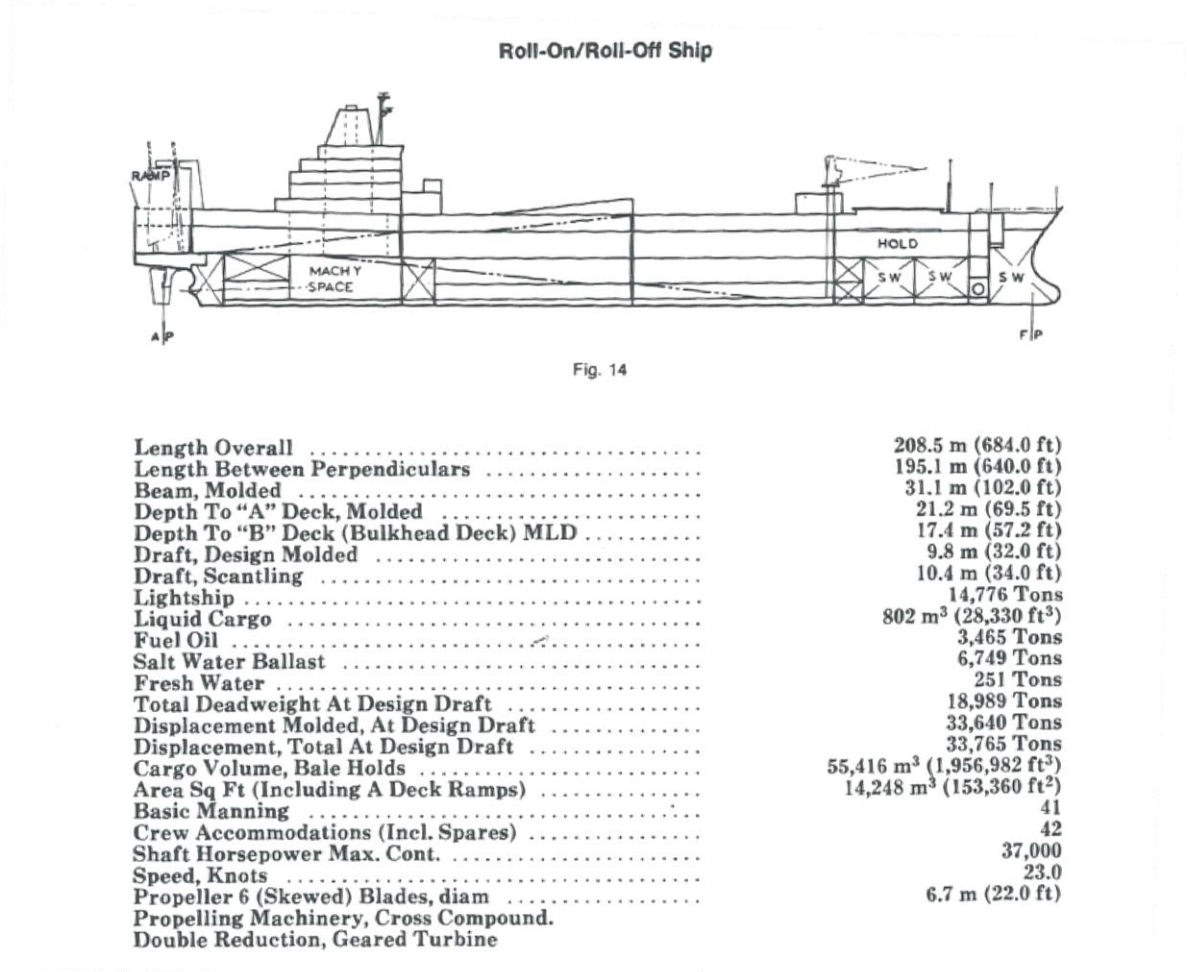

Figure 111: Ro-Ro ship example specification

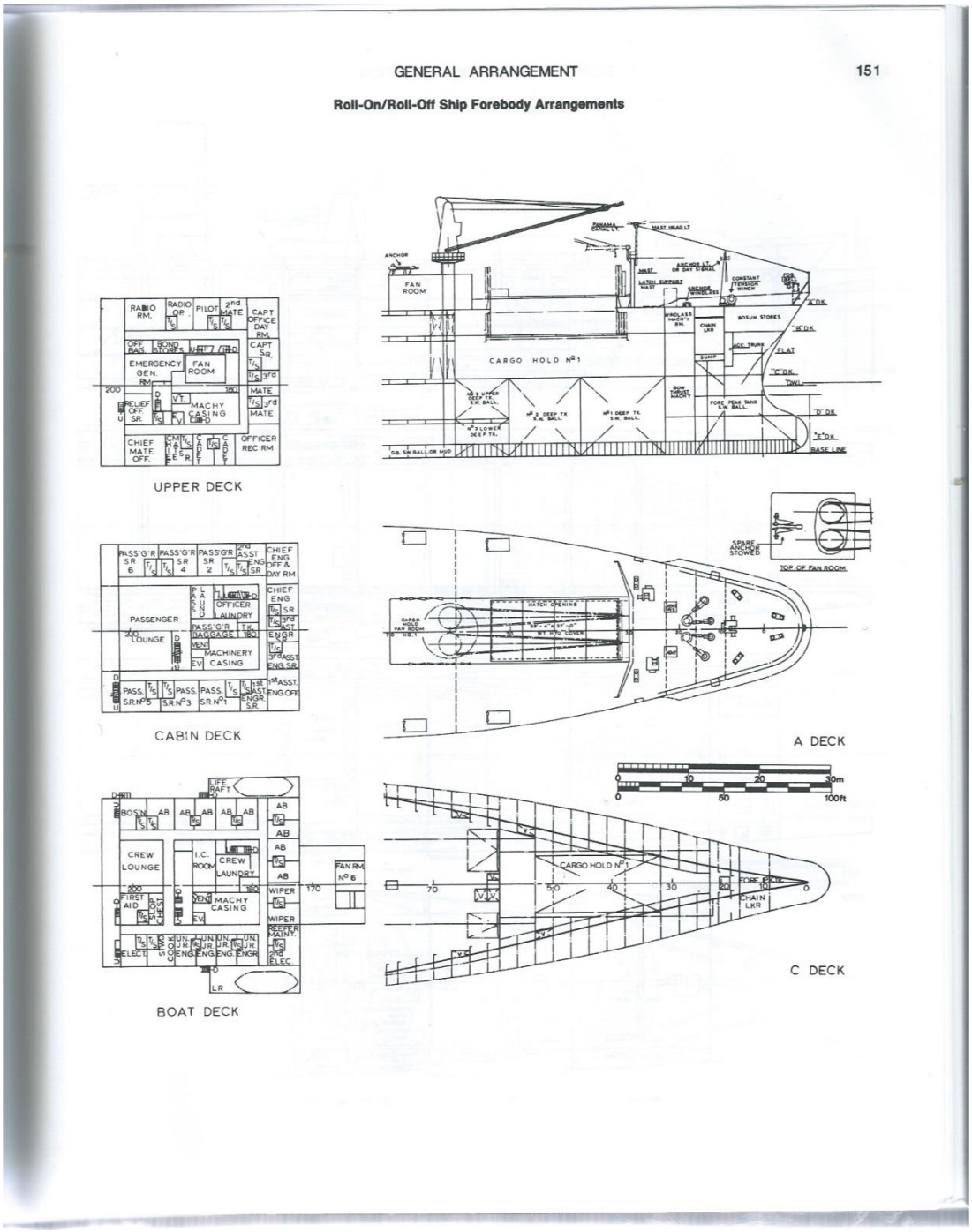

Figure 112: Ro-Ro ship example GA

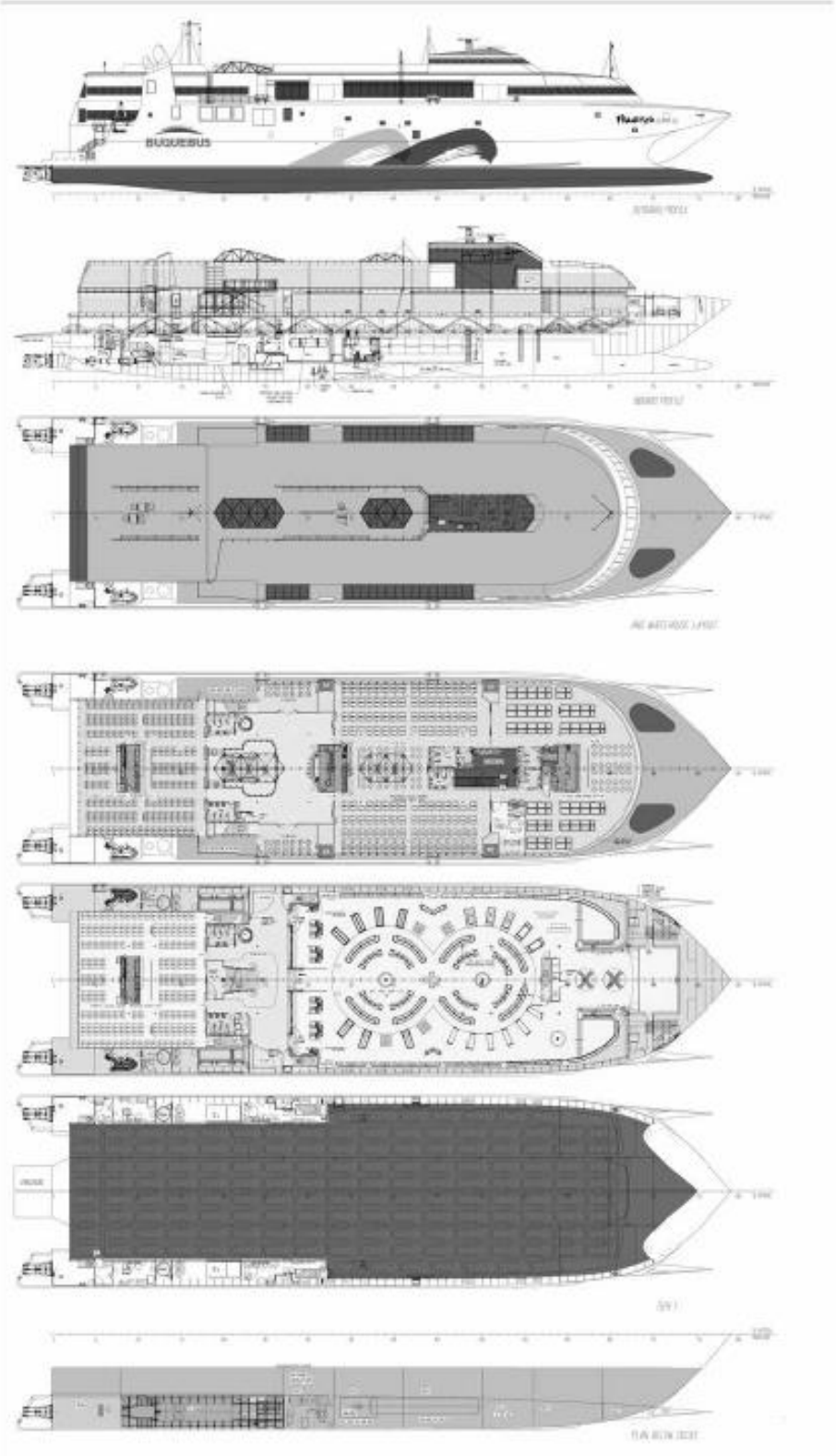

General Arrangement of *Francisco*
(Drawing Courtesy Incat Tasmania)

Figure 113: High speed catamaran example GA

19.8 ANNEX H: NUMERICAL EQUATIONS OF WIND RESISTANCE STUDY

TABLE IV. Values of independent variables

Variable	$\frac{2A_L}{L_{OA}^2}$	$\frac{2A_T}{B^2}$	$\frac{L_{OA}}{B}$	$\frac{S}{L_{OA}}$	$\frac{C}{L_{OA}}$	$\frac{A_{SS}}{A_L}$	M
Maximum	0·246	2·32	9·75	1·97	0·619	0·595	7
Minimum	0·072	0·88	4·00	1·23	0·401	0·138	1
Mean	0·143	1·78	7·39	1·51	0·506	0·246	4
Ship type							
1	0·192	1·95	7·66	1·44	0·492	0·398	2
2	0·111	1·67	7·80	1·51	0·490	0·258	4
3	0·149	2·04	7·80	1·58	0·489	0·188	4
4	0·122	1·75	7·80	1·51	0·550	0·253	5
5	0·151	2·06	7·80	1·58	0·526	0·175	5
6	0·076	1·03	7·46	1·33	0·547	0·252	3
7	0·117	1·43	7·46	1·40	0·522	0·161	3
8	0·100	1·59	7·46	1·33	0·568	0·211	3
9	0·121	1·68	7·46	1·40	0·537	0·139	3
10	0·166	1·80	6·47	1·45	0·476	0·229	2
11	0·236	1·43	4·05	1·86	0·405	0·396	1

(i) Fore and aft force coefficient

$$C_X = A_0 + A_1 \frac{2A_L}{L_{OA}^2} + A_2 \frac{2A_T}{B^2} + A_3 \frac{L_{OA}}{B} + A_4 \frac{S}{L_{OA}} + A_5 \frac{C}{L_{OA}} + A_6 M \quad (5)$$

(ii) Lateral force coefficient

$$C_Y = B_0 + B_1 \frac{2A_L}{L_{OA}^2} + B_2 \frac{2A_T}{B^2} + B_3 \frac{L_{OA}}{B} + B_4 \frac{S}{L_{OA}} + B_5 \frac{C}{L_{OA}} + B_6 \frac{A_{SS}}{A_L} \quad (6)$$

(iii) Yawing moment coefficient

$$C_N = C_0 + C_1 \frac{2A_L}{L_{OA}^2} + C_2 \frac{2A_T}{B^2} + C_3 \frac{L_{OA}}{B} + C_4 \frac{S}{L_{OA}} + C_5 \frac{C}{L_{OA}}$$

$$C_X = \frac{F_X}{\frac{1}{2}\rho V_R^2 A_T}$$

$$C_Y = \frac{F_Y}{\frac{1}{2}\rho V_R^2 A_L}$$

$$C_N = \frac{N}{\frac{1}{2}\rho V_R^2 A_L L_{OA}}$$

TABLE I. Fore and aft component of wind force

$$C_X = A_0 + A_1 \frac{2A_L}{L_{OA}^2} + A_2 \frac{2A_T}{B^2} + A_3 \frac{L_{OA}}{B} + A_4 \frac{S}{L_{OA}} + A_5 \frac{C}{L_{OA}} + A_6 M \pm 1{\cdot}96 \text{ S.E.}$$

γ_R°	A_0	A_1	A_2	A_3	A_4	A_5	A_6	S.E.
0	2·152	−5·00	0·243	−0·164	—	—	—	0·086
10	1·714	−3·33	0·145	−0·121	—	—	—	0·104
20	1·818	−3·97	0·211	−0·143	—	—	0·033	0·096
30	1·965	−4·81	0·243	−0·154	—	—	0·041	0·117
40	2·333	−5·99	0·247	−0·190	—	—	0·042	0·115
50	1·726	−6·54	0·189	−0·173	0·348	—	0·048	0·109
60	0·913	−4·68	—	−0·104	0·482	—	0·052	0·082
70	0·457	−2·88	—	−0·068	0·346	—	0·043	0·077
80	0·341	−0·91	—	−0·031	—	—	0·032	0·090
90	0·355	—	—	—	−0·247	—	0·018	0·094
100	0·601	—	—	—	−0·372	—	−0·020	0·096
110	0·651	1·29	—	—	−0·582	—	−0·031	0·090
120	0·564	2·54	—	—	−0·748	—	−0·024	0·100
130	−0·142	3·58	—	0·047	−0·700	—	−0·028	0·105
140	−0·677	3·64	—	0·069	−0·529	—	−0·032	0·123
150	−0·723	3·14	—	0·064	−0·475	—	−0·032	0·128
160	−2·148	2·56	—	0·081	—	1·27	−0·027	0·123
170	−2·707	3·97	−0·175	0·126	—	1·81	—	0·115
180	−2·529	3·76	−0·174	0·128	—	1·55	—	0·112
							Mean Standard Error	0·103

TABLE II. Lateral component of wind force

$$C_Y = B_0 + B_1 \frac{2A_L}{L_{OA}^2} + B_2 \frac{2A_T}{B^2} + B_3 \frac{L_{OA}}{B} + B_4 \frac{S}{L_{OA}} + B_5 \frac{C}{L_{OA}} + B_6 \frac{A_{SS}}{A_L} \pm 1{\cdot}96 \text{ S.E.}$$

γ_R°	B_0	B_1	B_2	B_3	B_4	B_5	B_6	S.E.
10	0·096	0·22	—	—	—	—	—	0·015
20	0·176	0·71	—	—	—	—	—	0·023
30	0·225	1·38	—	0·023	—	−0·29	—	0·030
40	0·329	1·82	—	0·043	—	−0·59	—	0·054
50	1·164	1·26	0·121	—	−0·242	−0·95	—	0·055
60	1·163	0·96	0·101	—	−0·177	−0·88	—	0·049
70	0·916	0·53	0·069	—	—	−0·65	—	0·047
80	0·844	0·55	0·082	—	—	−0·54	—	0·046
90	0·889	—	0·138	—	—	−0·66	—	0·051
100	0·799	—	0·155	—	—	−0·55	—	0·050
110	0·797	—	0·151	—	—	−0·55	—	0·049
120	0·996	—	0·184	—	−0·212	−0·66	0·34	0·047
130	1·014	—	0·191	—	−0·280	−0·69	0·44	0·051
140	0·784	—	0·166	—	−0·209	−0·53	0·38	0·060
150	0·536	—	0·176	−0·029	−0·163	—	0·27	0·055
160	0·251	—	0·106	−0·022	—	—	—	0·036
170	0·125	—	0·046	−0·012	—	—	—	0·022
							Mean Standard Error	0·044

TABLE III. Wind induced yawing moment

$$C_N = C_0 + C_1 \frac{2A_L}{L_{OA}^2} + C_2 \frac{2A_T}{B^2} + C_3 \frac{L_{OA}}{B} + C_4 \frac{S}{L_{OA}} + C_5 \frac{C}{L_{OA}} \pm 1{\cdot}96 \text{ S.E.}$$

γ_R°	C_0	C_1	C_2	C_3	C_4	C_5	S.E.
10	0·0596	0·061	—	—	—	−0·074	0·0048
20	0·1106	0·204	—	—	—	−0·170	0·0074
30	0·2258	0·245	—	—	—	−0·380	0·0105
40	0·2017	0·457	—	0·0067	—	−0·472	0·0137
50	0·1759	0·573	—	0·0118	—	−0·523	0·0149
60	0·1925	0·480	—	0·0115	—	−0·546	0·0133
70	0·2133	0·315	—	0·0081	—	−0·526	0·0125
80	0·1827	0·254	—	0·0053	—	−0·443	0·0123
90	0·2627	—	—	—	—	−0·508	0·0141
100	0·2102	—	−0·0195	—	0·0335	−0·492	0·0146
110	0·1567	—	−0·0258	—	0·0497	−0·457	0·0163
120	0·0801	—	−0·0311	—	0·0740	−0·396	0·0179
130	−0·0189	—	−0·0488	0·0101	0·1128	−0·420	0·0166
140	0·0256	—	−0·0422	0·0100	0·0889	−0·463	0·0162
150	0·0552	—	−0·0381	0·0109	0·0689	−0·476	0·0141
160	0·0881	—	−0·0306	0·0091	0·0366	−0·415	0·0105
170	0·0851	—	−0·0122	0·0025	—	−0·220	0·0057
					Mean Standard Error		0·0127